NOTICE

The quality of this microform is heavily dependent upon the quality of the original thesis submitted for microfilming. Every effort has been made to ensure the highest quality of reproduction possible.

If pages are missing, contact the university which granted the degree.

Some pages may have indistinct print especially if the original pages were typed with a poor typewriter ribbon or if the university sent us an inferior photocopy.

Reproduction in full or in part of this microform is governed by the Canadian Copyright Act, R.S.C. 1970, c. C-30, and subsequent amendments.

AVIS

La qualité de cette microforme dépend grandement de la qualité de la thèse soumise au microfilmage. Nous avons tout fait pour assurer une qualité supérieure de reproduction.

S'il manque des pages, veuillez communiquer avec l'université qui a conféré le grade.

La qualité d'impression de certaines pages peut laisser à désirer, surtout si les pages originales ont été dactylographiées à l'aide d'un ruban usé ou si l'université nous a fait parvenir une photocopie de qualité inférieure.

La reproduction, même partielle, de cette microforme est soumise à la Loi canadienne sur le droit d'auteur, SRC 1970, c. C-30, et ses amendements subséquents.

NOTICE

The quality of this microform is heavily dependent upon the quality of the original thesis submitted for microfilming. Every effort has been made to ensure the highest quality of reproduction possible.

If pages are missing, contact the university which granted the degree.

Some pages may have indistinct print especially if the original pages were typed with a poor typewriter ribbon or if the university sent us an inferior photocopy.

Reproduction in full or in part of this microform is governed by the Canadian Copyright Act, R.S.C. 1970, c. C-30, and subsequent amendments.

AVIS

La qualité de cette microforme dépend grandement de la qualité de la thèse soumise au microfilmage. Nous avons tout fait pour assurer une qualité supérieure de reproduction.

S'il manque des pages, veuillez communiquer avec l'université qui a conféré le grade.

La qualité d'impression de certaines pages peut laisser à désirer, surtout si les pages originales ont été dactylographiées à l'aide d'un ruban usé ou si l'université nous a fait parvenir une photocopie de qualité inférieure.

La reproduction, même partielle, de cette microforme est soumise à la Loi canadienne sur le droit d'auteur, SRC 1970, c. C-30, et ses amendements subséquents.

ISBN 0-315-60591-X

UNIVERSITÉ D'OTTAWA
UNIVERSITY OF OTTAWA

ACKNOWLEDGMENTS

Foremost I would like to thank Christian Detellier, my research supervisor, for his excellent guidance throughout my studies. I can truly say that his enthusiasm inspired and confirmed my desire to work towards a Ph.D.

I am much indebted to Heather Dettman and Raj Capoor for sharing their NMR expertise with me and providing assistance on numerous occasions. Heather and Raj have certainly been a catalyst in my studies.

Amongst the many friendly people in this department, I wish to especially thank Monique Frechette for her help and much appreciated advice and Helen Graves Smith for four years of enjoyable company and moral support as a fellow graduate student. My many thanks to Cass Guthridge, Wilma Schmiedel, Monique Levesque, Dan Lafleur, Robert Nadon, Eva Szabo, Fern Boucher and Mario Savage who were always willing to take the time to help me out.

I wish to thank John Nickifuruk and Barbara Blackwell from Agriculture Canada for running a few of my samples on their 500 MHz Bruker Spectrometer.

Finally, but certainly not least, I would like to thank my family: Milton, Brenda, Joyce and my parents, who were there for me every step of the way. I would especially like to thank my parents, Marguerite and Aldé, for their constant support throughout my studies and otherwise, and it is to them that I wish to dedicate this thesis.

to mom and dad

ABSTRACT

The structural, thermodynamic, kinetic and mechanistic behavior of alkali metal cation-crown ether complexes have been studied by ^{1}H, ^{13}C, ^{23}Na and ^{7} Li NMR. Insight into the solution structures of benzo-15-crown-5, dibenzo-18-crown-6, dibenzo-24-crown-8 and dibenzo-30-crown-10, as well as their lithium, sodium and potassium complexes in nonaqueous solvents has been obtained with ^{1}H NMR. The overall orientations of the oxygen atoms of the separate $O\text{-}CH_2\text{-}CH_2\text{-}O$ groups of the free and complexed crown ethers were shown to be gauche from the determinations of the $^{1}H\text{-}^{1}H$ coupling constants obtained from spin simulations. ^{13}C spectral assignments were done with heteronuclear chemical shift correlation NMR experiments.

^{23}Na and ^{7}Li NMR have proven to be very useful techniques for studying the extent of complexation reaction of lithium and sodium cations with 15-crown-5 (15C5) and benzo-15-crown-5 (B15C5) in nitromethane (NM), acetonitrile (AN), pyridine (PY) and dimethylformamide (DMF). Although the formation constants (K_{F1}) of $(Na{:}15C5)^{+}$, $(Na{:}B15C5)^{+}$, $(Li{:}15C5)^{+}$ and $(Li{:}B15C5)^{+}$ in NM were too large to be accurately measured ($\log K_{F1} > 4$), that of $(Na{:}B15C5)^{+}$ in DMF and PY were determined from ^{23}Na chemical shift and longitudinal relaxation rates: $\log K_{F1} = 2.9 \pm 0.3$ in PY and 1.2 ± 0.4 in DMF. A combined ^{23}Na and ^{7}Li NMR study for systems containing both lithium and sodium cations in the presence of B15C5 in NM revealed a selectivity for the complexation of lithium where the equilibrium constant, reflecting the ratio K_{FLi} / K_{FNa}, was determined: $\log K_{eq} = 1.9 \pm 0.2$.

In the two-site chemical exchange of the alkali metal cations, two exchange mechanisms have accounted for the ^{23}Na and ^{7}Li dynamic NMR results: associative and dissociative exchange. The chemical exchange of sodium and lithium individually with B15C5, was shown, by ^{23}Na and ^{7}Li NMR respectively, to follow the associative

pathway in NM whereas in AN the chemical exchange of sodium with B15C5 was shown to prefer the dissociative pathway. Kinetic studies of sodium-B15C5 in binary mixtures of AN-NM and DMF-NM have indicated that the change in observed mechanism is related to the solvent donicity where dissociative exchange is observed in high donicity solvents. An increase of the concentration of AN or DMF in the solvent mixture gives rise to an increase of the dissociative contribution to the exchange. The activation parameters of the dissociative exchange are highly solvent dependent indicating that the solvent, at the molecular level, must play an important role in this mechanism. However, the activation parameters for the associative exchange do not display such a dependence on the solvent; it was postulated that conformational rearrangements play the governing role in this mechanism. In studies with DMF-NM binary solvent mixtures, a model based on the direct participation of one DMF molecule in the coordination sphere of sodium in $(Na{:}B15C5)^+$, has accounted for the observed ^{23}Na chemical shift and longitudinal relaxation rate variations of $(Na{:}B15C5)^+$ as a function of the concentration of DMF in the solvent mixture. It was postulated that it is the formation of $(Na{:}B15C5{:}DMF)^+$ which is responsible for the observed increase of the rate of exchange as the concentration of DMF in the solvent increases. This direct participation of one solvent molecule in the dissociative exchange was qualitatively and quantitatively characterized.

The application of 2-dimensional ^7Li exchange NMR spectroscopy (EXSY), for the kinetic investigations of the exchange of the lithium cation in its solvated (NM) and complexed (B15C5) sites, is illustrated. Results obtained by this method are in agreement with the conventional 1D lineshape results.

TABLE OF CONTENTS

LIST OF FIGURES AND SCHEMES

LIST OF TABLES

SYMBOLS AND ABBREVIATIONS

15C5	15-crown-5
B15C5	benzo-15-crown-5
18C6	18-crown-6
DB18C6	dibenzo-18-crown-6
DB24C8	dibenzo-24-crown-4
DB30C10	dibenzo-30-crown-10
AN	acetonitrile
DMF	dimethylformamide
NM	nitromethane
PY	pyridine
PC	propylene carbonate
DME	dimethoxyethane
THF	tetrahydrofuran
DMSO	dimethylsulfoxide
HMPA	hexamethylphosphoric amide
DN	donor number
X	mole fraction
X_{AN}	mole fraction of acetonitrile
X_{DMF}	mole fraction of dimethylformamide
k_A, k_f, k_1, k_1^*	rate constant for complex formation
k_B, k_d	rate constant for complex dissociation
k_{-1}, k_{-1}^*	rate constant for dissociative exchange (equations 26 and 45)

k_2	rate constant for associative exchange (equation 31)
k	rate constant determined in 2D exchange spectroscopy
K_{F1}	formation constant for 1:1 complex (equation 18)
K_{F2}	formation constant for 1:2 complex (equation 20)
K_{eq}	equilibrium constant in cation competition (equation 64)
K_{CS}	equilibrium constant in formation of solvated complex (equation 44)
K_S	intrinsic equilibrium constant for solvent displacement
K_{IP}	ion-paring constant (equation 39)
K_{Li}	formation constant of lithium complex (equation 62)
K_{Na}	formation constant of sodium complex (equation 63)
$\Delta G^{\ddagger}_{di}$	free energy of activation for dissociative exchange
$\Delta H^{\ddagger}_{di}$	enthalpy of activation for dissociative exchange
$\Delta S^{\ddagger}_{di}$	entropy of activation for dissociative exchange

ΔG^{*}_{as}	free energy of activation for associative exchange
ΔH^{*}_{as}	enthalpy of activation for associative exchange
ΔS^{*}_{as}	entropy of activation for associative exchange
M^{+}	metal cation
C	crown ether
L	macrocyclic ligand
X^{-}	counteranion
$(M:C)^{+}$, $(M:L)^{+}$	alkali metal cation complex
$(M^{+})_S$	solvated cation
$[M^{+}]_T$	total concentration of metal cation
$[M^{+}]_{S,T}$	total concentration of solvated cation
$[M:C]_T$	total concentration of complexed cation
$[C]_T$	total concentration of crown ether
$(M,X)^{-}$	ion-pair
ϵ	dielectric constant
η	macroscopic solvent viscosity
f_r	microviscosity factor
χ	volume magnetic susceptibility
k_B	Boltzmann constant
h	Planck constant
$\hbar$	Planck constant / 2π

T	temperature
R	gas constant
S	signal height
σ	statistical standard error
γ	gyromagnetic ratio
B_o	static field
B_1	applied field
I	spin quantum number
Q, eQ	electric quadrupole moment
q, eq	electric field gradient
γ_∞	Sternheimer anitishielding factor
ν_o	observation frequency
ω	Larmor frequency
δ	chemical shift
δ_S	chemical shift of solvated cation
δ_C	chemical shift of complexed cation
σ	screening constant
σ_d	diamagnetic screening constant
σ_p	paramagnetic screening constant
ρ	$[C]_T / [M^+]_T$
ρ_T	$[C]_T / ([Na]_T + [Li]_T)$
J_{gem}	geminal ^1H-^1H coupling constant
J_{trans}	trans-vicinal ^1H-^1H coupling constant
J_{cis}	cis-vicinal ^1H-^1H coupling constant
R	ratio J_{trans} / J_{cis}

ϕ	dihedral angle
FID	free induction decay
HETCOR	heteronuclear chemical shift correlation
EXSY	exchange spectroscopy
DR	digital resolution
SW	spectral width
NP	number of points
PD	pulse delay
t_2	acquisition time
n	number of transients
T_1	longitudinal relaxation time
T_2	transverse relaxation time
T_1^{-1} or R_1	longitudinal relaxation rate
T_2^{-1} or R_2	transverse relaxation rate
$T_{2,obs}^{-1}$	observed transverse relaxation rate
$T_{2,inh}^{-1}$	inhomogeneity contribution to the transverse relaxation rate
$T_{2,ex}^{-1}$	exchange contribution to the transverse relaxation rate
T_q^{-1}	quadrupolar relaxation rate
T_q^{-1*}	reduced quadrupolar relaxation rate
$M_{x,y,z}$	magnetization on the *x*-, *y*- and *z*-axes respectively
M_o	initial (equilibrium) magnetization
χ	quadrupolar coupling constant

τ	recovery time
τ_c	correlation time
τ_A	lifetime of the cation in site A
τ_B	lifetime of the cation in site B
t_m	mixing time
P_A	population of site A
P_B	population of site B
$\nu_{1/2}$	linewidth at half-height
a_{AA}	contour peak volumes of site A
a_{BB}	contour peak volumes of site B
a_{AB}	contour cross-peak volumes

Chapter 1

Introduction

1.1 Alkali Metal Cation-Crown Ether Interactions

The detailed synthesis of *crown ethers*, an important class of organic compounds, was first reported by Charles J. Pedersen in 1967 [1]. The simplest traditional crown ethers are characterized by several $-CH_2-O-CH_2-$ ether groups linked together end on end where there is also a linkage between the beginning and end of the chain; this results in the formation of a cyclic compound. Pedersen also introduced a simple nomenclature for these compounds reflecting the total number of atoms as well as the number of oxygen atoms in the ring. For example, the common crown ether 18-crown-6 (1,4,7,10,13,16-hexaoxacyclooctadecane) is characterized by 6 of the above ether units containing a total of 18 atoms and 6 oxygen atoms in the ring. This discovery prompted the development of many related classes of macrocyclic compounds, two of which are the *cryptands* and the *spherands*, first synthesized by the groups of Jean-Marie Lehn [2] and Donald J. Cram [3] respectively. The impact that these compounds have had on

research in several fields is reflected in the fact that Pedersen, Lehn and Cram earned the Nobel Prize in chemistry in 1987 for their pioneering work [4-6]. When these cyclic compounds were shown to have high affinities for the complexation of alkali metal cations [7-9], research involving the cation-macrocycle interaction flourished and in the past two decades a wealth of information, gathered in several reviews [10-12] and books [13-16], has been published. The different aspects of these interactions include the synthesis of host ligands specific to a cation guest, the structural characterizations of the solid or solution complexes, by either experiment or theoretical molecular mechanics, the determination of thermodynamic characteristics of complexation in solution and the kinetic and mechanistic interpretations of the behavior of these ligands together with the metal cations in solution.

One of the important aspects of the complexation of alkali metal cations to synthetic macrocycles lies in the biological implications. Before the discovery of macrocyclic ligands, alkali metal cations were known to be very inert and it is the unusual affinities of macrocycles for important biological cations such and Na^+, K^+, Ca^{2+} and Mg^{2+} that sparked the interest of scientists. These synthetic hosts are structurally related to natural antibiotic ionophores by virtue of the similarities in the resulting complex structures where in each case the ligand is wrapped around the cation [17]. The presence of natural ionophores in biological systems will, for example, facilitate the transport of sodium and potassium cations across lipophilic membranes by either serving as a carrier of forming a channel. There are two types of natural ionophores: those which have preformed cavities such as valinomycin and enniatin and those which are not cyclic such as monensin and lasalocid. In either case the resulting complex is characterized by a cation completely or partially surrounded by a lipophilic ligand. Since crown ethers are structurally simpler than the natural ionophores, studies with the former predominate and experimental results can be used in understanding the

biological activities of the natural ionophores with cations.

Although the complexation of metal cations by macrocyclic ligands has been extensively studied, many aspects of the interaction are still not well understood. Kinetic aspects, which are central in understanding the underlying selectivities of the interaction, have not received much attention and there are still many questions about the kinetic and mechanistic nature of the processes occurring in solution. For example, knowledge of the actual mechanism of complexation and decomplexation in the transport of cations across membranes is crucial in the understanding of this phenomenon.

The global equilibrium associated with the formation of an alkali metal – macrocycle complex is given in equation 1:

$$(M^+)_S + L_S \underset{k_d}{\overset{k_f}{\rightleftharpoons}} (M{:}L)_S^+ \qquad (1)$$

where M^+ is the solvated alkali metal cation, L is the solvated ligand, $(M{:}L)^+$ is the solvated complex and k_f and k_d are the rate constants for the formation and dissociation respectively. There are several factors, such as the nature of the solvent, the nature of the counteranion and the relative size of the cation with respect to the ligand cavity size, which can influence the extent of the reaction in equation 1, as measured by the equilibrium formation constant K_{F1}. In studies of several systems, Cox et al. [18] and Lockhart [19,20] showed that the selectivity of complex formation was actually governed by the dissociation of the complex rather than by the complexation itself. This is illustrated in Figure 1.1 which shows a plot of log k_d as a function of log K_{F1} for a range of crowns and cryptands with alkali metal cations in several solvents [18-20]. Figure 1.1 shows a straight line of unit slope where the intercept gives the rate constant for the formation of the complex.

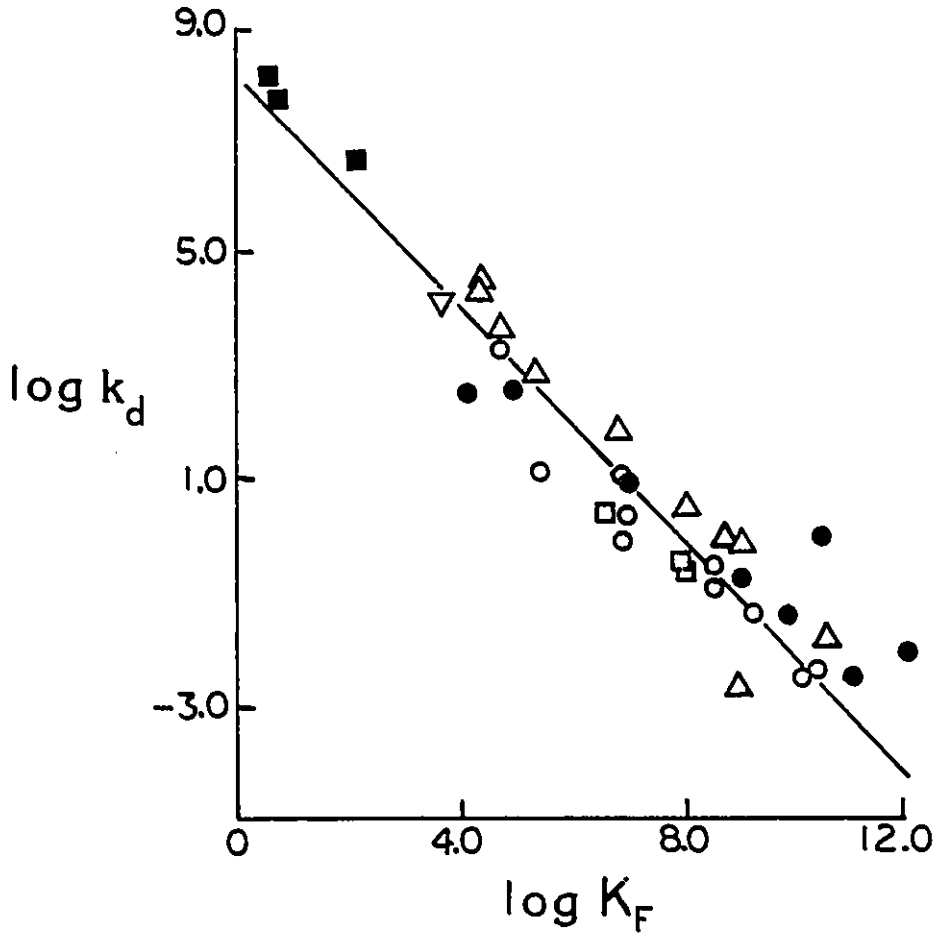

Figure 1.1: Plot of log k_d as a functions of log K_F for a range of crowns and cryptands with alkali metal cations in several solvents at 298 K. (△): MeOH, cryptands; (●): PC, cryptands; (□): DMF, cryptands; (■): H_2O, crowns; (▽): DME, crowns; (○): EtOH, cryptands. Reprinted with permission from reference 20 (© Academic Press, 1982).

In each separate case, k_f shows very little variation and is within a factor of about 100 of the diffusion controlled rate [18-20]. Variations in the K_{F1}, whether resulting from changes in solvent, cation or ligand, may thus be identified primarily with variations in k_d values.

The above discussion attests the importance of kinetic studies in order to characterize the cation - macrocycle interaction and encompasses a large part of the work presented in this thesis. By studying primarily the interactions of the crown ethers 15-crown-5 (15C5) (1,4,7,10,13-pentaoxacyclopentadecane) and benzo-15-crown-5 (B15C5) (2,3,5,6,8,9,11,12-octahydro-1,4,7,10,13-pentaoxacyclopentadecene), shown in Figure 1.2, with lithium and sodium cations in the nonaqueous solvents nitromethane (NM), acetonitrile (AN), dimethylformamide (DMF) and pyridine (PY), insight into the structures of the resulting complexes, thermodynamics of complexation and kinetics and mechanisms of the processes occurring in solution will be presented. Alkali metal *Nuclear Magnetic Resonance* is well suited for this study since the values of k_d for the dissociation of many crown ether complexes are typically in the order of 10^2 - 10^5 s^{-1} and fall in the range where they can be measured accurately by this technique.

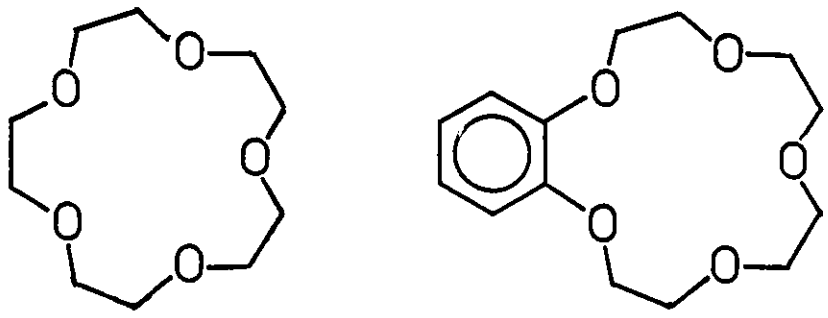

1 2

Figure 1.2: Structures of (1) 15-crown-5 and (2) benzo-15-crown-5.

1.2 Alkali Metal NMR

1.2.1 Alkali Metal Nuclei

Nuclear magnetic resonance has been a popular technique in the study of alkali metal cation-macrocyclic ligand complexes. Whereas ^{1}H and ^{13}C NMR can provide detailed information about the nature of cation complexation, alkali metal NMR has proven to be a powerful tool in this area of research [21]. With this technique, study of the alkali metal complex is possible by the direct observation of the alkali metal nucleus which is affected by its environment; that is, what is observed in alkali metal NMR is a direct reflection of the environment of the alkali metal cation as viewed through the cation.

The nuclear properties of the alkali metals, as well as those for the ^{1}H and ^{13}C nuclei, are shown in Table 1.1 [21-23]. Those nuclei shown in boldface have been used in this study. In NMR, the sensitivity, and thus signal height (S), is dependent on several factors as shown [23]:

$$S \propto \gamma^4 B_o^2 N B_1 g(v) T^{-1} \qquad (2)$$

where γ is the gyromagnetic ratio of the nucleus, B_o is the stationary magnetic field, N is the total number of nuclei, B_1 is the field associated with the Larmor precession frequency, g(v) is a lineshape factor and T is the temperature. The combined influences of their high gyromagnetic ratios and high natural abundances make the ^{1}H, ^{7}Li, ^{23}Na, and ^{133}Cs nuclei easily observable as compared to ^{13}C.

The alkali metal nuclei spins are all > 1 / 2 and therefore do not possess a spherical nuclear charge distribution; this results in an electric quadrupole moment (eQ).

Table 1.1: Nuclear Properties of the Alkali Metals, ^{1}H and ^{13}C [21-23].

Isotope	Natural abundance (%)	Spin	Gyromagnetic ratio γ (10^{7} rad T^{-1} s^{-1})	Quadrupole moment (10^{-28} m^{-2})	Receptivity referred to ^{13}C	Resonance frequency (7 Tesla) (MHz)
^{6}Li	7.42	1	3.9366	-8×10^{-4}	3.58	44.146
^{7}Li	92.58	3/2	10.3964	-4.5×10^{-2}	1540	116.571
^{23}Na	100	3/2	7.0761	0.12	525	79.346
^{39}K	93.1	3/2	1.2483	5.5×10^{-2}	2.69	13.997
^{41}K	6.88	3/2	0.6851	6.7×10^{-2}	0.0328	7.684
^{85}Rb	72.15	5/2	2.5828	0.25	43	28.965
^{87}Rb	27.85	3/2	8.7532	0.12	277	98.164
^{133}Cs	100	7/2	3.5087	-3×10^{-3}	269	39.342
^{1}H	99.99	1/2	26.7519	–	5670	299.944
^{13}C	1.11	1/2	6.7283	–	–	75.429

Because of this, quadrupolar alkali metal NMR, except for ^{6}Li, ^{7}Li and ^{133}Cs which have low quadrupole moments, is identified with relatively broad NMR lines . As well, the nuclei can assume (2I + 1) orientations in a magnetic field which theoretically results in more than one nuclear transition. In normal liquids however, these transitions will collapse to a single line because of fast reorientational averaging motions [24]. There are three important parameters in alkali metal NMR which provides information about a particular system. The *chemical shifts* and *relaxation rates* reflect the coordination sphere of the alkali metal cation and it is thus from these two parameters that structural and thermodynamical insight is obtained. Kinetic information however, is obtained primarily from the actual *lineshape* of the spectra which is related to the *relaxation rates*.

1.2.2 Quadrupolar NMR Chemical Shift

The phenomenon of chemical shift arises because of nuclear shielding due to the local magnetic fields generated at the nucleus by the circulations of the surrounding electrons induced by the applied field [23,25,26]. This nuclear shielding can be characterized by a dimensionless number, σ, called the screening constant and arises from two main factors: diamagnetic (σ_d) and paramagnetic (σ_p) [23,25,26]. A diamagnetic contribution arises from the effect of the atomic electrons circulating in the applied field, B_o, generating their own magnetic field which opposes B_o [23]. However, the presence of neighboring electrons and nuclei hinders this electron circulation giving rise to the paramagnetic contribution [23,25,26].

A sound theoretical understanding of the origin of the chemical shift in alkali metal NMR has yet to be put forth [24,27]. It is governed by the environment of the alkali cation which includes any combination of the solvent, counteranion and ligand. For an alkali metal nucleus in solution (except for ^{6}Li and ^{7}Li), the paramagnetic term,

σ_p, is predominant [24,28,29] and since this term depends on the average distance between the nucleus and the outermost p electron of the element [23,25,26,29], the magnitude and therefore the range of σ_p steadily increases in going from Li^+ to Cs^+ [30]. This is reflected in the usual range of the alkali metal chemical shifts which varies from approximately ten ppm for $^7Li^+$ to a few hundred ppm for $^{133}Cs^+$.

In 1971, Erlich and Popov [31] reported a linear relationship between the ^{23}Na chemical shift and the solvent donicity as expressed by the Gutmann Donor Number (DN) [32]. The DN of a solvent reflects its electron donating ability and is defined as the positive enthalpy of reaction for the dissociation of the adduct formed between the donor solvent and the acceptor antimony pentachloride in dichloroethane, a medium considered as inert [32]. The paramagnetic term for the chemical shift is predominant for the alkali metals [24,28,29] and since Na^+ has no unpaired electrons, it was originally assumed that partially unpaired electron density is donated by the solvent in the empty 3p orbitals of the sodium atom. However, later ab initio calculations could not confirm this transfer of electron density [33], and it was concluded that an electrostatic description was adequate for the bonding between Na^+ and coordinating dipolar solvent molecules [24]. Relationships between the chemical shift and solvent DN, although less admirable, have also been observed for ^{39}K [30,34] and ^{133}Cs [30,35], whereas in the case of ^7Li no such relationship is observed [30,36]. In the latter case, since the diamagnetic and the paramagnetic contributions to the screening constant are of the same order of magnitude, contributions to the shielding, other than paramagnetic ones, such as ring currents and neighbor anisotropy effects, have therefore a substantial influence on the magnitude and direction of the chemical shifts [30,37].

Although an understanding for the origin of the alkali metal chemical shift is still lacking, this parameter is nevertheless invaluable for the characterization of alkali metal complexes. For instance, in cases where the chemical shifts of the solvated and

complexed cation are different, one can obtain thermodynamic and structural information about the complex [21].

1.2.3 Quadrupolar Nuclear Relaxation

The conventional approaches to the NMR experiment are described in a number of books [22,23,25,38-40]. Basically, nuclear excitation is accomplished by "flipping" 90° the net *z* magnetization, M_z, (by the application of B_1) of a sample in a stationary magnetic field (B_o), to the *xy*-plane. Relaxation back to thermal equilibrium (the ground state) and observation of the free induction decay (FID) is described by the classical Bloch equations [41,42]:

$$dM_z / dt = -(M_z - M_o) / T_1 \qquad (3)$$

$$dM_x / dt = -M_x / T_2 \qquad dM_y / dt = -M_y / T_2 \qquad (4)$$

where t is the time, M_o is the initial magnetization and $M_{x,y,z}$ are the respective magnetizations on the *x*-, *y*- and *z*-axes. The relaxation is characterized by two times; T_1 and T_2. T_1 is the longitudinal or spin-lattice relaxation time, is enthalpy driven and results from a transfer of energy to the outside surroundings; this characterizes the return of M to the *z*-axis. T_2 is the transverse or spin-spin relaxation time, is entropy driven and results from a transfer of energy between the nuclei where there is no loss to the outside surroundings; this characterizes the dispersion of the Larmor frequencies and is a dephasing of the initial coherent magnetization in the *xy*-plane. Each of these relaxation times reflects the time required to attain a net magnetization of 0 in the *xy*-plane. T_2 is always $\leq T_1$ and under normal conditions in extreme narrowing, $T_2 = T_1$.

In general the relaxation of a quadrupolar nucleus can be represented by the sum

of several exponentials (this will depend on the spin number, I). For nuclei with spin 3/2, such as ^{23}Na, the relaxation can be described by the sum of two exponentials [43,44]:

$$M_z(t) = M_z(0)\,[0.6\exp(-t/T') + 0.4\exp(-t/T'')] \tag{5}$$

where $M_z(0)$ and $M_z(t)$ are the amplitudes of M_z at time 0 and time t respectively. The full expressions for T' and T'' are described by the following equations [43,44]:

$$1/T' = \frac{\pi^2}{5}\chi^2\left(\tau_c + \frac{\tau_c}{1+\omega^2\tau_c^2}\right) \tag{6}$$

$$1/T'' = \frac{\pi^2}{5}\chi^2\left(\frac{\tau_c}{1+\omega^2\tau_c^2} + \frac{\tau_c}{1+4\omega^2\tau_c^2}\right) \tag{7}$$

where χ is the quadrupolar coupling constant, described below, τ_c is the motional correlation time and ω is the Larmor frequency of the nucleus. If τ_c, characteristic of the electric field gradient fluctuation, has an origin purely reorientational, it should obey the Debye-Stokes-Einstein relationship [24]:

$$\tau_c = (V\,\eta\,f_r)/(k_B\,T) \tag{8}$$

where V is the molecular volume, f_r is a microviscosity coefficient [45] and η is the medium macroscopic viscosity.

All NMR active alkali nuclei have electric quadrupole moments due to their non-spherical charge distributions. The interaction between this nuclear electric

quadrupole moment (eQ) and the electric field gradient (eq) at the nucleus, arising from asymmetric charge distribution around the nucleus, produces an efficient pathway for nuclear relaxation referred to as quadrupolar relaxation. This interaction is characterized by the quadrupolar coupling constant (χ):

$$\chi = (eQ)(eq)(1 + \gamma_\infty) / \hbar \tag{9}$$

where $(1+ \gamma_\infty)$ is the Sternheimer antishielding factor for the quadrupolar nucleus. The parameter χ reflects the symmetry around the alkali metal cation. For example, the ^{23}Na quadrupolar coupling constant typically varies from 0.1 to 1.5 MHz [24,28].

In conditions of extreme motional narrowing ($\omega^2\tau_c^2 \ll 1$), which is the case for all the work presented in this thesis, the ^{23}Na quadrupolar longitudinal and transverse relaxation rates are equivalent, within inhomogeneity contributions, and they are given by [24,40]:

$$T_q^{-1} = \pi \nu_{1/2} = (2/5)\, \pi^2 \chi^2 \tau_c \tag{10}$$

where T_q^{-1} is the quadrupolar relaxation rate, $\nu_{1/2}$ is the linewidth at half-height and I is the nuclear spin number. Since in mobile liquids, τ_c is in the order of ps, the product $\omega^2\tau_c^2$ for ^{23}Na (ν_{Na} = 79.346 MHz, $\omega_{Na} = 2\pi\nu_{Na} = 4.9854 \times 10^8$ rad/s) $\ll 1$ and the relaxation rates are largely governed by the quadrupolar coupling constant. When the electric field around the cation is not symmetric, as is the case for alkali cations complexed by macrocyclic ligands compared to solvated cations, the relaxation is fast and the NMR lines can be broad. According to equation 8, the quadrupolar relaxation rate should be directly proportional to the viscosity of the solvent if the electric field gradient is independent of the solvent. In this context, the reduced quadrupolar

relaxation rate, T_q^{-1*}, may be referred to, where $T_q^{-1*} = T_q^{-1} / \eta$. As for the chemical shift, cations in a specific environment will have their own characteristic relaxation time and corresponding linewidth. Broad lines resulting from large T_q^{-1} values, is a reflection of a relatively non-symmetric environment of the nucleus under study. For example, the ^{23}Na linewidth at half-height of sodium complexed with the crown ether B15C5 in the solvent nitromethane was determined to be 217 Hz compared to that of solvated sodium which is 10 Hz. This gives an indication about the relative symmetry of coordination around the sodium cation in the two cases. The quadrupole moments of ^{7}Li and ^{133}Cs are relatively low and therefore typical linewidths for these nuclei are also relatively low. The linewidth at half-height of lithium complexed with B15C5 also in nitromethane is 1 Hz under similar conditions, while that of solvated lithium is 0.5 Hz.

1.2.4 Kinetic Studies by Lineshape Analysis

In addition to being subject to the same factors as the longitudinal relaxation rate, T_1^{-1}, the transverse relaxation rate, T_2^{-1}, can be sensitive to the chemical exchange of nuclei between different sites. Since the T_2^{-1} is related to the linewidth of thc observed spectrum, a change in this parameter can result in spectacular effects on the whole lineshape. The effect of dynamic processes in solution on the NMR lineshape was recognized early in the history of NMR and the underlying theory is now well understood [46-48]. When the chemical exchange rates are measurable on the NMR chemical shift timescale, one can distinguish three types of spectra whose lineshape is modified by the chemical exchange. This is illustrated in Figure 1.3 which shows a series of ^{23}Na NMR spectra for solutions containing equal populations of sodium complexed to B15C5 and sodium solvated in NM.

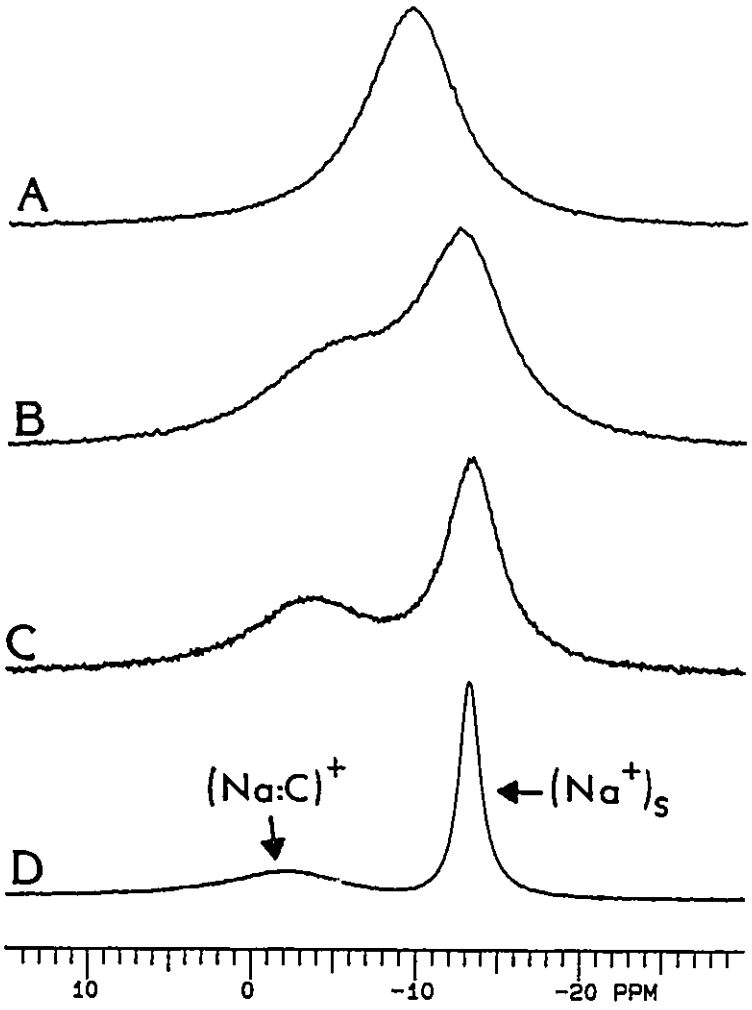

Figure 1.3: A series of ^{23}Na spectra as a function of temperature for a sample containing equal populations of solvated sodium (in nitromethane) and sodium complexed to B15C5. $\rho = [B15C5]_T / [NaBPh_4]_T = 0.5$; $[NaBPh_4]_T = 60.0$ mM. (A) T = 301.5 K; (B) T = 283.0 K; (C) T = 273.0 K; (D) T = 253.0 K.

The spectra shown in Figure 1.3 reflect the chemical exchange of the sodium cation in two possible sites: solvated (site A) and complexed (site B) (see equation 22 on page 84). As the temperature decreases, so does the rate for the two-site chemical exchange and there are distinct changes in the lineshape. In the fast exchange limit, only one single Lorentzian peak is observed which is characteristic of the population average of the two cation sites. This is the case for the chemical exchange of sodium at 301.5 K in the conditions listed (spectrum A in Figure 1.3). However, the line is broadened due to the presence of the chemical exchange and the respective rate constants involved can be calculated by determining the exchange contribution to the broadening (see section 4.3). In regions of intermediate exchange, there are spectacular changes in the NMR spectrum as it ceases to be Lorentzian. This is the case at 283.0 K and full lineshape analyses must be performed in order to obtained quantitative results for the rates of exchange.

Based on a two-site chemical exchange, mathematical expressions describing the lineshape of a spectrum altered by the exchange, have been derived (the equations are shown in Appendix 1) [46,49]. Essentially, the sum of the two pseudo-first order rate constants, $(k_A + k_B)$, involved in the chemical exchange (see equation 22 on page 84) is related to the populations, the transverse relaxation rates and the differences in chemical shifts of both sites (P_A and P_B, T_{2A}^{-1} and T_{2B}^{-1}, and $\nu_A - \nu_B$ respectively). A full lineshape analysis thus involves fitting an experimentally observed spectrum to the equations which describe it and quantitative kinetic information, in the form of $(k_A + k_B)$, is obtained. When the chemical exchange is slow on the NMR chemical shift timescale, the ^{23}Na NMR spectrum displays two separate peaks for the two sodium sites. This is the case at 253.0 K and full lineshape analyses are performed as well in order to extract quantitative rate values. The two-site chemical exchange is discussed in greater detail in section 4.3 and the lineshape analyses are discussed in section 2.3.

Chapter 2

Experimental Methods

2.1 Materials and Sample Preparation

All the crown ethers and alkali salts used in this study were purchased from the respective named companies and were either further treated as described or used as received. Unless otherwise stated, all crown ethers and alkali salts were vacuum dried in the presence of phosphorous pentoxide at 353 K for at least 24 hours prior to use. B15C5 (Aldrich 98%) was recrystallized from hexanes (dried at 303 K for at least 24 hours), 15C5 (Aldrich 98%) was vacuum distilled (dried at room temperature for 6-8 hours), DB24C8 (Aldrich, 98%) was recrystallized from acetonitrile and cyclohexane and DB18C6 (Parish) and DB30C10 (Aldrich 98%) were used as received. Sodium tetraphenylborate, $NaBPh_4$, (Aldrich 99%) was recrystallized from cyclohexane with a minimum amount of ethanol, sodium hexafluorophosphate, $NaPF_6$, (Aldrich 98%) was recrystallized from acetonitrile and a minimum of hexane and sodium perchlorate, $NaClO_4$, (Aldrich) and lithium perchlorate (Baker Analyzed Reagent) were used as

received. Nitromethane (NM) (BDH, Omnisolv and Aldrich 96% Gold Label), acetonitrile (AN) (BDH, certified ACS), dimethylformamide (DMF) (BDH, Omnisolv) and pyridine (PY) (BDH assured) were dried under reflux over calcium hydride for 3 hours, distilled under nitrogen and stored under argon. PY was stored with 4Å molecular sieves as well.

Samples for ^{1}H and ^{13}C NMR measurements were prepared by weighing the desired amount of crown ether directly in a 1.0 or 2.0 mL flask and either adding the appropriate amount of pure solvent (for a sample containing "free" crown ether) or stock solution containing a known amount of alkali salt (for a sample containing complexed crown ether); the concentration of either crown or complex was typically 0.02 to 0.1 M. In the solvents used for this part, the complexes are known to be quantitatively formed but a slight excess ($\leq$ 20%) of alkali metal was added to the crown ether to ensure that it was all complexed . These samples were prepared with deuterated solvents contained in sealed ampules: nitromethane-d_3, CD_3NO_2, (Aldrich 99% atom D), acetonitrile-d_3, CD_3CN, (Aldrich 99.5% atom D) or acetone-d_6, $(CD_3)_2CO$, (Aldrich 99.5% atom D). The solution samples were degassed by the freeze-thaw method under vacuum directly in the 5 mm NMR tubes and were sealed shut with a torch. The ^{7}Li and ^{23}Na NMR experiments typically involved recording the NMR spectra of a series of samples (see for example the results in Figure 4.1) which were prepared by weighing the desired amount of crown ether directly in a 5.0 or 10.0 mL flask and adding an appropriate amount of stock alkali salt solution of known concentration in the desired solvent. Binary solvent mixtures of desired mole fraction composition were prepared by adding the appropriate mass of AN, DMF and PY in preweighed amounts of NM. The mole fraction, X, of minor component was calculated from the masses of each component. Since the volumes of the individual components were not actually measured, the concentration, in moles / liter, of minor component was calculated using the density values for each

solvent [50] at ambient temperatures and assuming additive volumes in determining the total volume. The solution samples were transferred into 10 mm NMR tubes, argon was flushed over the solution and the tubes were sealed with Parafilm. The spectra of all 10 mm samples were recorded within 48 hours of preparation.

2.2 NMR Measurements

The basic 1-dimensional NMR experiment, described by the simple scheme shown in Figure 2.1, is characterized by 2 time periods: the preparation period primarily of length PD (pulse delay), preceding nuclear excitation by the 90° pulse, and the detection period of length t_2 (acquisition time).

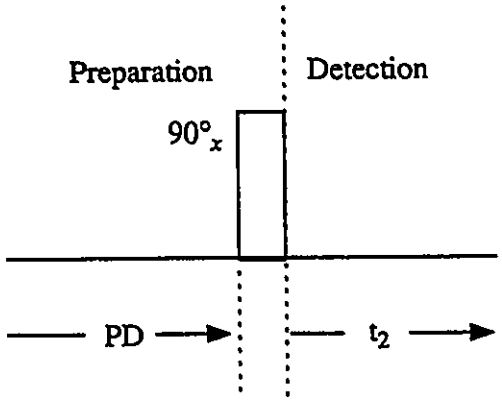

Figure 2.1: Basic scheme for 1-dimensional NMR Spectroscopy.

Nuclear excitation is accomplished by the $90°_x$ pulse which "flips" the equilibrium macroscopic magnetization (M_o) initially on the *z*-axis to the *xy*-plane. Immediately following this pulse and during the detection period, there is decay of the produced *xy* magnetization back to equilibrium. This decay is referred to as the free induction decay

(FID) and is monitored as a function of time. This simple 1 pulse sequence is repeated n times (number of transients) and the resulting signals are added. Fourier transform of the data in the time domain to the frequency domain results in the NMR spectrum as we know it. In normal experiments, a pulse delay was not used and the acquisition time depended upon the system under study.

2.2.1 Acquisition Parameters and Chemical Shift

Table 2.1: Typical NMR Acquisition Parameters.

Nucleus	^{1}H	^{13}C	^{7}Li	^{23}Na
Observation frequency (MHz)	299.994	75.429	116.571	79.346
Spectral width (Hz)	4000	16500	500	20000
Acquisition time (s)	3.0[a]	0.9[a]	1 - 2	0.05 - 0.2
Number of transients[b]	16	500 - 2000	10 - 1000	200 - 10000
90° pulse (μs)	12.9[a]	9.6[a]	15-20[c]	20-30[c]

(a) The actual tip angle used in the acquisition of the ^{1}H and ^{13}C NMR spectra (~30°) was calculated from the Ernst equation ($\cos \alpha_E = \exp(-AT / T_1)$) with the given acquisition time (AT) and average longitudinal ^{1}H and ^{13}C relaxation times (T_1) [38]. (b) this depended on the concentration and temperature of the sample (c) The 90° pulses were verified systematically by the 360° null method.

All NMR spectra were recorded on a Varian XL-300 NMR spectrometer. Typical NMR acquisition parameters for the nuclei used in this study are shown in Table 2.1. The ^{1}H (5 mm proton probe) and ^{13}C (5 mm broad band probe) NMR spectra were recorded at 299.994 and 75.429 MHz respectively at ambient temperature (~ 295 K) and the chemical shifts reported are referenced to TMS. In order to prepare samples free of TMS, the ^{1}H and ^{13}C chemical shifts of the central solvent lines of CD_3NO_2, CD_3CN and $(CD_3)_2CO$ were initially determined in the presence of TMS (see Table 2.2) and the sample spectra were subsequently referenced with the central solvent line.

Table 2.2: The Chemical Shifts of the Solvents vs TMS.

Solvent	^{1}H ± 0.001 ppm	^{13}C ± 0.007 ppm
Nitromethane-d_3	4.326	62.604
Acetonitrile-d_3	1.939	1.335
Acetone-d_6	2.040	29.800

The ^{7}Li and ^{23}Na NMR spectra were recorded at 116.571 and 79.346 MHz respectively (10 mm broadband probe) and referenced to a solution of LiCl or NaCl in 20% D_2O/H_2O (0.1 M). All alkali metal NMR spectra were recorded unlocked and all chemical shifts were corrected for differences in bulk magnetic susceptibilities between the organic samples and the aqueous reference. If the axis of the sample tube is parallel to the direction of the static magnetic field (such is the case with the XL-300):

$$\delta_{true} = \delta_{obs} + (4\pi/3)\,(\chi_{ref} - \chi_{samp}) \qquad (11)$$

and if the same axis is perpendicular to the direction of the static magnetic field:

$$\delta_{true} = \delta_{obs} - (2\pi/3)(\chi_{ref} - \chi_{samp}) \quad (12)$$

where δ_{true} is the true chemical shift, δ_{obs} is the observed chemical shift and χ_{ref} and χ_{samp} are the volume magnetic succeptibilities of the reference and sample solvents respectively (the effects of dissolved salts on the succeptibility can be neglected) [51]. The correction factors for each solvent are shown in Table 2.3.

Table 2.3: Solvent Magnetic Susceptibility Corrections.

Solvent	Volume Magnetic Susceptibility (χ)[a]	Correction[b] ppm
nitromethane	-0.391	-1.374
acetonitrile	-0.534	-0.775
dimethylformamide	-0.621[c]	-0.411
pyridine	-0.611	-0.452
water	-0.719	------

(a) $\times 10^{-6}$; reference [52]. (b) $\delta_{true} = \delta_{obs}$ + correction. (c) experimentally determined.

In order to determine the volume magnetic susceptibility of DMF, which is required to determine its chemical shift correction factor, the ^{23}Na chemical shift of a solution containing $NaBPh_4$ in DMF (0.02 M) was measured in two different field geometries: a Varian XL-300 and a Varian FT-80. χ_{DMF} was then determined by solving equations 11

and 12 simultaneously. For the dimethylformamide-nitromethane binary solvent mixtures, the mole fraction content of DMF in the solvent was always ≤ 0.1 and a chemical shift correction factor for pure NM was assumed.

The temperature of the probe was measured with a thermocouple dipped in nitromethane in a non-spinning 10 mm NMR tube. For a temperature range between 240 and 310K, the temperature of the sample was estimated to be reliable at ± 0.5 K. The temperature of the 10 mm broadband probe was calibrated periodically.

2.2.2 Longitudinal Relaxation Time

In cases where the spectra exhibited one Lorentzian shaped peak, the observed transverse relaxation rate was determined by simply measuring the linewidth at half-height, $\nu_{1/2}$, of the peak (see equation 10). The longitudinal relaxation rates were obtained by using the inversion-recovery, 180° - τ - 90°, pulse sequence shown in Figure 2.2 [39,53-55].

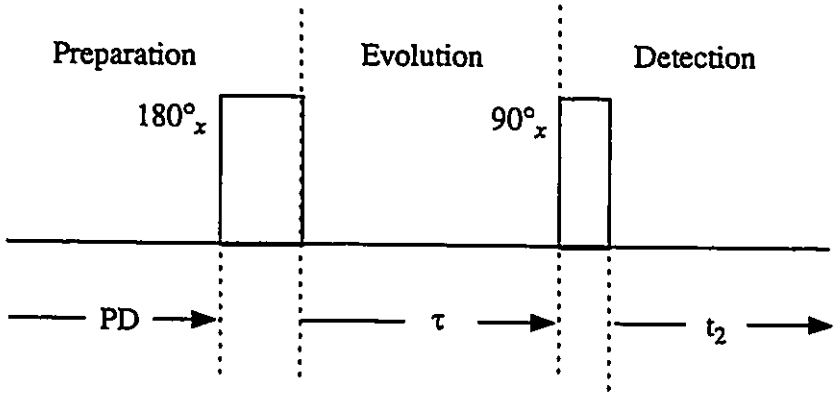

Figure 2.2: Scheme for the inversion recovery pulse sequence.

This 2-pulse sequence incorporates a third time period: the evolution period of length τ. The first 180° pulse inverts the magnetization along the *z*-axis (M_o becomes $-M_o$). Longitudinal relaxation back to equilibrium occurs during the evolution period and the second 90° pulse causes M_z to be rotated to the *y*-axis for detection. The magnitude and sign of the observed M_z, which are reflected in the signal height and phase respectively, depend on the length of τ. In any one experiment where the pulse sequence is repeated *n* times, τ is kept constant and several experiments with varying values of τ are repeated. This is illustrated in Figure 2.3 which shows a series of ^{23}Na spectra for a solution containing sodium and B15C5 in nitromethane at 301.5 K.

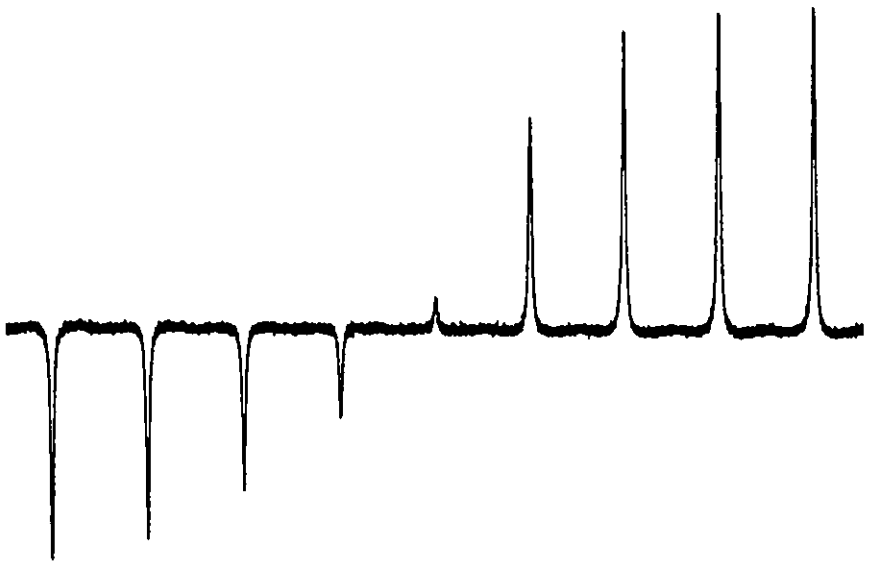

Figure 2.3: ^{23}Na NMR spectra for the measurement of T_1 by the inversion-recovery method for a sample containing sodium and B15C5 in nitromethane at 301.5 K. From left to right, τ = 0.0001, 0.0002, 0.0005, 0.001, 0.002, 0.005, 0.010, 0.020 and 0.050 s.

It is important that the spin should be at thermal equilibrium at the beginning of the 180° pulse and hence a pulse delay (PD ≅ 5 T_1) must be interposed between sequences [54]. In the case shown in Figure 2.3, as well as all ^{23}Na T_1 determinations, a pulse delay was not used since the longitudinal relaxation time was short compared to the detection time (AT ≥ 0.05 s). However, pulse delays were at times introduced in the determination of ^7Li longitudinal relaxation times, since these were longer.

A mathematical description for the decay of M_z was previously given in equation 3 (one of the Bloch equations). Integration of this equation with $M_z = -M_o$ at $t = 0$ gives:

$$M_z(t) = M_o (1 - 2 \exp(-\tau/T_1) \qquad (13a)$$

The observed intensity of the resulting NMR spectrum is proportional to M_z and is a function of τ. A nonlinear regression of the intensity (I) versus τ data, shown in Figure 2.4, can thus provide a value for T_1. The T_1 determinations were based on a 3 parameter nonlinear regressions performed on the XL-300 computer with at least nine experimental points (see equation 13b). In addition to the variables M_z and τ, a third variable, k′, is included which compensates for field inhomogeneities and imperfect pulses [55].

$$M_z(t) = M_o [1 - (1-k') \exp(-\tau/T_1)] \qquad (13b)$$

2.2.3 2-Dimensional Methods

The assignments of the ^{13}C NMR ether carbon peaks of the crown ethers was accomplished by ^1H-^{13}C heteronuclear chemical shift correlation spectroscopy (HETCOR) [38,56]. The basic pulse sequence for this technique is:

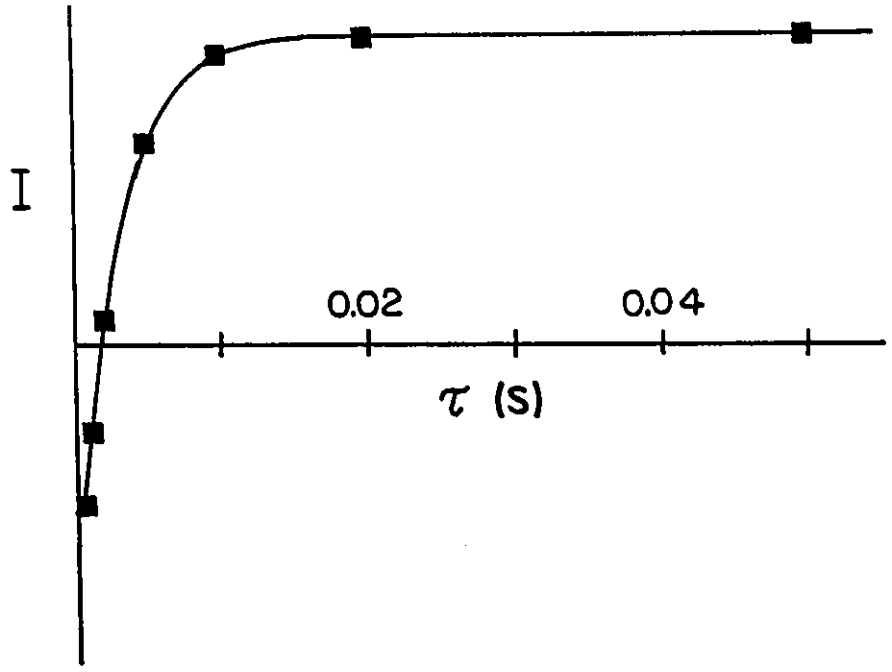

Figure 2.4: Arbitrary Intensity (I) as a function of τ. For clarity only 7 experimental data points, obtained from the spectra shown in Figure 2.3, are shown and the curve is calculated from a three parameter nonlinear regression; $T_1 = (2.99 \pm 0.07) \times 10^{-3}$ s.

$$(PD - 90°_x{}^{H} - t_1/2 - 180°_x{}^{C} - t_1/2 - \Delta_1 - 90°_\phi{}^{H}, 90°_x{}^{C} - \Delta_2 - \text{decouple protons},$$
$$\text{acquire } {}^{13}C -)_n$$

Typically, the spectral windows of both the ^1H and ^{13}C frameworks were narrowed down to the ether region and t_1 was varied in 64 or 128 equal increments. A pulse delay of one second was used and the fixed delays Δ_1 and Δ_2 were based on an average value for J_{CH} set to 140 Hz. The number of repetitions, n, varied from 16 to 32 and the time required for any one HETCOR experiment was usually never longer than two hours with samples containing ~0.02 M of material.

For the determination of the long-range ^{1}H-^{13}C couplings, the delay times Δ_1 and Δ_2 were based on the long-range J_{CCH} coupling constants (~ 10 Hz), n = 264 and the spectra were collected in overnight runs with samples which were more concentrated. The principles of the HETCOR experiment are described in section 3.4.

The EXSY pulse sequence used for acquiring 2D ^{7}Li spectra is [57]:

$$(PD - 90°_x - t_1 - 90°_x - t_m - 90°_x - \text{acquire } (t_2) -)_n$$

Typically, the t_1 varied in 64 equal increments, the mixing time, τ_m, varied from 0.005 to 0.15 s but is kept constant for any one 2D experiment, the pulse delay, PD, was one second and the number of scans, n, was 16. A very small spectral width was used (500 Hz) and because ^{7}Li is a very sensitive nucleus, 2D experiments were obtained in approximately one hour. The principles of this technique are discussed in section 5.3.

2.3 Data Analysis

2.3.1 Lineshape Analysis

Full lineshape analyses of the NMR spectral data which was obtained in the first year of research were carried out by using an optimization Simplex [58] routine on an Apple II computer. This involved manually recording 50-100 data points of the spectrum by visual inspection with cursors on the XL-300 computer screen and entering the data on the Apple computer (method 1). The corresponding errors on the resulting values for $k_A + k_B$, using this method for lineshape analysis, were estimated at ± 5%. A second method for the lineshape analyses was used for most of the rate determinations in this work and involved transferring the digitized spectra (100-200 points) from the XL-300 computer to a IBM compatible PC which was then further transferred to the

University of Ottawa main frame system (Amdahl). Full lineshape analyses were carried out by performing nonlinear regressions with a program developed from SAS® (Statistical Analysis Systems) [59] routines incorporating the equations describing an uncoupled spin system undergoing chemical exchange between two nonequivalent sites [46] (method 2); this overall program is shown in Appendix 1. An example of one experimental NMR spectrum along with the corresponding computer fit is shown in Figure 2.5. The slight deviation between the experimental data points and the theoretical curve observed in the middle portion of the spectrum, is due to a slight dephasing of the experimental curve. This problem was at times incurred but several tests showed that the $(k_A + k_B)$, resulting from the lineshape analysis, displayed very little deviation and remained within the reported errors even in relatively severe dephasing conditions.

2.3.2 Error Analysis

The error estimated for the ^1H NMR peaks is ± 0.001 ppm, corresponding to the theoretical digital resolution (DR = 2SW / NP) and that for ^{13}C is ± 0.007 ppm (with zero-filling) [38]. Since the linewidths of the ^7Li and ^{23}Na NMR peaks are broader than those of ^1H and ^{13}C, the chemical shift errors are larger than the digital resolution and were visually estimated with cursors on the computer screen of the XL-300 spectrometer. The linewidths of the ^7Li NMR peaks did not display much relative variation and the error on corresponding chemical shift is reported to be ± 0.01 ppm. Since the linewidth of the ^{23}Na NMR peaks varied extensively and depended on the experimental conditions, so did the reported errors on the ^{23}Na chemical shifts; typically ± 0.01 to ± 0.08 ppm. The error on the reported transverse relaxation rates depended on the errors of the chemical shifts since this parameter depends on the linewidth itself; $T_{2,obs}^{-1} = \pi\nu_{1/2}$.

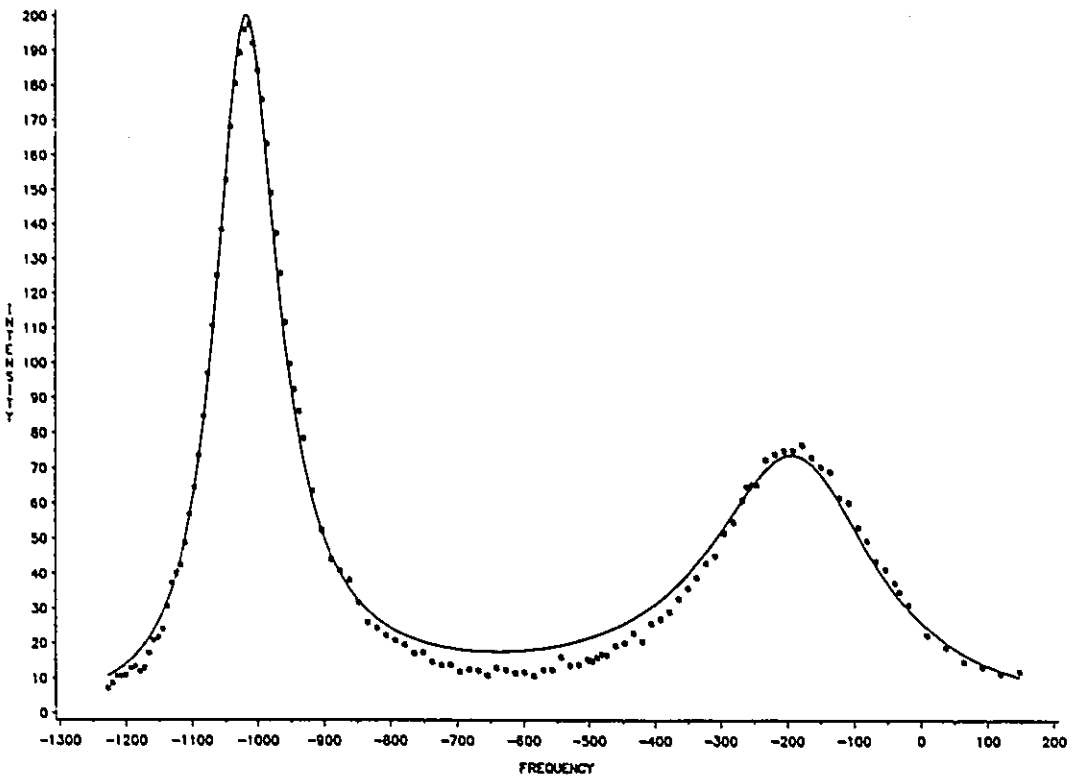

Figure 2.5: ^{23}Na NMR spectrum of a sample containing equal populations of solvated sodium, $(Na^+)_S$ in nitromethane, and sodium complexed to B15C5, $(Na{:}B15C5)^+$. $[NaBPh_4]_T$ = 4.0 mM and T = 301.5 K. The data points are experimental and the curve has been calculated from a nonlinear SAS® regression. The resulting value for $(k_A + k_B)$ is $(6.6 \pm 0.2) \times 10^2\ s^{-1}$.

The measurement of the linewidth at half-height entailed the estimation of two frequency positions on the NMR curve and thus the error on $\nu_{1/2}$ of a peak was reported to be twice that of its chemical shift in Hz. Typically the resulting errors for the ^{23}Na $T_{2,obs}^{-1}$ were in the order ± 1-40 Hz. The errors reported for the longitudinal relaxation rates were reported as ± 2σ, where σ is the standard error of the parameters of the nonlinear regressions performed directly on the computer of the XL-300 spectrometer. This represents a confidence level of 96% [60].

Many of the results reported in this thesis have been obtained from calculations involving either linear or nonlinear regressions based on the least squares method using SAS® [59]. The errors reported for (k_A+k_B) depended on the manner in which they were calculated: (a) if equation 25 (in section 4.2) was used, the sum of the errors of all contributions was taken into account, (b) if full lineshape analyses by method 1 was used the errors were estimated at about ± 5% and (c) if full lineshape analyses were carried out by method 2 the errors were reported as ± 2σ. Other nonlinear regressions were involved in the determination of equilibrium constant values and the corresponding limiting chemical shifts and limiting relaxation rates (Figures 4.1, 4.2, 4.21, 4.25 and 5.13) and in the determination of the exchange rate constant k by 2D EXSY spectroscopy (Figure 5.12). The errors of all values which resulted from nonlinear regressions were reported as ± 2σ. Those calculations which involved linear regressions, such as in the determinations of k_{-1} and k_2 (see section 4.4 for the definitions of k_{-1} and k_2), were reported with errors equal to ± 1σ from the regression; this represents a 68% confidence level (Figures 4.7-4.10, 4.12, 4.14, 4.16, 4.18, 4.19 and 4.22). The values obtained from nonlinear regressions were reported with a greater error, ± 2σ, as compared to the linear regressions, ± 1σ; this reflects the fact that the linear fits generally displayed an overall better agreement with the experimental data. All other values resulting from linear regressions, such as the enthalpy of activation, $\Delta H^{\ddagger}$, and entropy of

activation, ΔS^{*}, were also reported with $\pm$ 1σ for the error. The free energies of activation, ΔG^{*}, were calculated directly from the determined rate constants [46]:

$$\Delta G^{*} = -RT \ln(k\hbar / k_B T) \tag{14}$$

where k is k_{-1} or k_2. The corresponding errors in ΔG^{*} ($\Delta\Delta G^{*}$) were calculated using equation 15 [61]:

$$\frac{\Delta\Delta G^{*}}{\Delta G^{*}} = \frac{\left\{\left[\frac{\Delta T}{T}\left(\ln\frac{k_B T}{\hbar k} + 1\right)\right]^2 + \left(\frac{\Delta k}{k}\right)^2\right\}}{\ln\left(\frac{k_B T}{\hbar k}\right)} \tag{15}$$

The errors associated with sample preparations, such as the sample concentrations and ρ, were deemed negligible.

2.3.3 Spin Simulations

^{1}H spin simulations were carried out in order to determine the ^{1}H-^{1}H spin coupling constants of the protons in the ether fragments of the crown ethers (see section 3.2.2). These were carried out on the computer of the XL-300 spectrometer using a program based on the LAOCOON procedure [62,63]. Initially, the 4-spin AA'BB' system is defined where it is characterized by 5 unknown parameters: (1) the chemical shift of A = A', (2) the chemical shift of B = B', (3) the geminal coupling constants $J_{AA'}$ and $J_{BB'}$ are assumed to be equivalent (J_{gem}), (4) $J_{trans} = J_{A'B} = J_{AB'}$ and (5) $J_{cis} = J_{AB} = J_{A'B'}$. Reasonable initial values are given for each variable parameter and a set of

theoretical lines are generated. These lines are subsequently matched to those experimentally observed and then a minimization procedure is performed where values for the 5 variables, corresponding to the best fit, are obtained. It was noted that the simulations were not very sensitive to J_{gem}.

Chapter 3

Structural Elucidation of Complexes in Solution: ^{1}H and ^{13}C NMR Study

3.1 Introduction

A key to understanding the nature of the underlying kinetic processes involving crown ethers and their metal complexes in solution, lies in the precise knowledge of the structures of the molecules themselves. Structures of crown ether complexes are in general characterized by several factors such as the position of the cation within the cavity of the ligand, the stoichiometry of the complex and the actual conformations of the bonds in the ligands. The two first factors are largely governed by the relative size of the metal cation with respect to the size of the ligand cavity [64]. When the cation is much smaller than the ligand cavity, a "wrap around" structure may result where the metal cation is completely or partially wrapped around by the crown ether. This is the case for potassium complexed to DB30C10, shown as a solid in Figure 3.1 [65] as well

as in solution [66]. A complex with 2:1 (cation:ligand) stoichiometry may also result with a relatively small cation. In solution the "wrap around" structure of $(Na:DB24C8)^+$ is formed [67-69] and as a solid $(Na_2:DB24C8)^{2+}$ is observed [70,71]. In solution, aggregates of $(Na^+_{n+1}:DB24C8_n)$ have also been observed [69]. When the cation is larger than the crown ether on the other hand, there can be formation of a 1:1 complex where the cation lies above the plane of the ligand, as is the case for $(Cs:18C6)^+$ [72-74], or the formation of a 1:2 (cation:ligand) complex, $(Cs:18C6_2)^+$, may result [75]. This is also the case for sodium with B15C5 where the sodium cation sits just slightly above the plane of the crown ether as shown in Figure 3.1 [76,77]. When the diameter of the cation is matched to that of the ligand, the cation is centered in the ring plane of the crown ether; this is the case for $(K:18C6)^+$ also shown in Figure 3.1 [78].

As solids, the structures of several crown ethers and their respective alkali metal complexes have been well characterized by X-ray crystallography, where not only a knowledge of the overall structures is obtained but also a precise knowledge of inter-atomic coordinates and conformations of the rigid molecules [65,70,71,73,76-87].

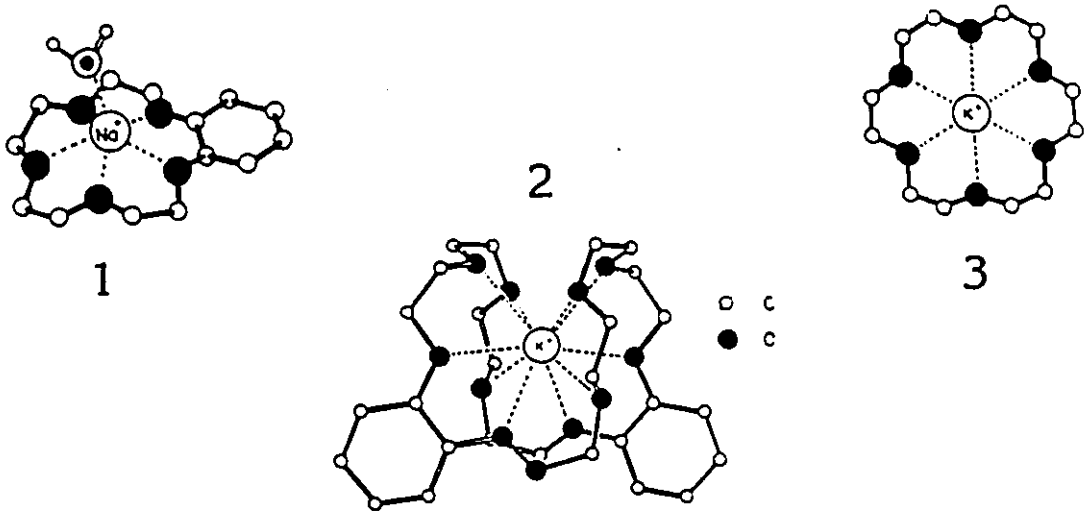

Figure 3.1: The solid structures of (1) Na^+ complexed to B15C5 [76], (2) K^+ complexed to DB30C10 [65] and (3) K^+ complexed to 18C6 [78].

From the structures of sodium complexed with B15C5 and potassium complexed to DB30C10 shown in Figure 3.1, a general *gauche* orientation about the C-C bonds of the crown ethers can be observed whereas there is a general *anti* preference about the C-O bonds. There is overwhelming evidence, from the X-ray data of solids [13-16,65,70,71,73,76-87], theoretical molecular mechanics studies [89-90] and solution NMR studies [91-98], some of which is reviewed by Dale [99,100], that this specific conformational orientation is in general typical of all crown ethers as well as crown ethers complexed to alkali metal cations.

Structural elucidation in solution however, is not so readily achieved and factors such as rapid conformational averaging as well as the influence of the solvent must be taken into account. Information about the overall structures of crown ether complexes can be obtained by alkali metal NMR. The stoichiometries of several crown ether complexes in solution have been determined by ^{23}Na [67,72,88,101], ^{7}Li [102] and ^{33}Cs [67,74,75] NMR. As well, information about the presence, or absence, of solvent molecules in the coordination sphere of the complexed cation can be obtained by alkali metal NMR. For example, it has been shown by ^{23}Na and ^{39}K NMR respectively, that the first coordination sphere of Na^+ in $(Na:DB24C8)^+$ [68] and K^+ in $(K:DB30C10)^+$ [66] is exclusively filled by the oxygens of the crown ether whereas for $(Na:DB30C10)^+$ there is participation of at least one solvent molecule [103]. It is not possible by alkali metal NMR however, to obtain specific information about the conformational status of the crown ether.

^{1}H and ^{13}C NMR have been successful in providing various types of information about macrocyclic ligands and their complexes in solution. The chemical shifts of the ether protons and carbons will to some extent depend on the solvent where in some cases the formation of an actual weak complex between the macrocycle and the solvent may be observed [104,105]. A change in the chemical shift upon addition of metal cations,

indicates the formation of a cation complex whereby the stoichiometry [91,92,106-110] and the equilibrium constant [91,106,110] for complex formation may be determined by ^{1}H or ^{13}C NMR . Information on the structures and the motions of crown ethers and their complexes in solution can be obtained from ^{13}C NMR relaxation (T_1) measurements [66,68,111-114]. Of particular interest, is the determination of the actual conformations of the ether segments of the "free" and complexed crown ethers in solution. The ^{1}H and ^{13}C NMR spectra obtained for these systems, reflect the rapid conformational averaging due to the great molecular flexibility of crown ethers even down to 153 K [93]. The observed spectra thus represent the average of all possible orientations of the molecules in solution. The study of these fast processes has been limited to cases in which relatively large substituents have been introduced on the crown ethers [115,116] or there is complexation with metal cations, possibly slowing down the conformational averaging allowing the determination of quantitative rate data [95-98,115,116]. In these cases, the degeneracy of the spectra is uplifted at low temperatures, usually indicating an equilibrium between two conformers and the energy barriers for the conversion can be determined from classical coalescence temperature studies.

The ^{1}H and ^{13}C NMR spectra of simple non-substituted crown ethers such as 15C5 and 18C6, do not yield much structural information because of chemical equivalence due to symmetry of the protons and carbons; as a result, only one peak is observed. Those crown ethers having aromatic benzene substituents however, are well suited for this kind of study since the ring current magnetic anisotropy of the benzene ring leads to a spectroscopic resolution of the ether protons which can easily be assigned based on the spatial relationship between the protons and the aromatic group. Furthermore, the multiplets which are observed in the ^{1}H NMR ether region are characteristic of 4-spin, AA'BB', spin systems involving the separate O-CH_2-CH_2-O

segments of the crown ethers. The corresponding values for the ^{1}H-^{1}H coupling constants may be determined from spin simulations from which conformational information may subsequently be obtained. The ^{13}C spectral assigments are achieved with 2D heteronuclear chemical shift correlation (HETCOR) experiments.

In this chapter, the solution structures of benzo-15-crown-5 (B15C5), dibenzo-18-crown-6 (DB18C6), dibenzo-24-crown-8 (DB24C8) and dibenzo-30-crown-10 (DB30C10), shown in Figure 3.2, as well as the respective 1:1 sodium complexes in nitromethane (CD_3NO_2), will be characterized with the use of ^{1}H and ^{13}C NMR results.

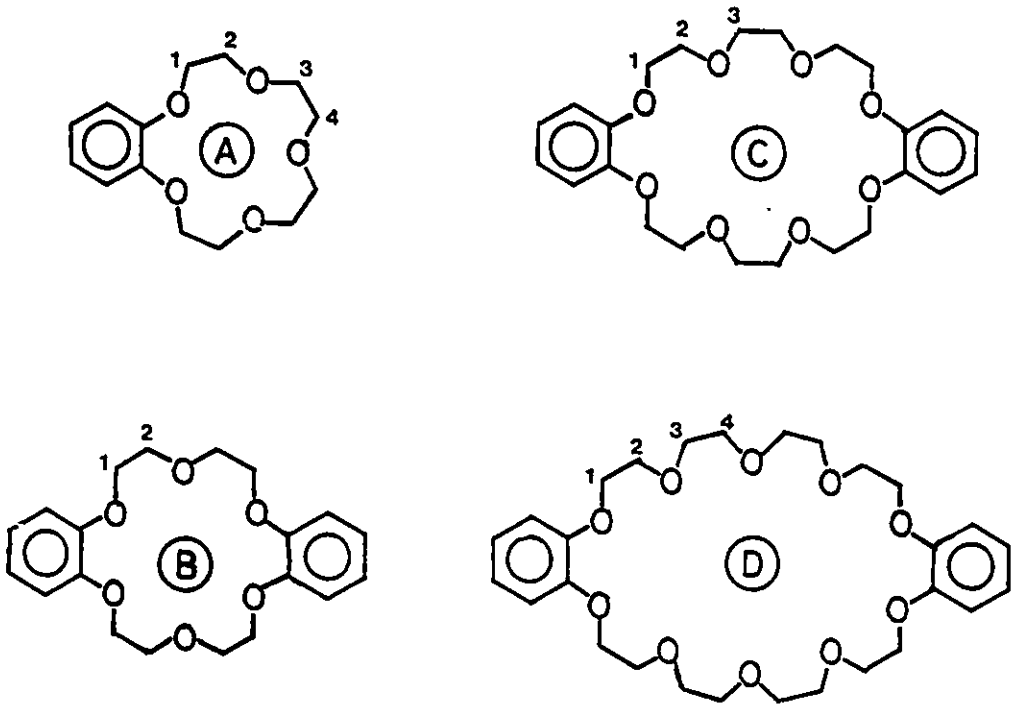

Figure 3.2: (A) Benzo-15-crown-5, (B) Dibenzo-18-crown-6, (C) Dibenzo-24-crown-8 and (D) Dibenzo-30-crown-10.

3.2 ^1H NMR

3.2.1 ^1H Spectral Assignments

The ^1H NMR spectra of B15C5, DB18C6, DB24C8 and DB30C10, and their respective alkali metal complexes in CD_3NO_2, are shown in Figures 3.3, 3.4, 3.5 and 3.6 respectively. The spectra of B15C5 and DB24C8, correspond to solution concentrations of approximately 0.1 M and a slight excess in alkali salt to form the complex was added to ensure that all the crown was present in the complexed form. Since DB18C6 and DB30C10 exhibited limited solubilities in CD_3NO_2, saturated solutions of these were used to obtain the spectra, but the concentrations of the respective complexes were approximately 0.1 M. The ^1H spectrum and chemical shifts of $(Na:B15C5)^+$ in CD_3CN at approximately 0.02 M, was identical to that at 0.1 M. The proton spectra for B15C5 and $(Na:B15C5)^+$ in CD_3CN and $(CD_3)_2CO$ and $(Li:B15C5)^+$ and $(K:DB30C10)^+$ in CD_3NO_2 were also obtained under the same conditions. Of primary concern is the ether region which is involved in the complexation and a summary of the proton chemical shifts of the ether protons of the various crown ethers and corresponding alkali complexes is shown in Table 3.1. In all cases, the aromatic benzene protons are located between 6.9 and 7.2 ppm. The circulating electrons of the benzene ring produce a so-called "ring-current effect" whereby a magnetic field is induced in the direction of the stationary magnetic field, B_o, resulting in the substantial deshielding of the aromatic protons which are located in the space outside the benzene ring [117]. This ring-current magnetic anisotropy of the aromatic substituent also affects the chemical shift of nearby protons, where those which are closest to the benzene ring are located downfield relative the others. The assignment of the protons in positions 1 and 2 (see Figure 3.2) for all crown ethers was made on this basis.

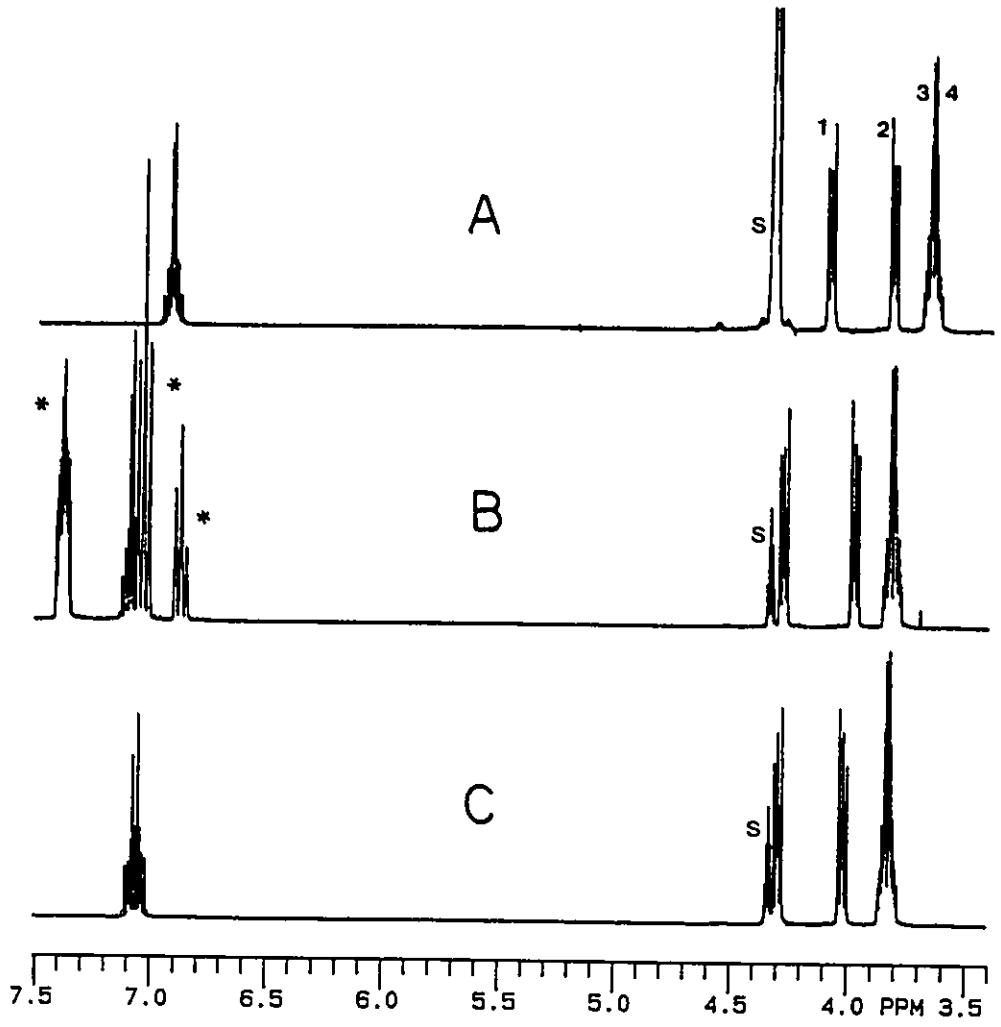

Figure 3.3: ^1H NMR spectra of (A) B15C5 (~ 0.1 M), (B) $(Na:B15C5)^+$ (~ 0.1 M) and (C) $(Li:B15C5)^+$ (~ 0.1 M). A slight excess of $NaBPh_4$ and $LiClO_4$ was added to ensure that all crown was complexed. Resonances marked with a * are those of the counteranion, BPh_4^-. Recorded at ambient temperature in CD_3NO_2 (s).

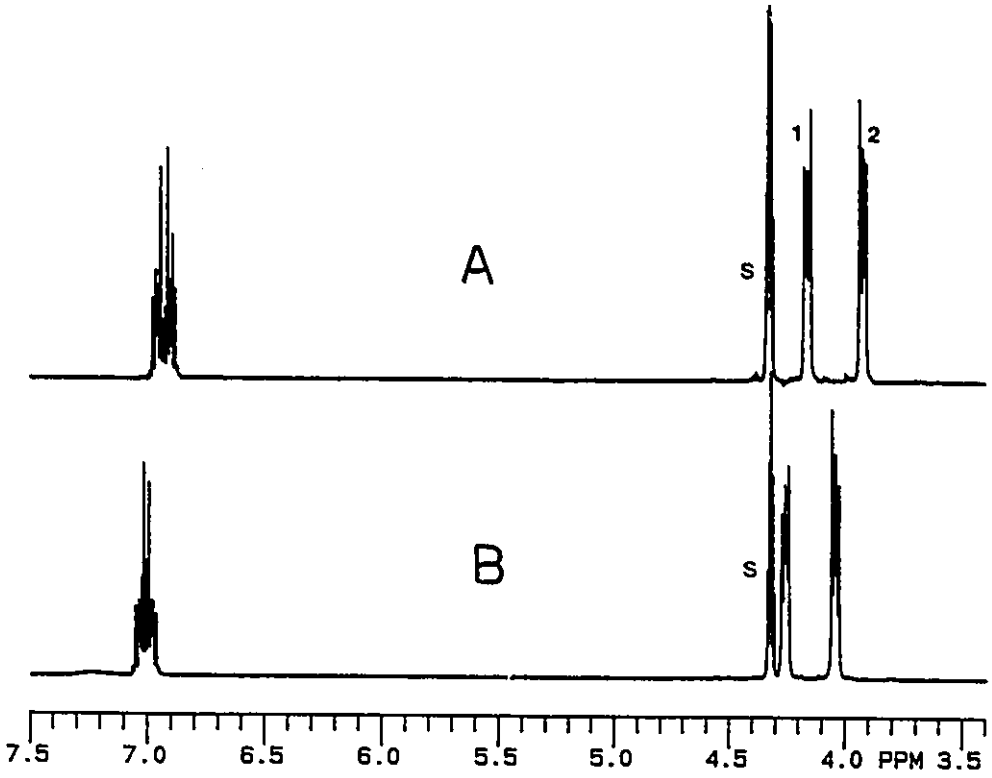

Figure 3.4: ^{1}H NMR spectra of (A) DB18C6 (saturated) and (B) $(Na:DB18C6)^+$ (~ 0.1 M). A slight excess of $NaPF_6$ added to ensure that all crown was complexed. Recorded at ambient temperature in CD_3NO_2 (s).

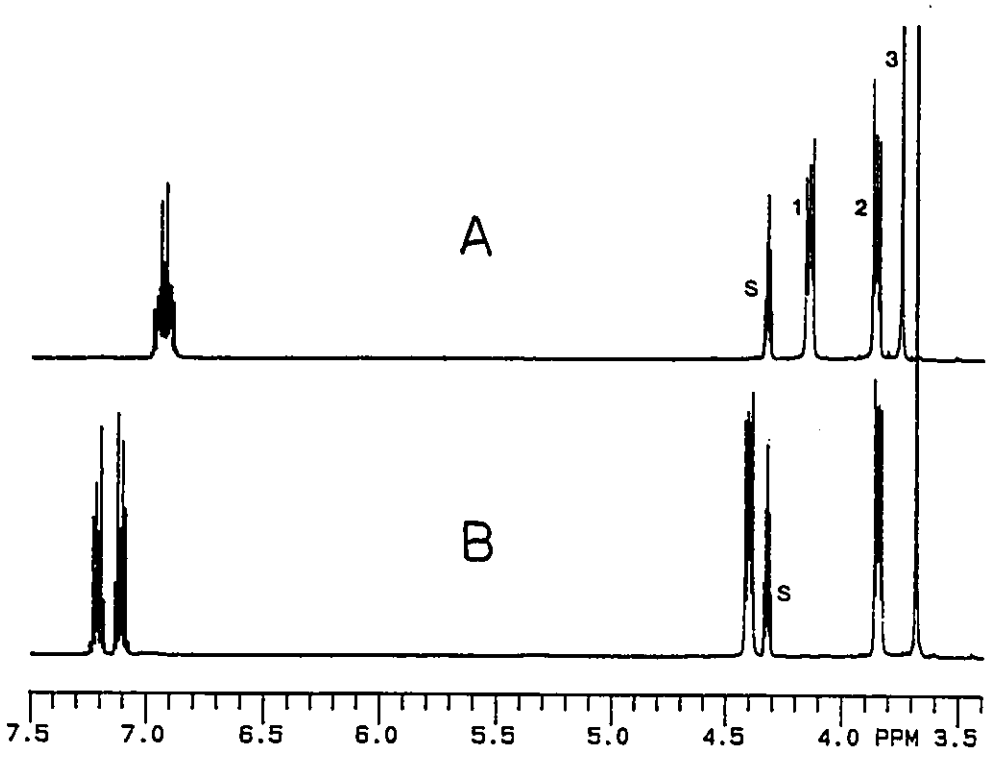

Figure 3.5: ^{1}H NMR spectra of (A) DB24C8 (~ 0.1 M) and (B) $(Na{:}DB24C8)^+$ (~ 0.1 M). A slight excess of $NaPF_6$ added to ensure that all crown was complexed. Recorded at ambient temperature in CD_3NO_2 (s).

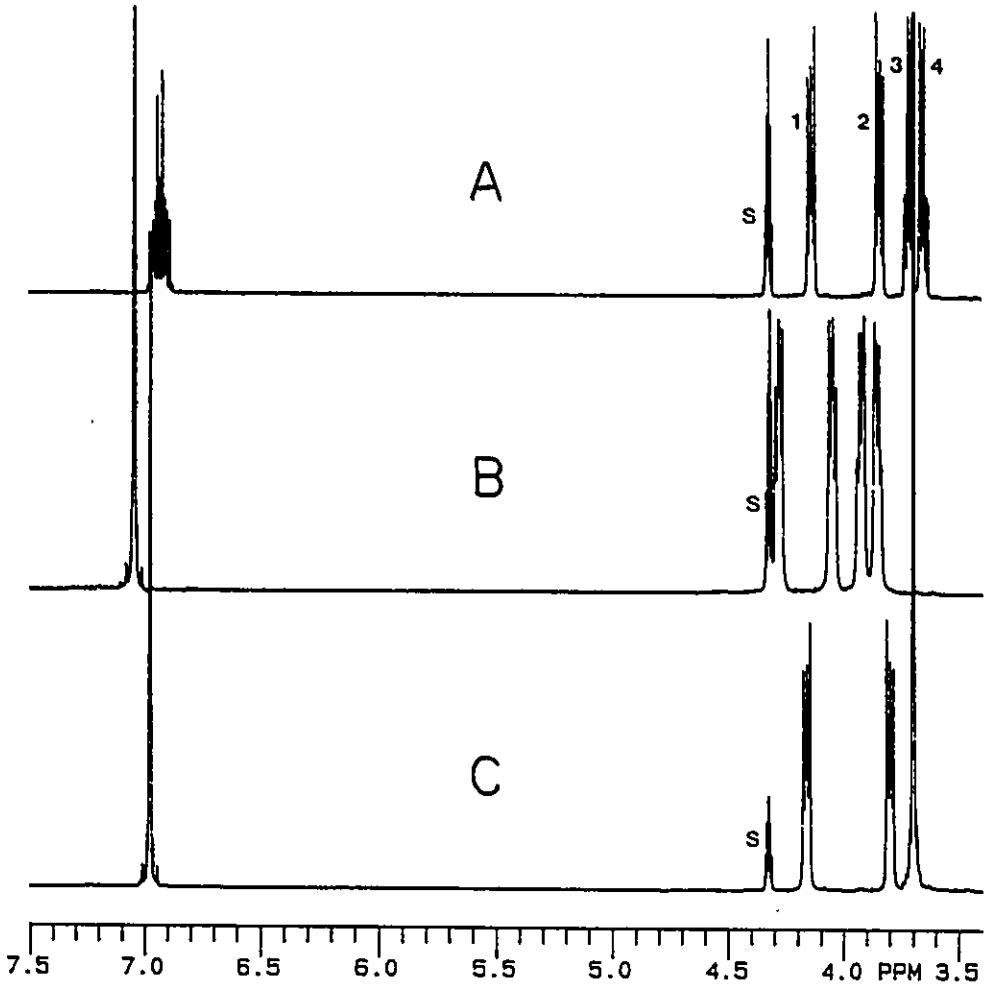

Figure 3.6: ^1H NMR spectra of (A) DB30C10 (saturated), (B) $(Na:DB30C10)^+$ (~ 0.1 M) and (C) $(K:DB30C10)^+$ (~ 0.1 M). A slight excess of $NaPF_6$ and KPF_6 was added to ensure that all crown was complexed. Recorded at ambient temperature in CD_3NO_2 (s).

Table 3.1: ^1H Chemical Shifts for Various Crown Ethers (C) and Crown Ether Complexes $(M:C)^+$ [a].

C or $(M:C)^+$	Solvent	H_1 [b]	H_2	H_3	H_4
15C5	CD_3NO_2	3.589	–	–	–
$(Li:15C5)^+$	CD_3NO_2	3.757	–	–	–
$(Na:15C5)^+$	CD_3NO_2	3.723	–	–	–
B15C5	CD_3NO_2	4.091	3.825	3.673	3.640
B15C5	CD_3CN	4.051	3.782	3.646	3.615
B15C5	$(CD_3)_2CO$	4.078	3.826	3.666	3.658
B15C5[c]	CD_3OD	3.944	3.944	3.678	3.678
$(Li:B15C5)^+$	CD_3NO_2	4.285	4.011	3.836	3.802
$(Li:B15C5)^+$[c]	CD_3OD	4.033	4.033	3.722	3.722
$(Na:B15C5)^+$	CD_3NO_2	4.272	3.972	3.829	3.791
$(Na:B15C5)^+$	CD_3CN	4.144	3.823	3.706	3.666
$(Na:B15C5)^+$	$(CD_3)_2CO$	4.187	3.876	3.750	3.730
$(Na:B15C5)^+$[c]	CD_3OD	4.022	4.022	3.767	3.767
DB18C6	CD_3NO_2	4.158	3.920	–	–
DB18C6[d]	$(CD_3)_2CO$	4.147	3.965	–	–
$(Na:DB18C6)^+$	CD_3NO_2	4.252	4.027	–	–
$(Na:DB18C6)^+$[d]	$(CD_3)_2CO$	4.255	4.002	–	–
DB24C8	CD_3NO_2	4.143	3.856	3.750	–
$(Na:DB24C8)^+$	CD_3NO_2	4.401	3.844	3.685	–
DB30C10	CD_3NO_2	4.140	3.840	3.714	3.651
DB30C10[d]	$(CD_3)_2CO$	4.131	3.826	3.712	3.632
$(Na:DB30C10)^+$	CD_3NO_2	4.346	4.112	3.923	3.855
$(Na:DB30C10)^+$[d]	$(CD_3)_2CO$	4.232	3.965	3.689	3.815
$(K:DB30C10)^+$	CD_3NO_2	4.163	3.800	3.699	3.699
$(K:DB30C10)^+$[d]	$(CD_3)_2CO$	4.197	3.807	3.718	3.718

(a) recorded at ambient temperature using $NaBPh_4$ and $NaPF_6$ for the sodium complexes, $LiClO_4$ for the lithium complex and KPF_6 for the potassium complex. (b) $H_{1,2,3,4}$ correspond to the chemical shifts of the protons at the position 1, 2, 3 and 4 respectively as shown in Figure 3.2; chemical shift ± 0.001 ppm; exact values for the chemical shifts were determined from spin simulations. (c) ± 0.002 ppm from reference 92; at 298 K and [C], [LiBr] and [NaI] = 0.5 M. (d) ± 0.002 ppm from reference 91; at ~288 K and [C], $[NaClO_4]$ and $[KClO_4]$ = 0.002 to 0.02 M.

The assignments of the protons in positions 3 and 4 for B15C5 and DB30C10 were unambiguously obtained by long-range ^{1}H-^{13}C chemical shift correlation experiments described in section 3.4.

The chemical shifts obtained for B15C5 in CD_3NO_2 are similar to results previously reported in CD_3OD [92] where at 90 MHz the protons on C(1) could not be distinguished from those on C(2) and those on C(3) from those on C(4). A downfield shift, induced by an electric field caused by the presence of charged cations, was also observed upon complexation with Na^+. The chemical shifts obtained for DB18C6 and DB30C10 in CD_3NO_2 are very similar to the values reported by Live and Chan [91] in $(CD_3)_2CO$. They also observed a general downfield shift of the protons upon complexation of the crown ethers with Na^+. The similarities in chemical shifts observed for B15C5 in three different solvents indicate that there is no significant participation or influence of the solvent in the environment of the crown ether. Live and Chan [91] observed a slight upfield shift in the ether proton resonances of DB18C6, B18C6 and DB30C10 in $(CD_3)_2CO$ compared to $CDCl_3$ which was attributed to the chemical shift anisotropy of the acetone solvent molecules which presumably have a preferential orientation in the proximity of the ether linkages. The slight differences in B15C5 chemical shifts that we observe might also be attributed to any such solvent anisotropy. As well, there is only a small difference between the chemical shifts of $(Na{:}B15C5)^+$ and $(Li{:}B15C5)^+$ in CD_3NO_2 indicating similar interactions of the two cations where B15C5 is concerned. Previous studies in solution by alkali metal NMR have indicated that whereas DB30C10 forms a complex with the potassium cation where the solvent is completely expelled from the coordination sphere of the cation [66], this is not so with the sodium cation [103]. As well, whereas $(K{:}DB30C10)^+$ displays protons on C(3) and C(4) which are equivalent, this is not the case for $(Na{:}DB30C10)^+$. This may be a reflection of the greater symmetry of the potassium complex compared to that with

sodium which is not perfectly adapted to DB30C10 [103]. The cation-induced shifts resulting from crown ether complexation in CD_3NO_2 are shown in Table 3.2. With a few exceptions, the downfield shift is consistently 0.1 to 0.2 ppm. The protons in position 1 of DB24C8 exhibit a downfield shift of 0.25 ppm upon sodium complexation and a small upfield shift is observed for the protons in position 2 and 3. This is a possible indication that the sodium cation, in its DB24C8 solution complex, is in closer proximity to the oxygens closest to the benzene ring (O_1) compared to the other oxygens of the crown ether. Since only the crystal structure of a solid sodium complex with 2:1 cation to ligand stoichiometry is available [70], a direct comparison of our solution observations is not possible.

Table 3.2: Cation-Induced ^1H Shifts for Crown Ethers upon Complexation, $(M:C)^+$ in Nitromethane-d_3.

Complex	H_1[a]	H_2	H_3	H_4
$(Li:B15C5)^+$	0.194	0.186	0.163	0.162
$(Na:B15C5)^+$	0.181	0.147	0.157	0.151
$(Na:DB18C6)^+$	0.094	0.107	–	–
$(Na:DB24C8)^+$	0.258	-0.012	-0.065	–
$(Na:DB30C10)^+$	0.206	0.272	0.209	0.204
$(K:DB30C10)^+$	0.023	0.040	0.015	0.048

(a) $H_{1,2,3,4}$ corresponds to the differences in chemical shifts between the complexed and free crown ethers of the protons at the position 1, 2, 3 and 4 respectively as shown in Figure 3.2.

In the $(Na_2:DB24C8)^{2+}$ solid complex however, the sodium cations are observed to be in closer proximity to the oxygens closest the benzene rings: the Na^+-O_1 bond lengths are 2.468 and 2.534 Å compared to 2.615 and 2.965 Å for Na^+-O_2 [70]. The same reasoning could be applied in the case of the protons in position 2 of $(Na:DB30C10)^+$ which are near O_2, since a significantly larger downfield shift is observed (0.272 ppm). However, a direct comparison to the solid counterpart is again not possible since the formation of a solid sodium-DB30C10 complex also exhibits 2:1 stoichiometry [87]. In this case, the sodium-oxygen bond lengths increase in the order Na^+-O_1 (2.413 Å), Na^+-O_2 (2.493 Å) and Na^+-O_3 (2.531 Å), which does not confirm the solution observations [87].

3.2.2 Conformational Analysis

All of the spectra shown in Figures 3.3 to 3.6, exhibit the same basic spectral characteristics. The peaks in the aromatic region are characteristic of a 1,2-disubstituted benzene and exhibit a typical 4-spin AA′BB′ pattern. Any observed differences in the coupling pattern come from changes in the chemical shift. All of the spectra also exhibit two ^1H multiplets in the ether region, again characteristic of a 4-spin AA′XX′ system for the O-C(1)H_2-C(2)H_2-O segments of the crown ethers. In addition, B15C5 and DB30C10 exhibit a third 4-spin AA′BB′ system in the ether region, for the C(3)-C(4) fragment. It should be mentioned that lowering the temperature to approximately 283 K did not affect the ^1H spectra of both B15C5 and $(Na:B15C5)^+$ in acetone-d_6, indicating a very rapid conformational averaging. Keeping in mind the preferred gauche orientation of the oxygen atoms in the fragments, the ^1H spectra observed at ambient temperature reflect the averaging due to the rapid rotamer conversion depicted in Figure 3.7.

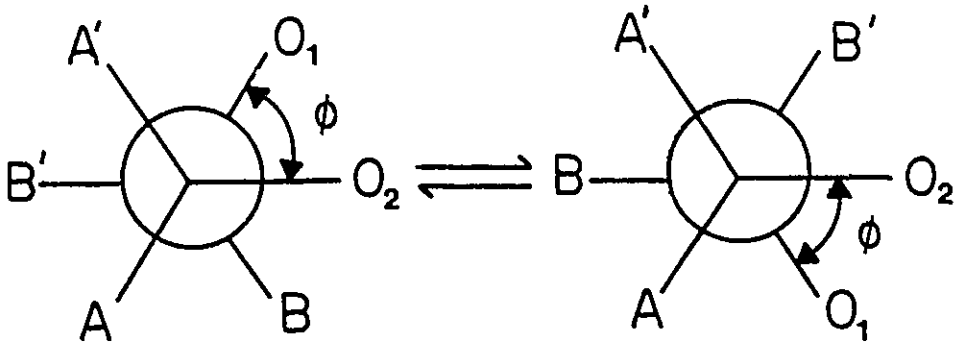

Figure 3.7: Newman projections showing the rotamer conversion of the two rotational isomers of the crown ether OCH_2CH_2O fragment. ϕ is the dihedral angle subtended by the oxygen atoms in two adjacent carbons.

The ^1H-^1H coupling in the O-CH_2-CH_2-O fragments is characterized by two geminal coupling constants, $^2J_{AA'}$ and $^2J_{BB'}$ assumed to be equivalent, and average values of two vicinal coupling constants, $^3J_{AB} = {}^3J_{A'B'}$ and $^3J_{AB'} = {}^3J_{A'B'}$. Values for these coupling constants were obtained from spin simulations, as described in section 2.3.3, for the 4-spin systems. As an example, the simulated spectra for both fragments of B15C5 in CD_3NO_2 are shown in Figure 3.8. The ether region of the ^1H spectrum of B15C5 is characteristic of the two separate 4-spin systems. The simulated spectra of the first order C(1) - C(2) AA'XX' fragment corresponds very well to the experimental one and this is a good indication that there is no significant long-range ^1H-^1H coupling. The simulated spectra of the second order C(3) - C(4) AA'BB' fragment also corresponds very well to the experimental one. The geminal coupling constant is not affected by the rotamer conversion and only average values for the vicinal coupling constants, which are effectively J_{trans} and J_{cis}, can be determined. A summary of the coupling constants obtained from spin simulations of several crown ether systems are shown in Table 3.3.

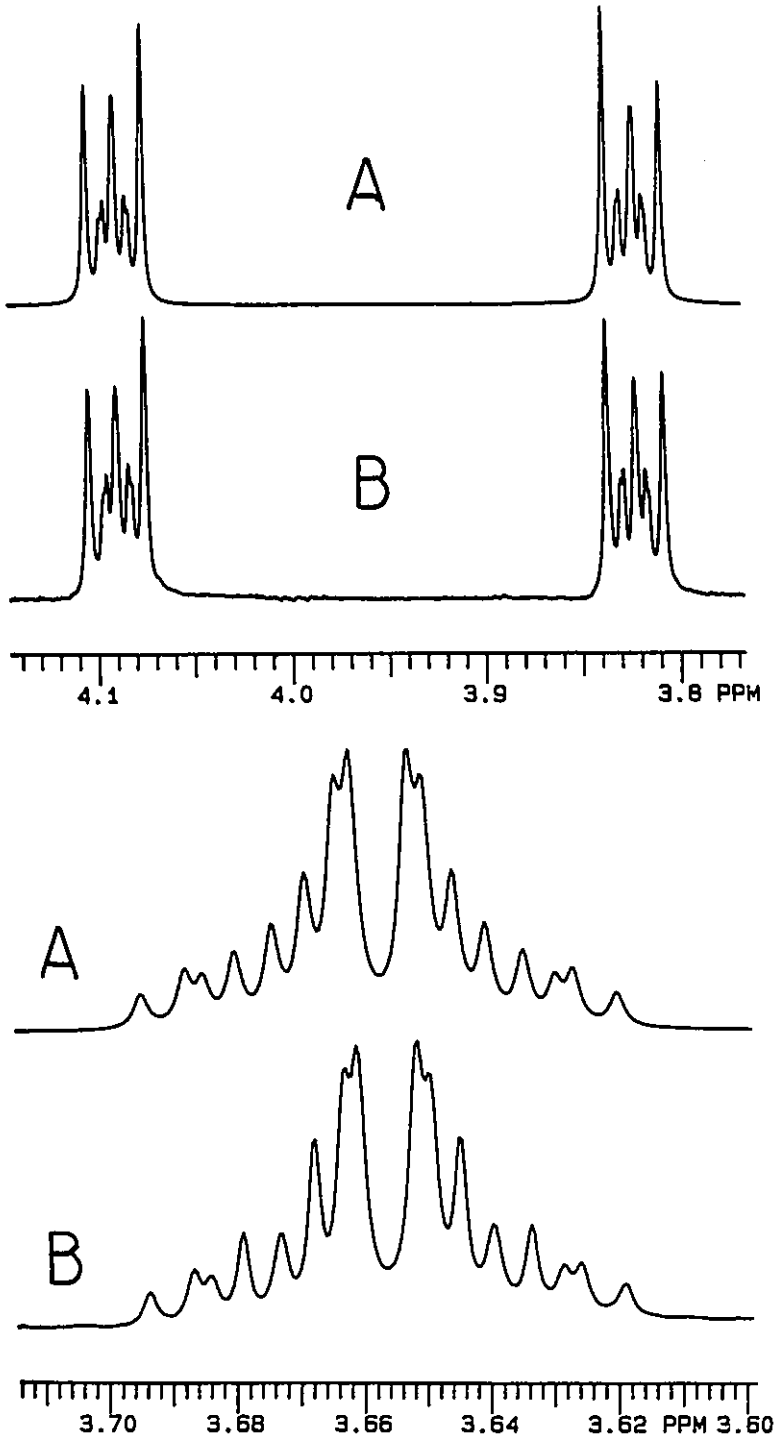

Figure 3.8: ^1H Spin simulations for B15C5 in CD_3NO_2. Top: O-C(1)H_2-C(2)H_2-O fragment, bottom: O-C(3)H_2-C(4)H_2-O fragment. (A) Simulated spectrum, (B) experimental spectrum.

Table 3.3: Coupling Constants for the Protons in the Ether Fragments of Crown Ethers and Crown Ether Complexes.

C or $(M:C)^+$	Solvent	J_{gem}[a]	J_{trans}[a]	J_{cis}[a]
B15C5	CD_3NO_2	-9.5(-10.0)	6.6(6.5)	1.9(2.8)
B15C5	CD_3CN	-10.2(-10.1)	6.7(6.4)	2.5(3.3)
B15C5	$(CD_3)_2CO$	-9.8[b]	6.5	2.9
B15C5[c]	CD_3OD	–	5.75	3.1
$(Li:B15C5)^+$	CD_3NO_2	-10.2(-10.1)	6.2(6.2)	4.3(3.2)
$(Na:B15C5)^+$	CD_3NO_2	-10.3(-10.0)	6.7(6.4)	3.0(2.2)
$(Na:B15C5)^+$	CD_3CN	-10.0(-10.0)	6.4(6.3)	2.9(2.4)
$(Na:B15C5)^+$	$(CD_3)_2CO$	-10.0(-10.0)	6.6(6.4)	2.7(2.6)
$(Na:B15C5)^{+c}$	CD_3OD	–	6.8	2.1
DB18C6	CD_3NO_2	-9.8	7.0	1.1
DB18C6[d]	$(CD_3)_2CO$	–	5.8	3.5
$(Na:DB18C6)^+$	CD_3NO_2	-10.0	6.0	3.0
DB24C8	CD_3NO_2	-9.6	6.6	2.2
$(Na:DB24C8)^+$	CD_3NO_2	-10.1	6.7	2.8
DB30C10	CD_3NO_2	-10.4(-10.0)	6.8(6.0)	2.6(2.9)
DB30C10[d]	$(CD_3)_2CO$	–	6.2(6.0)	3.1(3.3)
$(Na:DB30C10)^+$	CD_3NO_2	-10.0(-10.0)	6.3(6.4)	3.1(2.9)
$(K:DB30C10)^+$	CD_3NO_2	-9.9	6.7	2.2
1,4 dioxane[c]		–	6.1	2.7

(a) $J_{gem} = J_{AA'} = J_{BB'}$ $J_{cis} = J_{AB} = J_{A'B'}$ and $J_{trans} = J_{A'B} = J_{AB'}$; number in brackets corresponds to the coupling constants of the O-C(3)H_2-C(4)H_2-O fragment. (b) The difference in chemical shifts for the protons on C(3) and C(4) for B15C5 in $(CD_3)_2CO$ was too small to get accurate results in the simulation. (c) from reference 92. (d) from reference 91.

A geminal coupling constant, reflecting the geminal H-C-H angle, of approximately -10 Hz is obtained for all the systems shown in Table 3.3. Based on the geminal Karplus correlation, at first approximation (not taking into account the electronegative substituents), this corresponds to a geminal H-C-H angle approximately equal to 110° [117].

It is through the vicinal coupling constants however, that specific conformational information may be obtained. Vicinal coupling constants obtained by Lockhart et al. for B15C5 in CD_3OD [92] and by Live and Chan for DB18C6 and DB30C10 in $(CD_3)_2CO$ and $CDCl_3$ [91], correspond very closely those determined in this work. Furthermore, the coupling constants of the O-CH_2-CH_2-O fragments of other unusual crown ethers also are similar [92,93]. The smallest crown ether, 1,4-dioxane (6C2), can only exist in a gauche conformation and in solution this compound also exhibits the rotamer conversion shown in Figure 3.7 [91,118]. Since values for the average vicinal coupling constants for 1,4-dioxane correspond very closely to those of many other crown ether systems, this is an initial indication that the conformations of the O-CH_2-CH_2-O fragments of the studied crown ethers and the complexes in solution must be gauche as well (see Table 3.3). In order to determine exact values of the dihedral angle between the oxygens subtended on two adjacent carbons, ϕ shown in Figure 3.7, a method based on the Karplus vicinal correlation, shown in equation 16, has been appled. The original Karplus vicinal correlation relates the ^1H-^1H vicinal coupling constants, ^3J, to the dihedral angle subtended by the protons on different carbons in a C-C bond [23,119,120-122].

$$^3J = A\cos^2\phi + B\cos\phi + C \qquad (16)$$

Since this relationship does not account for electronegative substituents, bond angles and bond lengths, the three constants A, B and C may differ considerably from compound to

compound and its use is therefore rather limited [23]. The R value method, where $R = J_{trans} / J_{cis}$, for determining dihedral angles was originally developed by Lambert [121] for six-membered rings and a quantitative relationship between ϕ and R, shown in equation 17, was developed by Buys [122].

$$\phi = \cos^{-1} [3 / (2 + 4R)]^{1/2} \qquad (17)$$

This relationship is based on the Karplus correlation shown in equation 16, assuming that the parameters B and C are small with respect to A and therefore can be neglected, and as well assuming that there are only gauche dihedral angles. R is independent of the electronegativity of the oxygen substituents in the ether fragments and can be used as a criterion of conformational change free from electronegativity effects [92]. This method has been successfully used by Lockhart et al. [92] and Kleinpeter et al. [93] for crown ethers with rings having more than 6 members. The values for the dihedral angles of the segments shown in Figure 3.7 for the crown ethers in this study have been calculated using equation 17 and are shown in Table 3.4. The observed dihedral angles, all corresponding approximately to 60°, do in fact agree with the previously stated gauche preference of C-C bonds in crown ethers. These results also generally agree with the dihedral angles obtained for other crown ethers [92,93] and crown ether complexes [92] in solution which ranged from 55-64°. Although Lockhart et al. [92] and Live and Chan [91] observed a slight increase in dihedral angle upon complexation of the crown ethers, we do not observe such a trend using the R method. A more direct approach to determine a trend in ϕ is to examine directly the values for J_{cis} which are the same in the two rotamers shown in Figure 3.7 ($J_{cis} = J_{AB} = J_{A'B'}$). As the crown ethers are complexed, a general increase in J_{cis} is observed (see Table 3.3). Based on the Karplus vicinal correlation in the region 0° < dihedral angle < 80° [117], this corresponds to a

Table 3.4: *R* Values and Corresponding Dihedral Angles, ϕ, of the Oxygen Atoms in the O-C(1)H_2-C(2)H_2-O Fragments in Various Crown Ethers (C) and Their Alkali Metal Complexes $(M:C)^+$.

C	Solvent	R^a	ϕ (°)	$(M:C)^+$	*R*	ϕ (°)
B15C5	CD_3NO_2	3.5(2.3)	64(59)	$(Na:C)^+$	2.2(2.9)	58(62)
				$(Li:C)^+$	1.4(1.9)	51(55)
B15C5	CD_3CN	2.7(1.9)	61(55)	$(Na:C)^+$	2.2(2.6)	58(61)
B15C5	$(CD_3)_2CO$	2.2	58	$(Na:C)^+$	2.4(2.5)	59(60)
B15C5[b]	CD_3OD	1.9	55	$(Na:C)^+$	3.2	63
DB18C6	CD_3NO_2	6.4	71	$(Na:C)^+$	2.0	57
DB18C6[c]	$(CD_3)_2CO$	1.7	54			
DB24C8	CD_3NO_2	3.0	62	$(Na:C)^+$	2.4	59
DB30C10	CD_3NO_2	2.6(2.0)	61(57)	$(Na:C)^+$	2.1(2.2)	57(58)
				$(K:C)^+$	3.0	62
DB30C10[c]	$(CD_3)_2CO$	3.4	64			

(a) number in brackets corresponds to the *R* value for the O-C(3)H_2-C(4)H_2-O fragment where applicable. (b) from reference 92. (c) calculated from the J values reported in reference 91.

a decrease in the dihedral angle described by J_{cis} and therefore also corresponds to a decrease in ϕ (see Figure 3.7).

The overall solution gauche orientations of the oxygen atoms in the ether fragments of B15C5 agree with what is observed for this crown ether as a solid [79]. This is illustrated in Figures 3.9a and 3.9b which show diagrams of space filling models for solid B15C5 and solid B15C5 complexed to sodium, built from crystal structure coordinates using the ALCHEMY software [77,79]. The sodium cation, which is not

shown in Figure 3.9b, sits on top of the macrocyclic B15C5 ring and is coordinated to all five oxygen atoms (the inter-atomic distances vary from 2.4 to 2.6 Å [77]). The crystal structures for B15C5 show that this crown ether exhibits only gauche O-C-C-O dihedral angles, ϕ, which vary from 66-72° [79], and there is a slight decrease in dihedral angle upon complexation to sodium, 57-61° [77]. A decrease in ϕ upon complexation of B15C5 is also observed in solution. Although all the oxygen atoms have gauche orientations in both cases, the oxygen atom farthest from the benzene ring has a different relative orientation. The crystal structure of complexed DB18C6 [85] show that the corresponding C-C dihedral angles are also gauche, vary from 66-69° and are in agreement with the present NMR studies, whereas the uncomplexed solid DB18C6 exhibits much larger dihedral angles: 77° (gauche) and 105° (trans). DB24C8 forms 2:1 cation:ligand solid complexes with sodium, exhibiting both trans (117°) and gauche (60 and 61°) conformations of the O-CH_2-CH_2-O fragments [70]. Solid DB30C10, $(K{:}DB30C10)^+$, $(Rb{:}DB30C10)^+$ [86] and $(Na_2{:}DB30C10)^{2+}$ [87] exhibit gauche dihedral angles only. Save a few exceptions, the overall conformations of the crown ethers and their complexes in solution agree with the corresponding solid structures.

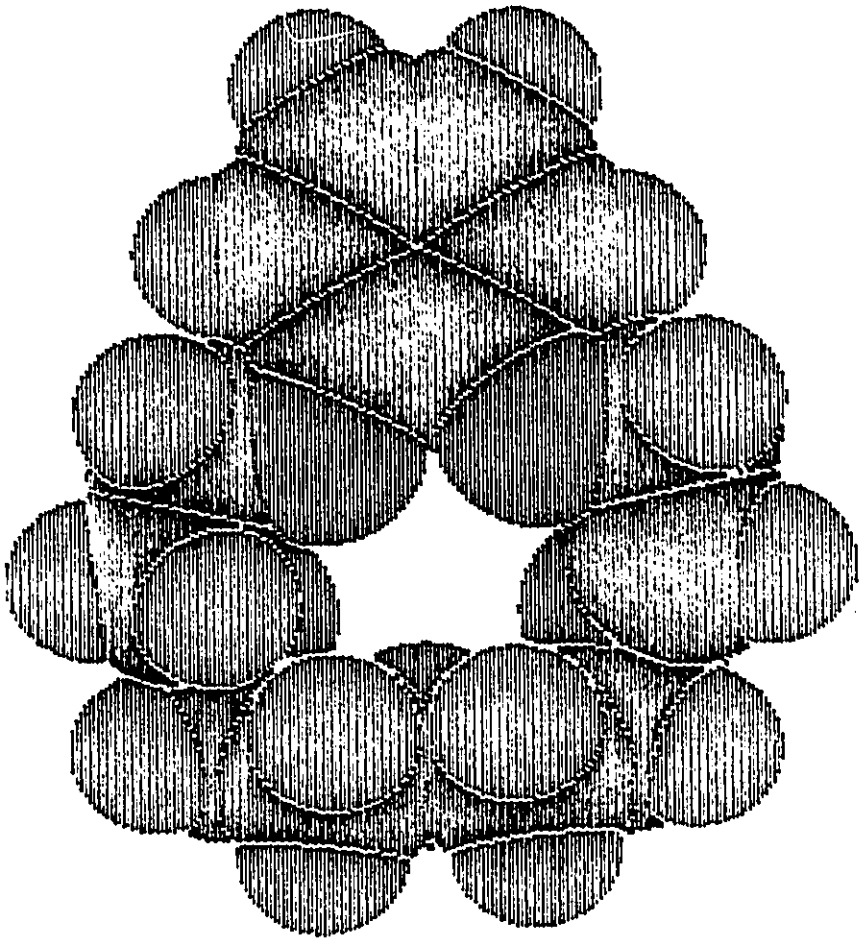

Figure 3.9a: Space filling model of B15C5 constructed from the crystal structure coordinates [79].

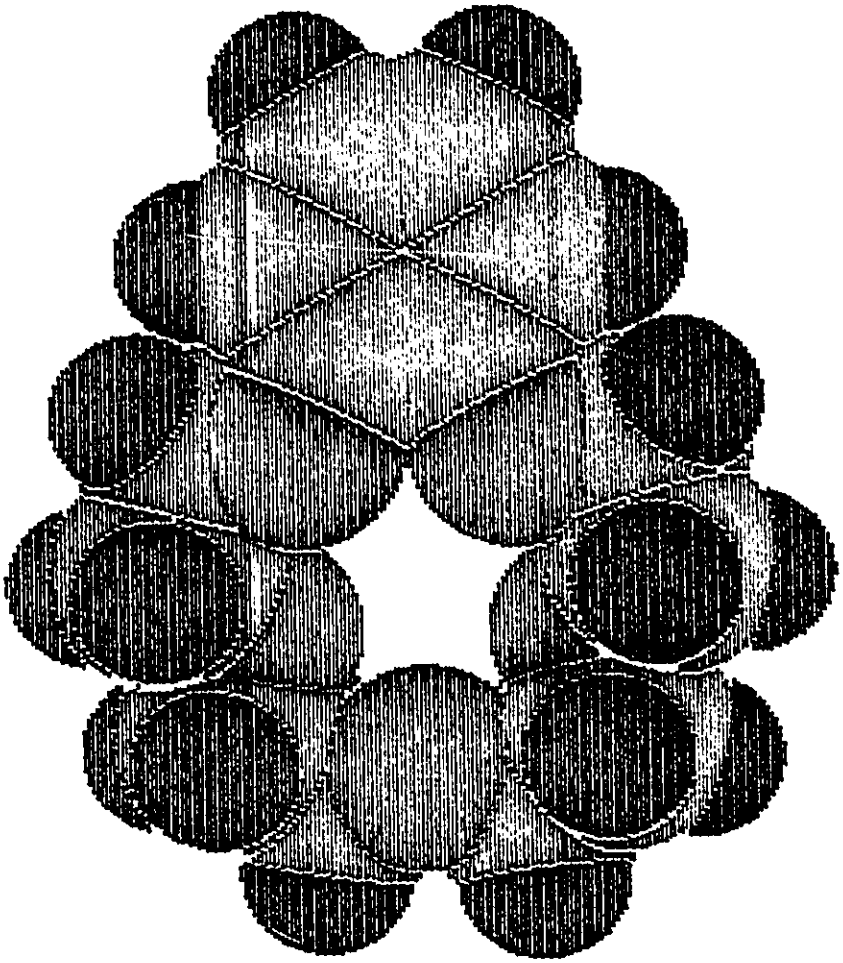

Figure 3.9b: Space filling model of B15C5 complexed to sodium constructed from the crystal structure coordinates [77].

3.3 ^{13}C NMR

Although ^{13}C chemical shifts are known to be sensitive to conformations, there is an insufficient understanding of the ^{13}C chemical shift to establish the details of small structural changes on the basis of the spectral positions of the ^{13}C resonances alone [91,110,123]. Nevertheless in order to completely characterize the crown ethers and their respective complexes in CD_3NO_2 by NMR, ^{13}C spectra were obtained and are shown in Figures 3.10 to 3.13. The assignment of the ^{13}C resonances was done using heteronuclear chemical shift correlation described is section 3.4. The aromatic carbons, whose chemical shifts do not vary appreciably, were not rigorously experimentally assigned. The α carbon (see Figure 3.2) can be easily assigned: it is the most downfield, at 145-150 ppm, since it is next to the oxygen which deshields it and it is the "shortest" peak since the α carbon is quaternary. The β carbon is located at approximately 115 ppm and the γ carbon at 122 ppm (this is an empirical assignment based on a collection of results obtained for substituted benzenes [123]). The ^{13}C chemical shifts of the ether carbons of all the systems studied are between 67 and 71 ppm and are shown in Table 3.5. There is a small difference in the ^{13}C chemical shifts of DB18C6 and DB30C10 in CD_3NO_2 compared to those reported by Live and Chan [91] for the same crown ethers in $CDCl_3$. However, they have also observed a general upfield shift upon complexation. As do the ^1H results, the ^{13}C chemical shifts indicate similar interactions of both sodium and lithium where B15C5 is concerned. However, there is a significant difference between the chemical shift of carbon 1 in $(Li:B15C5)^+$ which is shifted one ppm more upfield upon complexation in CD_3NO_2 than that of $(Na:B15C5)^+$. This might be a reflection of the different positions of the cations within the cavity of B15C5. The chemical shifts of $(Na:DB24C8)^+$, DB30C10, $(Na:DB30C10)^+$ and $(K:DB30C10)^+$ are similar to those previously reported [68,66,108].

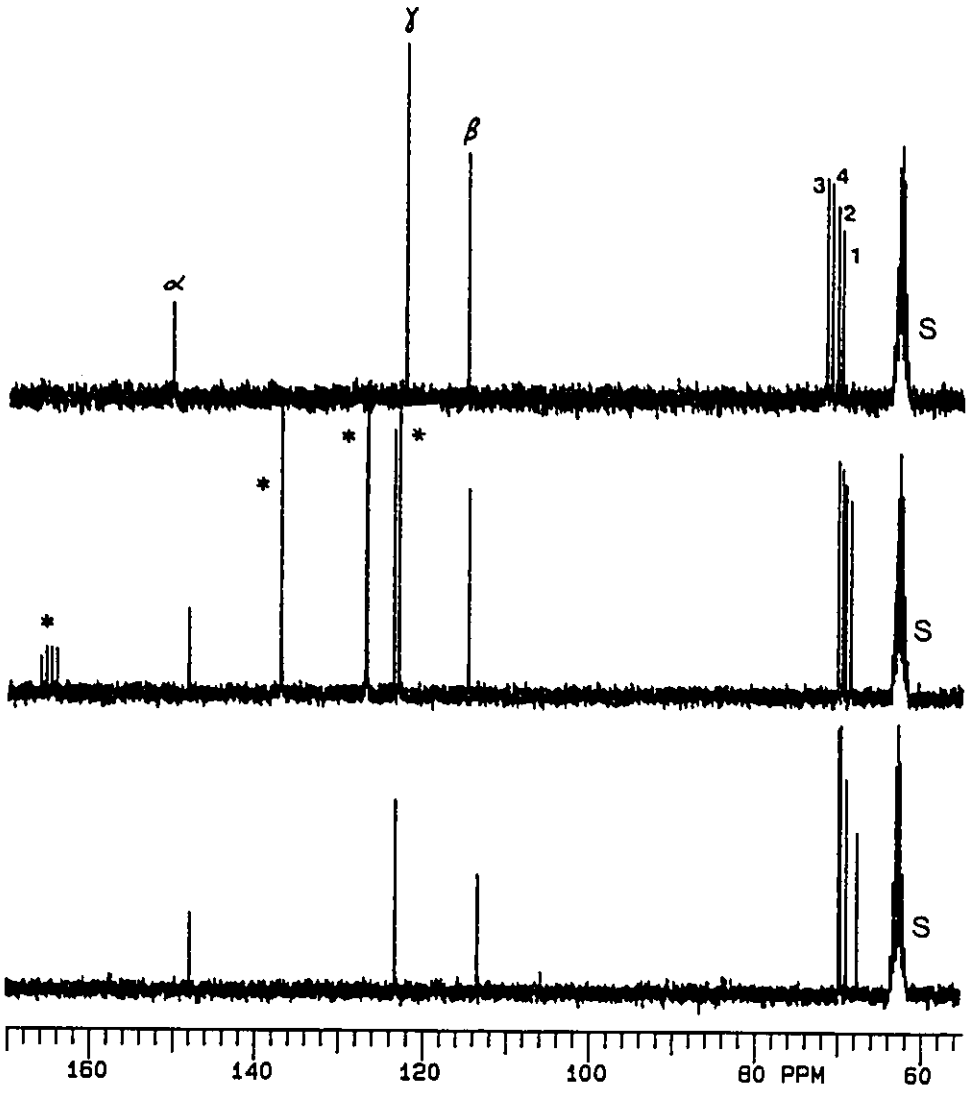

Figure 3.10: ^{13}C proton decoupled NMR spectra of (A) B15C5, (B) $(Na:B15C5)^+$ (resonances marked with a * are those of the BPh_4^- counteranion) and (C) $(Li:B15C5)^+$. Recorded at ambient temperature in CD_3NO_2 (s).

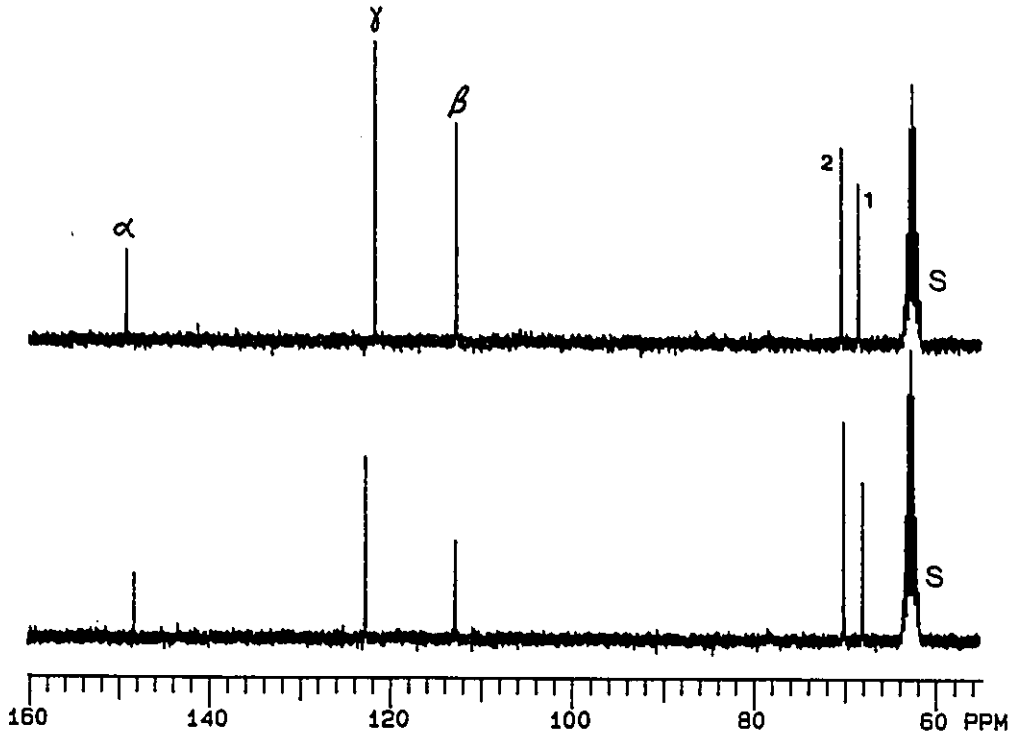

Figure 3.11: ^{13}C proton decoupled NMR spectra of (A) DB18C6 and (B) $(Na:DB18C6)^+$. Recorded at ambient temperature in CD_3NO_2 (s).

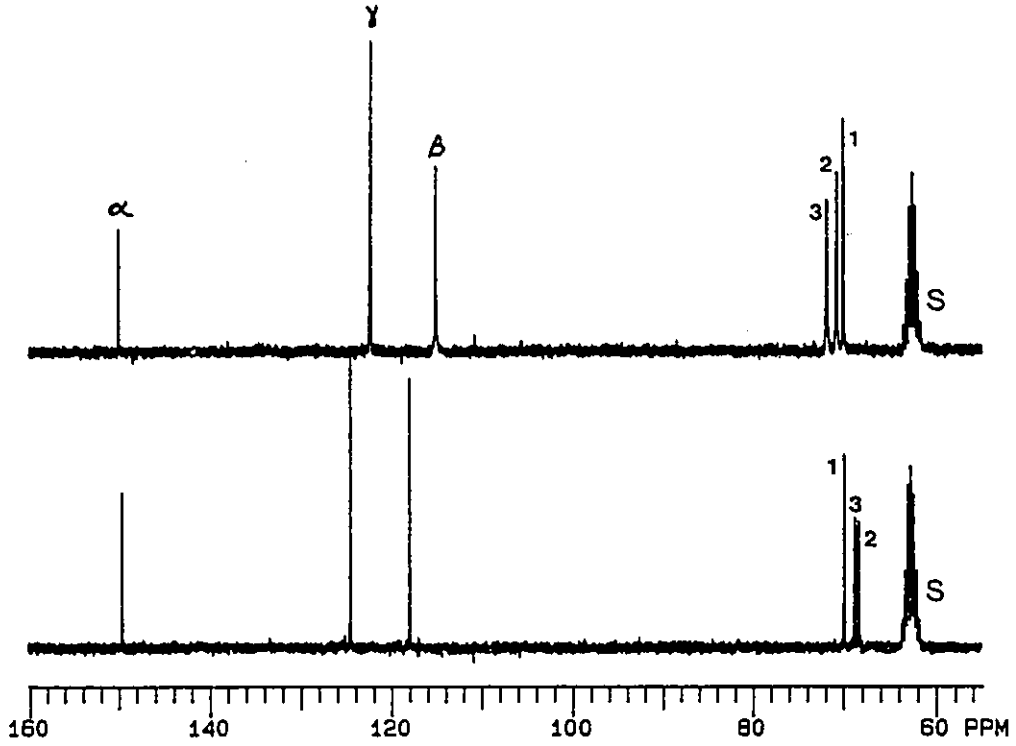

Figure 3.12: ^{13}C proton decoupled NMR spectra of (A) DB24C8 and (B) $(Na:DB24C8)^+$. Recorded at ambient temperature in CD_3NO_2 (s).

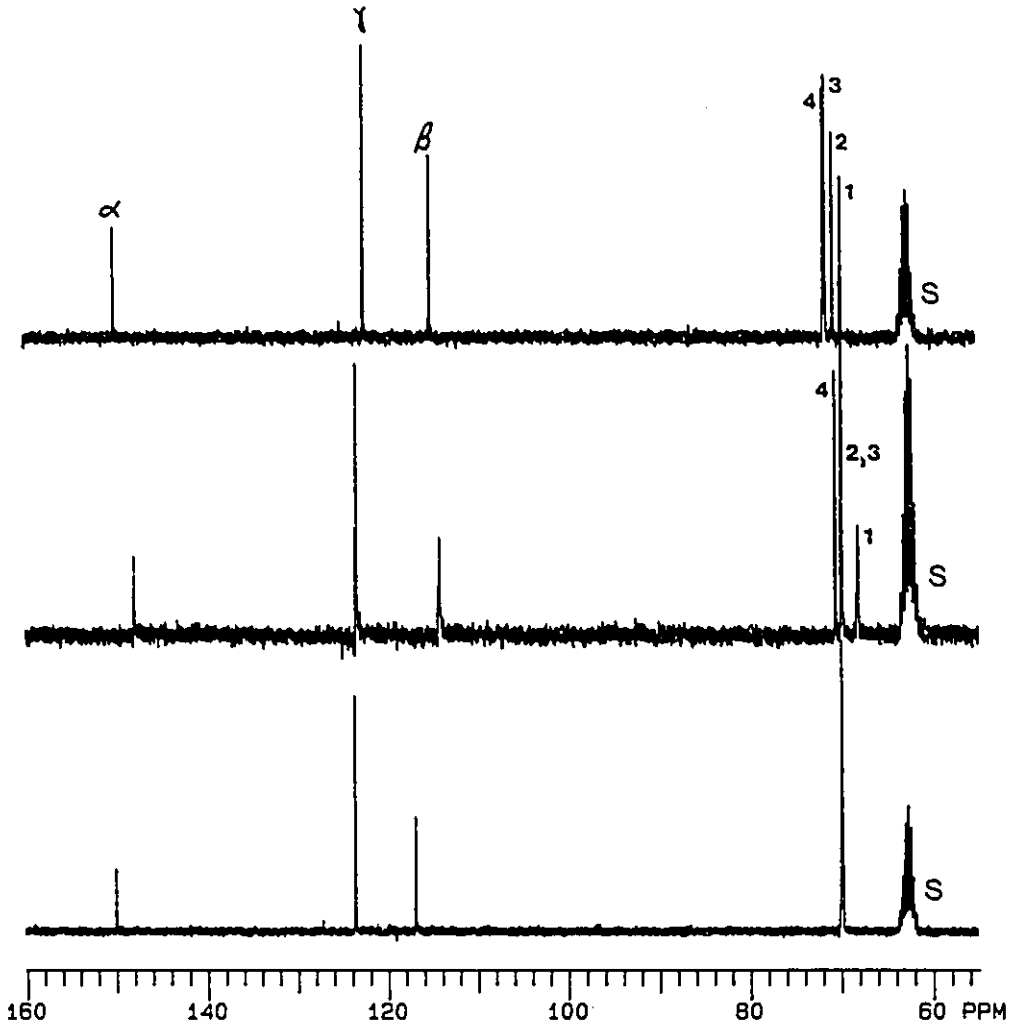

Figure 3.13: ^{13}C proton decoupled NMR spectra of (A) DB30C10, (B) $(Na:DB30C10)^+$ and (C) $(K:DB30C10)^+$. Recorded at ambient temperature in CD_3NO_2 (s).

Table 3.5: ^{13}C Chemical Shifts of the Ether Carbons for the Various Crown Ethers (C) and Crown Ether Complexes $(M:C)^+$.[a]

C or $(M:C)^+$	Solvent	C_1[b]	C_2	C_3	C_4
15C5	CD_3NO_2	71.193	–	–	–
$(Li:15C5)^+$	CD_3NO_2	69.227	–	–	–
$(Na:15C5)^+$	CD_3NO_2	69.778	–	–	–
B15C5	CD_3NO_2	69.632	70.184	71.540	70.942
B15C5	CD_3CN	69.589	70.050	71.442	70.900
B15C5	$(CD_3)_2CO$	69.818	70.262	71.856	71.325
$(Li:B15C5)^+$	CD_3NO_2	67.447	68.786	69.702	69.475
$(Na:B15C5)^+$	CD_3NO_2	68.454	69.115	69.978	69.482
$(Na:B15C5)^+$	CD_3CN	68.262	68.676	69.440	68.876
$(Na:B15C5)^+$	$(CD_3)_2CO$	68.072	68.575	69.288	68.725
DB18C6	CD_3NO_2	68.493	70.381	–	–
DB18C6[c]	$CDCl_3$	69.39	70.19	–	–
$(Na:DB18C6)^+$	CD_3NO_2	67.886	69.949	–	–
DB24C8	CD_3NO_2	70.003	70.757	71.859	–
$(Na:DB24C8)^+$	CD_3NO_2	69.763	68.187	68.857	–
DB30C10	CD_3NO_2	69.724	70.572	71.609	71.418
DB30C10[c]	$CDCl_3$	69.50	70.30	71.06	70.89
$(Na:DB30C10)^+$	CD_3NO_2	68.011	69.897	69.897	70.587
$(K:DB30C10)^+$	CD_3NO_2	69.205	69.205	69.205	69.205
$(K:DB30C10)^{+c}$	$CDCl_3$	69.40	69.07	68.84	68.80

(a) recorded at ambient temperature using $NaBPh_4$ and $NaPF_6$ for the sodium complexes, $LiClO_4$ for the lithium complex and KPF_6 for the potassium complex. (b) $C_{1,2,3,4}$ corresponds to the chemical shifts of the carbons at the position 1, 2, 3 and 4 respectively as shown in Figure 3.2; chemical shift ± 0.007 ppm. (c) ± 0.02 ppm from reference 91; at ~320 K.

However, whereas we observe only one peak for $(K:DB30C10)^+$ in CD_3NO_2, reflecting the symmetry of this complex compared to $(Na:DB30C10)^+$, others have observed two peaks in $(CD_3)_2CO$ [66] and 4 peaks in $CDCl_3$ [91]. An unusual effect is observed in the case of $(Na:DB24C8)^+$: the carbons of this complexed crown ether do not follow the usual trend and the chemical shift of the carbon at position 1 is located downfield relative to the other carbons in this molecule. The ^1H studies also indicated unusual behavior at position 1 which was attributed to a shorter Na-O_1 bond length compared to the other Na-O bond lengths in the sodium-DB24C8 complex. The ^{13}C results probably also reflect the relative position of the sodium cation in the same manner.

3.4 Heteronuclear Chemical Shift Correlation

The development of sophisticated multiple pulse sequences and 2-dimensional techniques in NMR, has provided today's chemist with several possibilities for peak assignments and compound structural elucidation [38,56,124,125]. One of the techniques that enjoys widespread use for assigning ^{13}C resonances is *heteronuclear chemical shift correlation* (HETCOR). It is a 2-dimensional technique which labels the ^{13}C resonances, conventionally in the second dimension (f_2 domain), to the protons, in the first dimension (f_1 domain), which are attached to them via the ^1H - ^{13}C couplings. The standard HETCOR pulse sequence is shown in Figure 3.14 [38]. Polarization transfer from the high-γ protons to the low-γ carbons is accomplished with the proton pulses, the 180° ^{13}C pulse at the midpoint of the evolution time t_1, which is incremented during the experiment, is designed to suppress the effects of the ^1H - ^{13}C couplings in the f_1 domain and Δ_1 and Δ_2 are fixed delays related to the ^1H - ^{13}C coupling constants [38,125]. In general, the Δ_1 and Δ_2 delays are optimized as $(2\ J_{CH})^{-1}$ and $(3\ ^1J_{CH})^{-1}$ respectively; since the J_{CH} of directly attached protons is 100-200 Hz, Δ_1 is normally

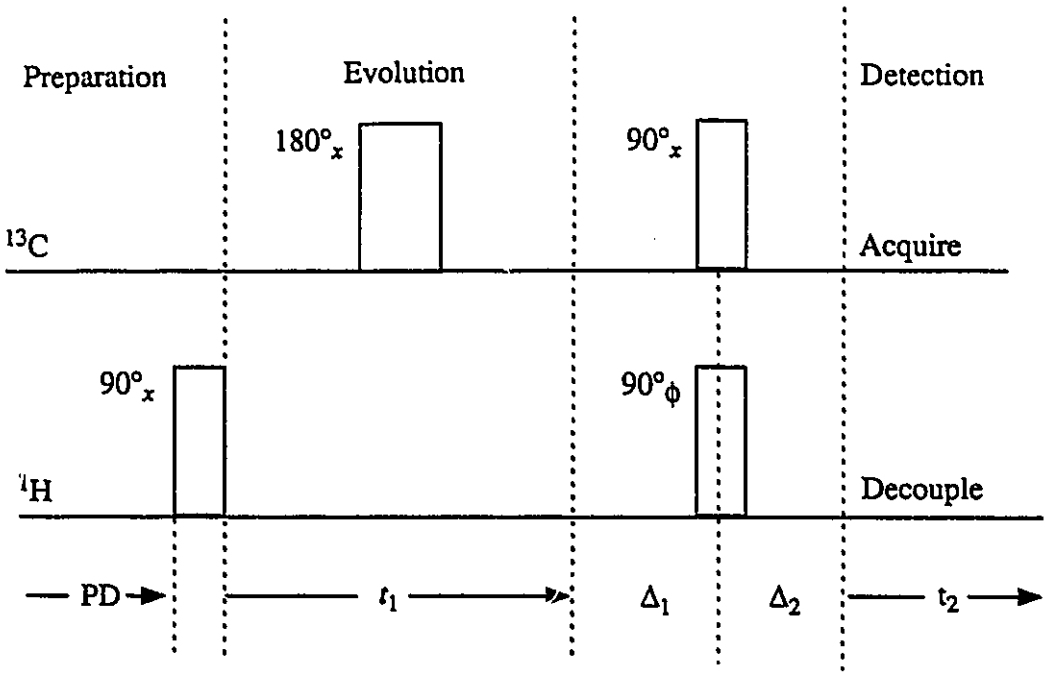

Figure 3.14: The standard pulse sequence for ^{1}H - ^{13}C chemical shift correlation.

2.5-5 ms and Δ_2 is about 2 ms [38,125]. The value of t_1 is incremented during an experiment resulting in a series of spectra in which Fourier transform with respect to t_2 gives the resulting 2-dimensional spectrum. The details of our HETCOR experiments are described in section 2.2.3.

This technique was used in order to assign the ^{13}C resonances of the spectra shown in Figures 3.10 to 3.13. Values for ^{1}H - ^{13}C coupling constants were determined for B15C5 in CD_3NO_2 from a fully coupled spectrum; the J_{CH} values varied from 143 to 146 Hz. It was assumed that the J_{CH} values for the carbons in all the other crown ethers and their complexes were approximately the same and a standard value of 140 Hz was used for all HETCOR experiments. The results obtained are represented by the 2D contour plots shown in Figures 3.15 to 3.18.

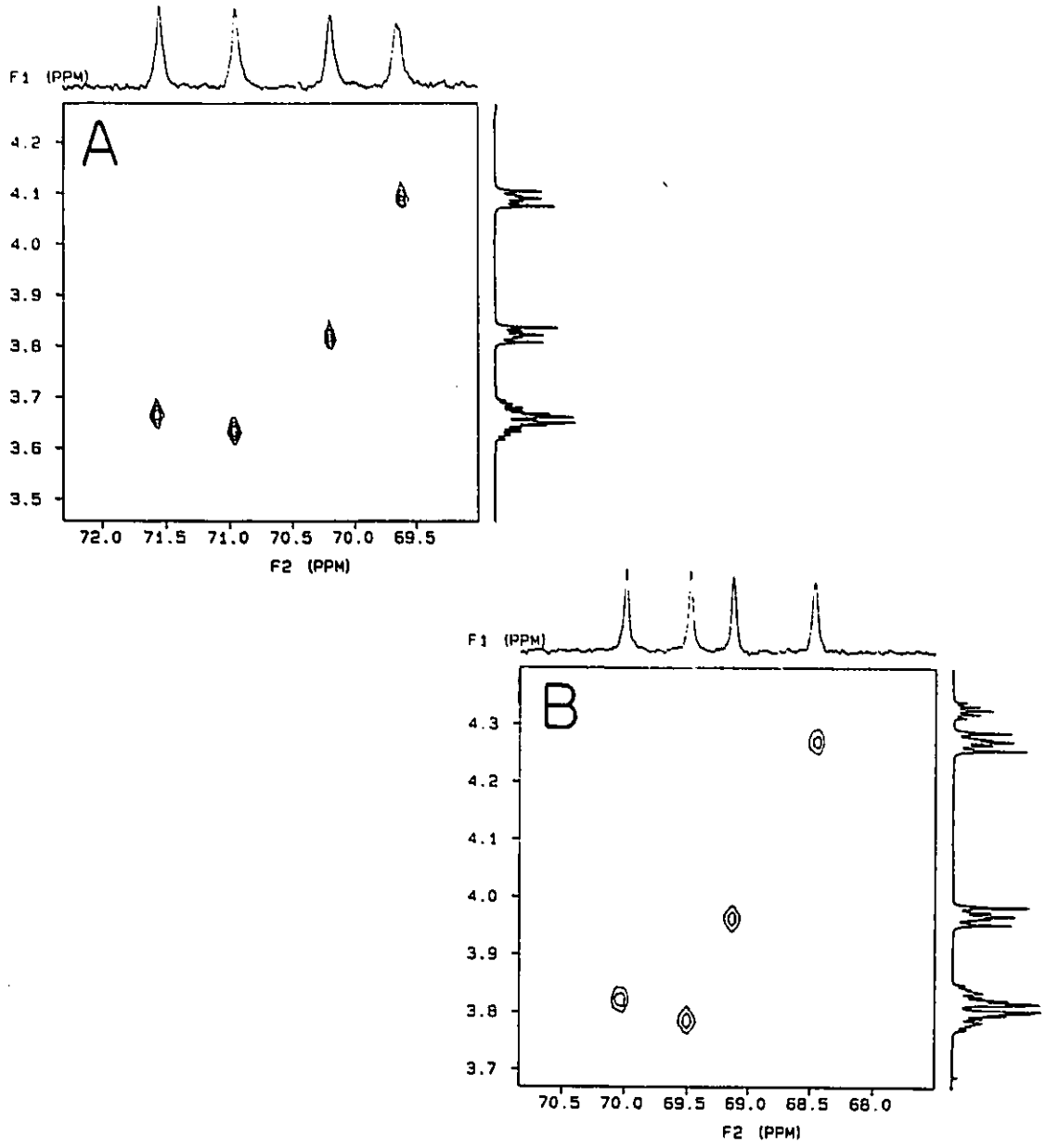

Figure 3.15: HETCOR contour plot of (A) B15C5 and (B) $(Na:B15C5)^+$ in CD_3NO_2 at ambient temperature.

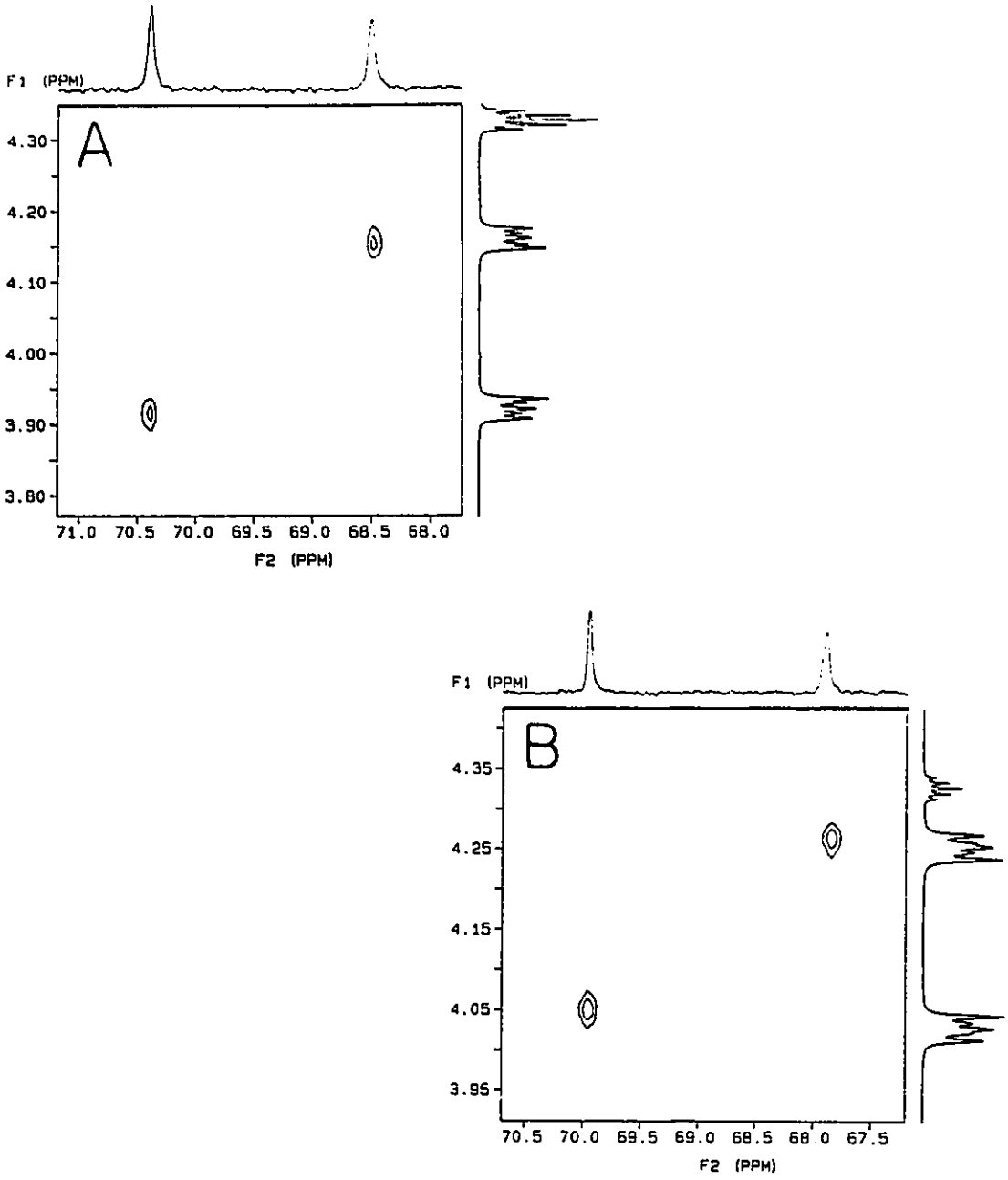

Figure 3.16: HETCOR contour plot of (A) DB18C6 and (B) $(Na:DB18C6)^+$ in CD_3NO_2 at ambient temperature.

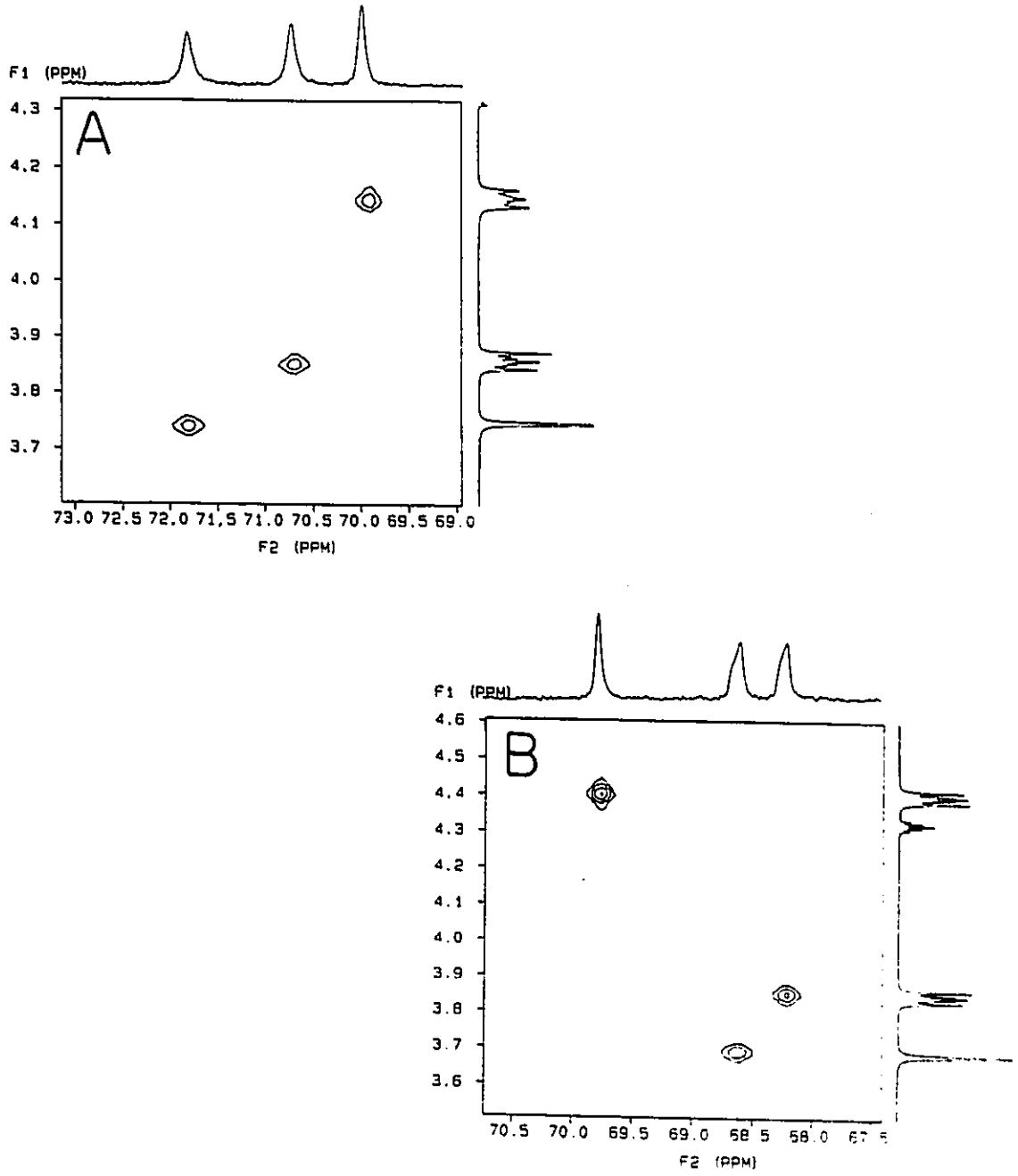

Figure 3.17: HETCOR contour plot of (A) DB24C8 and (B) $(Na:DB24C8)^+$ in CD_3NO_2 at ambient temperature.

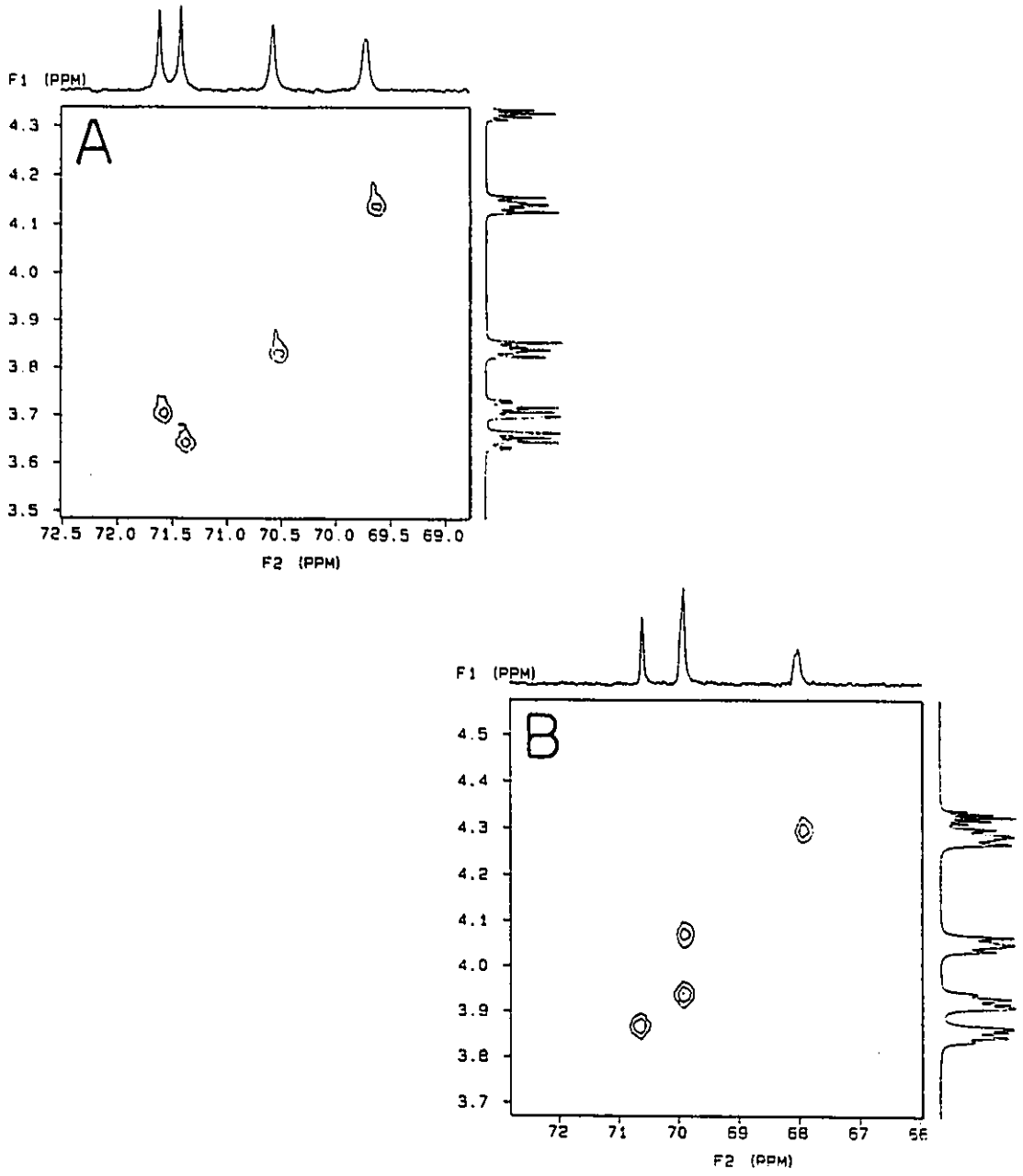

Figure 3.18: HETCOR contour plot of (A) DB30C10 and (B) $(Na{:}DB30C10)^+$ in CD_3NO_2 at ambient temperature.

This method proved to be very successful in the assignment of the crown ether ^{13}C resonances. The assignment of the protons in positions 1 and 2 was based on the ring current anisotropy of the aromatic substituent and from the correlations shown in Figures 3.15 - 3.18, the ^{13}C assignments of those two positions followed. However, since the ^{1}H chemical shifts values of the protons in positions 3 and 4 of B15C5 and DB30C10 were so close, long-range heteronuclear chemical shift correlation experiments were performed in order to unambiguously assign the positions of those protons. In the past five years, several techniques for long-range heteronuclear chemical shift correlation have been developed, the simplest based on optimization for long-range couplings of the standard pulse sequence shown in Figure 3.14 [125]. Since information transfer in 2-D heteronuclear chemical shift correlation, is accomplished through the ^{1}H - ^{13}C couplings, a knowledge of the sizes of the long-range couplings, J_{CCH}, is required. Values of coupling constants for these long-range interactions could not be determined from a fully coupled ^{13}C spectrum of B15C5 since the long-range information consisted of several couplings. The assignments for the protons on C(1) and C(2) for B15C5 and DB30C10 have been unambiguously determined, and we thus wish to observe a long-range coupling between either C(2) and the protons on C(3) or C(3) and the protons on C(2). The first long-range HETCOR experiments consisted of using trial values for J_{CCH} equal to 9 and 12 Hz, selected on the basis of several published results for long-range coupling constants [125]. The HETCOR contour plots, resulting from a concentrated sample of B15C5 in CD_3NO_2, are shown in Figure 3.19. Clearly, the selection of J_{CCH} has a large influence on the final appearance of the contour plots. Since the pulse sequence is optimized for the long-range interactions, it is difficult to predict the appearance or absence of direct one bond C-H interactions [125] and as a consequence, only three of the four direct C-H interactions, also varying in contour intensity, are observed in Figure 3.19(B).

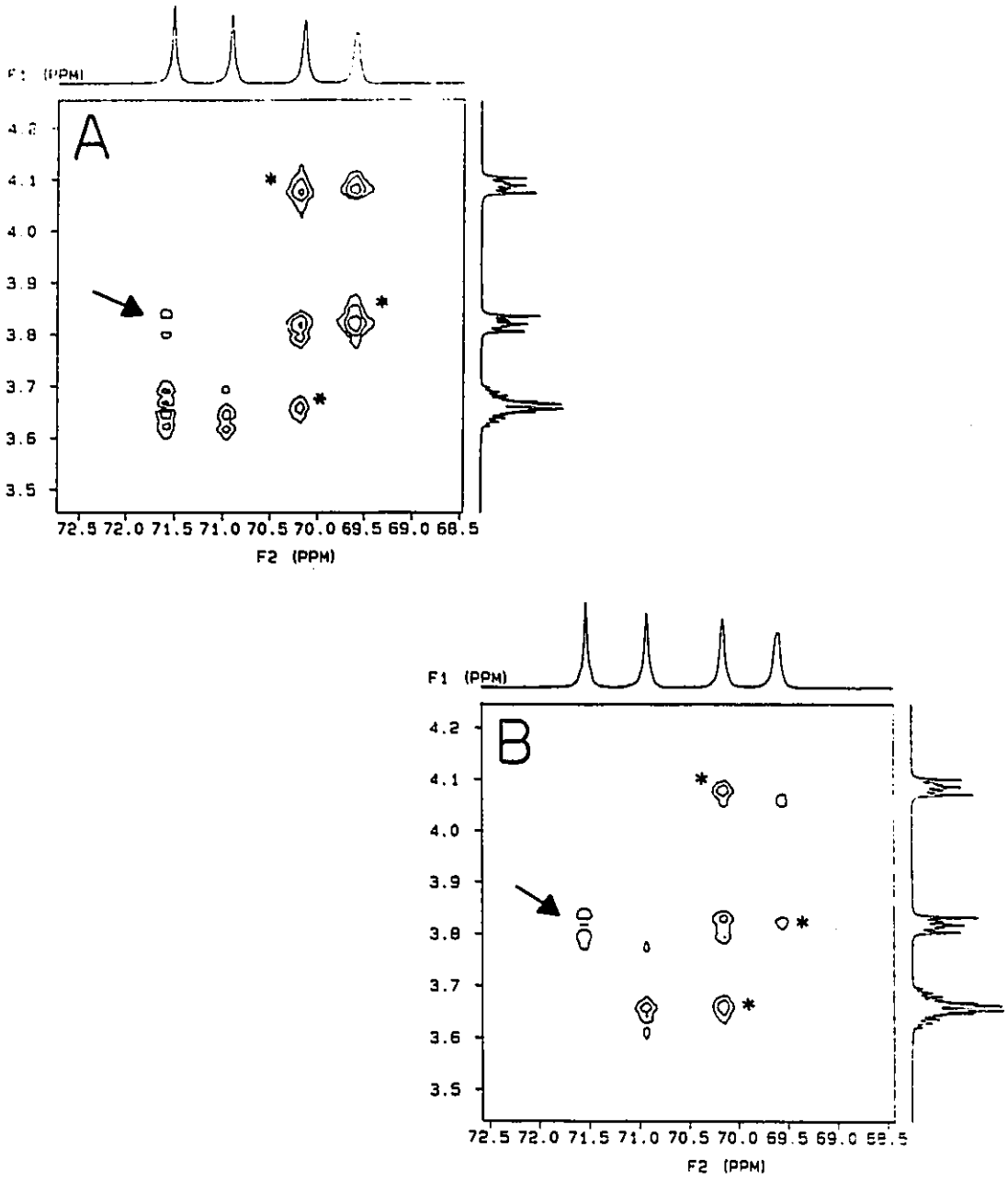

Figure 3.19: Long-range HETCOR contour plot of B15C5 (approximately 200 mg in 1 mL of solvent) in CD_3NO_2 at ambient temperature. (A) $J_{CCH} = 9$ and (B) $J_{CCH} = 12$. The contours marked with a * correspond to the long-range C-C-H interactions only . The contour marked with an arrow is that of interest (see discussion).

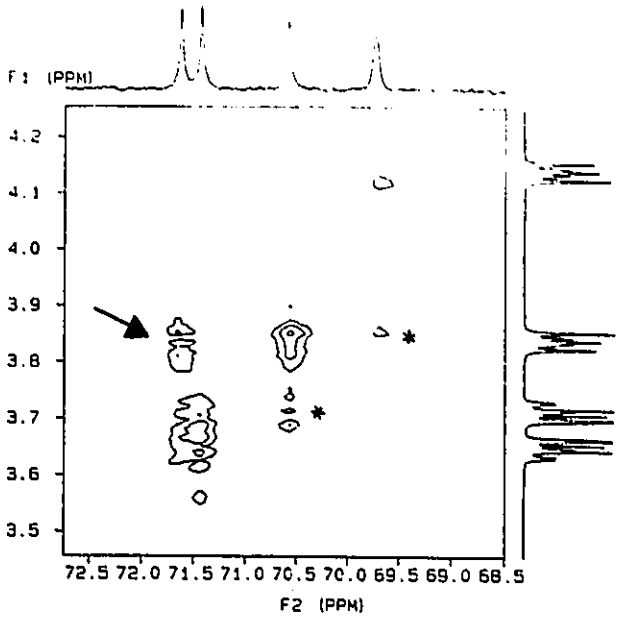

Figure 3.20: Long-range HETCOR contour plot of DB30C10 in CD_3NO_2 at ambient temperature. The contours marked with a * correspond to the long-range C-C-H interactions only. The contour marked with an arrow is that of interest (see discussion).

The following long-range couplings are observed: (a) between C(1) and the protons on C(2), (b) between C(2) and the protons on C(1), (c) an overall long-range coupling between C(2) and the protons on C(3) and C(4) which cannot be distinguished, (d) between C(4) and the protons on C(3) (this is presumably mixed in with the direct C(4)-H coupling), (e) between C(3) and the protons on C(4) (this can only be observed in Figure 3.19(A)) and most importantly (f) a long-range coupling is observed between C(3) and the protons on C(2) which is clearly seen in both Figure 3.19A and 3.19B. It is also clear that there is no long-range interaction between C(4) and the protons on C(2) and this provides conclusive evidence for the assignment. Furthermore, the same

experiment was done with DB30C10 (J_{CCH} = 12 Hz) which also clearly revealed a long-range interaction between C(3) and the protons on C(2) (see Figure 3.20).

Although previous studies have involved ^{1}H and ^{13}C NMR of crown ethers in solution [91,92,110], this is the first mention of unambiguous ^{1}H and ^{13}C ether assignments by determining long-range couplings using the heteronuclear chemical shift correlation technique. The assignment also agrees with that by Live and Chan in 1976 [91] for DB18C6 and DB30C10, who used off-resonance heteronuclear decoupling to assign their ^{13}C spectra.

Chapter 4

Structures, Thermodynamics, Kinetics and Mechanisms: ^{23}Na NMR Study of Sodium Complexes

4.1 Introduction

Sodium is the 6th most abundant element on earth, present in the rocks, oceans, upper atmosphere and many organisms; this element is indeed essential to life [24]. Sodium cations are of great biological importance, for instance, the active transport of both sodium and potassium across cellular membranes, by interaction with natural ionophores, is an essential function in human bodies and accompanies various phenomena such as the firing of the nerve, muscular contractions, brain activity and salt and water transport in the kidneys [24,126]. It is not thus surprising that many studies of cation - macrocycle complexes have implicated the sodium cation where ^{23}Na NMR has been a choice technique with regards to such investigations. As a NMR nucleus, ^{23}Na has a high natural abundance and a high gyromagnetic ratio (see Table 1.1 on page 7)

which makes it easily observed and a good probe for the characterization of Na^+-macrocycle complexes as viewed through the cation. The usual ^{23}Na chemical shift range spans about 40 ppm and macrocyclic complexes of sodium have been observed to fall between 0 and -20 ppm. In this chapter, important insight into the interactions of the sodium cation with benzo-15-crown-5 (B15C5) and 15-crown-5 (15C5) will be shown with the use of ^{23}Na NMR.

4.2 Complexes in Solution

Table 4.1 lists the solvents used in this study along with some relevant properties. Except for PY, these nonaqueous solvents all have similar dielectric constants but the donor numbers span a relatively large range.

Table 4.1: Solvent Properties at 298 K.

Solvent	DN[a]	ϵ[b]	η (mP)[c]	ρ (g/mL)[d]	δ_{corr}[e]
NM	2.7	35.9[f]	6.14	1.131	-1.374
AN	14.1	35.9	3.41	0.776	-0.775
DMF	26.6	36.7	8.02	0.944	-0.415
PY	33.1	12.9	8.84	0.978	-0.452

(a) donor number; reference 32. (b) dielectric constant; reference 50. (c) viscosity; reference 50. (d) density; reference 50. (e) magnetic susceptibility correction; $\delta_{true} = \delta_{obs} + \delta_{corr}$(see section 2.2). (f) at 303 K.

The Gutmann donor number of a solvent [32] is essentially a measure of its electron donating ability (Lewis basicity), where the quantitative value assigned is the positive enthalpy for the dissociation of the donor solvent molecule–antimony(V)-chloride adduct in dichloroethane. As will be shown, it is this property of a solvent which largely governs many aspects of the cation-macrocycle interaction.

The overall equilibrium associated with the formation of the 1:1 sodium-B15C5 (or 15C5) complex is shown in equation 18:

$$(Na^+)_S + (B15C5)_S \overset{K_{F1}}{\rightleftharpoons} (Na{:}B15C5)^+_S \qquad (18)$$

where each separate entity is solvated to some extent. Since information on the coordination sphere of the sodium cation can be obtained by ^{23}Na NMR, the above equilibrium can be monitored by this technique, as shown in Figures 4.1a, 4.1b, 4.2a and 4.2b, where the ^{23}Na chemical shift (δ) and longitudinal relaxation rate (T_1^{-1}) are plotted as a function of $\rho = [C]_T / [Na]_T$ (C = B15C5 or 15C5). These plots are equivalent to titration curves where the concentration of metal cation is kept constant but the concentration of ligand is varied. As can be seen, the relationships displayed between the chemical shifts and ρ (Figures 4.1a and 4.2a) parallel that of the longitudinal relaxation rates (Figure 4.1b and 4.2b) and essentially the same structural and thermodynamic information can be obtained from both ^{23}Na parameters. The overall relationships observed for δ and T_1^{-1} as a function of ρ are governed primarily by two factors: 1) the magnitude of K_{F1} for the formation of $(Na{:}C)^+$ and 2) the possibility for the formation of a second complex, $(C{:}Na{:}C)^+$ referred to as a "sandwich" complex.

As expected, the relationships between δ and ρ, shown in Figure 4.1a, and T_1^{-1} and ρ, shown in Figure 2a, for both 15C5 and B15C5 in NM, are very similar.

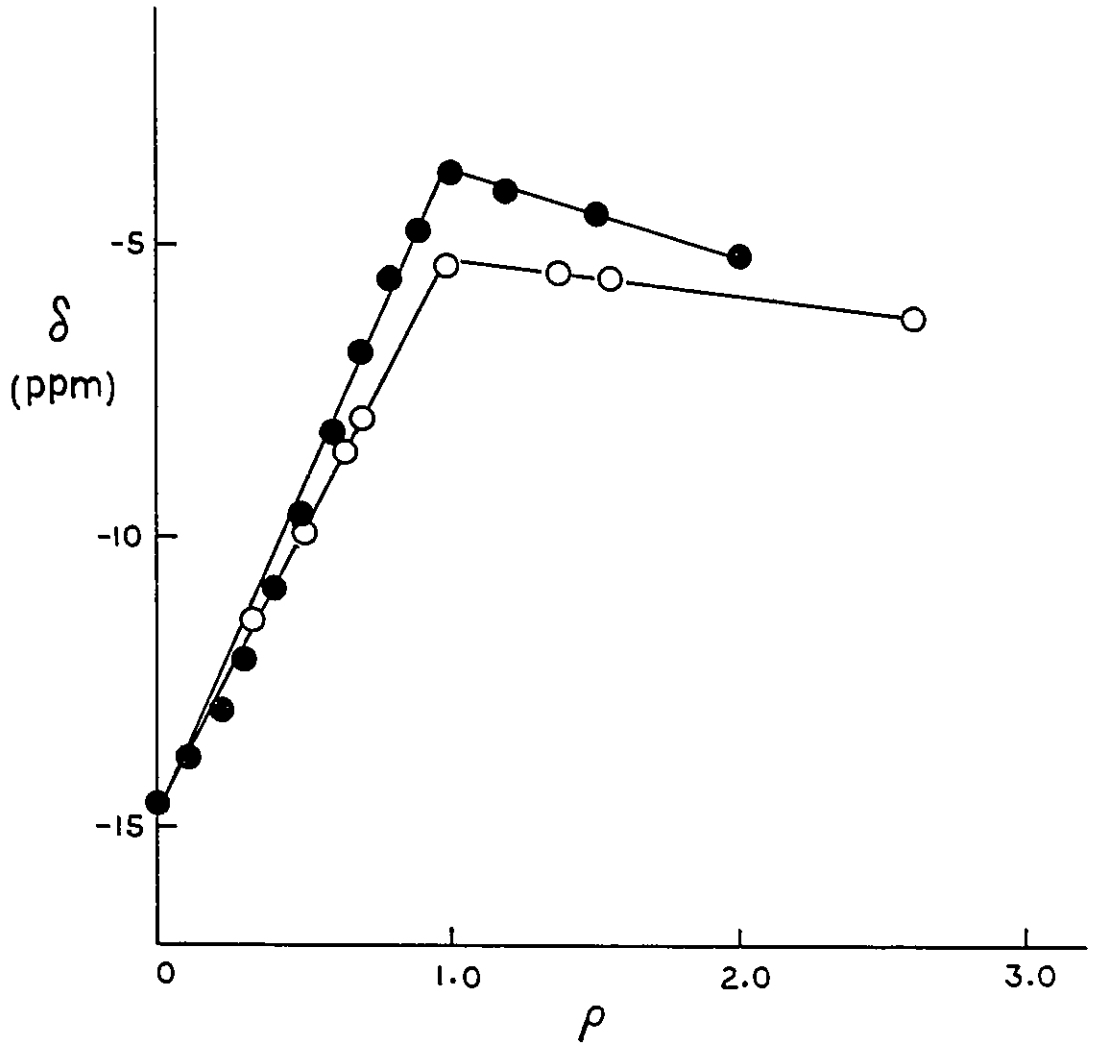

Figure 4.1a: ^{23}Na chemical shift (δ) as a function of $\rho = [C]_T / [NaBPh_4]_T$ in nitromethane at 301.5 K. C = B15C5 (●) and C = 15C5 (○). $[NaBPh_4]_T = 80.0$ mM.

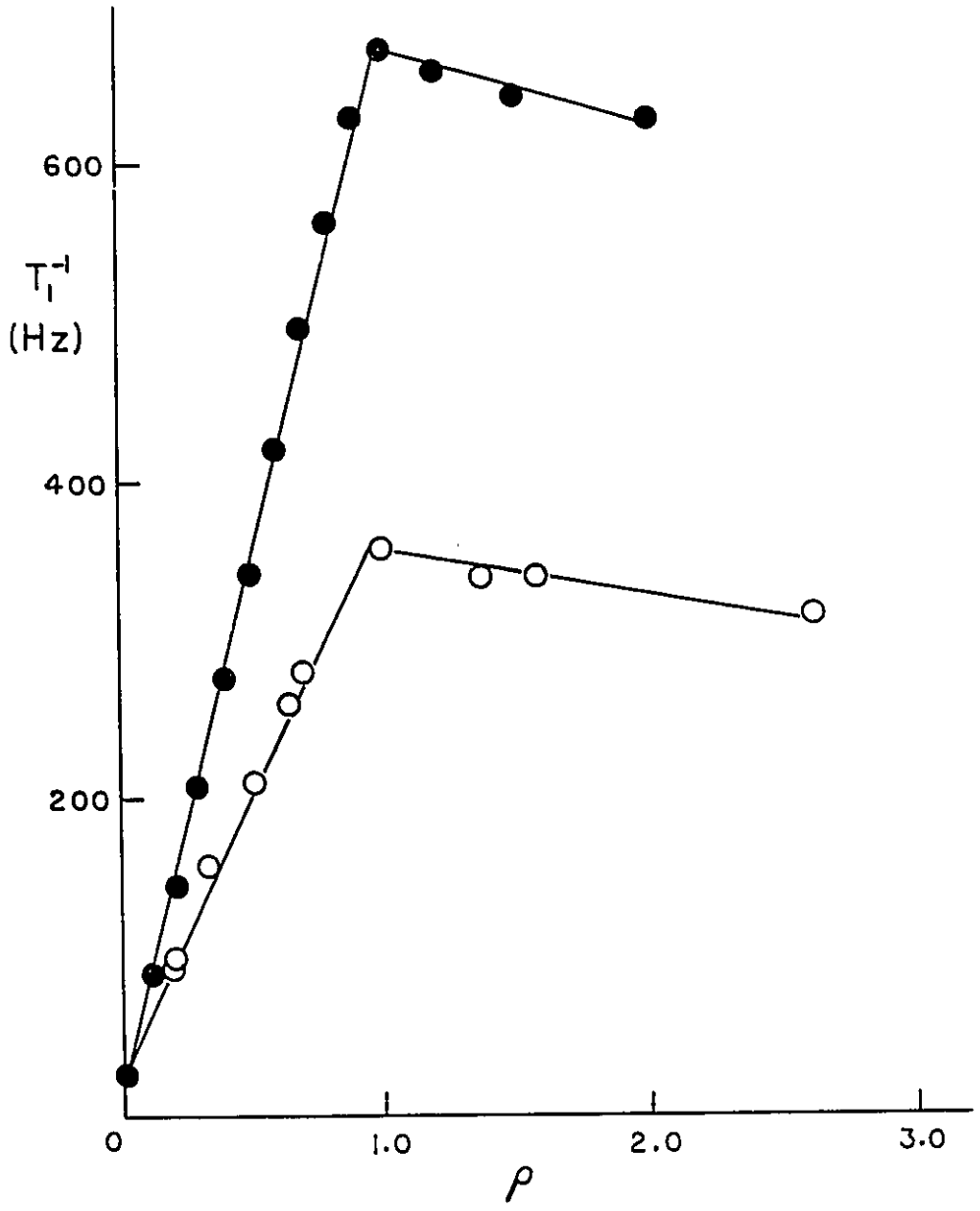

Figure 4.1b: ^{23}Na longitudinal relaxation rates (T_1^{-1}) as a function of $\rho = [C]_T / [NaBPh_4]_T$ at 301.5 K in nitromethane. C = B15C5 (●) and C = 15C5 (○). $[NaBPh_4]_T$ = 80.0 mM.

These results, agree very well with those observed by Lin and Popov for the same systems [88]. At $\rho = 0$ there is no crown ether present and the sodium is completely solvated. The linearity of the plots in the region $0 < \rho \leq 1$ in Figures 4.1a and 4.1b is an indication that the formations of the 1:1 $(Na:B15C5)^+$ and $(Na:15C5)^+$ complexes in NM are quantitative where the formation constants (equation 18) are high: $\log K_{F1} > 4$ [88]. Also, in this region, there is the presence of sodium in two possible sites: solvated, $(Na^+)_S$ (site A), and complexed, $(Na:C)^+_S$ (site B), where there is actually a chemical exchange of sodium in these two sites. This kinetic aspect will be discussed in section 4.3. In the conditions of Figures 4.1a and 4.1b, the chemical exchange is fast on the chemical shift timescale and only one average Lorentzian signal is observed; the chemical shift observed (δ_{obs}) is a weighted average of the two sites:

$$\delta_{obs} = P_A\delta_A + P_B\delta_B \tag{19}$$

where P_A and P_B are the populations of sodium in both sites while δ_A and δ_B are the corresponding chemical shifts. The longitudinal relaxation rate can be substituted for the chemical shift in equation 19.

Since the K_{F1} for complex formation is high, all the sodium present is complexed at $\rho \geq 1$ in Figure 4.1a and 4.1b, but as well in this case, there is further formation of a sandwich complex as indicated by the variation of the chemical shift at $\rho > 1$: $\log K_{F2} = 0.8 \pm 0.3$ for the formation of $(Na:B15C5_2)^+$ in NM [88].

$$(Na:C)^+_S + (C)_S \overset{K_{F2}}{\rightleftharpoons} (C:Na:C)^+ \tag{20}$$

The reversal in chemical shift at $\rho = 1$ is indicative of the formation of a sandwich complex where this has also been observed for other alkali metal cation-crown ether

complexes: $(Li:12C4_2)^+$ [102,127], $(Na:15C5_2)^+$ [88] and $(Cs:18C6_2)^+$ [128,129]. The formation of 1:2 cation-crown ether complexes usually occurs in low donicity solvents when the diameter of the cation is greater than that of the ligand cavity. In this present case, the diameter of Na^+ (2.04 Å) is probably only slightly larger than the cavity of 15C5 / B15C5 (1.7-2.2 Å) [14,16] since the formation of the sodium-B15C5 sandwich complex is only observed in NM (compare with Figure 4.2a). The significant difference observed in the T_1^{-1} values of $(Na:15C5)^+$ and $(Na:B15C5)^+$, at $\rho = 1$ in Figure 4.1b, reflects the overall higher symmetry about sodium in the former complex.

Figures 4.2a and 4.2b show the ^{23}Na chemical shift and longitudinal relaxation rate as a function of $\rho = [B15C5]_T / [NaBPh_4]_T$ in AN, DMF and PY. The linearity of the relationship observed in AN reflects the high degree of formation of $(Na:B15C5)^+$ in this solvent: $\log K_{F1} > 4$ [88]. However, the curved relationships observed in PY and DMF are indicative of a substantially lower extent of the reaction shown in equation 18, which thus results in a lower value for K_{F1}. Based on this equilibrium, it is possible to derive a relationship for the observed chemical shift or longitudinal relaxation rate which is a function of $[Na]_T$, $[B15C5]_T$ and K_{F1} (see Appendix 2). Nonlinear SAS® regressions of both the chemical shift and longitudinal relaxation rate data in PY, gave $\log K_{F1} = 2.9 \pm 0.3$ in both cases, $\delta_{lim} = -1.9 \pm 0.2$ (this represents the chemical shift of $(Na:B15C5)^+$) and $T_1^{-1}{}_{lim} = 265 \pm 18$ (this represents the longitudinal relaxation rate of $(Na:B15C5)^+$). This agrees well with values previously reported by Lin and Popov [88]: $\log K_{F1} = 2.6 \pm 0.1$ and $\delta_{lim} = -2.4 \pm 0.3$. In DMF, $\log K_{F1}$ was determined to be 1.2 ± 0.4 from both the δ and T_1^{-1} data; $\delta_{lim} = -5.9 \pm 0.6$ ppm and $T_1^{-1}{}_{lim} = 273 \pm 84$. This also agrees well with that determined again by Lin and Popov; $\log K_{F1} = 1.6 \pm 0.1$ and $\delta_{lim} = -6.0 \pm 0.3$ ppm [88]. The lower values for K_{F1} in DMF and PY as compared to AN and NM is a reflection of the higher donor numbers of the two former solvents (see Table 4.1).

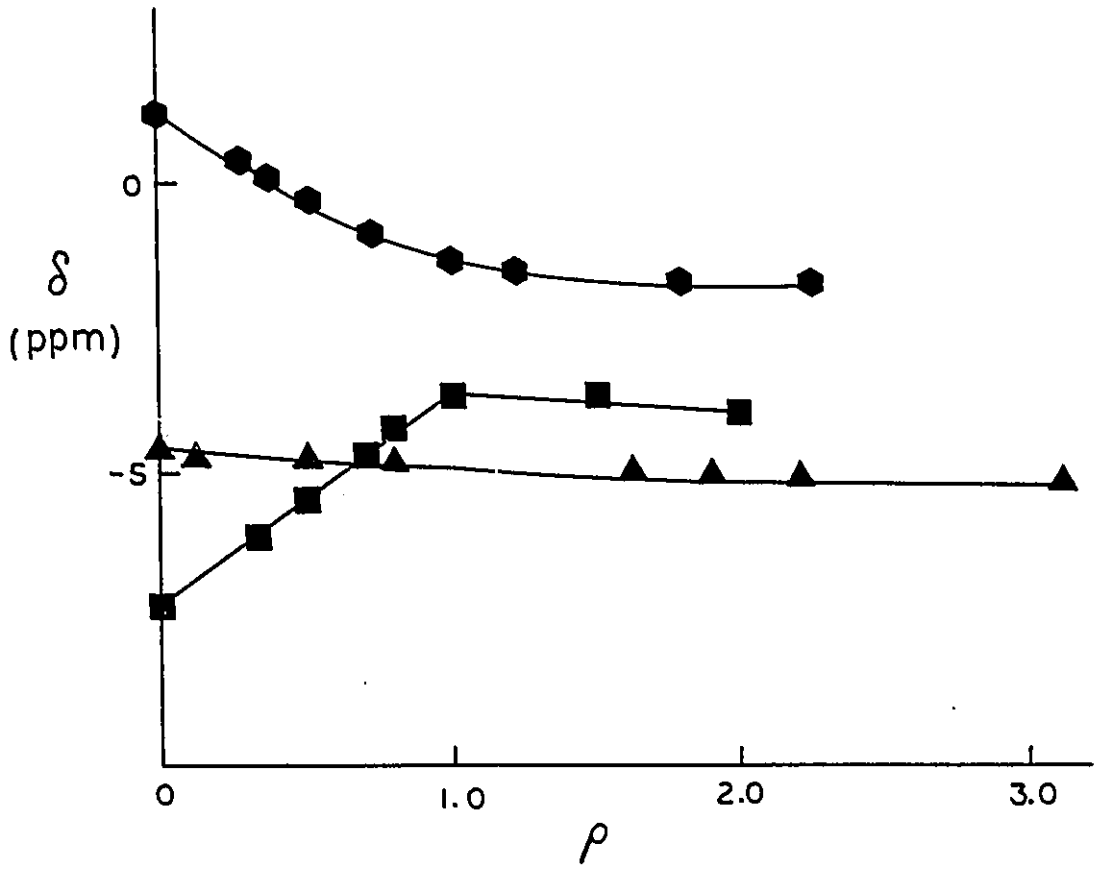

Figure 4.2a: ^{23}Na chemical shift (δ) as a function of $\rho = [B15C5]_T / [NaBPh_4]_T$ at 301.5 K in PY (●), DMF (▲) and AN (■). For PY and DMF, $[NaBPh_4]_T = 20.0$ mM and for AN, $[NaBPh_4]_T = 80.0$ mM. For PY and DMF, the data points are experimental and the curves are calculated based on a model for the formation of the 1:1 complex (see Appendix 2).

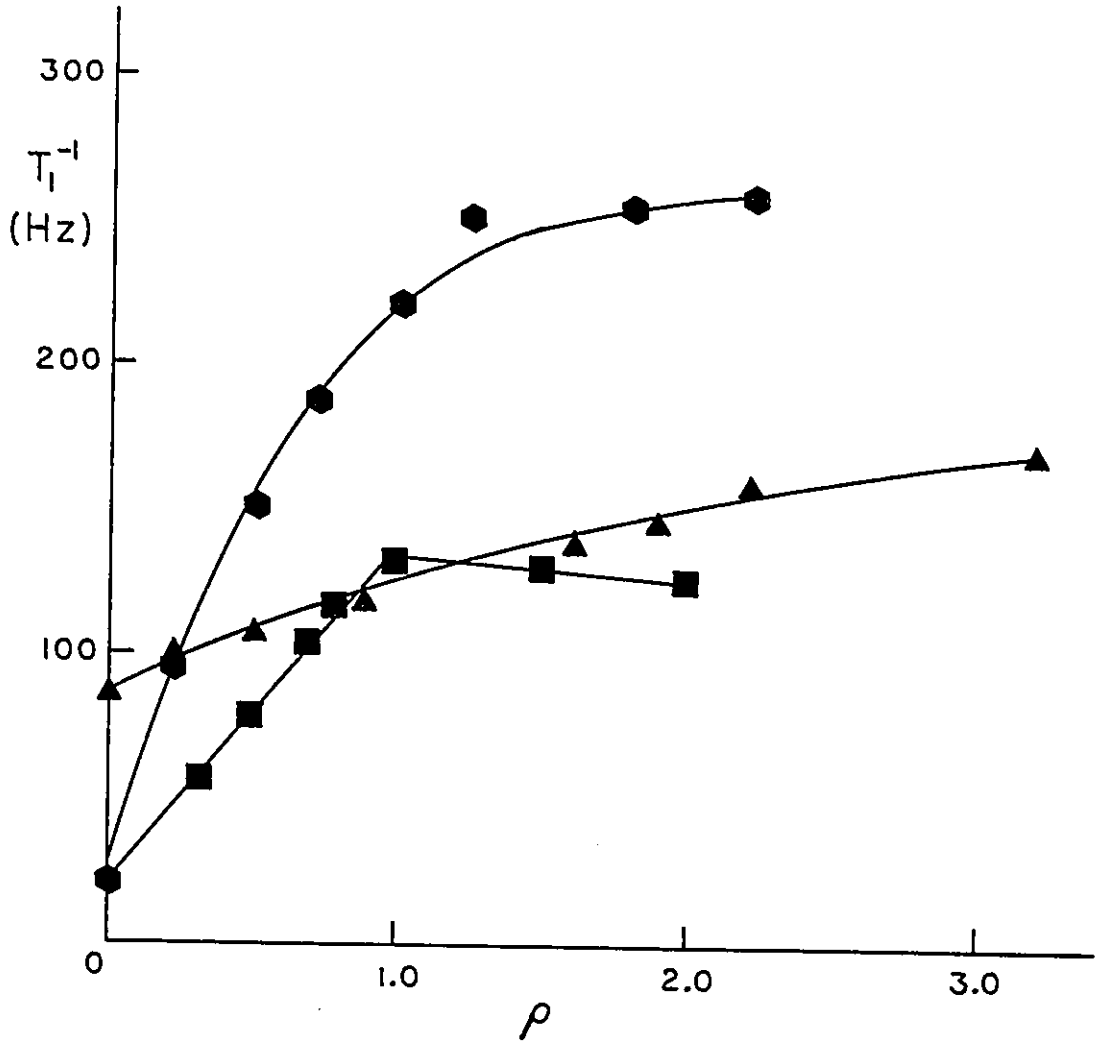

Figure 4.2b: ^{23}Na longitudinal relaxation rates (T_1^{-1}) as a function of $[C]_T$ / $[NaBPh_4]_T$ (ρ) at 301.5 K in PY (●), DMF (▲) and AN (■). For PY and DMF, $[NaBPh_4]_T$ = 20.0 mM and for AN, $[NaBPh_4]_T$ = 80.0 mM. For PY and DMF, the data points are experimental and the curves are calculated based on a model for the formation of the 1:1 complex (see Appendix 2).

DMF and PY effectively compete with B15C5 for sodium coordination sites resulting in the formation of a weaker complex in these two solvents. This also explains the fact that the formation of sandwich complexes is not observed in these two solvents.

A summary of the results shown in Figures 4.1a, 4.1b, 4.2a and 4.2b can be found in Table 4.2. The trend followed for the ^{23}Na chemical shift of $(Na)^+_S$ (at $\rho = 0$) is directly related to the DN of the solvent as discussed in section 1.2.2. Since the chemical shift values for $(Na{:}B15C5)^+$ are not identical in all four solvents, this indicates the direct participation of the solvent in the first coordination sphere of the complexed sodium cation in at least some of the solvents. Looking at equations 8 and 10 shown earlier, one can determine that the measured quadrupolar relaxation rate should be directly proportional to the solvent viscosity if the electric field gradient is independent of the solvent; thus a constant value for the reduced T_1^{-1} (T_1^{-1} / η) is expected. As can be seen in Table 4.2, this is not the case which again indicates a different immediate environment of the sodium cation in each of the solvents.

The results for $(Na{:}B15C5)^+$ can be compared with other ^{23}Na NMR results in a similar study by Detellier and co-workers for $(Na{:}DB30C10)^+$ [103]. This sodium complex also exhibits different chemical shifts and reduced longitudinal relaxation rates indicating the participation of at least one solvent molecule, as well as the ether oxygens of the ligand, in the first coordination sphere of the sodium cation. The behavior of both $(Na{:}B15C5)^+$ and $(Na{:}DB30C10)^+$ is in contrast to that of $(Na{:}DB24C8)^+$ [66] and $(K{:}DB30C10)^+$ [68], where the respective ^{23}Na and ^{39}K NMR studies show that the solvent is completely expelled from the cation coordination sphere. DB24C8 and DB30C10 can form three-dimensional cavities precisely adapted to Na^+ and K^+ respectively, whereas the large DB30C10 and smaller B15C5 do not perfectly adapt themselves to Na^+. The values for the formation constants themselves can also give insight into the degree of "adaptability" of the ligand towards the cation.

Table 4.2: ^{23}Na NMR Characteristics of $(Na)^+_S$ and $(Na:B15C5)^+_S$.

Solvent	δ_S ppm	$T_{1,S}^{-1}$ Hz	δ_C ppm	$T_{1,C}^{-1}$ Hz	$T_{1,C}^{-1}/\eta$ Hz /mP	log K_{F1}
NM[a]	-14.48 ± 0.01	26 ± 1	-3.75 ± 0.05	662 ± 6	108 ± 1	> 4[b]
AN[a]	-7.29 ± 0.01	21 ± 1	-3.71 ± 0.01	157 ± 6	46 ± 2	> 4[b]
DMF[c]	-4.55 ± 0.01	86 ± 1	-5.9[d] ± 0.1	273[d] ± 84	34 ± 5	1.2 ± 0.4
PY[c]	1.20 ± 0.01	48 ± 1	-1.9[d] ± 0.1	265[d] ± 10	30 ± 1	2.9 ± 0.3
NM[a,e]	-	-	-5.30 ± 0.02	365 ± 4	59 ± 1	> 4[b]

(a) $[NaBPh_4]_T$ = 80.0 mM and T = 301.5 K ± 0.5 K. (b) reference 88. (c) $[NaBPh_4]_T$ = 20.0 mM and T = 301.5 ± 0.5 K. (d) limiting values from nonlinear regressions of the data in Figures 4.2a and 4.2b. (e) characteristics of $(Na:15C5)^+$.

Overall, the K_{F1} values for $(K:DB30C10)^+$ are larger than those for $(Na:DB30C10)^+$ [66,68] and those for $(Na:18C6)^+$ larger than those for $(Na:B15C5)^+$ [88]. The crown ether 18C6 thus displays a marked selectivity over B15C5 in the complexation of the sodium cation.

In the complexation equilibria, the possibility of ion-pairing must be considered:

$$(Na)^+_S + (X^-)_S \rightleftharpoons (Na^+,X^-)_S \qquad (21)$$

where X^- is the counteranion in the sodium salt. Others have shown that the presence of ion-pairing, in related studies, can have profound effects on experimental observations [130-132]. With relevance to these types of studies, the extent of ion-pairing, K_{IP}, can be quantitatively determined from alkali metal NMR experiments by observing the desired alkali metal chemical shift as a function of the concentration of alkali metal salt [30,133]. Throughout this work the counteranion associated with the sodium complexes is tetraphenylborate (BPh_4^-). As can be seen in Table 4.3, there is little or no variation in the ^{23}Na chemical shift of $(Na^+)_S$ in NM as a function of $[NaBPh_4]_T$. This is a good indication that ion-pairing, as shown in equation 21, between the sodium cations and the bulky tetraphenylborate anion is minimal in this solvent [134]. This is also the case in AN and since the tendency for sodium ions to form contact ion-pairs is related to solvent donicity [135] one could predict that ion-pairing between the Na^+ and BPh_4^- ions would be nonexistent in DMF and PY. Sodium perchlorate, $NaClO_4$, has limited solubility in NM but again in the range of sodium concentration studied, no ion-pairing effect is observed. A relatively small ion-pairing effect is observed for sodium hexafluorophosphate, $NaPF_6$, also in NM. The chemical shifts of $(Na{:}B15C5)^+$ do not vary significantly as a function of $[Na^+]_T$ and thus it is not likely that these three counteranions are associated with the complexed sodium. Those sodium salts listed in Table 4.3 are the only three used in this study. The data shown in Table 4.3 was included in this thesis in order to illustrate and confirm the negligible role of ion-pairing in any equilibria or mechanism which is presented here. These variations (or absence of) in chemical shifts are also paralleled by the relaxation rates.

Table 4.3: ^{23}Na NMR Chemical Shifts of $(Na)^+_S$ and $(Na:B15C5)^+$ in Nitromethane and Acetonitrile.

Counteranion (solvent)	$[Na^+]_T$ mM	δ_S[a] ± 0.01 ppm	δ_C[b] ± 0.05 ppm
BPh_4^- (NM)	80.0	-14.48	-3.75
	59.9	-14.42	-3.74
	40.0	-14.45	-3.75
	20.0	-14.41	-3.71
	8.0	-14.43	-3.74
	4.0	-14.37	-3.67
BPh_4^- (AN)	80.1	-7.29	-3.71[c]
	50.0	-7.29	-3.71
	40.1	-7.29	-3.70
	5.0	-7.25	-3.68
ClO_4^- (NM)	10.0	-14.27	-3.73
	5.0	-14.27	-3.64
PF_6^- (NM)	20.6	-14.60	-3.83
	10.3	-14.46	-3.82
	5.0	-14.33	-3.74

(a) δ_S is the ^{23}Na chemical shift of $(Na^+)_S$. (b) δ_C is the ^{23}Na chemical shift of $(Na:B15C5)^+$. (c) in AN the error on δ_C is ± 0.01.

4.3 Two-Site Chemical Exchange

Since the interactions between alkali metal cations and macrocyclic ligands are dynamic in nature, these systems can also be studied kinetically by alkali metal NMR. We have already seen that the formation of these complexes in nonaqueous solution is usually close to the diffusion control limit (see section 1.1) [18,19], and it is thus the dissociation of the complex, responsible for the selectivity of interaction, which is of interest. The corresponding values of the rate constants involved in the dissociation of alkali metal-crown ether complexes often fall in the range where they can be measured by alkali metal NMR (typically 10^2 - 10^5 s^{-1}), making this a choice technique for such investigations.

Generally, two sites are considered when describing the chemical exchange of the alkali metal cation:

$$(M^+)_S \underset{k_B}{\overset{k_A}{\rightleftharpoons}} (M{:}C)^+_S \qquad (22)$$

where $(M^+)_S$ refers to the solvated metal cation (site A), $(M{:}C)^+_S$ refers to the complexed cation (site B) and k_A and k_B are the rate constants for the forward and reverse reactions respectively. The lifetime of the cation is site A is $\tau_A = 1 / k_A$ and the lifetime of the cation is site B is $\tau_B = 1 / k_B$. The mean lifetime, τ, of M^+ in the two sites = $P_A / k_B = P_B / k_A = (k_A + k_B)^{-1}$ where P_A and P_B are the respective populations of the cation in both sites.

In the absence of chemical exchange the observed transverse relaxation rate has quadrupolar relaxation and instrument inhomogeneity contributions:

$$T_{2,obs}^{-1} = \pi\nu_{1/2} = T_{2,q}^{-1} + T_{2,inh}^{-1} \quad (23)$$

Since the $T_{2,obs}^{-1}$ is also related to the line-width of a Lorentzian peak, it may be determined directly from the observed spectrum. In extreme narrowing conditions, the presence of chemical exchange markedly affects the transverse relaxation rate, T_2^{-1}, while not affecting the longitudinal relaxation rate, T_1^{-1}. As a result the lineshape of the observed spectrum is altered and another contribution to the observed T_2^{-1} is introduced: $T_{2,ex}^{-1}$. If the spectrum remains Lorentzian shaped, an increase in $T_{2,obs}^{-1}$ will result in a broadening of the line. Since in extreme narrowing conditions $T_{2,q}^{-1}$ and $T_{1,q}^{-1}$ are equivalent:

$$T_{2,ex}^{-1} = T_{2,obs}^{-1} - T_{1,q}^{-1} - T_{2,inh}^{-1} \quad (24)$$

Essentially then, the exchange contribution to the observed transverse relaxation, is the difference between the observed transverse relaxation rate, which is measured directly from the spectrum (equation 23), and the longitudinal relaxation rate, which is independently measured. A graphical representation of this is shown in Figures 4.3 and 4.4 [136,137]. In these figures, both the transverse and longitudinal relaxation rates are plotted as a function of ρ, where $\rho = [C]_T / [NaBPh_4]_T$ (C = 15C5 in Figure 4.3 and B15C5 in Figure 4.4). The experimental conditions are identical in both cases; the $[NaBPh_4]_T$ remains constant at 80.0 mM and as ρ increases the $[C]_T$ increases. The behavior of T_1^{-1} as a function of ρ was described in section 4.2 (Figure 4.1b) and since under ideal conditions in the absence of chemical exchange the two relaxation rates should be equivalent, the instrument inhomogeneity contribution to the observed transverse relaxation can be determined when $\rho > 1.0$ (in the absence of chemical exchange); it is about 30 and 10 Hz in Figures 4.3 and 4.4 respectively.

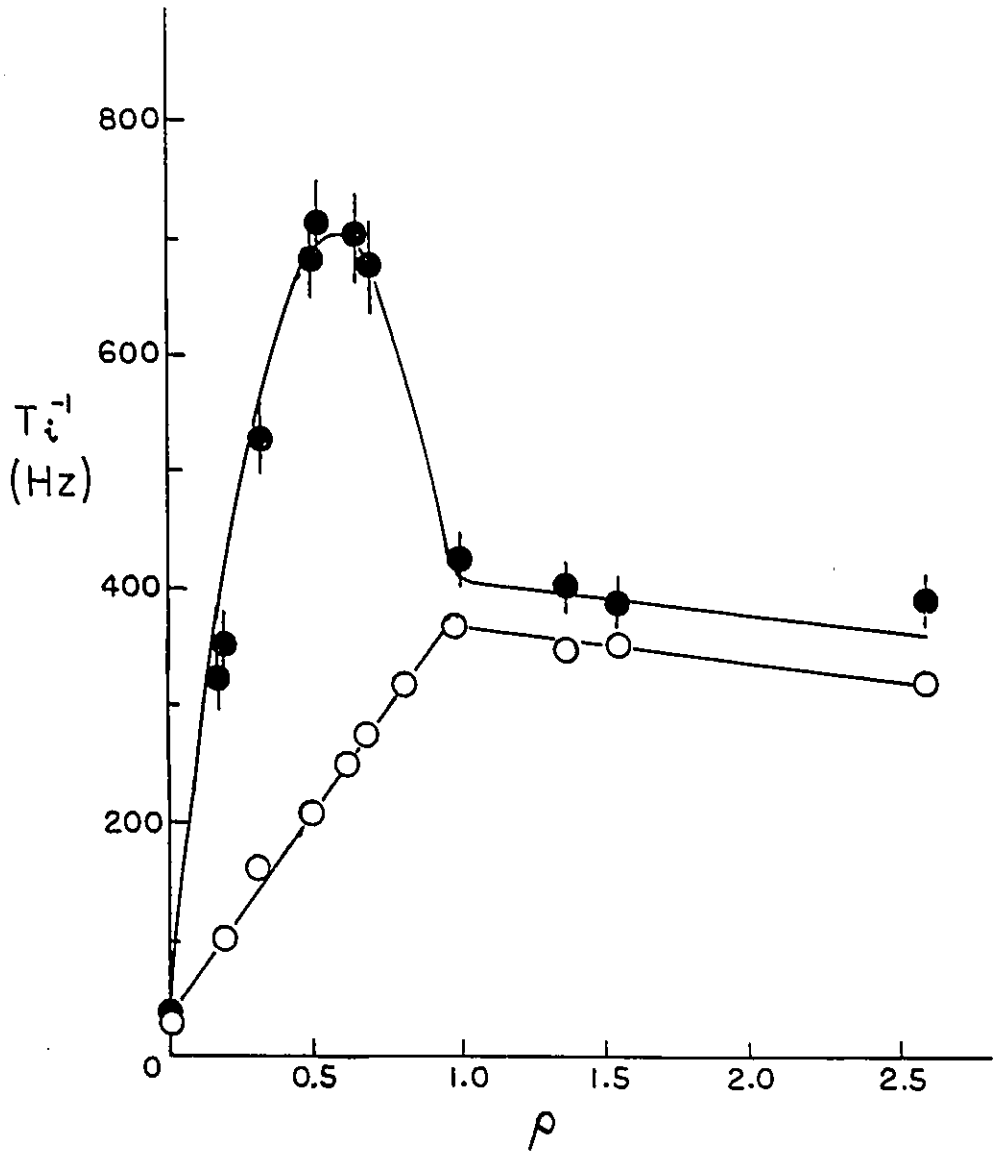

Figure 4.3: ^{23}Na transverse (i = 2; ●) and longitudinal (i = 1; ○) relaxation rates as a function of the ratio $\rho = [15C5]_T / [NaBPh_4]_T$ in nitromethane. T = 301.5 ± 0.5 K; $[NaBPh_4]$ = 80.0 mM. The data points are experimental and the T_2^{-1} curve has been calculated based on equation 25 from the determined k_2 value: ($k_2 = 1.45 \pm 0.05$) × 10^5 M^{-1} s^{-1}.

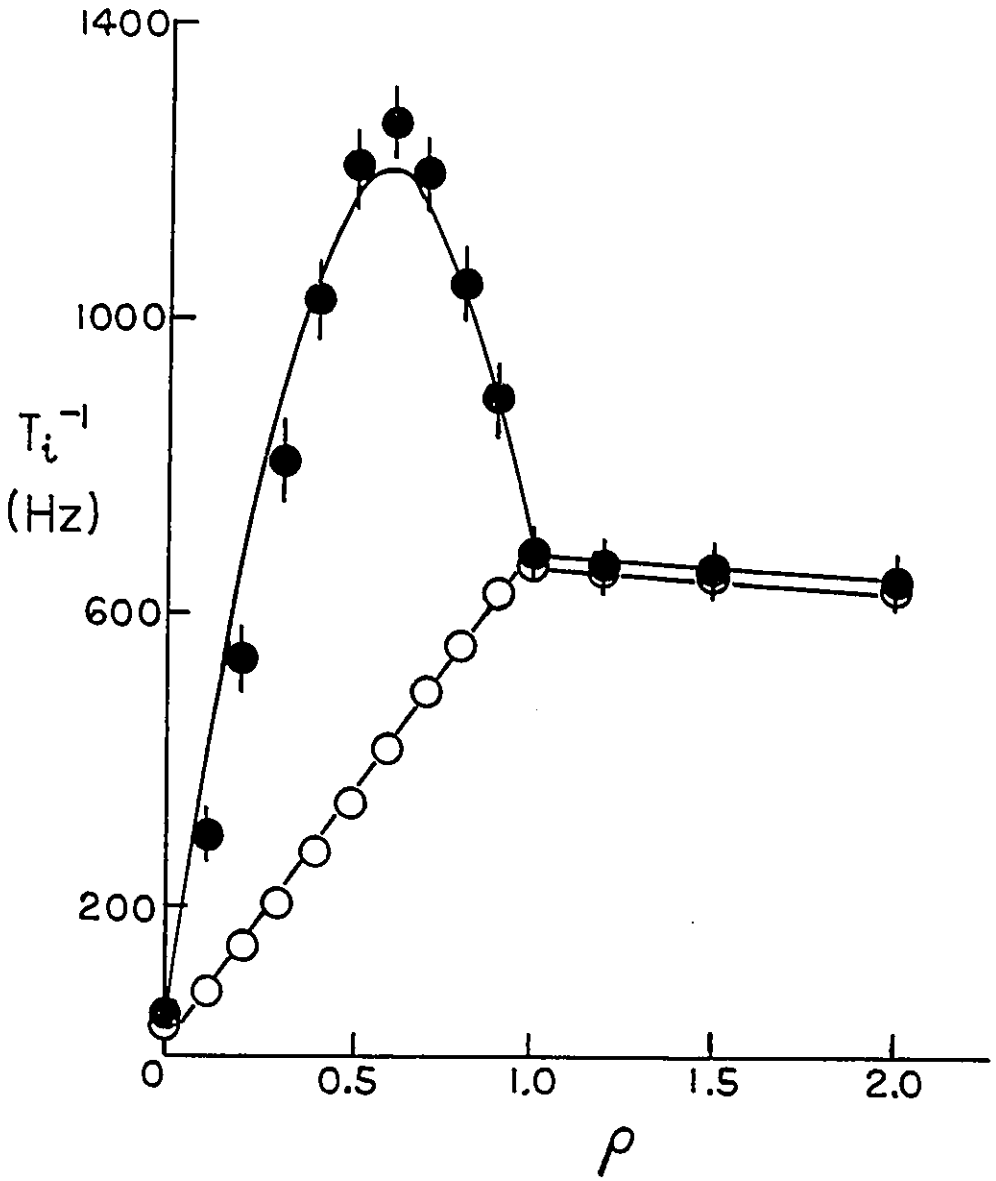

Figure 4.4: ^{23}Na transverse (i = 2; ●) and longitudinal (i = 1; ○) relaxation rates as a function of the ratio $\rho = [B15C5]_T / [NaBPh_4]_T$ in nitromethane. T = 301.5 ± 0.5 K; $[NaBPh_4]$ = 8.01 mM. The data points are experimental and the T_2^{-1} curve has been calculated based on equation 25 from the determined k_2 and k_{-1} values: $k_2 = (1.09 \pm 0.04) \times 10^5\ M^{-1}\ s^{-1}$ and $k_{-1} = (1.1 \pm 0.1) \times 10^2\ s^{-1}$.

As well, the lower value of T_1^{-1} (365 Hz) for $(Na:15C5)^+$ (ρ = 1.0 in Figure 4.3) as compared to the value of T_1^{-1} (660 Hz) for $(Na:B15C5)^+$ (ρ = 1.0 in Figure 4.4) reflects the greater symmetry around sodium in $(Na:15C5)^+$. As can be seen, in the region where the sodium cation can occupy the two different sites ($0 < \rho < 1$), the linewidth of the ^{23}Na NMR spectrum, as denoted by the transverse relaxation rate, has been broadened due to the presence of chemical exchange. This behavior is characteristic of a system undergoing "moderately rapid" exchange (the lineshapes remain Lorentzian shaped) and it can be shown that in these conditions [138,139]:

$$T_{2,ex}^{-1} = 4 P_A P_B \pi^2 (\nu_A - \nu_B)^2 (k_A + k_B)^{-1} \qquad (25)$$

where ν_A and ν_B are the chemical shifts, expressed in Hz, of the two respective sodium sites. Equation 25 is valid when k_A , $k_B > T_{2A}^{-1}$, T_{2B}^{-1}, $2\pi |(\nu_A - \nu_B)|$ and $4\pi^2 (\nu_A - \nu_B)^2 \gg (T_{2A}^{-1} - T_{2B}^{-1})^2$. The second condition can be verified in the cases shown in Figures 4.3 and 4.4: $4\pi^2 (\nu_A - \nu_B)^2$ is at least two orders of magnitude greater than $(T_{2A}^{-1} - T_{2B}^{-1})^2$ for sodium with 15C5 and B15C5. Therefore, quantitative values of $(k_A + k_B)$, describing the dynamic activity in solution, may be relatively easily obtained from the exchange contribution to $T_{2,obs}^{-1}$. Figure 4.5 illustrates this exchange contribution by showing a plot of $T_{2,ex}^{-1}$ as a function of ρ for $(Na:B15C5)^+$ in NM obtained from the data in Figure 4.4. The parabolic shape of the curve with a maximum at $\rho = 0.5$ is in agreement with equation 25 and indicates that the $(k_A + k_B)$ is constant throughout the range $0 < \rho < 1$. Since the equilibrium constant for the formation of $(Na:B15C5)^+ > 10^4$ [88], one can equate ρ with P_B ($P_A = 1 - \rho$) and the product $P_A P_B$ has a maximum value of 0.5. The kinetic behavior of Na^+ with 15C5 (Figure 4.3) and B15C5 (Figure 4.4) under identical conditions is similar except that there is a greater contribution of $T_{2,ex}^{-1}$ to $T_{2,obs}^{-1}$ in the case of B15C5 which indicates a lower overall rate of exchange, $(k_A + k_B)$.

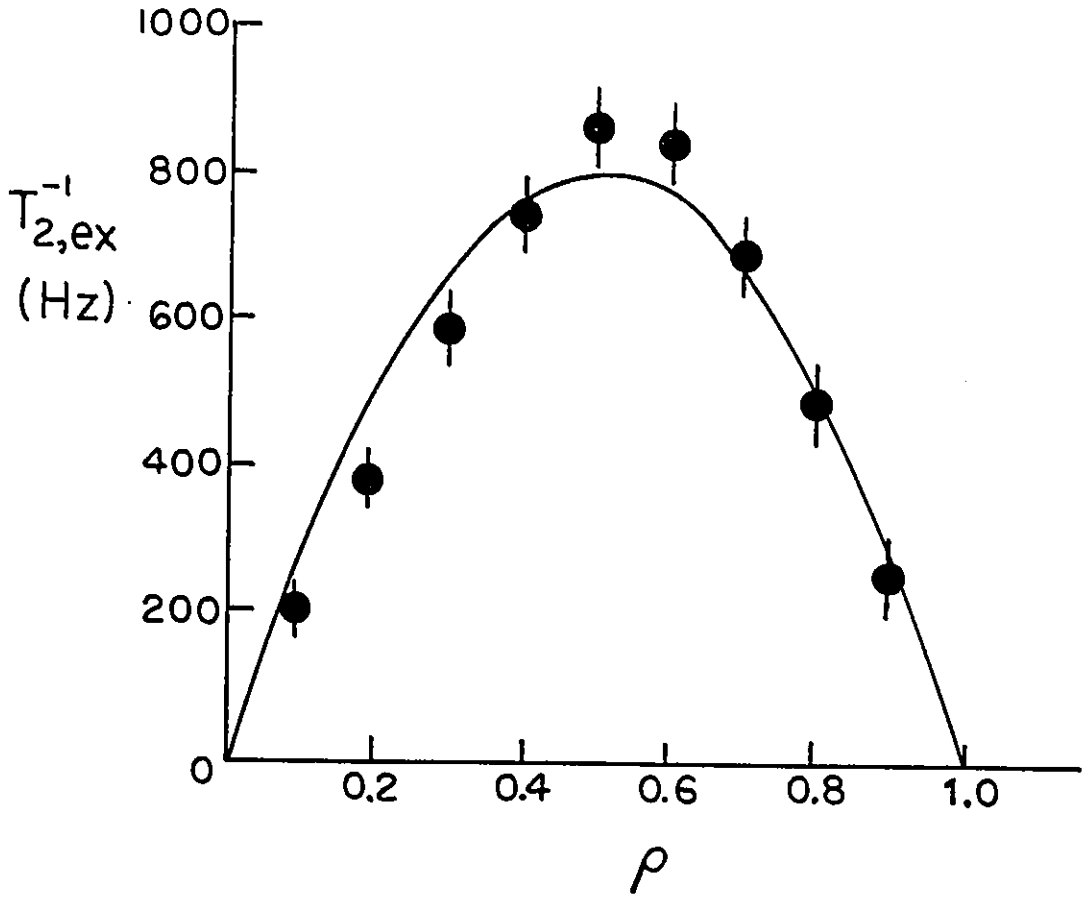

Figure 4.5: $T_{2,ex}^{-1}$ as a function of $\rho = [B15C5]_T / [NaBPh_4]_T$. T = 301.5 ± 0.5 K. $[NaBPh_4]_T$ = 80.0 mM. The data points are calculated from the data shown in Figure 4.4 and the solid line is calculated based on equation 25 from the determined k_2 and k_{-1} values: $k_2 = (1.09 \pm 0.04) \times 10^5\ M^{-1}\ s^{-1}$ and $k_{-1} = (1.1 \pm 0.1) \times 10^2\ s^{-1}$.

Table 4.4 contains values for the sum of the two pseudo-first order rate constants, (k_A + k_B), calculated with equation 25, as well as determined from complete lineshape analyses (see section 2.3.1).

Table 4.4: Kinetic Data for Sodium Chemical Exchange in Nitromethane[a].

C = 15C5 ν_A = -1142 ± 13 Hz ν_B = -424 ± 1 Hz	P_B (ρ)	$T_{2,ex}^{-1}$ (Hz)	$(k_A + k_B)^b$ ($\times 10^3$ s^{-1})	$(k_A + k_B)^c$ ($\times 10^3$ s^{-1})
	0.18	198 ± 14	13.3 ± 1.4	13.3 ± 0.7
	0.20	224 ± 16	14.5 ± 1.6	13.6 ± 0.7
	0.33	347 ± 28	13.0 ± 1.6	12.3 ± 0.6
	0.51	442 ± 33	11.5 ± 1.2	11.8 ± 0.6
	0.52	472 ± 42	10.7 ± 1.4	11.5 ± 0.6
	0.64	421 ± 46	11.1 ± 1.6	11.4 ± 0.6
	0.70	373 ± 31	11.4 ± 1.4	11.0 ± 0.6
C = B15C5 ν_A = -1155 ± 25 Hz ν_B = -298 ± 1 Hz				
	0.22	385 ± 26	12.4 ± 2.0	9.9 ± 0.5
	0.30	592 ± 45	10.2 ± 1.7	8.7 ± 0.4
	0.40	743 ± 43	9.4 ± 1.1	8.7 ± 0.4
	0.50	856 ± 45	8.5 ± 0.9	9.1 ± 0.5
	0.60	839 ± 43	8.3 ± 0.9	9.0 ± 0.5
	0.70	693 ± 43	8.8 ± 1.0	8.6 ± 0.4
	0.80	476 ± 41	9.7 ± 1.4	8.9 ± 0.5
	0.90	253 ± 44	11.1 ± 2.5	8.3 ± 0.4

(a) $[NaBPh_4]_T$ = 80.0 mM and T = 301.5 ± 0.5 K. (b) calculated using equation 25. (c) determined from complete lineshape analyses (method 1; see section 2.3.1).

As they should be, the results obtained for $(k_A + k_B)$ by both methods are identical within experimental error. The $(k_A + k_B)$ values for 15C5 are greater than the $(k_A + k_B)$ values for B15C5 reflecting the greater overall rate of exchange of sodium with 15C5 in otherwise identical conditions. The observation that $(k_A + k_B)$ is independent of ρ with both crown ethers, is significant and will be discussed later.

As the rate of exchange decreases on the NMR chemical shift timescale, there are spectacular changes in the lineshape as it ceases to be Lorentzian. This is illustrated in Figure 4.6 for a series of solutions containing equal populations of sodium in solvated (NM) and complexed to B15C5 forms. For spectra which are non-Lorentzian, full lineshape analyses must be performed in order to extract a value for $(k_A + k_B)$ [46]. As the sodium concentration decreases from 80.0 to 4.0 mM, the $(k_A + k_B)$ also decreases from $(9.1 \pm 0.5) \times 10^3$ to $(7.0 \pm 0.4) \times 10^2$ s^{-1}. The observed dependence of the exchange rate by the concentration of sodium cations is indicative about the specific mechanism by which the exchange takes place.

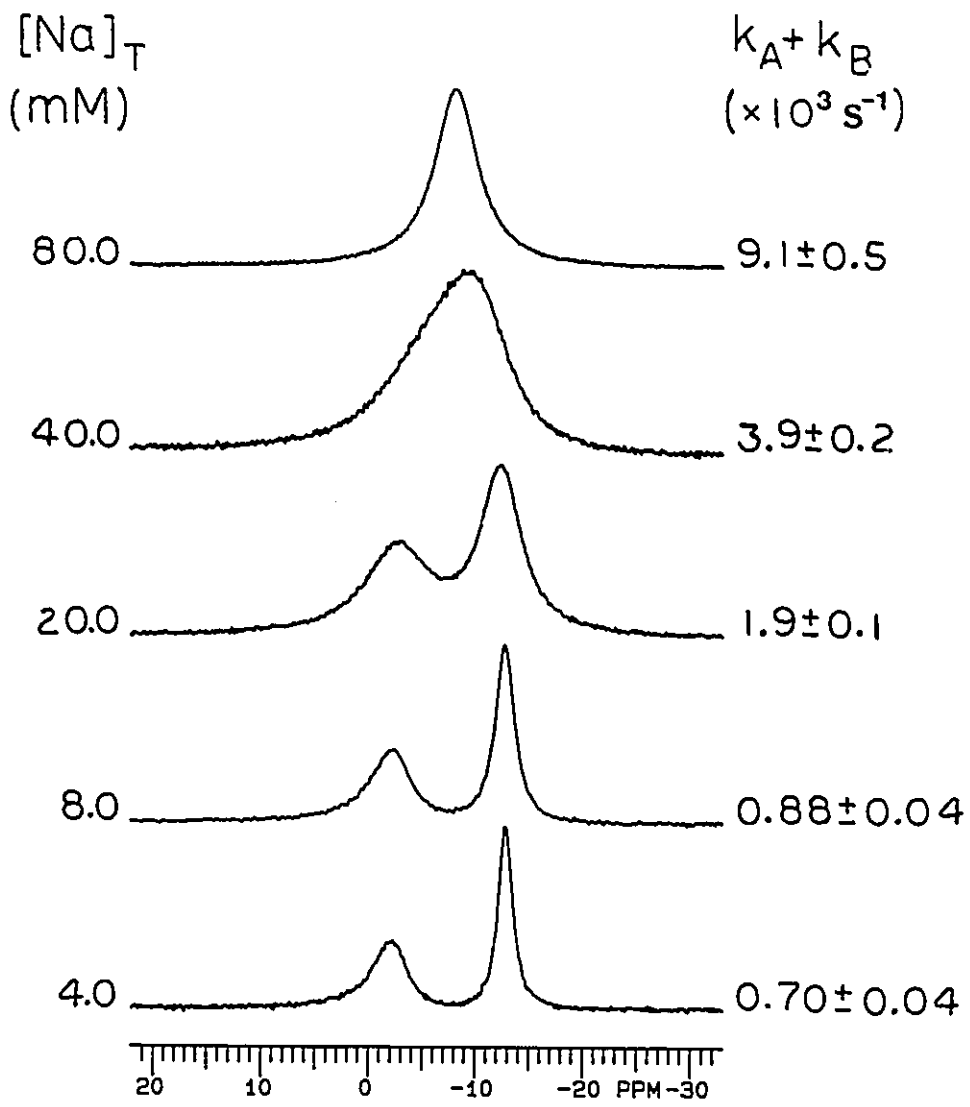

Figure 4.6: ^{23}Na NMR spectra of solutions containing equal populations of $(Na^+)_S$ and $(Na{:}B15C5)^+$ (ρ = $[B5C5]_T$ / $[NaBPh_4]_T$ = 0.50) in nitromethane at T = 301.5 ± 0.5 K. From top to bottom, the $[NaBPh_4]_T$ and sum of the pseudo-first order rate constants, (k_A + k_B), vary as shown.

4.4 Mechanistic Interpretation of the Chemical Exchange

The sum of the two pseudo-first order rate constants ($k_A + k_B$), can be interpreted in a meaningful way only if the corresponding mechanism of exchange is known, and, for this purpose, models have to be designed and tested. Two simple mechanisms for the two-site chemical exchange (equation 22), initially postulated by Shchori et al. [140,141], have been successful in accounting for the kinetic data obtained in several related NMR studies (see Appendix 3) [17,19,128,130-132,136,137,140-164]. The first mechanism is referred to as ***dissociative exchange*** and is comprised of the following two equations:

$$(M{:}C)^+ \underset{k_1}{\overset{k_{-1}}{\rightleftharpoons}} M^+ + C \qquad (26a)$$

$$M^{+*} + C \underset{k_{-1}}{\overset{k_1}{\rightleftharpoons}} (M^*{:}C)^+ \qquad (26b)$$

As it is shown, the chemical exchange of sodium in its solvated and complexed sites is accomplished by the dissociation of the complex to give the free cation and free ligand or by the association of the free cation and free ligand to give the complex (equation 26a). This mechanism is propagated with the interaction of different species in solution (equation 26b). In this case, the rates for the appearance of the solvated and complexed sodium can be expressed as:

$$d[M^+] / dt = k_{-1} [M{:}C^+] = k_B [M{:}C^+] \qquad (27)$$

$$d[M:C^+] / dt = k_1 [M^+][C] = k_A [M^+] \quad (28)$$

and therefore:

$$(k_A + k_B) = k_1 [C] + k_{-1} \quad (29)$$

Since equilibrium constants for the formation of these complexes are typically very high, $[M:C^+]_T \equiv [C]_T$, equation 30 may be derived from equation 29:

$$k_A + k_B = k_{-1} (1-\rho)^{-1} \quad (30)$$

where again $\rho = [C]_T / [M^+]_T$. The chemical exchange may also proceed via a second mechanism referred to as ***associative exchange***:

$$M^{*+} + (M:C)^+ \overset{k_2}{\rightleftharpoons} M^+ + (M^*:C)^+ \quad (31)$$

where the chemical exchange of sodium by this mechanism is achieved with the interaction of another sodium cation where in the transition state one can visualize the simultaneous binding of two cations, wholly or partially bound on opposite faces of the ligand. Equation 31 is the sum of equations 26a and 26b where the exchange is accomplished in one step. In this case, the rates for the appearance of the solvated and complexed sodium can be expressed as:

$$d[M^+] / dt = k_2 [M^+][M:C^+] = k_B [M:C^+] \quad (32)$$

$$d[M:C^+] / dt = k_2 [M^+][M:C^+] = k_A [M^+] \quad (33)$$

and therefore:

$$(k_A + k_B) = k_2 [M^+] + k_2 [M{:}C^+] = k_2 [M^+]_T \quad (34)$$

At this stage we can obtain qualitative information about the chemical exchange of sodium between its solvated (NM) and its complexed (B15C5 and 15C5) states. If the exchange proceeded via the dissociative pathway (equation 26) then there should be a variation of $(k_A + k_B)$ as a function of ρ (equation 30). From the results shown in Table 4.4, we can conclude that this is not so.

If these two mechanisms for the chemical exchange are the only ones considered then:

$$(k_A + k_B) = k_{-1}(1-\rho)^{-1} + k_2[M^+]_T \quad (35)$$

where the overall $(k_A + k_B)$, measured by NMR, comes from dissociative and associative contributions to the exchange. The relative simplicity and linear form of equation 35 provides a convenient mechanistic test for determining the exchange mechanism. This does not preclude, however, the possibility of other mechanisms which could be implicated in the chemical exchange, such as the possible participation of the counteranion. Highly coordinating counteranions such as SCN^-, have been shown to influence the pathway for exchange [132] as well as to influence the magnitude of the observed rates [130,131]. Since the counteranions used in this study (BPh_4^-, ClO_4^- and PF_6^-) are relatively non-coordinating, a counteranion effect is not anticipated (this will be confirmed later). In the case of a solvated crown ether (C), coexisting in solution with the complex $(M{:}C)^+$, an associative mechanism for the ligand exchange should also be considered [166]:

$$C^* + (M{:}C)^+ \rightleftharpoons C + (M{:}C^*)^+ \quad (36)$$

However, this particular chemical exchange cannot be studied by the present method, ^{23}Na NMR, since the cation occupies only one site in solution. In this case, ^{13}C NMR might prove to be useful if the rates involved can be measured on the ^{13}C chemical shift timescale.

If the two mechanisms described in equations 26 and 31 are the only ones responsible for the chemical exchange of the sodium cation between the solvated and complexed sites, then from equation 35 the relationship between $(k_A + k_B)$ and $(1-\rho)^{-1}$ at a constant $[M^+]_T$, or $(k_A + k_B)$ and $[Na^+]_T$ at a constant ratio of ρ, should be linear. Figure 4.7 shows plots of $(k_A + k_B)$ as a function of $(1-\rho)^{-1}$ for $(Na:15C5)^+$ at various concentrations of $NaBPh_4$ in NM. The linearity of the plots is an indication that equation 35 is valid where the slope and intercept values are related respectively to the dissociative and associative contributions of the overall exchange. The observed lines are horizontal which confirms the absence of the dissociative pathway for the chemical exchange. The values of k_2, which are proportional to $[Na^+]_T$, can be obtained from the Y-intercepts. Figure 4.8 shows the same plot for $(Na:B15C5)^+$ again at various concentrations of $NaBPh_4$ in NM. Again the relationships between $(k_A + k_B)$ and $(1-\rho)^{-1}$ are linear and near horizontal. At the lower sodium concentrations (20.0, 8.0 and 4.0 mM) there is evidence for a measurable residual contribution of dissociative exchange. The rate constant for complex dissociation in the dissociative exchange mechanism (equation 26) can be determined from the slope of these lines: $k_{-1} = (1.1 \pm 0.2) \times 10^2\ s^{-1}$ at 301.5 ± 0.5 K. At the higher sodium concentrations (80.0 and 40.0 mM), the errors preclude any useful determination of k_{-1}.

Plots of $(k_A + k_B)$, this time as a function of $[Na^+]_T$ at constant ρ, shown in Figures 4.9 and 4.10, confirm that the preferred exchange mechanism is via the associative pathway for $(Na:15C5)^+$ and $(Na:B15C5)^+$ in NM.

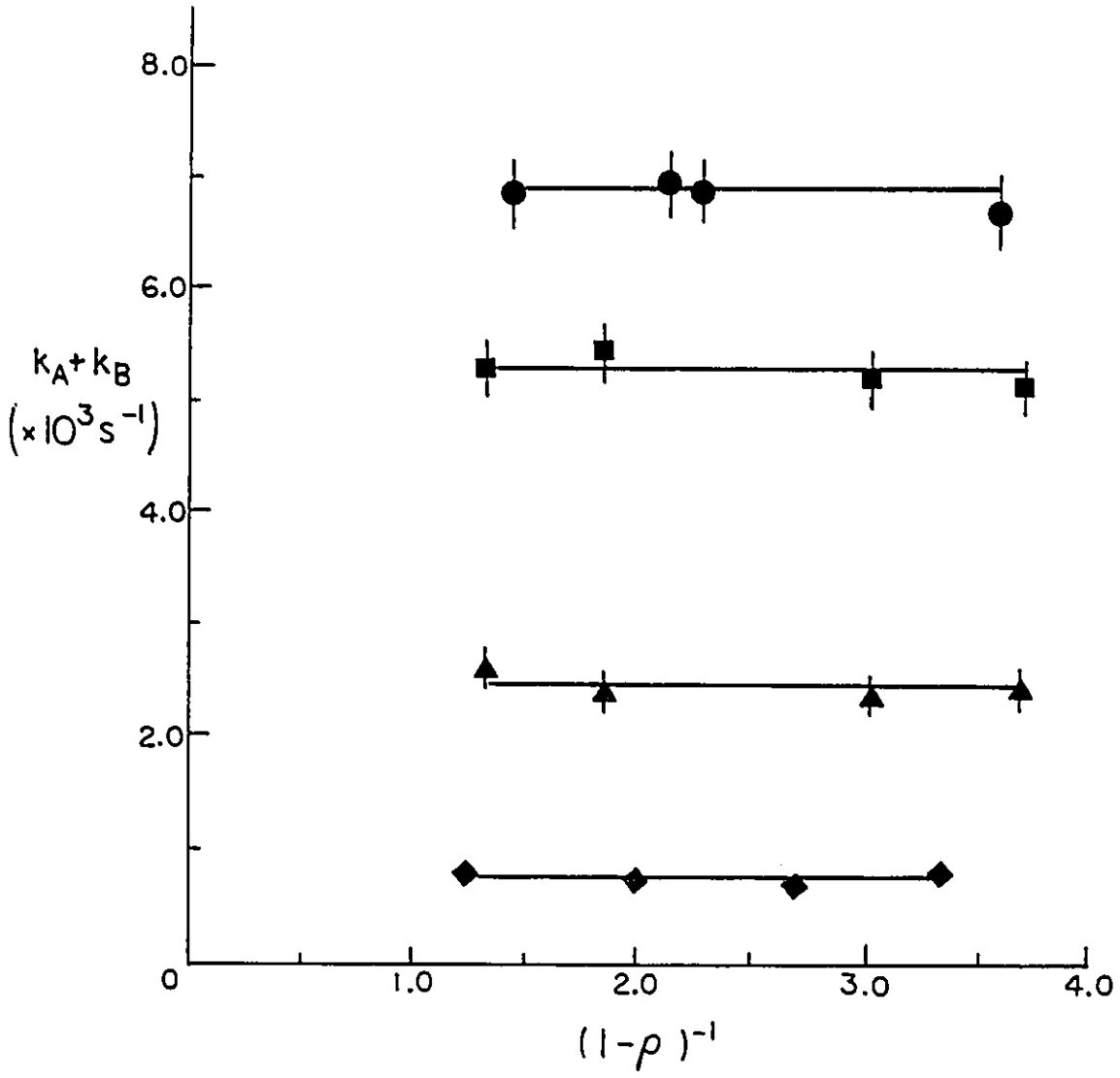

Figure 4.7: ($k_A + k_B$) a function of $(1-\rho)^{-1}$ for various concentrations of $NaBPh_4$ in NM at 301.5 ± 0.5 K; $\rho = [15C5]_T / [NaBPh_4]_T$: 50.1 mM (●); 40.0 mM (■); 20.0 mM (▲); 8.0 mM (◆).

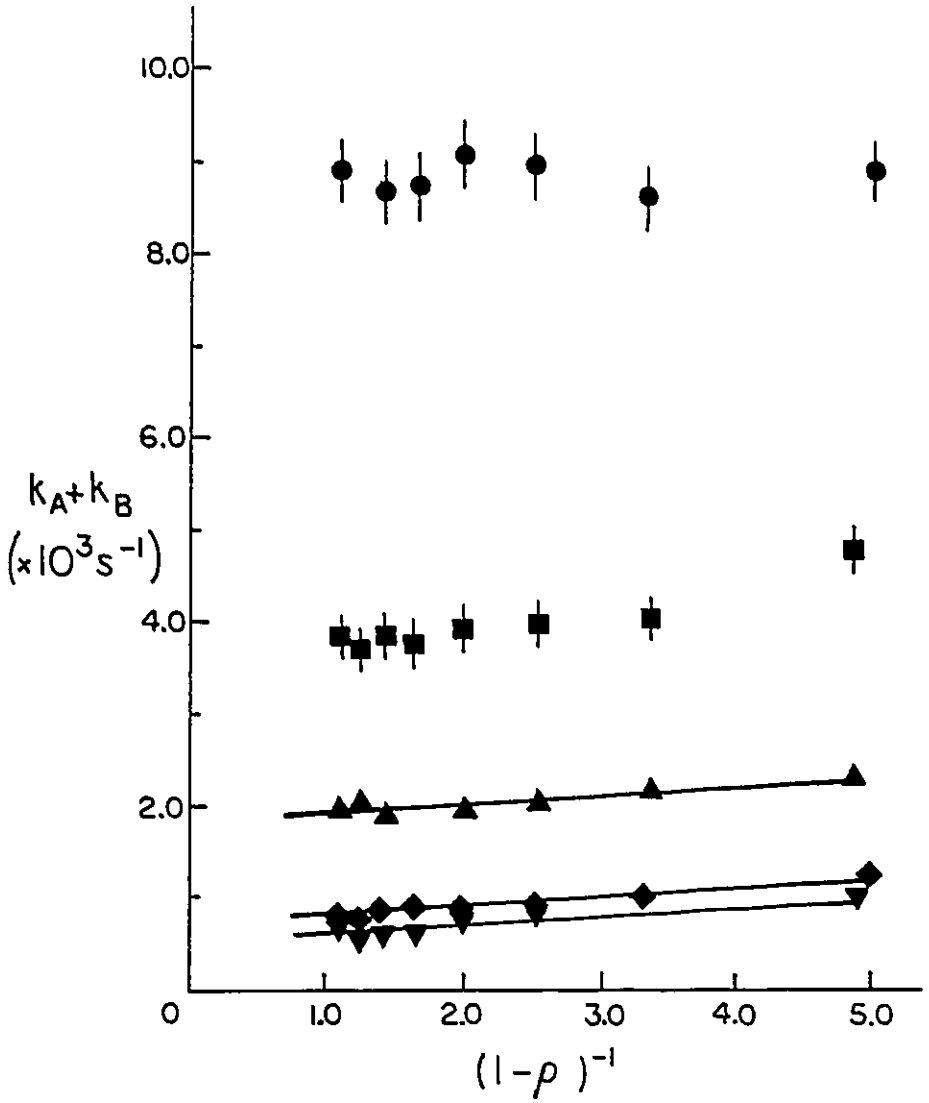

Figure 4.8: (k_A + k_B) as a function of $(1-\rho)^{-1}$ for various concentrations of $NaBPh_4$ in NM at 301.5 ± 0.5 K; ρ = $[B15C5]_T$ / $[NaBPh_4]_T$: 80.0 mM (●); 40.0 mM (■); 20.0 mM (▲); 8.0 mM (◆); 4.0 mM (▼).

The plots are linear, extrapolate to the origin and k_2 is obtained from their slopes: k_2 = (1.45 ± 0.05) × 10^5 $M^{-1}s^{-1}$ for $(Na:15C5)^+$ and k_2 = (1.09 ± 0.04) × 10^5 $M^{-1}s^{-1}$ for $(Na:B15C5)^+$ at 301.5 in NM.

The activation parameters for the associative exchange of $(Na:15C5)^+$ and $(Na:B15C5)^+$ in NM were determined from a temperature study for ρ = 0.50 at $[NaBPh_4]_T$ = 60.0 mM. The Eyring equation relates the determined rate constants with the activation parameters as shown [46]:

$$k = (k_B T / h) \exp(-\Delta G^* / RT) \quad (37)$$

$$k = (k_B T / h) \exp(-(\Delta H^* - T\Delta S^*) / RT) \quad (38)$$

where k_B Boltzmann's constant, h is Planck's constant and ΔH^*, ΔS^* and ΔG^* are the enthalpy, entropy and free energy of activation respectively. The Eyring plots shown in Figure 4.11 are linear in the temperature range studied (six temperatures, 253.0 ≤ T ≤ 301.5 K) and the activation parameters for the associative exchange of $(Na:15C5)^+$ and $(Na:B15C5)^+$ in NM are given in Table 4.6: ΔH^* = 21 ± 2 and 28 ± 3 $kJ.mol^{-1}$ and ΔS^* = -76 ± 2 and -57 ± 3 $J.mol^{-1}.K^{-1}$ respectively. The slightly higher enthalpy of activation in the case of B15C5, which is compensated by a less negative entropy of activation, reflects the rigidity of this crown ether compared to the nonsubstituted 15C5. The highly negative values of entropies of activation for both crowns reflects the associative nature of the chemical exchange.

It was previously shown that in the complexation of sodium with B15C5 in NM, ion association between Na^+ and the three counteranions used in this study, BPh_4^-, ClO_4^- and PF_6^-, was minimal (see Table 4.3). A parallel analysis can be done in relation to kinetic aspects of the interaction again showing relatively little kinetic influence of these counteranions.

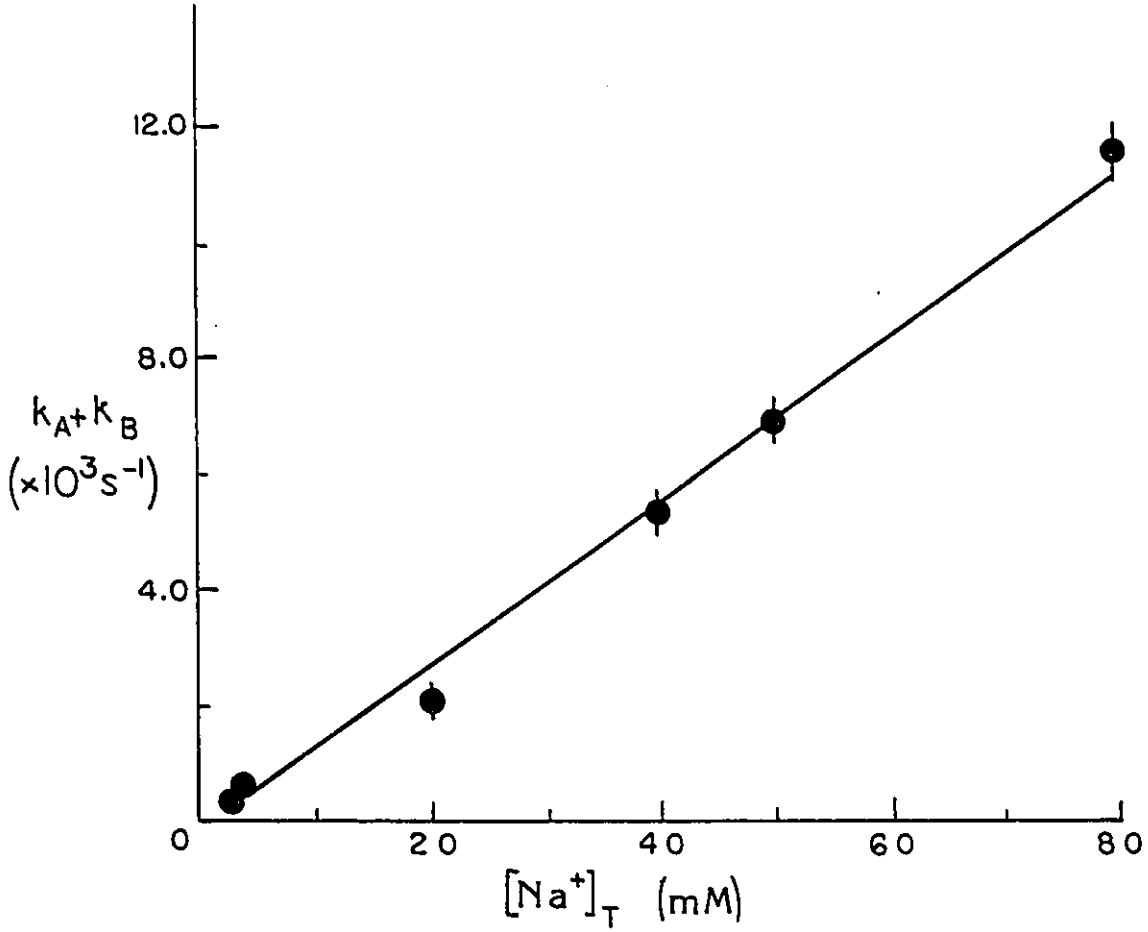

Figure 4.9: $(k_A + k_B)$ as a function of $[NaBPh_4]_T$ in nitromethane at T = 301.5 ± 0.5 K. $\rho = [15C5]_T / [NaBPh_4]_T = 0.57$ in all cases. The data points are experimental and the line is a result of a linear regression: $(k_A + k_B) = (-0.2 \pm 0.2) \times 10^3 + (1.45 \pm 0.05) \times 10^5 [Na^+]_T$, (see equation 35).

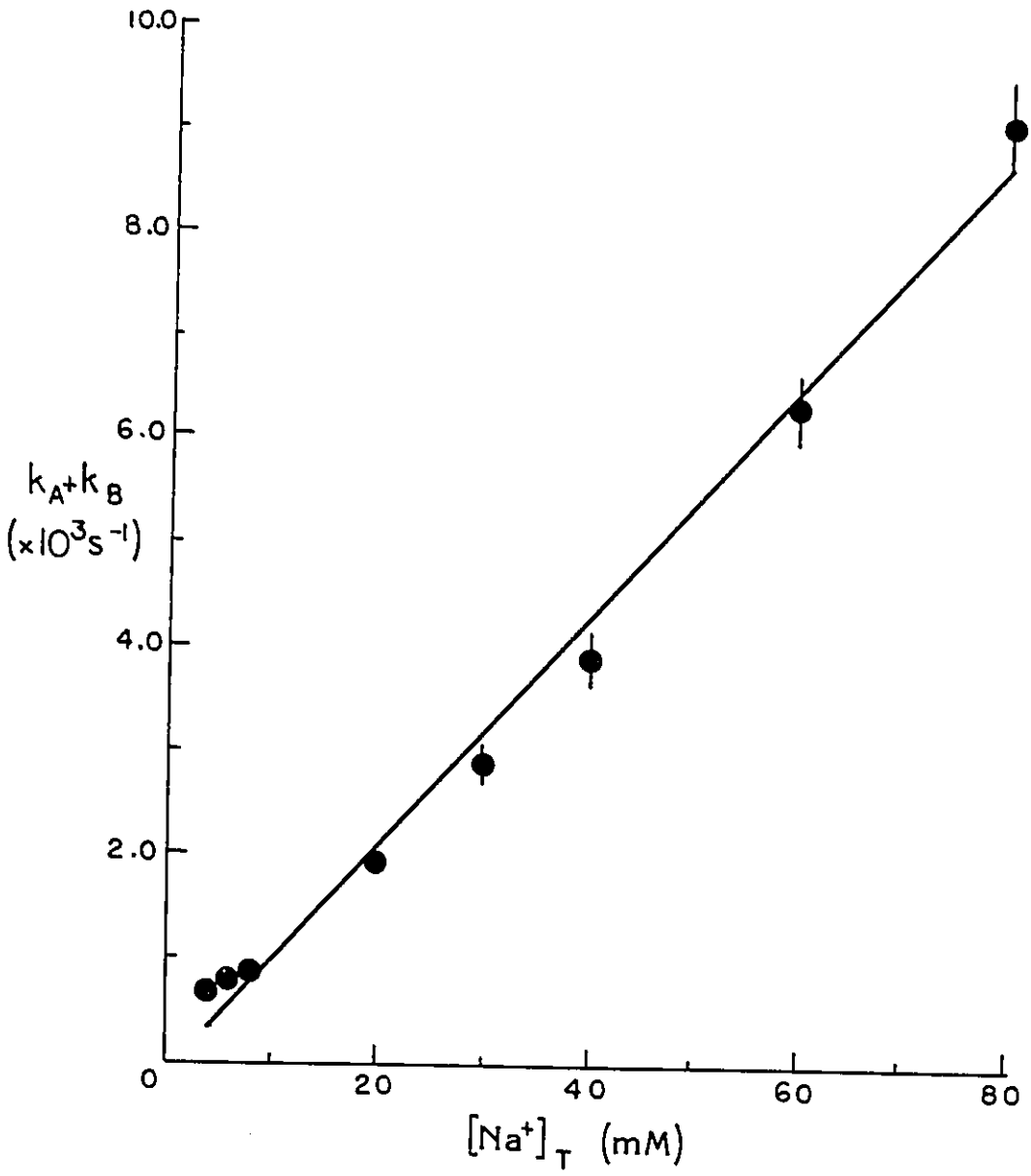

Figure 4.10: ($k_A + k_B$) as a function of $[NaBPh_4]_T$ at T = 301.5 ± 0.5 K in nitromethane. $\rho = [B15C5]_T / [NaBPh_4]_T = 0.50$ in all cases. The data points are experimental and the line is a result of a linear regression: $(k_A + k_B) = (-0.6 \pm 1.8) \times 10^2 + (1.09 \pm 0.04) \times 10^5 [Na^+]_T$, (see equation 35).

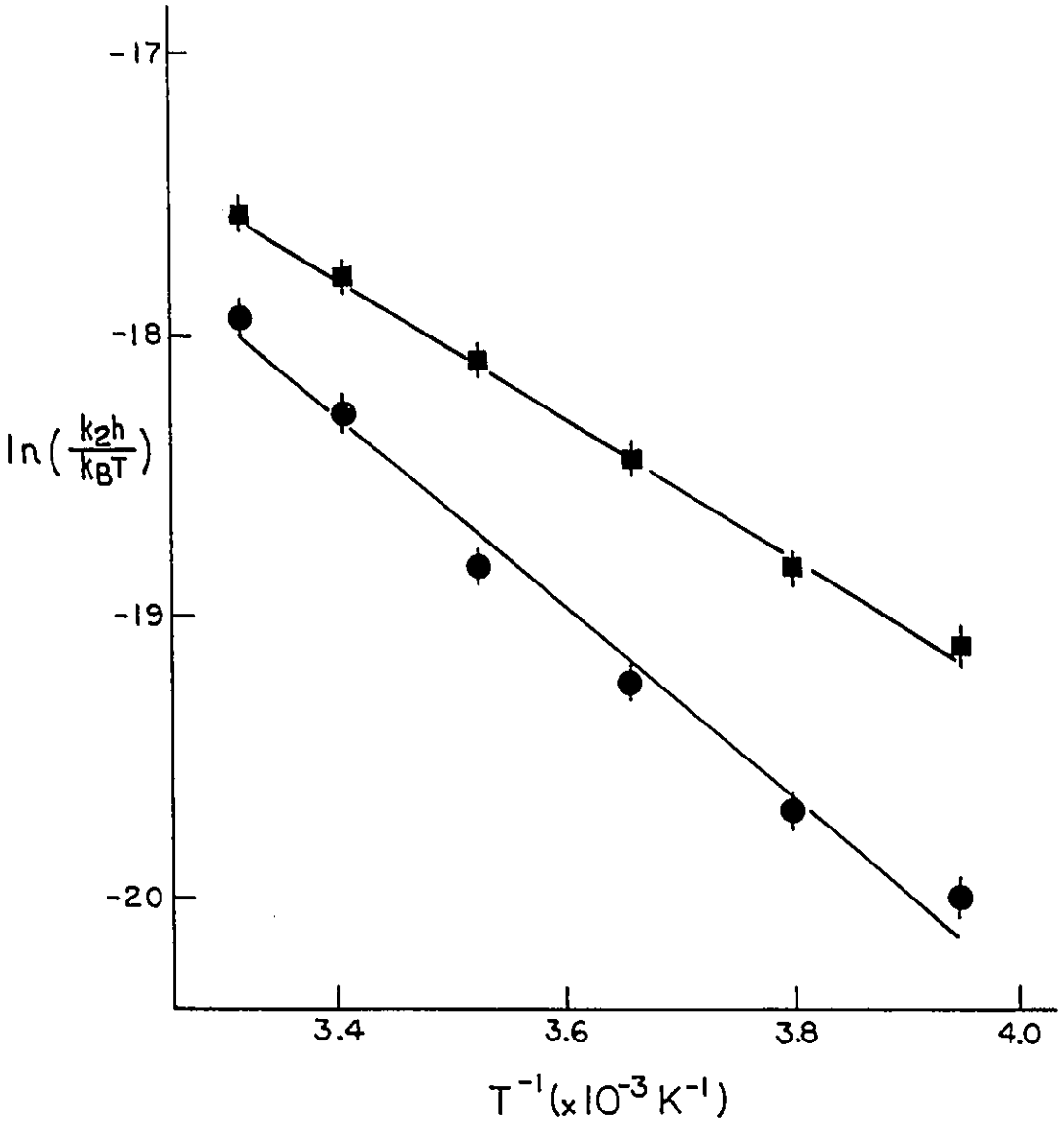

Figure 4.11: $\ln(k_2h / k_BT)$ as a function of T^{-1}. $[NaBPh_4]_T$ = 60.0 mM in nitromethane. k_2 at each temperature was calculated assuming associative exchange only (equation 35 becomes $(k_A + k_B) = k_2[Na^+]_T$). (●): B15C5, $\rho = 0.50$; (■): 15C5 $\rho = 0.65$.

Table 4.5 shows the measured $(k_A + k_B)$ for the exchange of sodium between $(Na^+)_S$ and $(Na:B15C5)^+$ in NM as a function of $[NaX]_T$, where X^- is the counteranion. Assuming that the exchange of sodium is purely associative in these conditions, the corresponding rate constant k_2, which displays very little change as the counteranion and its concentration varies, is calculated from the corresponding $(k_A + k_B)$: $k_2 \cong 1.0 \times 10^5$ $M^{-1}s^{-1}$. The values of k_2 are slightly higher in the presence of the perchlorate anion. Plots of $(k_A + k_B)$ as a function of $(1-\rho)^{-1}$ for the exchange of sodium in the presence of the hexafluorophosphate anion in NM at 300.0 K are shown in Figure 4.12. As in the case of $NaBPh_4$ at these relatively low salt concentrations, there is evidence for a residual contribution of dissociative exchange. Analysis of the three linear plots yields an average value of $k_2 = (0.83 \pm 0.08) \times 10^5$ $M^{-1}s^{-1}$ and $k_{-1} = (1.7 \pm 0.5) \times 10^2$ s^{-1} at 300.0 K which is comparable to $k_2 = (1.09 \pm 0.04) \times 10^5$ $M^{-1}s^{-1}$ and $k_{-1} = (1.1 \pm 0.1) \times 10^2$ s^{-1} for $NaBPh_4$ at 301.5 K.

Although PF_6^- is known to be a relatively non-coordinating counteranion [144,145], the results shown in Table 4.3 indicate that there is a small ion-pairing effect for this counteranion (the ^{23}Na chemical shift displays a slight dependence on the $[NaPF_6]_T$). The ion-pairing equilibrium is represented by equation 39:

$$Na^+ + X^- \underset{}{\overset{K_{IP}}{\rightleftharpoons}} Na^+,X^- \qquad (39)$$

The chemical exchange of sodium can be thus effected by a third possible mechanism:

$$Na^+,X^- + C \underset{k_-}{\overset{k_+}{\rightleftharpoons}} (Na:C)^+ + X^- \qquad (40)$$

Table 4.5: The Effect of the Counteranion (X^-) on ($k_A + k_B$) for the Exchange of Sodium Between $(Na^+)_S$ and $(Na:B15C5)^+$ in Nitromethane.

X^-	[NaX][a] mM	$(k_A + k_B)$ $\times 10^2 s^{-1}$	k_2 [b] $\times 10^5 M^{-1}s^{-1}$
BPh_4^-	80.0	91 ± 4	1.1 ± 0.1
BPh_4^-	59.9	63 ± 3	1.1 ± 0.1
BPh_4^-	40.0	39 ± 2	0.99 ± 0.01
BPh_4^-	30.0	29 ± 2	0.97 ± 0.01
BPh_4^-	20.0	19 ± 1	0.95 ± 0.01
BPh_4^-	8.0	8.8 ± 0.5	1.1 ± 0.1
BPh_4^-	6.0	8.1 ± 0.5	1.3 ± 0.1
BPh_4^-	4.0	7.0 ± 0.5	1.8 ± 0.1
ClO_4^-	10.0	19.7 ± 0.5	1.97 ± 0.05
ClO_4^-	5.0	10.4 ± 0.3	2.08 ± 0.06
PF_6^-	20.6	22.6 ± 0.5	1.10 ± 0.02
PF_6^-	10.3	11.7 ± 0.4	1.14 ± 0.04
PF_6^-	5.0	7.7 ± 0.4	1.54 ± 0.08

(a) $X^- = BPh_4^-$, $\rho = 0.50$, $T = 301.5$ K; $X^- = ClO_4^-$, $\rho = 0.48$, $T = 300.0$ K; $X^- = PF_6^-$, $\rho = 0.52$, $T = 300.0$ K. (b) assuming associative exchange only: $(k_A + k_B) = k_2[Na^+]_T$.

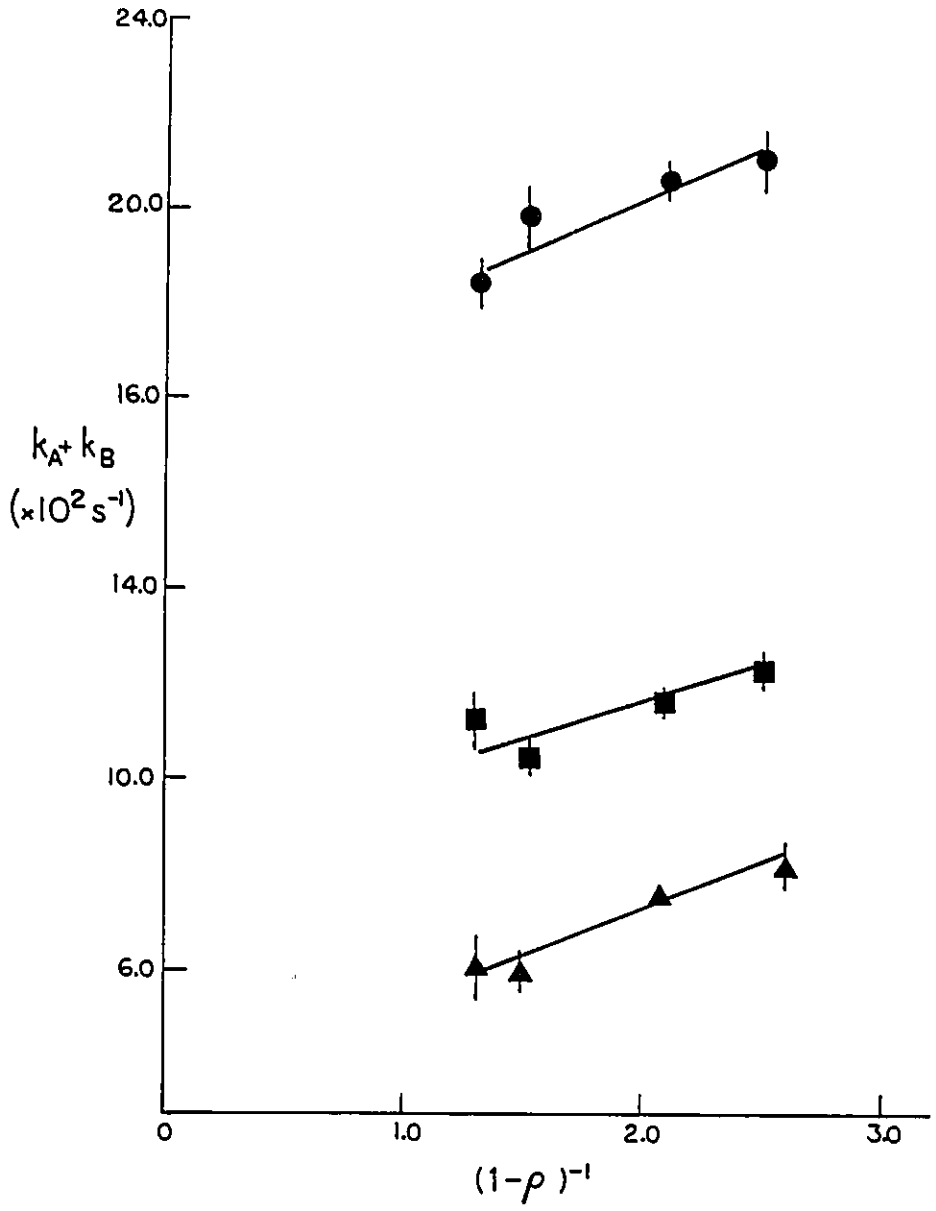

Figure 4.12: $(k_A + k_B)$ as a function of $(1-\rho)^{-1}$ in nitromethane at 300.0 ± 0.5 K. ρ = $[B15C5]_T$ / $[NaPF_6]_T$ and $[NaPF_6]_T$ = 20.6 mM (●); 10.3 mM (■); 5.0mM (▲).

For PF_6^-, one can assume that K_{IP} is very small, and, using the appropriate approximations, equation 41 is obtained [130].

$$(k_A + k_B) = (k_{-1}[Na^+]_T \rho) / ((1-\rho) K_{IP}) \qquad (41)$$

The increase in $(k_A + k_B)$ observed as a function of ρ, as well as a function of $[Na]_T$, shown in Figure 4.12, could therefore be due to slight ion-pairing effects rather than a residual dissociative contribution. If this was the case however, the plots shown in Figure 4.12 would not be linear. Since a value of K_{IP} cannot be accurately determined, and given the limited range of ρ values accessible, a full analysis could not be performed giving enough precision on the rate constants.

Thus in NM, the exchange of sodium between its solvated and B15C5 complexed sites, proceeds almost exclusively via the associative exchange mechanism shown in equation 31. In AN however, the behavior of sodium with the same ligand is completely different. In this solvent at 300 K, no detectable broadening of the ^{23}Na NMR signal is observed for $NaBPh_4$ - B15C5 ($[NaBPh_4]_T$ = 10.0 mM), and only a lower limit of 3.8×10^4 s^{-1} can be estimated for $(k_A + k_B)$. This lower limit for $(k_A + k_B)$ is calculated from equation 25, knowing the chemical shifts of both sodium sites and assuming that reliable $T_{2,ex}^{-1}$ data can be obtained only when the exchange broadening is at least 20% of $T_{1,obs}^{-1}$ [143]. At 258 K, the transverse relaxation rate is sufficiently different from the longitudinal relaxation rate and a meaningful chemical exchange contribution, $T_{2,ex}^{-1}$, can be measured. This is illustrated in Figure 4.13 which shows plots of the relaxation rates as a function of ρ for Na^+-B15C5 in AN. The corresponding variation of $(k_A + k_B)$ as a function of $(1-\rho)^{-1}$ is shown in Figure 4.14. Figure 4.13 shows the experimental data points and a set of curves calculated for various values of k_{-1} (equations 25 and 35). It is worth noticing that the graph of T_2^{-1} as a function of ρ displays an inflection point, resulting from the form of equation 25 when $(k_A + k_B) = k_{-1} (1-\rho)^{-1}$. Since $K_{FI} > 10^4$, as

shown by the linearity of T_1^{-1} with ρ, $P_B = 1 - P_A = \rho$. Under these conditions, $T_2^{-1} = f(\rho)$ is a cubic equation. The curves shown in Figure 4.13 were calculated without taking into account any contribution from the associative exchange mechanism ($k_2 = 0$). This can explain the slight discrepancy between the experimental data points and the curve (C). The linear variation of $(k_A + k_B)$ with $(1-\rho)^{-1}$, shown in Figure 4.14, is diagnostic of mainly dissociative exchange for sodium in AN since the line has a definite slope which extrapolates near the origin: $k_{-1} = (3.5 \pm 0.1) \times 10^3\ s^{-1}$. Evidence for some residual contribution of the associative exchange can also be found in the non-negligible value of the Y-intercept, giving $k_2 = (0.9 \pm 0.3) \times 10^5\ M^{-1}s^{-1}$. A summary of the kinetic results obtained for $(Na:15C5)^+$ and $(Na:B15C5)^+$ in NM and AN from this work, as well as other published results for closely related systems, are shown in Table 4.6.

The completely different mechanistic behavior in NM and AN maybe at first surprising considering that these two solvents are characterized by many similar properties; the dielectric constant for both is 35.9 at 303 and 298 K, the dipole moments are 3.56 and 3.53 D and the solubility parameters (Hildebrand's δ) are 26.0 and 24.8 $MPa^{1/2}$ all respectively [50]. These two solvents have however significantly different donicity numbers (2.7 for NM and 14.1 for AN). While the contribution of the dissociative exchange process (equation 26) to the overall exchange rate accounts for only 9% in NM (B15C5, 301.5 K, $[Na^+]_T = 20.0$ mM, $\rho = 0.50$), it reaches 85% in AN (258.0 K, identical conditions otherwise; see Table 4.6). The change of predominant exchange mechanism observed comes mainly from an increase of the absolute value of the dissociative exchange rate constant, k_{-1}, seen in the solvent with the higher donicity number (AN). It can be seen in Table 4.6 that for similar values of k_2 (B15C5 in AN at 258.0 K, in NM at 301.5 K), the k_{-1}'s differ by a factor of 30 in going from NM to AN. A similar trend has been observed for $(Na:DB18C6)^+$ in NM and AN [145].

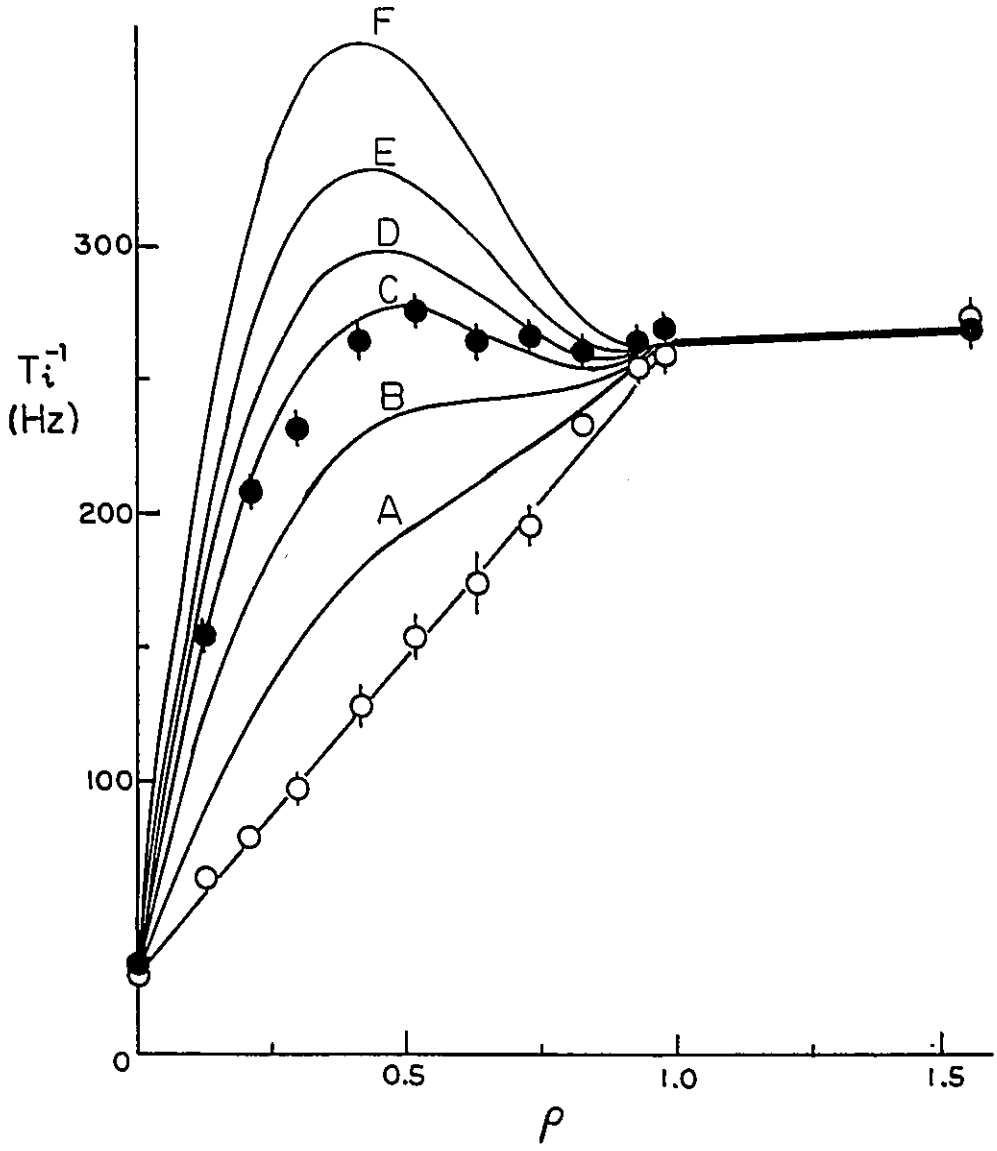

Figure 4.13: ^{23}Na transverse ($i = 2$; ●) and longitudinal ($i = 1$; ○) relaxation rates as a function of $\rho = [B15C5]_T / [NaBPh_4]_T$ in acetonitrile at T = 258.0 ± 0.5 K. $[NaBPh_4]_T$ = 10.0 mM. The data points are experimental and the curves have been calculated from different values of k_{-1}: (A) 10.0×10^3; (B) 5.0×10^3; (C) 3.5×10^3; (D) 3.0×10^3; (E) 2.5×10^3; (F) 2.0×10^3 (see equations 25 and 35).

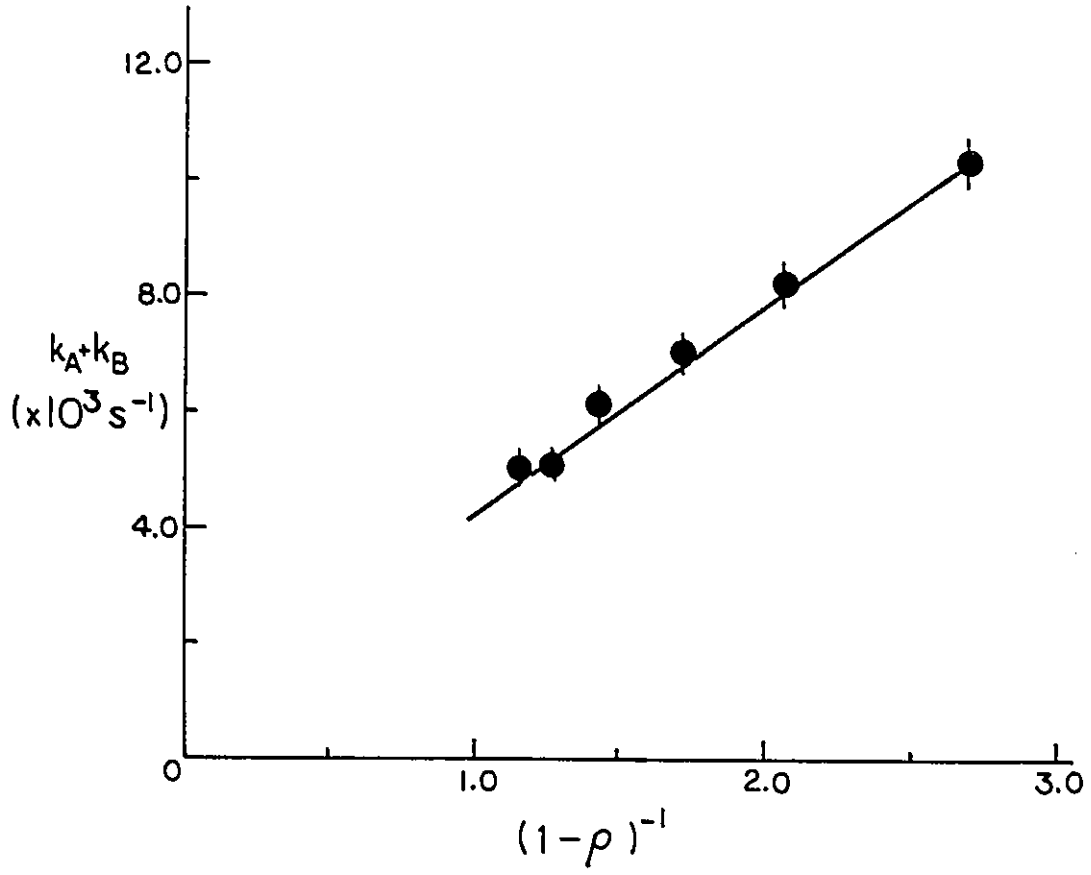

Figure 4.14: $(k_A + k_B)$ as a function of $(1-\rho)^{-1}$ in acetonitrile at T = 258.0 ± 0.5 K. ρ = $[B15C5]_T$ / $[NaBPh_4]_T$ and $[NaBPh_4]_T$ = 10.0 mM. The result of the linear regression is: $(k_A + k_B) = (3.5 \pm 0.1) \times 10^3 (1-\rho)^{-1} + (9 \pm 3) \times 10^2$ (see equation 35).

Table 4.6: Kinetic Parameters of $(Na:crown)^+$ in Nitromethane and Acetonitrile[a].

crown	solvent[a]	k_{-1} [b] (s^{-1})	k_2 [c] ($M^{-1}s^{-1}$)	ΔH^*_{as} [d] ($kJ.mol^{-1}$)	ΔS^*_{as} [d] ($J.mol^{-1}.K^{-1}$)	ΔG^*_{as} [d,f] ($kJ.mol^{-1}$)	ΔH^*_{di} [e] ($kJ.mol^{-1}$)	ΔS^*_{di} [e] ($J.mol^{-1}.K^{-1}$)	ΔG^*_{di} [e,f] ($kJ.mol^{-1}$)
15C5	NM	g	$(1.45\pm0.05)\times10^5$	21±1	−76±2	44.1±0.1	g	g	g
B15C5	NM	$(1.1\pm0.1)\times10^2$	$(1.09\pm0.04)\times10^5$	28±3	−57±3	44.8±0.1	h	h	62.1±0.3
B15C5	AN	$(3.5\pm0.1)\times10^3$ [j]	$(0.9\pm0.3)\times10^5$ [j]	i	i	38.4±0.8 [j]	i	i	45.4±0.4[j]
18C6	NM	g	$>6\times10^5$	g	g	<40	g	g	g
18C6[k]	AN	$(3.8\pm0.5)\times10^3$	$(2.6\pm0.4)\times10^5$	h	h	42.6±0.4	32±2	−65±8	53.2±0.4
DB18C6[l]	NM	$(1.7\pm0.1)\times10^2$ [m]	$(2.3\pm0.4)\times10^4$ [m]	h	h	47.4±0.4[m]	37±3	−78±8	59.4±0.2[m]
DB18C6[l]	AN	$(2.2\pm0.1)\times10^3$ [m]	g	g	g	g	40±2	−44±8	53.2±0.2[m]
DB24C8[n]	NM	$\sim0.6\times10^2$ [o]	$(3.5\pm0.3)\times10^5$ [o]	31±3	−32±10	40.9±0.2[o]	h	h	62[o]

Table 4.6: footnotes

(a) NM = nitromethane; AN = acetonitrile; the counteranion is BPh_4^- in all cases. (b) dissociative exchange rate constant (see equation 26) at 301.5 K. (c) associative exchange rate constant (see equation 31) at 301.5 K. (d) activation parameters for the associative exchange. (e) activation parameters for the dissociative exchange. (f) ΔG^* is given at 301.5 K unless otherwise indicated and calculated from k_2 and k_{-1} determined at this temperature (see equation 37). (g) not observed. (h) not determined because of experimental errors. (i) not determined. (j) at 258.0 K. (k) from reference 143. (l) from reference 145. (m) at 294.0 K. (n) from reference 144. (o) at 295.0 K.

Unfortunately a direct comparison with $(Na:18C6)^+$ is not possible since the difference between the chemical shifts of the complexed and solvated sodium is only 121 Hz (at 79.346 MHz) in NM at 303.0 K, and the highest observable pseudo-first order rate constant ($k_A + k_B$) is 3.4×10^3 s^{-1} [143]. This value corresponds to a lower limit of $\sim 6 \times 10^5$ $M^{-1}s^{-1}$ at 303 K for k_2, since the values obtained for T_2^{-1} and T_1^{-1} were almost the same for $[Na]_T = 5$ mM [143].

The results shown in Table 4.6 give some preliminary indications of the influence of the solvent on the exchange kinetics of alkali metal cation-crown ether systems. In general, excluding the case of B15C5 in AN, the free energy of activation for the dissociative exchange, ΔG_{di}^*, at about 300 K is approximately 8 $kJ.mol^{-1}$ higher in NM (59-62 $kJ.mol^{-1}$) than in AN ($\sim$ 53 $kJ.mol^{-1}$), while all the measured ΔG_{as}^*, for the associative exchange, are in the same range (41-47 $kJ.mol^{-1}$). This is an indication that the solvent plays a crucial role in the dissociative process. For $(Na:18C6)^+$ [148] Strasser and Popov have shown that there is a correlation between the donicity number of a solvent and the free energy of activation in cases where the dissociative mechanism predominates; as the donicity of the solvent increases the free energy of activation decreases. Lincoln et al. [155] have found that the activation parameters are also

strongly dependent on the solvent. Since the free energies of activation for the associative exchange appear to be independent of the solvent (see Table 4.6 and Appendix 3) the solvent would play a minor role in this exchange. The major controlling factor of the associative process is plausibly the conformational rearrangements of the ligand; this will be discussed in more detail later. The independence of solvent on the associative process was also observed for $(K:18C6)^+$ [150], $(Cs:DB21C7)^+$, $(Cs:DB24C8)^+$ and $(Cs:DB30C10)^+$ [152,153] where no correlation between the free energies of activation and solvent donicity was observed. A compiled list of kinetic results, obtained by alkali metal NMR, which have been published to date for all alkali-ionophore systems is shown in Appendix 3.

Rate constants for the exchange kinetics of $(Na:15C5)^+$ and $(Na:B15C5)^+$ in NM and AN were accessible by ^{23}Na NMR for two main reasons: (1) there is an appreciable difference in the chemical shifts of the two sites in both solvents (10.8 ppm in NM and 3.6 ppm in AN; see equation 22, Figure 4.1a and Figure 4.2a) and the exchange rates themselves were in the moderate to slow region of the ^{23}Na NMR chemical shift timescale. Kinetic studies were attempted for $(Na:B15C5)^+$ in PY, but at $[NaBPh_4]_T$ = 10 mM, no detectable broadening of the peak was observed even at 249 K indicating that the exchange of sodium in this solvent is fast on the ^{23}Na NMR chemical shift timescale. This is not surprising considering the high donicity of the solvent (33.1) where a faster observed rate of exchange than in AN is, a priori, expected based on the DN of the solvent alone. The chemical shift difference between both sodium sites in PY is also quite small (3.1 ppm). Based on the high donicity number of PY, one could also speculate that the dominant exchange mechanism observed would be dissociative in this solvent. Since the K_{F1} for the formation of $(Na:B15C5)^+$ in DMF is low, kinetic studies in this solvent were not attempted, but once again a dissociative mechanism might be predicted on the basis of the high donicity number (26.6) of this solvent.

4.5. Role of the Solvent in the Chemical Exchange

In order to understand the exact role of the solvent in the chemical exchange of sodium, kinetic studies, paralleling those discussed in the previous section, were done for $(Na:B15C5)^+$ in binary solvent mixtures of AN-NM, DMF-NM and PY-NM. Except for PY, all have similar dielectric constants, but differ in donicities increasing in the order NM, AN, DMF and PY (see Table 4.1 on page 72).

4.5.1 Acetonitrile-Nitromethane Binary Solvent Mixtures

Figure 4.15 shows several ^{23}Na NMR spectra for solutions containing $(Na^+)_S$ and $(Na:B15C5)^+$ ($\rho = 0.50$) obtained in binary solvent mixtures of AN-NM. The bottom spectrum is that obtained in pure NM where two peaks for the two sodium sites can be observed. Upon increasing the content of AN in the solvent mixture, there is a coalescence of the two peaks indicating that the overall rate of exchange, and therefore $(k_A + k_B)$, increases. At T = 301.5 K, the rate of exchange in pure AN is too rapid to be measured and there is no observable line broadening. Figure 4.16 shows the usual plots of $(k_A + k_B)$ as a function of $(1-\rho)^{-1}$ for several AN-NM binary mixtures varying in composition. As the content of AN in the solvent mixture increases, there is an increase of the slope, indicative of an increase in the dissociative contribution to the exchange. However, the intercept values, pertaining to the associative contribution, remain constant within experimental error (see equation 35). The increase in slope value corresponds to an increase in k_{-1} whereas the constant values for the intercepts correspond to a constant value of k_2. Table 4.7 contains the results of the linear regressions of the plots shown in Figure 4.16, as well as the calculated free energies of activation, for the dissociative and the associative contributions of the exchange in several AN-NM solvent mixtures.

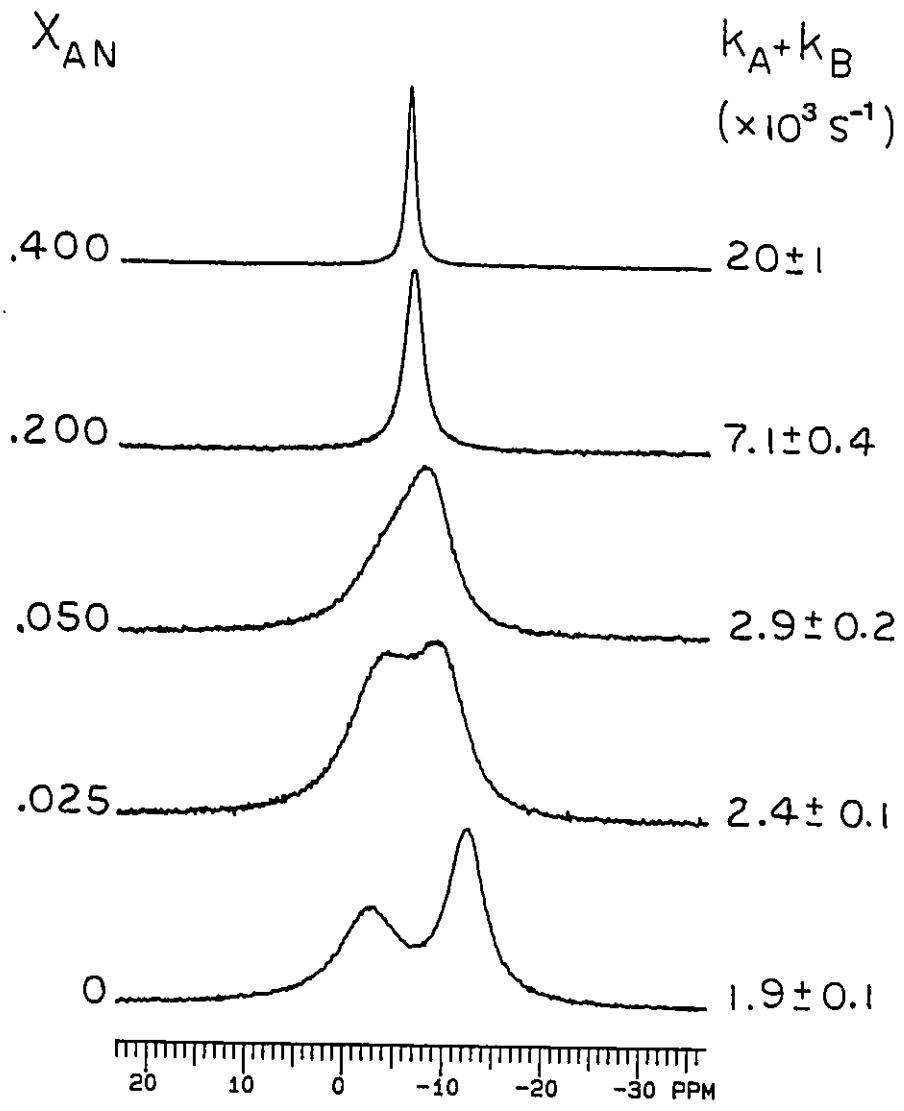

Figure 4.15: ^{23}Na spectra of samples containing equal populations of $(Na^+)_S$ and $(Na{:}B15C5)^+$ ($\rho = 0.50$). $[NaBPh_4]_T$ = 20 mM and T = 301.5 K. From top to bottom, mole fraction of AN (X_{AN}) and ($k_A + k_B$) in AN-NM binary mixtures vary as shown.

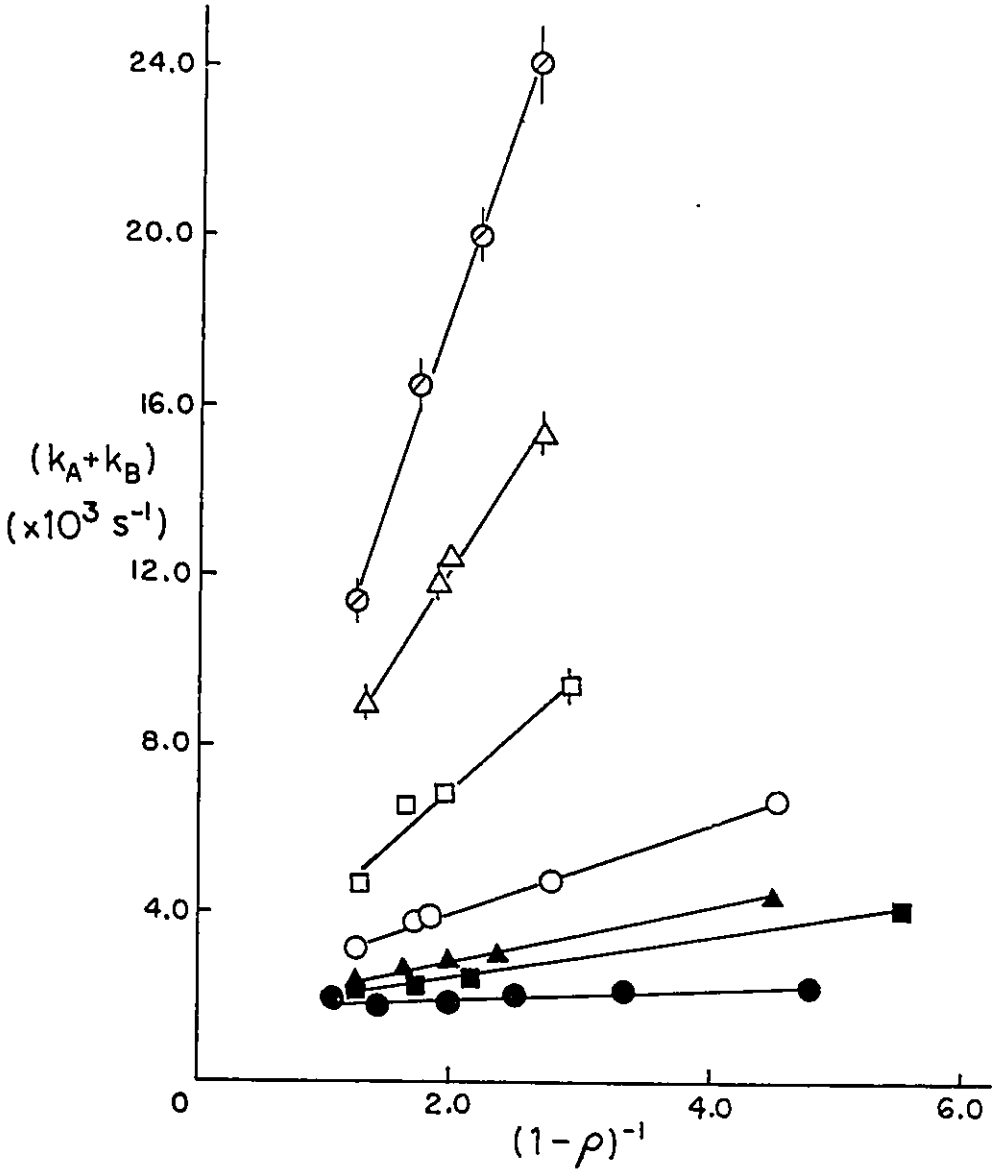

Figure 4.16: $(k_A + k_B)$ as a function of $(1-\rho)^{-1}$ for several AN-NM binary solvent mixtures. $[NaBPh_4]_T = 20.0$ mM and $T = 301.5 \pm 0.5$ K. X_{AN}: (⊘) 0.40; (△) 0.30; (□) 0.20; (○) 0.10; (▲) 0.050; (■) 0.025; (●) 0.

Table 4.7: Kinetic Parameters for the Dissociative and Associative Exchange of Sodium with B15C5 in Acetonitrile - Nitromethane Binary Solvent Mixtures[a].

X_{AN}	[AN] M	k_{-1} $\times 10^2$ s^{-1}	$\Delta G^{\ddagger}_{di}$ $kJ.mol^{-1}$	k_2 $\times 10^4$ $M^{-1}s^{-1}$	$\Delta G^{\ddagger}_{as}$ $kJ.mol^{-1}$
0	0	1.1 ± 0.1	62.1 ± 0.3	10.9 ± 0.4	44.8 ± 0.1
0.025	0.46	3.5 ± 0.1	59.2 ± 0.1	8.4 ± 0.1	45.9 ± 0.1
0.050	0.92	6.2 ± 0.9	57.8 ± 0.4	8.0 ± 0.8	45.6 ± 0.5
0.100	1.85	10 ± 1	56.5 ± 0.2	9.7 ± 0.9	45.1 ± 0.5
0.200	3.67	27 ± 3	54.1 ± 0.3	7.7 ± 3.5	45 ± 1
0.300	5.60	46 ± 1	52.7 ± 0.1	14 ± 2	44.1 ± 0.4
0.400	7.50	89 ± 5	51.1 ± 0.2	1.5 ± 4.8	50 ± 8

(a) all values of k_{-1}, k_2, $\Delta G^{\ddagger}_{di}$ and $\Delta G^{\ddagger}_{as}$ are reported at 301.5 ± 0.5 K.

The results shown in Table 4.7 indicate that an increase in the concentration of AN in the solvent mixture results in an increase of the rate for dissociative exchange with a corresponding decrease in the free energy of activation for this mechanism. This is not surprising considering the observations obtained in the two neat solvents discussed in section 4.4. This trend is expected based upon an increased solvating ability of the global solvent . The increased coordinating ability of the solvent, as reflected by its donicity number, facilitates the separation of the sodium from the crown ether in the dissociation process, thereby increasing the overall rate of exchange. The decrease in free energy of activation could be related to a decrease in enthalpy of activation in the replacement of a sodium-ether oxygen bond by a sodium-solvent bond (in a solvent with high donicity). Very little has been published concerning kinetic studies of alkali metal cation-crown ether systems in binary solvent mixtures. Results obtained for $(Na{:}18C6)^+$

by Popov and his coworkers (counteranion BPh_4^-) in solvent mixtures containing THF (DN = 20.0) and PC (DN = 15.1), indicate that the dissociative mechanism is predominant in a mixture of 0.8-0.2 mole % of THF-PC [148], as is the case in neat THF [132]. Increasing the amount of lower donor solvent in the solution (0.4-0.6 mole % of THF-PC) however, results in a mechanism for the exchange which is predominantly associative as is the case in pure PC [148]. This trend agrees with the present studies where the donicity of a solvent greatly influences the exchange mechanism and that solvents with high donor values will favour the dissociative mechanism. It should be mentioned that although the data obtained in this work so far indicates a model for the dissociative exchange which can be rationalized based on the donicity of the solvent, other published results indicate that this is not so. For example, the values of ΔG^*_{di} and ΔH^*_{di} for the dissociative exchange of $NaBPh_4$-18C6 in AN (DN = 14.1), PC (DN = 15.1), AC (DN = 17.0) and PY (DN = 33.1) do not decrease in this order [143]. This is also the case for NaSCN-18C6 [155]. It is interesting to note that although the ΔG^*_{di} versus donicity trend is followed for $(Na:DB18C6)^+$ in NM (BPh_4^- [145]), AN (BPh_4^- [145]) and DMF (SCN^- [140,141]), the ΔH^*_{di} does not follow this trend. This shows that the electron-donating ability of a solvent, as measured by its donicity number, is not the only parameter involved in the dissociative exchange mechanism which is not a simple process. It has been suggested that the conformational rearrangements leading to the transition state in the dissociative exchange are accompanied by partial desolvation of the complexed cation, reorganization of the solvent cage around the complex and solvation of the partially decomplexed crown ether [145].

Although properties of solvents in mixtures cannot usually be predicted from their behavior in the neat state [32b,148], it is reasonable to assume that the donicity of the global solvent increases as the concentration of AN in the AN-NM binary mixture increases. The strong dependence of the free energy of activation on the concentration

of AN for the dissociative exchange suggests that the AN molecules must be directly implicated in this mechanism for sodium exchange. Figure 4.17 shows a plot of, ΔG^{*}_{di}, as a function of the mole fraction content of AN (X_{AN}) in the solvent mixture. The plot shown in Figure 4.17 is not linear (this is also the case for ΔG^{*}_{di} as a function of the concentration of AN in the solvent mixture), but since the donor properties of solvent mixtures cannot be predicted from those of the neat solvents [32b], and there are considerable differences in previous ΔG^{*}_{di} versus DN trends [143,148,155], it is difficult to predict the exact relationship between ΔG^{*}_{di} and X_{AN}. The donor numbers of other solvent mixtures have been inferred to on the basis of ^{23}Na NMR chemical shifts. It was shown that the donor numbers of several nitromethane binary mixtures increased in a nonlinear fashion with increasing mole fraction contents of HMPA, PY, DMSO and AN [31,167]. The same nonlinear observation was reported for DMSO-AN and PY-AN solvent mixtures [31,168]. Based on these observations, it is possible that the nonlinearity of the plot in Figure 4.17 is a reflection on the nonlinearity of the DN versus solvent composition.

The results in Table 4.7 also indicate that the associative mechanism for the chemical exchange is influenced very little, if at all, by increasing amounts of AN in the global solvent (there is little variation in ΔG^{*}_{as}). Whereas it has been shown that there is a direct implication of the solvent at the molecular level in the dissociative process, the solvent plays a minor role in the associative exchange. The free energies of activation, ΔG^{*}_{as}, for many systems involving various combinations of macrocyclic ligands and alkali-metal cations, in solvents varying in donicity from NM to PY, have values in the order of 40-50 kJ.mol^{-1} at ~ 300 K (see Appendix 3). This is a very strong indication that the controlling factor of the associative exchange, which does not involve the solvent, always has the same origin.

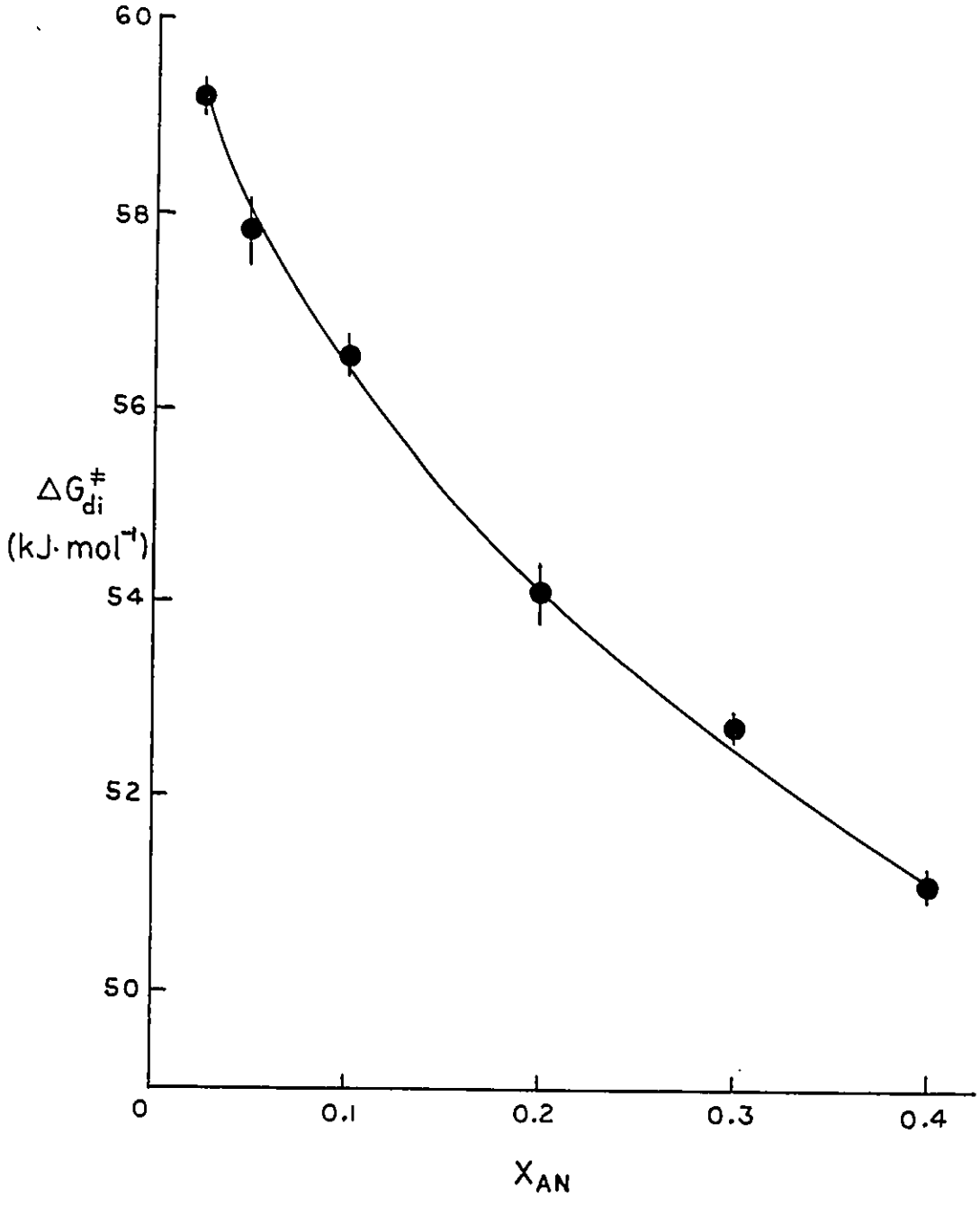

Figure 4.17: $\Delta G^{\bullet}_{di}$ as a function of mole fraction content of acetonitrile, X_{AN}, in AN-NM binary solvent mixtures. $T = 301.5 \pm 0.5$ K.

Variable temperature studies of the exchange processes in the various binary mixtures has given access to the enthalpies and entropies of activation for both exchange mechanisms. Some of the results are shown in Figures 4.18 and 4.19 which show our usual plots of $(k_A + k_B)$ as a function of $(1-\rho)^{-1}$. Figure 4.18 first illustrates the overall decrease in $(k_A + k_B)$ as the temperature decreases in 4.18a to 4.18d and secondly illustrates the increase in k_{-1} as X_{AN} is increased, in each of Figures 4.18a to 4.18d, whereas the k_2 is unaffected. Figure 4.19 shows a different perspective of the same data, as well as including data at T = 264.5 and 255.0 K. Figure 4.19 first illustrates again an overall decrease in $(k_A + k_B)$ this time as X_{AN} is lowered in 4.19a to 4.19d and secondly, illustrates that a decrease in temperature, in each of Figures 4.19a to 4.19d, results in a decrease in both k_{-1}(slope) and k_2 (intercept). Table 4.8 contains the values of the rate constants for both exchange mechanisms, k_{-1} and k_2, calculated from linear regressions of the plots shown in Figure 4.19. In these types of studies it is typical that only one major mechanism is observed for a particular system and that although a residual second mechanism may be observed, only the major contribution can be reliably characterized (e.g. activation parameters). Figures 4.18 and 4.19 show that both mechanisms can be observed for the exchange of sodium in the AN-NM binary solvents, but also this is a rare case where both mechanisms can be somewhat characterized.

A summary of the activation parameters for the dissociative and associative exchange determined from Eyring plots for each binary solvent mixture is shown in Table 4.9. Unfortunately, reliable values for the activation parameters for the dissociative exchange contribution could not be determined since the errors associated with this determination were relatively large.

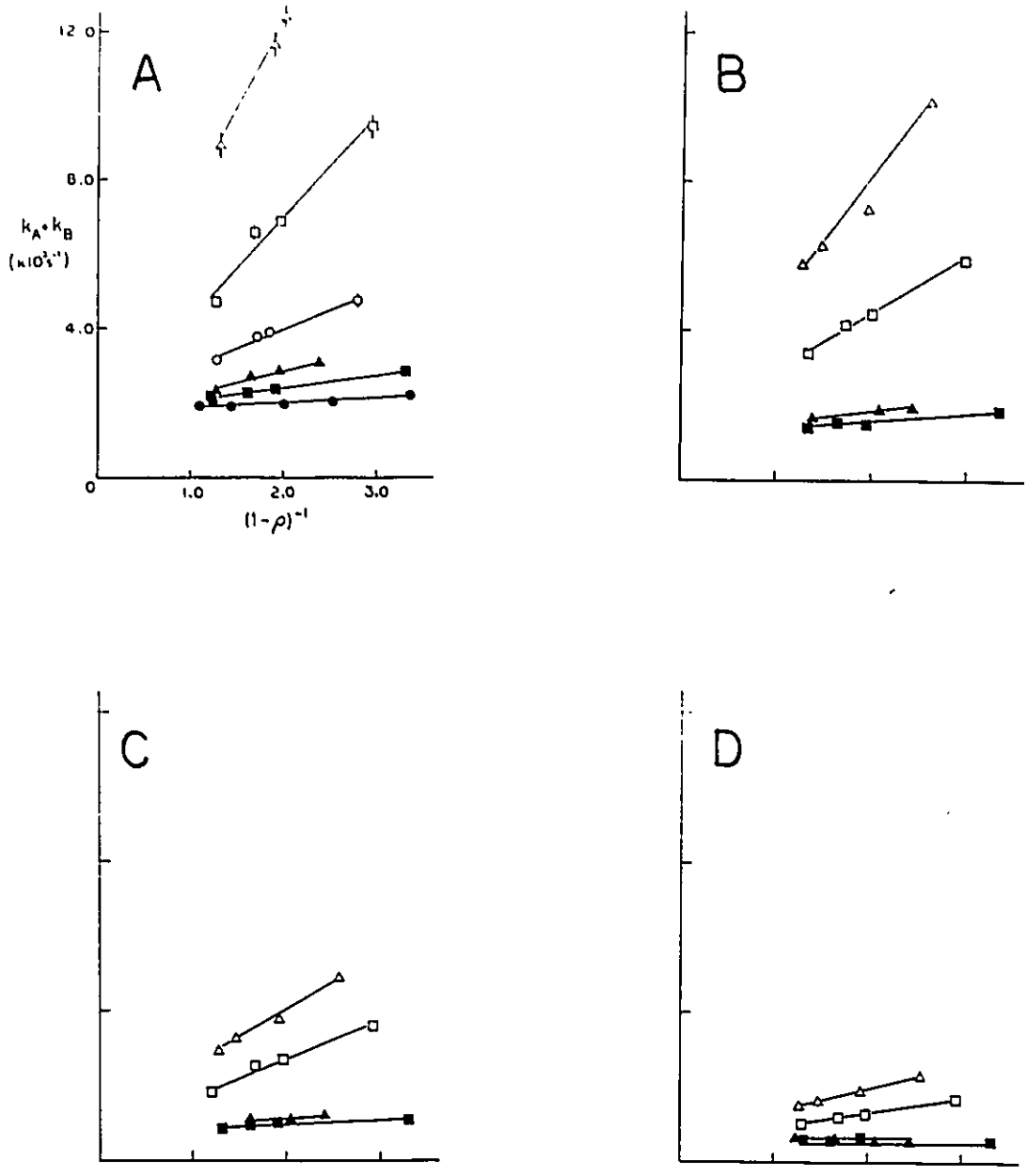

Figure 4.18: ($k_A + k_B$) as a function of $(1-\rho)^{-1}$ for a series of solvent mixtures ranging in X_{AN}: (△) 0.300; (□) 0.200; (○) 0.100; (▲) 0.050; (■) 0.025. Plot at T = (A) 301.5 K; (B) 293.0 K; (C) 284.0 K and (D) 274.0 K.

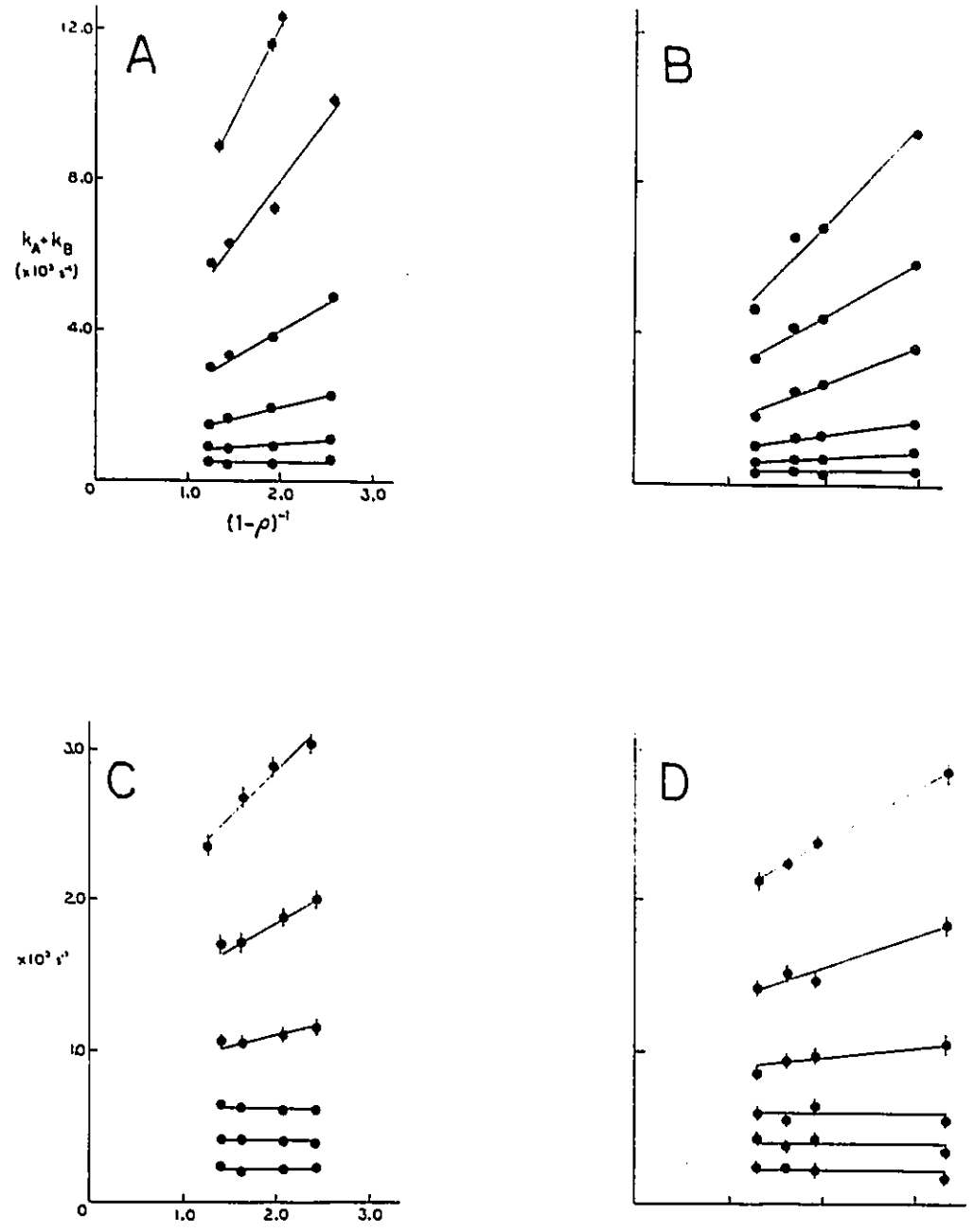

Figure 4.19: $(k_A + k_B)$ as a function of $(1-\rho)^{-1}$ for a series of temperatures: from top to bottom T = 301.5, 293.0, 284.0, 274.0, 264.5 and 255.0 K. Plot for X_{AN} = (A) 0.300; (B) 0.200; (C) 0.050 and (D) 0.025. Note the two different scales (A=B and C=D).

Table 4.8: Rate Constants for the Dissociative, k_{-1}, and Associative, k_2, Exchange as a Function of Temperature for Various Acetonitrile - Nitromethane Binary Mixtures.

X_{AN}[a]	T K	k_{-1} $\times 10^2\ s^{-1}$	k_2 $\times 10^4\ M^{-1}s^{-1}$
0.0252	255.0	–	1.1 ± 0.2
	264.5	–	2.0 ± 0.2
	274.0	–	3.0 ± 0.2
	284.0	0.8 ± 0.4	4.1 ± 5.7
	293.0	2.0 ± 0.4	5.7 ± 0.4
	301.5	3.5 ± 0.1	8.4 ± 0.1
0.0500	255.0	–	1.0 ± 0.1
	264.5	–	2.0 ± 0.1
	274.0	–	3.1 ± 0.1
	284.0	1.5 ± 0.1	3.9 ± 0.1
	293.0	3.5 ± 0.1	5.7 ± 0.1
	301.5	6.2 ± 0.9	8.0 ± 0.8
0.200	255.0	0.4 ± 0.2	1.4 ± 0.3
	264.5	1.6 ± 0.1	1.9 ± 0.1
	274.0	3.6 ± 0.2	3.0 ± 0.2
	284.0	10 ± 1	3.4 ± 1.2
	293.0	14 ± 1	7.9 ± 0.9
	301.5	27 ± 3	7.7 ± 3.5
0.300	255.0	1.0 ± 0.1	1.4 ± 0.1
	264.5	2.7 ± 0.6	2.1 ± 0.6
	274.0	5.9 ± 0.1	3.8 ± 0.1
	284.0	14 ± 1	5.8 ± 0.9
	293.0	33 ± 4	7.3 ± 3.0
	301.5	46 ± 1	14 ± 2

(a) $[NaBPh_4]_T = 20.0$ mM.

Table 4.9: Activation Parameters for the Dissociative and Associative Exchange of Sodium with B15C5 in Acetonitrile - Nitromethane Solvent Mixtures.

X_{AN}	ΔG^{*}_{di}[a] kJ.mol^{-1}	ΔH^{*}_{as} kJ.mol^{-1}	ΔS^{*}_{as} J.K^{-1}.mol^{-1}	ΔG^{*}_{as}[a] kJ.mol^{-1}
0	62.1 ± 0.3	28 ± 3	-57 ± 3	44.8 ± 0.1
0.0252	59.2 ± 0.1	25 ± 1	-66 ± 8	45.9 ± 0.1
0.0500	57.8 ± 0.4	24 ± 2	-66 ± 8	45.6 ± 0.5
0.100	56.5 ± 0.2	–	–	45.1 ± 0.5
0.200	54.1 ± 0.1	23 ± 2	-75 ± 8	45 ± 1
0.300	52.7 ± 0.1	28 ± 2	-58 ± 8	44.1 ± 0.4
0.400	51.1 ± 0.2	–	–	50 ± 8

(a) at T = 301.5 ± 0.5 K.

The results shown in Table 4.9 corroborate previous conclusions that the associative exchange mechanism for sodium in its solvated and complexed to B15C5 sites is insensitive to the solvent since the activation parameters are affected very little upon change in solvent composition. Again the highly negative values for the ΔS^{*}_{as} are indicative of an associative type mechanism. Earlier, a conformational origin of the associative mechanism was alluded to. If this hypothesis is combined with the solution structural studies in chapter 3 of this thesis, a relatively simple scenario for the associative chemical exchange of sodium in its solvated and complexed to B15C5 sites can be devised. This is shown in Scheme 1. The evidence that was presented in chapter 3 indicated that the overall structures of B15C5 and $(Na{:}B15C5)^{+}$ in solution are similar those as solids determined by X-ray crystallography [77,79].

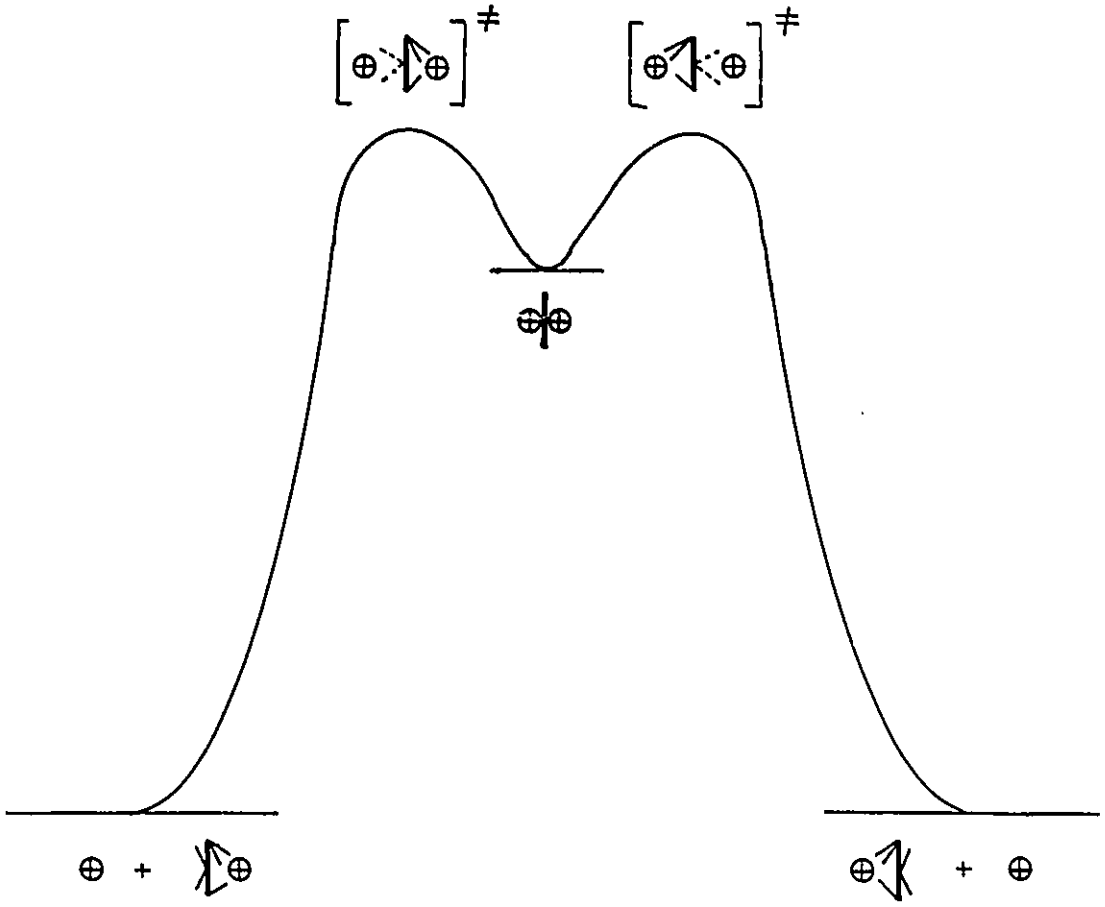

Scheme 1: Scenario of the associative exchange mechanism of Na^+ in the Na^+-B15C5 complex.

More specifically, an overall preferred conformation of the complexed and free B15C5 in solution was shown, where the oxygens in a C-C bond are gauche with respect to each other. Upon closer examination of the actual solid structures, shown in Figure 3.9, a difference in relative orientation of the five oxygen atoms in B15C5 free and complexed, is observed: this specific information cannot be obtained in solution. In the scenario shown in Scheme 1, the relative orientations of the five oxygen atoms in B15C5 complexed to the sodium cation were assumed to be identical to what is observed as a solid. In this scheme, the benzene group of B15C5 is omitted for clarity and the crown ether is represented by a thick line. Although all the oxygens are known to participate in the electrostatic bonding of sodium in $(Na:B15C5)^+$ [77], the orientations of the oxygen atoms, represented by lines which stem from the central one, relative to the plane of the crown ether are denoted as shown. Whereas the solvent is still implicated in the solvation-desolvation processes which must occur in this exchange mechanism, the scenario shown in Scheme 1 implies that the exchange is controlled by conformational reorientations. As far as the dissociative exchange mechanism is concerned the solvent must play a governing role and one of the objects of this work is to characterize its participation on a molecular level.

4.5.2 Dimethylformamide-Nitromethane Binary Solvent Mixtures

Figure 4.20 shows the ^{23}Na NMR spectra of samples containing equal populations of $(Na^+)_S$ and $(Na:B15C5)^+_S$ ($\rho = 0.50$) in DMF-NM binary mixtures. As was the case for the AN-NM mixtures, as the content of higher donor solvent increases, so does the observed $(k_A + k_B)$. However, the concentrations of DMF (0.03 to 0.2 M) in the DMF-NM solvent mixtures are very low compared to the concentration of AN in the AN-NM mixtures (0.5 to 8 M).

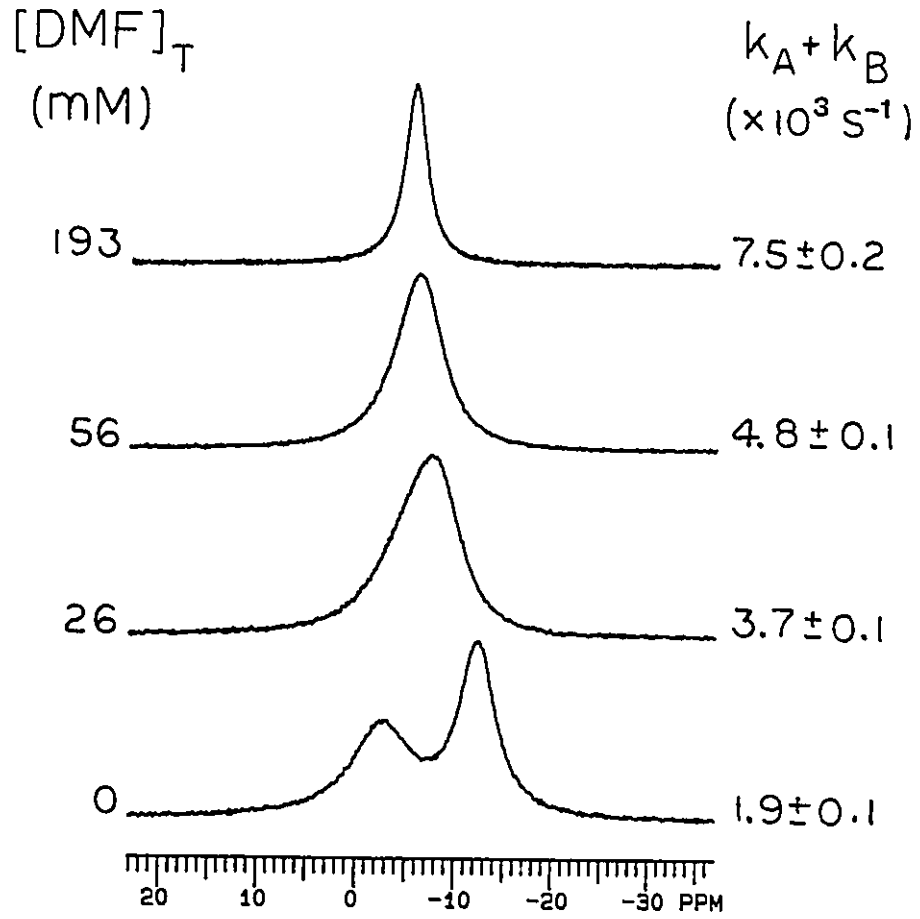

Figure 4.20: ^{23}Na spectra of samples containing equal populations of solvated sodium and sodium complexed with B15C5 ($\rho = 0.50$). $[NaBPh_4]_T = 20.0$ mM and T = 301.5 ± 0.5 K. From top to bottom the concentration of dimethylformamide in the DMF-NM binary solvent mixtures and $(k_A + k_B)$ vary as shown.

Very little DMF, which is in the order of the $[Na^+]_T$ (0.02 M), results in a considerable increase in the overall exchange rate. This is not surprising considering that the donor ability of DMF (DN = 26.6) is much higher than that of AN (DN = 14.1). Since the relative concentrations of DMF in the solvent mixtures are very small, one can consider that the macroscopic properties of the global solvent, such as magnetic susceptibility, are as those of pure NM. We have seen that whereas in pure NM the formation constant of $(Na:B15C5)^+$ is high, that in pure DMF is much lower. Figure 4.21 shows the chemical shift as a function of ρ for the complexation of sodium with B15C5 in various DMF-NM binary solvent mixtures. Since the chemical shift variations are linear in the solvent mixtures containing mole fraction contents of DMF, X_{DMF}, equal to 0.0052 (0.107 M) and 0.0150 (0.279 M), this indicates that in these conditions the formation constant of B15C5 is still high: $\log K_{F1} > 4$. It is not until X_{DMF} reaches 0.0250 (0.460 M) that the presence of DMF causes an observable decrease in the extent of complex formation, which is reflected by the appearance of a slight curvature in the variation. In this case, a value of K_{F1} may be determined from a nonlinear regression of the data (see Appendix 2): $\log K_{F1} = 2.8 \pm 0.5$

Plots of $(k_A + k_B)$ as a function of $(1-\rho)^{-1}$ for several DMF-NM mixtures at 301.5 K, shown in Figure 4.22, again show an increase in the dissociative contribution (slope) as the content of DMF in the solvent increases. The rate constants for the two exchange mechanisms determined from linear regressions of the plots in Figure 4.22 are shown in Table 4.10. As observed in the AN-NM case, there is a respective increase and decrease of k_{-1} and ΔG^*_{di} as the concentration of the minor component increases. There also appears to be a slight increase in k_2 as the [DMF] increases. However, whereas this increase is only approximately 2 fold in going from $X_{DMF} = 0$ to 0.0151 M, the observed increase in k_{-1} is 30 fold.

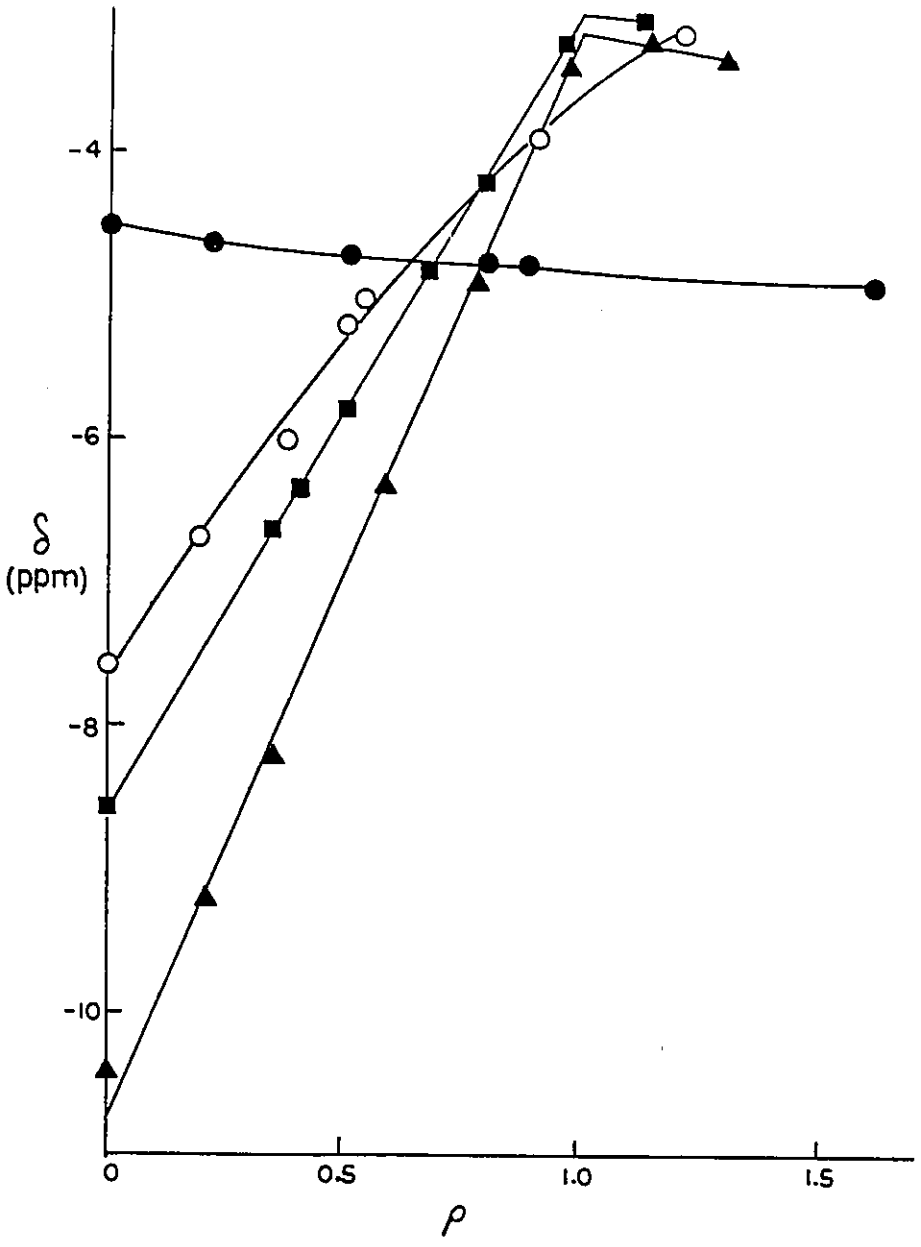

Figure 4.21: ^{23}Na chemical shift as a function of $\rho = [B15C5]_T / [NaBPh_4]_T$ in various dimethylformamide - nitromethane binary solvent mixtures at 301.5 ± 0.5 K. Mole fraction content of dimethylformamide, X_{DMF}, is: (▲) 0.0052; (■) 0.0150; (○) 0.0250 and (●) 1.0.

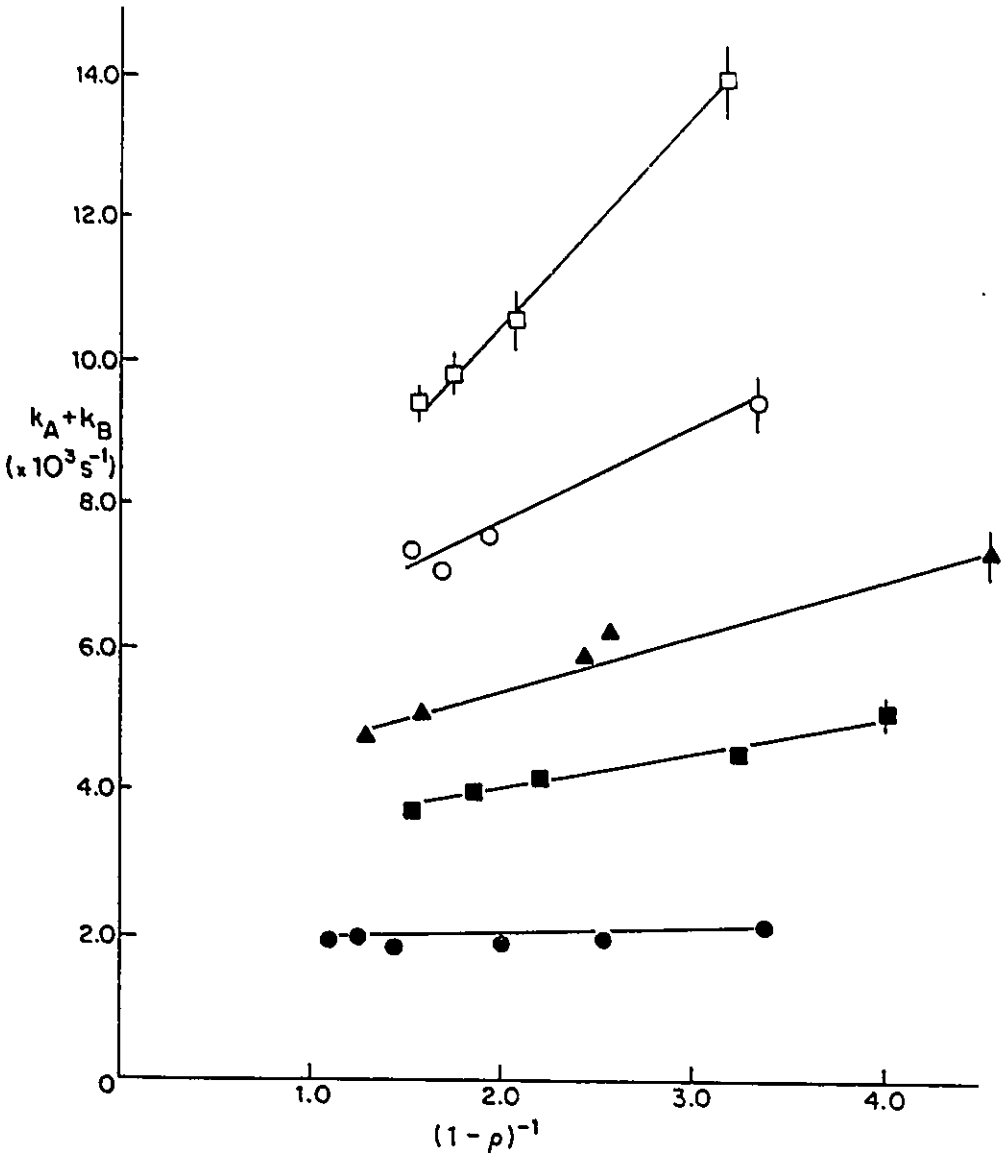

Figure 4.22: (k_A + k_B) as a function of $(1-\rho)^{-1}$ for several DMF-NM binary solvent mixtures. $[NaBPh_4]_T$ = 20.0 mM and T = 301.5 ± 0.5 K. Mole fraction of DMF (X_{DMF}): (□) 0.015; (○) 0.0100; (▲) 0.0052; (■) 0.0030; (●) 0.

Table 4.10: Kinetic Parameters for the Dissociative and Associative Exchange of Sodium with B15C5 in Dimethylformamide - Nitromethane Binary Solvent Mixtures[a].

X_{DMF}	[DMF] M	k_{-1} $\times 10^2\ s^{-1}$	$\Delta G^{\ddagger}_{di}$ $kJ.mol^{-1}$	k_2 $\times 10^5\ M^{-1}s^{-1}$	$\Delta G^{\ddagger}_{as}$ $kJ.mol^{-1}$
0	0	1.1 ± 0.1	62.1 ± 0.3	1.09 ± 0.04	44.8 ± 0.1
0.0030	0.056	4.9 ± 0.6	58.3 ± 0.3	1.5 ± 0.1	44.0 ± 0.2
0.0052	0.107	7.7 ± 1.0	57.2 ± 0.3	2.0 ± 0.1	43.3 ± 0.2
0.0100	0.193	14 ± 2	55.7 ± 0.3	2.5 ± 0.1	42.7 ± 0.2
0.0150	0.279	29 ± 1	53.9 ± 0.3	2.4 ± 0.1	42.8 ± 0.2

(a) all values of k_{-1}, k_2, $\Delta G^{\ddagger}_{di}$ and $\Delta G^{\ddagger}_{as}$ reported at 301.5 ± 0.5 K

At this point the kinetic results obtained for the DMF-NM binary solvent mixtures do not yet offer any new perspectives about the direct implication of the solvent molecules in the dissociative chemical exchange. The kinetic studies in binary mixtures have clearly illustrated contributions of both exchange mechanisms which are in direct competition with each other and it was concluded that it is not until the rate for the dissociative mechanism becomes appreciable, that this contribution is even observed. It has also been surmised, that whereas the solvent has a minor influence on the associative mechanism, it plays a crucial role in the dissociative exchange mechanism. The question is then, how exactly does the solvent participate in the dissociative exchange at the molecular level and can this participation be quantified?

4.5.3 Coordination of Sodium by Dimethylformamide

By looking at the solution ^{23}Na NMR chemical shifts and longitudinal relaxation times, two parameters reflecting the immediate coordination environment of sodium, we hope to gain insight into the actual participation of the solvent molecules themselves. Since $(Na:B15C5)^+$ displays chemical shifts and reduced longitudinal relaxation rates which are different in the four neat solvents (NM, AN, DMF and PY; see Table 4.2 on page 81), it can be concluded that the solvent, along with the ligand, must be present in the coordination sphere of the complexed cation in at least some of the solvents. It is thus reasonable to assume that one or two solvent molecules may bond to the partially exposed sodium cation. Table 4.11 shows a summary of the ^{23}Na NMR characteristics of the solvated and complexed sodium (B15C5) in several DMF-NM binary solvent mixtures. As the concentration of DMF increases, the observed chemical shift of $(Na)^+_S$ increases from its value in pure NM, -14.41 ppm, to that in pure DMF, -4.55 ppm. This variation of δ_S as a function of DMF content is consistent with a solvent competition between NM and DMF for the coordination sites of the sodium cation. This curved relationship, shown in Figure 4.23, reflects the overall equilibrium shown in equation 42:

$$(Na^+)_{xNM} + yDMF \rightleftharpoons (Na^+)_{yDMF} + xNM \qquad (42)$$

where y DMF molecules are replacing x NM molecules in a successive fashion. It is reasonable to assume that x and $y = 4$ for solvent coordination of the sodium cation in nonaqueous solvents [169,170] and therefore the equilibrium in equation 42 describes four successive equilibria having an intrinsic equilibrium constant associated with each step.

Table 4.11: ^{23}Na NMR Characteristics of $(Na^+)_S$ and $(Na:B15C5)^+_S$ in DMF-NM Solvent Binary Mixtures[a].

X_{DMF}	[DMF] M	δ_S[b] ppm	$T_{1,S}^{-1}$ Hz	δ_C[c] ppm	$T_{1,C}^{-1}$ Hz
0	–	-14.41	26 ± 1	-3.71	610 ± 12
0.0014	0.026	-12.39	145 ± 3	-3.58	540 ± 15
0.0030	0.056	-11.62	224 ± 4	-3.41	510 ± 30
0.0052	0.107	-10.50	316 ± 9	-3.35	472 ± 10
0.0070	0.132	-10.08	353 ± 4	-3.29	446 ± 13
0.0090	0.168	-9.56	383 ± 8	-3.30	422 ± 16
0.0100	0.188	-9.46	403 ± 16	-3.21	418 ± 12
0.0150	0.279	-8.57	410 ± 12	-3.17	376 ± 10
0.0025	0.460	-7.67	413 ± 20	-3.11	337 ± 13
0.0050	0.913	-6.50	355 ± 14	–	–
0.070	1.27	-6.10	330 ± 10	–	–
0.077	1.40	-5.99	300 ± 11	-3.79	–
0.100	1.97	-5.60	265 ± 3	-3.94	–
1.00[d]	–	-4.55	86 ± 1	-5.9	273 ± 84

(a) $[NaBPh_4]_T$ = 20.0 mM at 301.5 ± 0.5 K. (b) the error on the chemical shift depends on the linewidth of the line: typically δ_S ± 0.01 to 0.02 ppm (c) δ_C ± 0.02 to 0.05 ppm (d) characteristics determined from nonlinear regressions in Figures 4.2a and 4.2b.

A model based on the application of the *Hill* formalism [171], widely used in biochemical studies of phenomena such as cooperative oxygen bonding to hemoglobin, is adequate in the mathematical treatment of this type of problem [172,173], since preferential solvation of a tetracoordinated ion and binding of a ligand to one of four sites in a biomolecule constitute one and the same problem. The *Hill* formalism was previously successfully applied by Delville et al. [172] in a study of the preferential solvation of the sodium cation in binary mixtures of THF with amines. This situation is very similar to the present one and from a parallel mathematical treatment, it is possible to find out if there is cooperativity in the successive steps of solvent displacement and to obtain the intrinsic K_S for each step if there is no cooperativity. The relationship between δ_S and X_{DMF} observed can be directly translated to a Hill plot which is shown in Figure 4.24 for both the AN-NM and DMF-NM binary mixtures. The Hill plot relates a parameter Y, determined from the observed chemical shift and thus reflecting the fraction of the Na^+ cation sites occupied by a ligand such as DMF or AN, with another A, based on the composition of the solvent in the medium [172,173]. The linearity of the ln (Y/1-Y) as a function of ln (A) plots, where $Y = (\delta_{obs} - \delta_{NM}) / (\delta_{DMF \text{ or } AN} - \delta_{NM})$ (assuming additive chemical shifts for all intermediate species formed) and $A = [DMF \text{ or } AN]_T / [NM]_T$, indicates that there is no cooperativity in the successive displacement of NM by AN or DMF. Furthermore, the value of the intercept is equal to ln (K_S) where K_S is the intrinsic equilibrium constant for each step. Linear regressions for both binary mixtures give the following linear equations: for AN-NM; $y = (1.03 \pm 0.03)x + (2.31 \pm 0.05)$ and for DMF-NM; $y = (0.83 \pm 0.01)x + (3.81 \pm 0.02)$ and from the values of the intercepts, the K_S values are obtained: $K_S = 10.0 \pm 0.3$ and 45 ± 2 for AN and DMF in NM respectively. The higher K_S for DMF is expected since this solvent has a higher DN and competes more effectively than AN for the sodium cation.

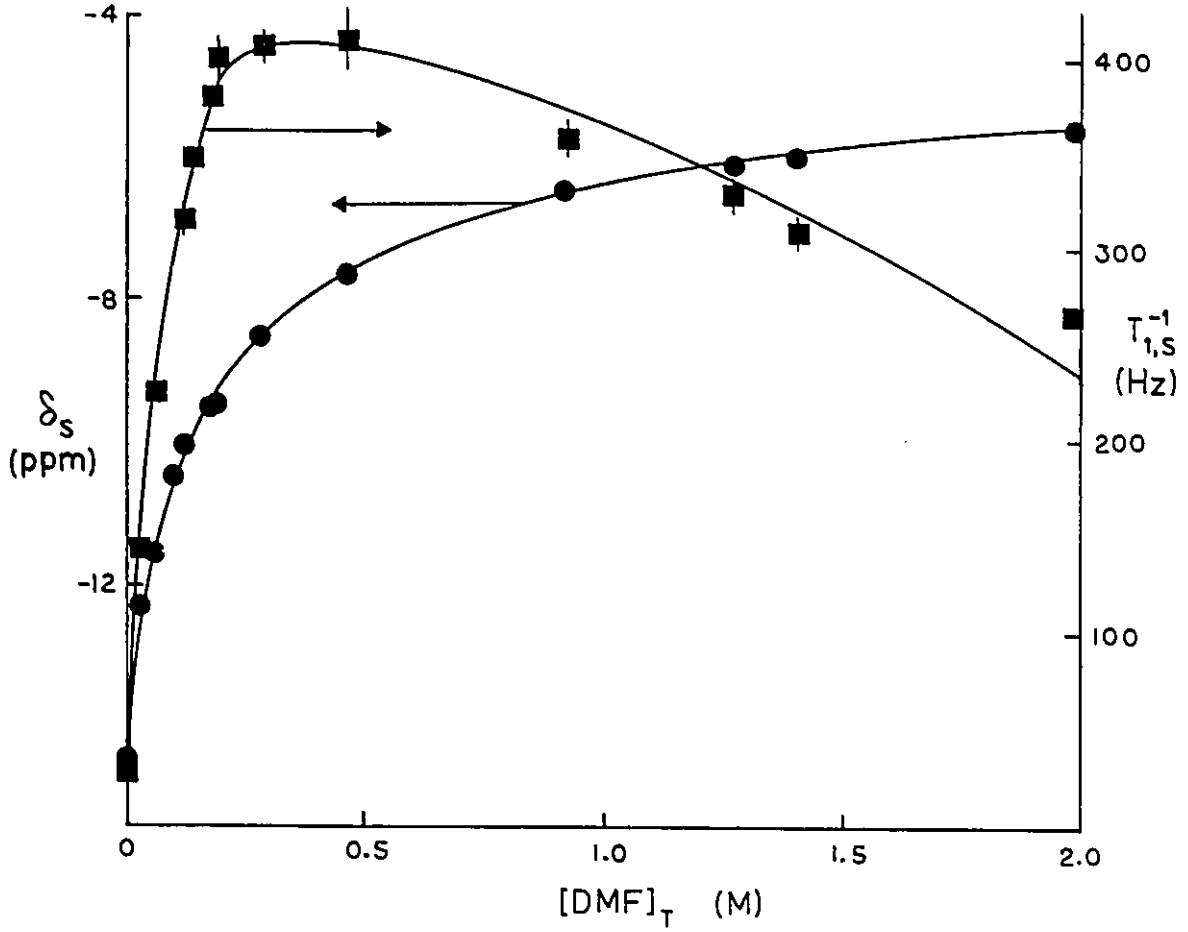

Figure 4.23: The ^{23}Na chemical shift: (●) and longitudinal relaxation rate: (■) of $(Na^+)_S$ as a function $[DMF]_T$ in DMF-NM binary solvent mixtures. T = 301.5 and $[NaBPh_4]_T = 20.0$ mM.

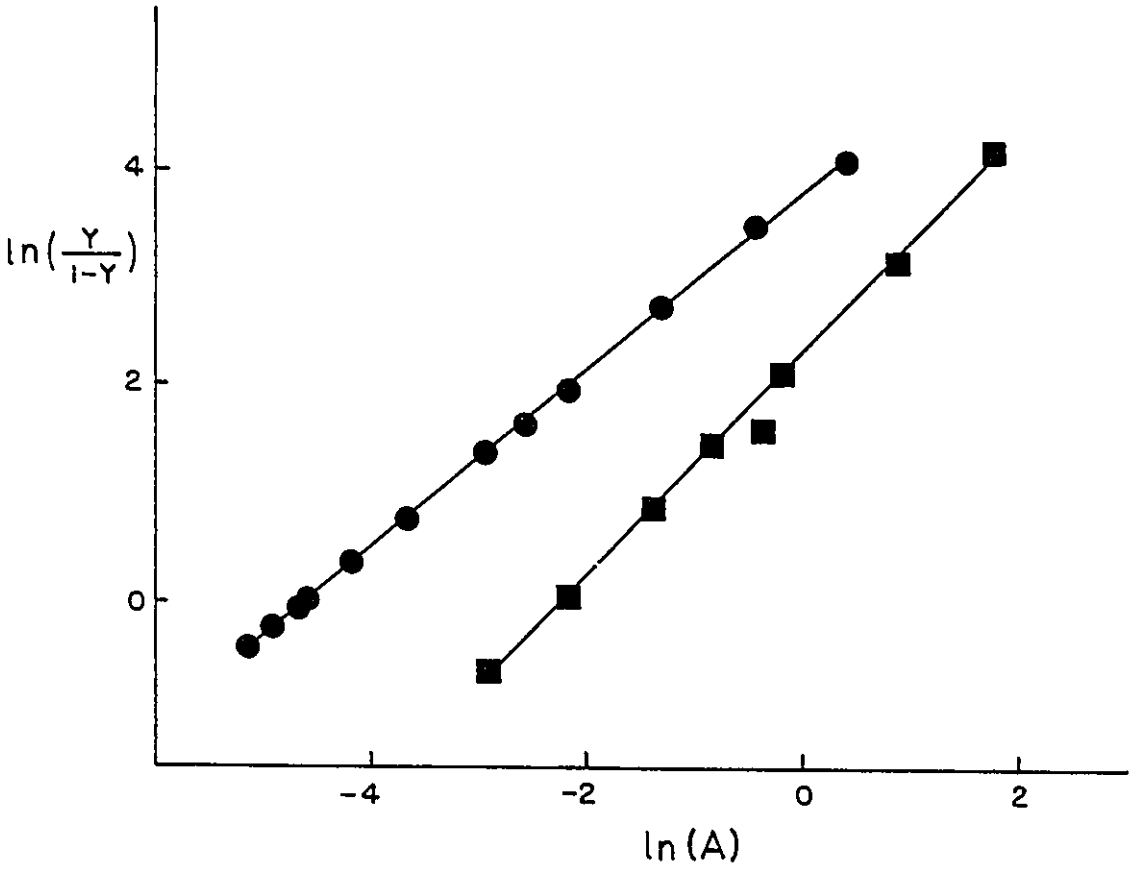

Figure 4.24: Hill plots involving $(Na^+)_S$ in binary mixtures of (■) AN-NM and (●) DMF-NM.

Figure 4.23 also shows the variation and sensitivity of the longitudinal relaxation rate as a function of the concentration of DMF. Although these results still reflect the overall equilibrium shown in equation 42, the trend does not display a steady variation exhibiting a maximum of ~ 400 Hz at $[DMF]_T$ = 0.35 M. The magnitude of the relaxation rate reflects the overall symmetry about the sodium cation and any one point on this curve reflects an average of the sodium species present in solution. Initially at $[DMF]_T$ = 0, the sodium is surrounded by nitromethane molecules in a symmetrical coordination. This results in the relatively low value for the observed longitudinal relaxation rate. In pure DMF, again a relatively low value for T_1^{-1} is observed since the sodium is again in a symmetrical environment. In the region 0 > $[DMF]_T$ > 2, sodium can be coordinated by various combinations of DMF and NM resulting in an unsymmetrical sodium coordination sphere and thus in the observation of higher T_1^{-1} values.

Figure 4.25 shows the variation of δ_C and $T_{2,C}^{-1}$ for $(Na:B15C5)^+$ as a function of the $[DMF]_T$ in DMF-NM binary solvent mixtures. The steady increase and decrease respectively of these two ^{23}Na NMR parameters indicates that the coordination sphere of sodium in $(Na:B15C5)^+$ is changing. The variations may be explained if one considers that a possible one molecule of NM in the first coordination sphere of sodium in $(Na:B15C5)^+$ is replaced by one molecule of DMF, as shown equation 43.

$$(Na:B15C5)^+_{NM} + DMF \overset{K_{CS}}{\rightleftharpoons} (Na:B15C5)^+_{DMF} + NM \qquad (43)$$

or if it is assumed that the poorly donating NM is not involved in the first coordination sphere of the complex then the equilibrium shown in equation 43 may be further simplified:

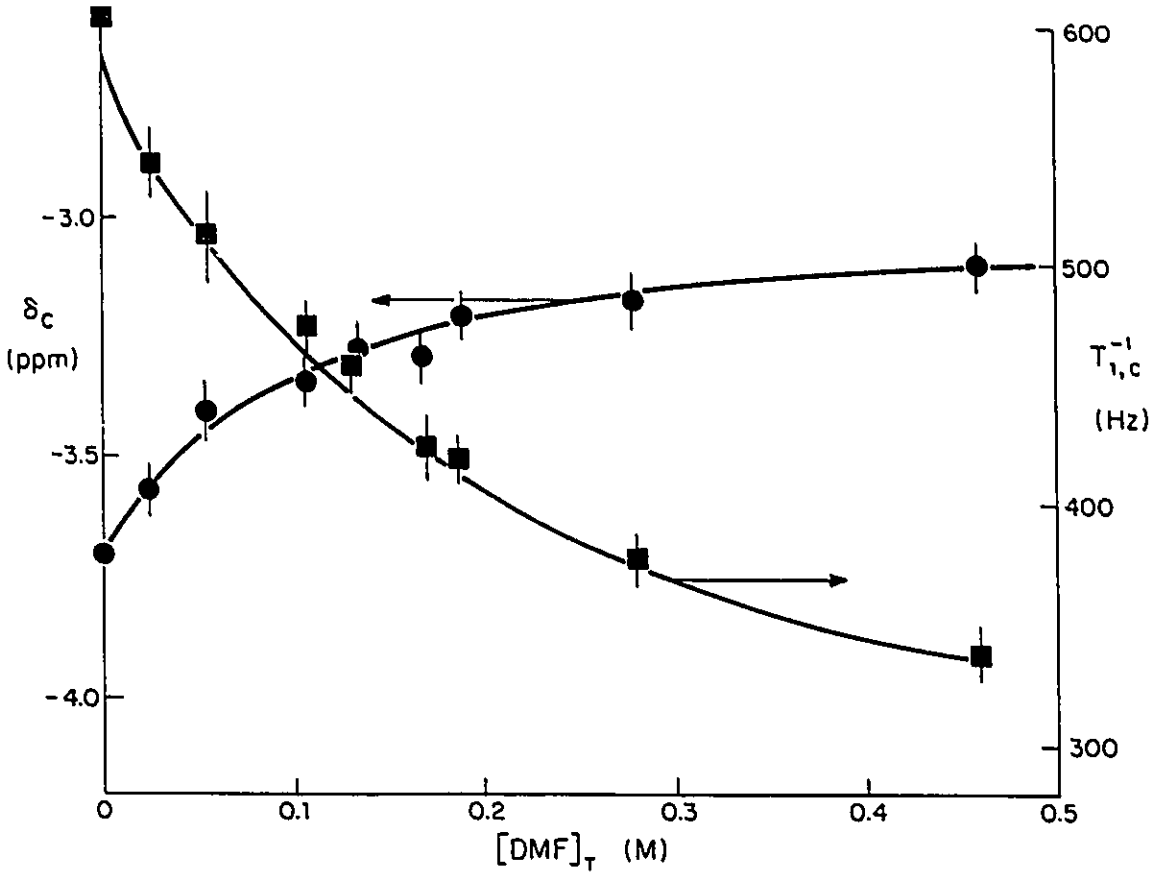

Figure 4.25: The chemical shift: (●) and longitudinal relaxation rate: (■) of $(Na:B15C5)^+$ as a function of $[DMF]_T$ in DMF-NM binary solvent mixtures. T = 301.5 and $[NaBPh_4]$ = 20.0 mM. The points are experimental and the drawn curves are based on a model involving the formation of $(Na:B15C5:DMF)^+$ (see equation 44 and text).

$$(Na{:}B15C5)^{+} + DMF \overset{K_{CS}}{\rightleftharpoons} (Na{:}B15C5{:}DMF)^{+} \qquad (44)$$

A model, based on the equilibrium shown in equation 44, was formulated and K_{CS} was obtained from the data shown in Figure 4.25; this is shown in Appendix 4. Nonlinear regressions from the chemical shift and longitudinal relaxation rate data have given log K_{CS} = 1.04 and 0.61 respectively with an average log K_{CS} = (0.8 ± 0.3). As the $[DMF]_T$ increases so does therefore the concentration of a newly formed species which will be referred to as $(Na{:}B15C5{:}DMF)^{+}$. This complexed sodium species is different than the previously referred to $(Na{:}B15C5)^{+}$, by virtue of the direct implication of one DMF molecule in the coordination sphere of sodium. The values of $T_{1,C}^{-1}$ as a function of $[DMF]_T$ steadily decrease from a value in pure NM, 610 Hz, towards that in pure DMF, 273 Hz. This is not a variation due to viscosity effects (see equations 8 and 10) since an opposite trend would be expected as the concentration of the more viscous solvent (DMF) increases. Moreover, the concentrations of DMF are very low, so that the change in overall solvent viscosity is minimal [174]. The variation of δ_C, on the other hand, is not in the direction expected: Figure 4.25 shows an increase from -3.71 ppm to a limiting value of -2.98 ± 0.04 ppm, determined from the nonlinear regression whereas one would expect an opposite trend towards -5.9 ppm (see Table 4.2 on page 81). Since very similar values of K_{CS} can be obtained from the data in both curves shown in Figure 4.25, the chemical shift trend shown is real. This implies that the involvement of DMF at the complexed cation site, as reflected by the observed chemical shift, is different in a solvent medium containing low concentrations of DMF to one which is pure in DMF. In the first case, there is only one DMF molecule in the first coordination sphere of sodium in a bulk NM medium, and in the second case there is plausibly more than one molecule in the first coordination sphere of the complexed sodium in a bulk DMF medium.

Studies in binary mixtures of PY-NM have proven to be anomalous if one considers only the donicity number of this solvent (DN=33.1). In binary solvent mixtures where the $[PY]_T$ in the overall solvent is comparable to that of DMF, no appreciable increase in the sum of the two pseudo-first order rate constant for chemical exchange, $(k_A + k_B)$, compared to that in pure NM was observed. There was also very little variation in the ^{23}Na parameters of $(Na:B15C5)^+$ upon increasing the PY content in the overall solvent, reflecting the lack of participation of PY in the coordination of complexed sodium. On the basis of the high donor value of PY, one would expect a kinetic effect even more dramatic than DMF. Since this is not the case, one can surmise that other factors play a role in the kinetic and mechanistic participation of PY molecules. Steric hindrance preventing the interaction of PY may be a consideration. Unexpected behaviors in PY have also been reported where the formation constants of cation-macrocycle complexes were found to be relatively large [128,175]. In these cases, it has been postulated that since PY, being a nitrogen donor or a "soft base", does not solvate strongly a "hard acid" such as the sodium cation [128,175] and as a result, the Gutmann Donor Number does not work well in amine solvents.

4.5.4 Mechanistic Interpretation of the Participation of Dimethylformamide

A summary of the kinetic results for the chemical exchange of sodium in $(Na^+)_S$ and $(Na:B15C5)^+_S$, obtained in AN-NM, DMF-NM and PY-NM binary solvent mixtures can be represented by Figure 4.26. At these relatively low concentrations of AN or PY in the solvent mixtures, there is no appreciable increase in the $(k_A + k_B)$ which remains close in value to that in pure NM. On the other hand, the increase in $(k_A + k_B)$ is linearly related to an increase in the $[DMF]_T$. Earlier, we observed that this increase comes mainly from an increase in the dissociative exchange contribution (see Figure 4.22). We have also speculated that as the $[DMF]_T$ increases, so does the concentration of $(Na:B15C5:DMF)^+$ and it is plausible to consider that it is this new species which is responsible for the observed increase in the dissociative contribution of $(k_A + k_B)$. The overall expression for $(k_A + k_B)$ shown in equation 35, has been very successful up until now, in relating the observed kinetic data to mechanistic aspects of the actual chemical exchange which has included contributions of two proposed mechanisms. In order to represent the data obtained in the DMF-NM solvent mixtures shown in Figure 4.26, another contribution to the $(k_A + k_B)$ must be taken into account: a dissociative exchange involving $(Na:B15C5:DMF)^+$:

$$(Na:DMF)^+ + B15C5 \underset{k_{-1}^*}{\overset{k_1^*}{\rightleftharpoons}} (Na:B15C5:DMF)^+ \qquad (45)$$

For the two-site chemical exchange (equation 22) in binary solvent DMF-NM mixtures, one must consider that the solvated metal cation (site A) can exist in two forms where the total concentration of solvated cation, $[M^+]_{S,T}$, is equal to $[Na^+] + [Na^+:DMF]$.

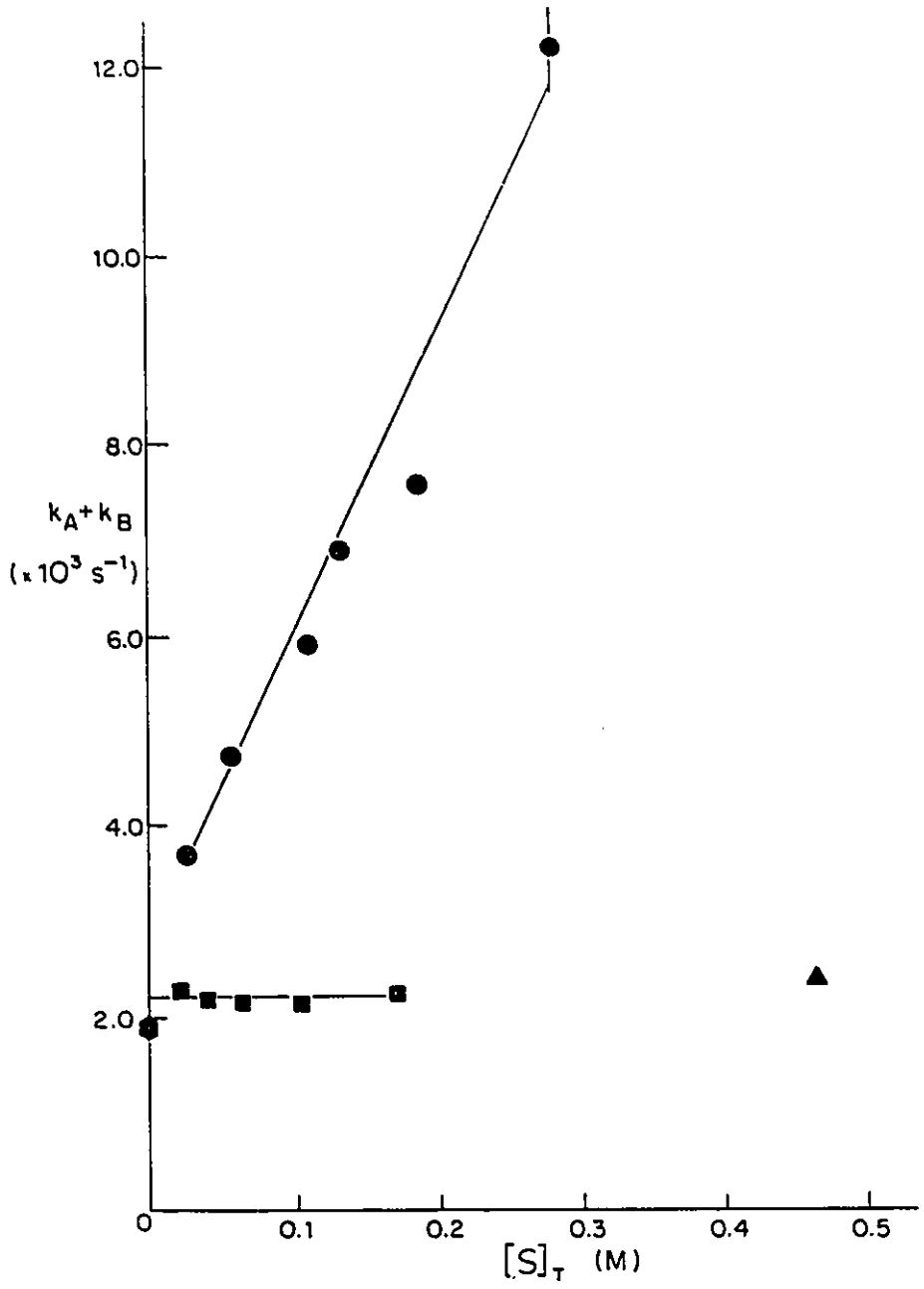

Figure 4.26. (k_A + k_B) as a function of the concentration of the minor solvent component, $[S]_T$, in the S-NM binary mixtures. S is AN (▲); DMF (●); and PY (■). As well (⬢) in pure NM. T =301.5, $[NaBPh_4]_T$ = 20.0 mM and ρ = 0.50.

The complexed metal cation (site B) also has two possible forms where $[M^+:C]_T$ = $[Na^+:B15C5]$ + $[Na^+:B15C5:DMF]$. The total concentration of sodium cation, $[Na^+]_T$, is equal to $[M^+]_{S,T}$ + $[M^+:C]_T$ and it is straightforward to derive the dissociative contribution to $(k_A + k_B)$ from the reaction shown in equation 45. The rates for the appearance $(M^+)_S$ and $(M:C)^+$ can be, for this mechanism, expressed as:

$$d[M^+]_{S,T}/dt = k_B [M^+,C]_T = k_{-1}^* [Na^+:B15C5:DMF] \quad (46)$$

$$d[M^+:C]_T/dt = k_A [M^+]_{S,T} = k_1^* [Na^+:DMF] [B15C5] \quad (47)$$

and therefore:

$$(k_A + k_B) = k_{-1}^*[Na^+:B15C5:DMF] ([Na^+]_T/([M^+]_{S,T}[M^+,C]_T)) \quad (48)$$

The linear variation of $(k_A + k_B)$ as a function of $[DMF]_T$ shown in Figure 4.25, is obtained for samples containing equal populations of $(M^+)_S$ and $(M:C)^+$ ($\rho = 0.5$). At these low concentrations of DMF (0 - 0.28 M), we have determined that log K_F for the formation of $[M^+,C]$ is still > 4. This was shown in Figure 4.21 which illustrates that at the highest [DMF] in the kinetic studies (0.28 M), the relationship between δ and ρ is still linear reflecting the high extent of complex formation. Therefore for $\rho = 0.5$, $[M^+]_{S,T} \cong [M^+,C]_T = 0.5[Na^+]_T$ and therefore equation 48 is reduced to:

$$(k_A + k_B) = k_{-1}^*[Na^+:B15C5:DMF] (4 / [Na^+]_T) \quad (49)$$

The $[Na^+:B15C5:DMF]$ can be related to K_{CS} (see equation 44) and thus:

$$(k_A + k_B) = k_{-1}^*(K_{CS} [Na^+:B15C5] [DMF]_F)(4 / [Na^+]_T) \quad (50)$$

where $[DMF]_F$ is the concentration of free DMF. The following assumptions can be made since K_{CS} was determined to be relatively low (log K_{CS} = 0.8 ± 0.3): 1) $[Na^+:B15C5] \sim [M^+:C]_T$ (that is, $[Na^+:B15C5:DMF]$ is negligible compared to $[Na:B15C5]^+ \equiv 0.5\ [Na^+]_T$ at these low DMF concentrations) and 2) $[DMF]_F \equiv [DMF]_T$ (again a very small amount of $[Na^+:B15C5:DMF]$ is formed) and thus:

$$(k_A + k_B) = 2\ k_{-1}^*\ K_{CS}\ [DMF]_T \qquad (51)$$

Combining the contribution of this mechanism with the contributions of the other two usual mechanisms (equations 26 and 31), the following overall relationship between the $(k_A + k_B)$ and $[DMF]_T$ is obtained for $\rho = 0.5$:

$$(k_A + k_B) = 2\ k_{-1} + k_2\ [Na^+]_T + 2\ k_{-1}^*\ K_{CS}\ [DMF]_T \qquad (52)$$

A plot of $(k_A + k_B)$ as a function of $[DMF]_T$ should therefore be linear where the k_{-1}^* for the dissociative exchange of sodium in $(Na^+)_S$ and $(Na^+:B15C5:DMF)^+$ can be determined from the slope of this line since a value for K_{CS} is known. A linear regression of this plot shown in Figure 4.26 gives $k_{-1}^* = (2 \pm 1) \times 10^3\ s^{-1}$ and an intercept value = $(2.6 \pm 0.5) \times 10^3\ s^{-1}$ which corresponds very well with a value calculated from the previously reported values of k_{-1} and k_2 in pure NM: $k_{-1} = (1.1 \pm 0.1) \times 10^2\ s^{-1}$, $k_2 = (1.09 \pm 0.04) \times 10^5\ M^{-1}s^{-1}$ and therefore $(2\ k_{-1} + k_2\ [Na^+]_T) = (2.4 \pm 0.1) \times 10^3\ s^{-1}$.

The DMF-NM binary solvent mixtures is an excellent system for the study of the specific role of the solvent in the kinetic interactions between sodium cations and B15C5. Based on the ^{23}Na NMR results, we have surmised the implication of one

molecule of DMF in the coordination sphere of complexed sodium and from this a kinetic model has been proposed. In pure nitromethane, which is a poorly donating solvent, the associative mechanism overshadows the presence of the dissociative mechanism where the rate of dissociation of $(Na:B15C5)^+$, k_{-1} (see equation 26), in this solvent is relatively slow: $k_{-1} = (1.1 \pm 0.1) \times 10^2\ s^{-1}$. Upon the addition of small amounts of DMF, a highly donating solvent, in concentrations comparable to that of sodium, a phenomenal increase is observed in the overall exchange rate. This reflects the very favourable coordination of DMF to sodium, already coordinated to B15C5 and surrounded by the abundant nitromethane solvent molecules. Coordination of the sodium cation by the one molecule of DMF, results in an increased lability of the sodium complex. This is reflected by the rate constant for the dissociation of $(Na:B15C5:DMF)^+$, k_{-1}^* (see equation 45) which was determined to be $(2 \pm 1) \times 10^3\ s^{-1}$. An increase in over one order in magnitude in the dissociative rate constant has resulted from the participation of one molecule of high donor solvent. This has facilitated complex dissociation and this dissociative contribution now offers a significant competition to the associative exchange, where the rate constant for this mechanism does not depend on the solvent medium, and can be observed.

Chapter 5

Kinetics and Mechanisms:

^{7}Li NMR Study of (Li:B15C5)$^{+}$

5.1 Introduction

The abundance of lithium in the earth's crust, as well as its biological importance, is relatively small compared to that of sodium. This element, in the form of lithium carbonate, has however been successfully applied in the treatment of manic-depressive disorders. The molecular basis for the biological action of lithium cations is unknown, although it has been postulated that Li^{+} competes with biological cations such as Na^{+}, K^{+}, Mg^{2+} and/or Ca^{2+} for binding sites [176-178]. Recent studies by Pettegrew et al. [177] and Espanol and Mota de Freitas [178], have provided insight into the possible biological role of lithium as a therapeutic drug. In ^{7}Li NMR studies conducted on human erythrocytes in relevant in vivo conditions (310 K, 0.2 - 2.5 mM Li^{+}), the intra- and extra- cellular lithium cations were differentiated by the use of a shift

reagent. The cellular uptake of the lithium cations, even in the presence of the physiologically relevant above cations, is a clear indication that lithium plays a significant role where the transport of cations across cell membranes is concerned [177,178]. The noninvasive use of ^{7}Li NMR to study intra-cellular lithium shows great promise as a tool for the investigation of the bioinorganic chemistry of lithium [178].

It was previously stated that the selectivity of alkali metal cation complexation to macrocyclic ligands is largely dependent on the size ratio of the metal cation and ligand cavity. In the previous chapter, the interaction of sodium with B15C5 was investigated by ^{23}Na NMR, where structural, kinetic and mechanistic information was obtained thereby well characterizing $(Na{:}B15C5)^{+}$. A parallel study of $(Li{:}B15C5)^{+}$, implicating the smaller lithium cation, could give fundamental insight into the influence of the metal cation to ligand size ratio where both structures and kinetics with crown ethers are concerned. Another justification for studying the kinetic interaction of crown ethers with lithium cations was alluded to by Eyring and coworkers [179], involving possible applications in lithium batteries. It was recently demonstrated that the addition of crown ethers to a solid electrolyte containing a lithium salt enhanced the charge transfer [180].

The quadrupole moment of the ^{7}Li nucleus is relatively low compared to that of ^{23}Na (see Table 1.1 on page 7) resulting in spectral linewidths which are relatively narrow compared to the other NMR active alkali nuclei (^{133}Cs and ^{6}Li also have low quadrupole moments and are also characterized by narrow linewidths). For example, the measured ^{23}Na linewidth at half-height of NaCl in water (0.1 M) at 300 K is 10 Hz whereas that of ^{7}Li for LiCl under identical conditions is 0.5 Hz. As well, relaxation mechanisms other than quadrupolar relaxation can influence this nucleus [28,181]. The chemical shift span of ^{7}Li NMR varies from -10 to 5 ppm (referred to LiCl in water) and macrocyclic lithium complexes have been observed to fall between -3 and 3 ppm [102,146,147,161,182,183].

Alkali metal NMR of crown ether complexes has been largely dominated by ^{23}Na NMR in the study of sodium complexes and ^{7}Li has not been a very popular choice despite its high sensitivity as a NMR nucleus. As a matter of fact it is the most sensitive of the NMR active alkali metal nuclei. Results using ^{7}Li NMR and concerning alkali metal macrocyclic complexes were first published in 1974 by Popov and coworkers [182]. In this first study, it was shown that the ^{7}Li chemical shift of Li^{+} complexed with the cryptand C211 was independent of the solvent illustrating the complete encasing of the lithium cation which forms an "exclusive" complex with this ligand. Kinetic studies with this system were possible since the ^{7}Li NMR (23.3 Mz) spectrum of a solution containing both lithium sites displayed two peaks indicating a slow rate of exchange on the ^{7}Li NMR chemical shift timescale [146,147]. It is interesting to note that at 23.3 MHz the lithium exchange between $(Li^{+})_S$ and Li^{+} complexed to C222 and C221 was fast on that ^{7}Li NMR chemical shift timescale and only one population average unbroadened resonance is observed [146,183] but a study at 69.591 MHz reported 12 years later for the same systems [147], displayed spectra which were broadened or contained two resonances thus allowing for kinetic studies. ^{7}Li NMR was also used in dynamic studies of the lithium cation with 16C4 derivatives [161].

In this chapter, the use of ^{7}Li NMR as a structural, thermodynamic, kinetic and mechanistic probe for $(Li{:}15C5)^{+}$ and $(Li{:}B15C5)^{+}$ will be illustrated and results will be compared to those obtained by ^{23}Na NMR for the corresponding sodium complexes. Furthermore, the application of 2D ^{7}Li EXSY (EXchange SpectroscopY) to also obtain exchange rates, will be shown. Finally, a study combining the two cations and the two alkali NMR nuclei will be presented and insight into the selectivity of B15C5 will be presented.

5.2 Lithium Chemical Exchange

Figure 5.1 shows the variation of the ^{7}Li chemical shift as a function of ρ ($[C]_T$ / $[LiClO_4]_T$) for both 15C5 and B15C5 in NM. The results obtained for 15C5 in NM ($[LiClO_4]_T$ = 0.02 M) agree with those of Smetana and Popov for the same system at 23.3 MHz [127]. Initially at ρ = 0, the observed chemical shift, -0.62 ppm, is characteristic of $(Li^+)_S$ in NM. Upon the addition of the individual crown ethers, there is complexation of lithium and an upfield shift is observed. The linearity of the plots in the region $0 < \rho < 1$ shown in Figure 5.1 is a clear indication that the formation of both $(Li{:}15C5)^+$ and $(Li{:}B15C5)^+$ in NM is quantitative and the K_F cannot be precisely determined by this technique. Smetana and Popov have reported a lower limit for the formation constant of $(Li{:}15C5)^+$ in NM at 300 K, where $\log K_F > 4$ [127]. Whereas $\log K_F > 4$ was also reported for the formation of $(Na{:}B15C5)^+$ in NM [88], the formation of a sandwich complex is observed with B15C5 and Na^+ where the formation of one is not obvious with Li^+ in the same solvent. A plateau for the chemical shift is reached at ρ = 1.0 indicating that all the lithium is complexed and no further interaction of this cation is observed. The chemical shift of $(Li{:}B15C5)^+$ is approximately 0.15 ppm further downfield that of $(Li{:}15C5)^+$. This probably reflects the ring current magnetic anisotropy of the aromatic substituent in B15C5 which has an effect on the ^{7}Li chemical shift. In the region of lithium concentrations studied, (1 - 11 mM) the chemical shift of $LiClO_4$, $(Li{:}15C5)^+$ and $(Li{:}B15C5)^+$ in NM varied minimally (maximum variation of 0.1 ppm), indicating a negligible amount of ion-pairing. Although $NaClO_4$ exhibited a limited solubility in NM, we also observed minimal ion-pairing with this salt (see Table 4.3 on page 83).

In kinetic studies involving lithium complexes, the same two-site exchange for the cation and mechanistic approach, described in sections 4.3 and 4.4, can be applied.

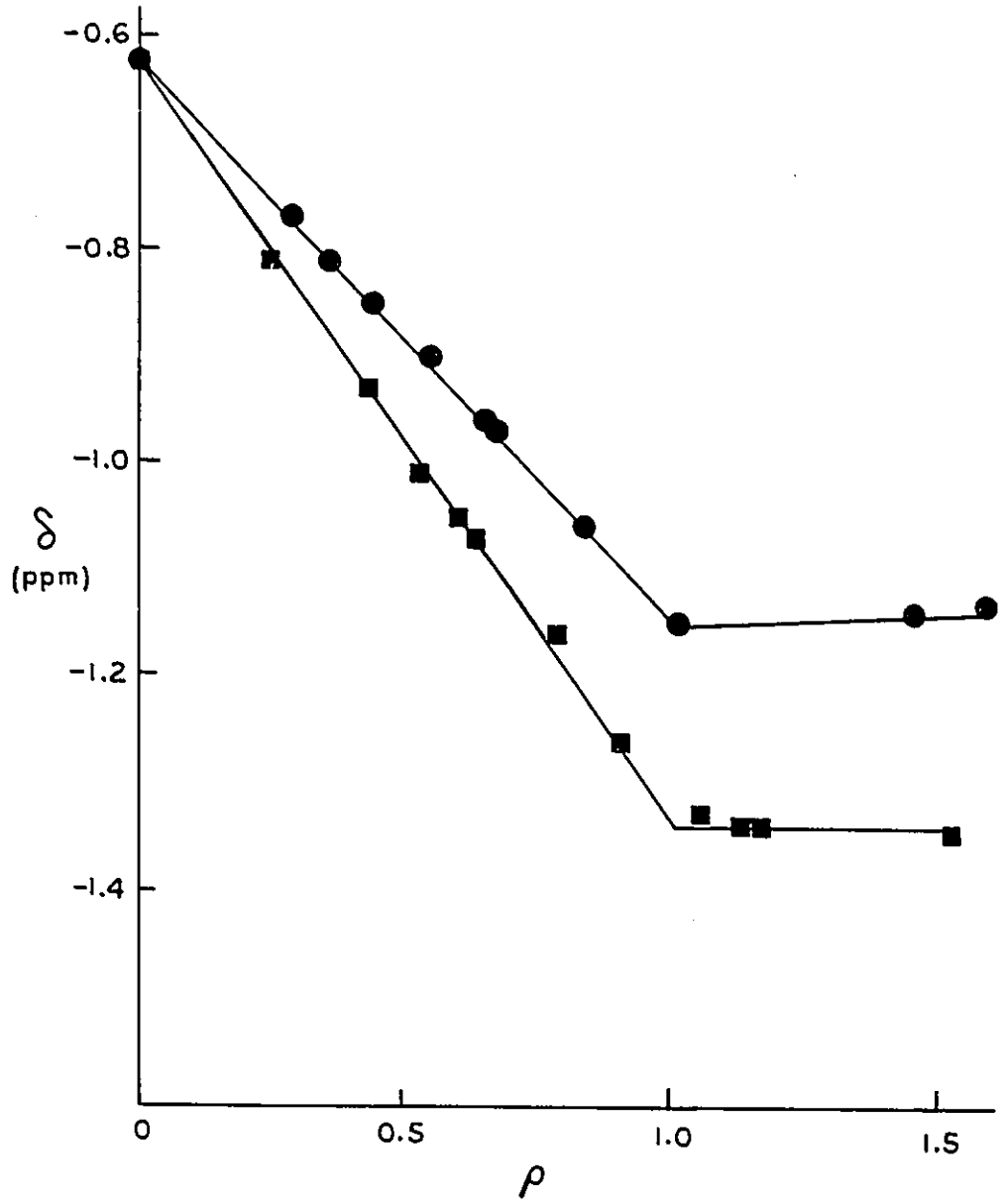

Figure 5.1: ^{7}Li chemical shift as a function of $[C]_T$ / $[LiClO_4]_T$ in nitromethane at 300.0 K. C = 15C5 (■) $[LiClO_4]_T$ = 10.0 mM; B15C5 (●) $[LiClO_4]_T$ = 10.6 mM.

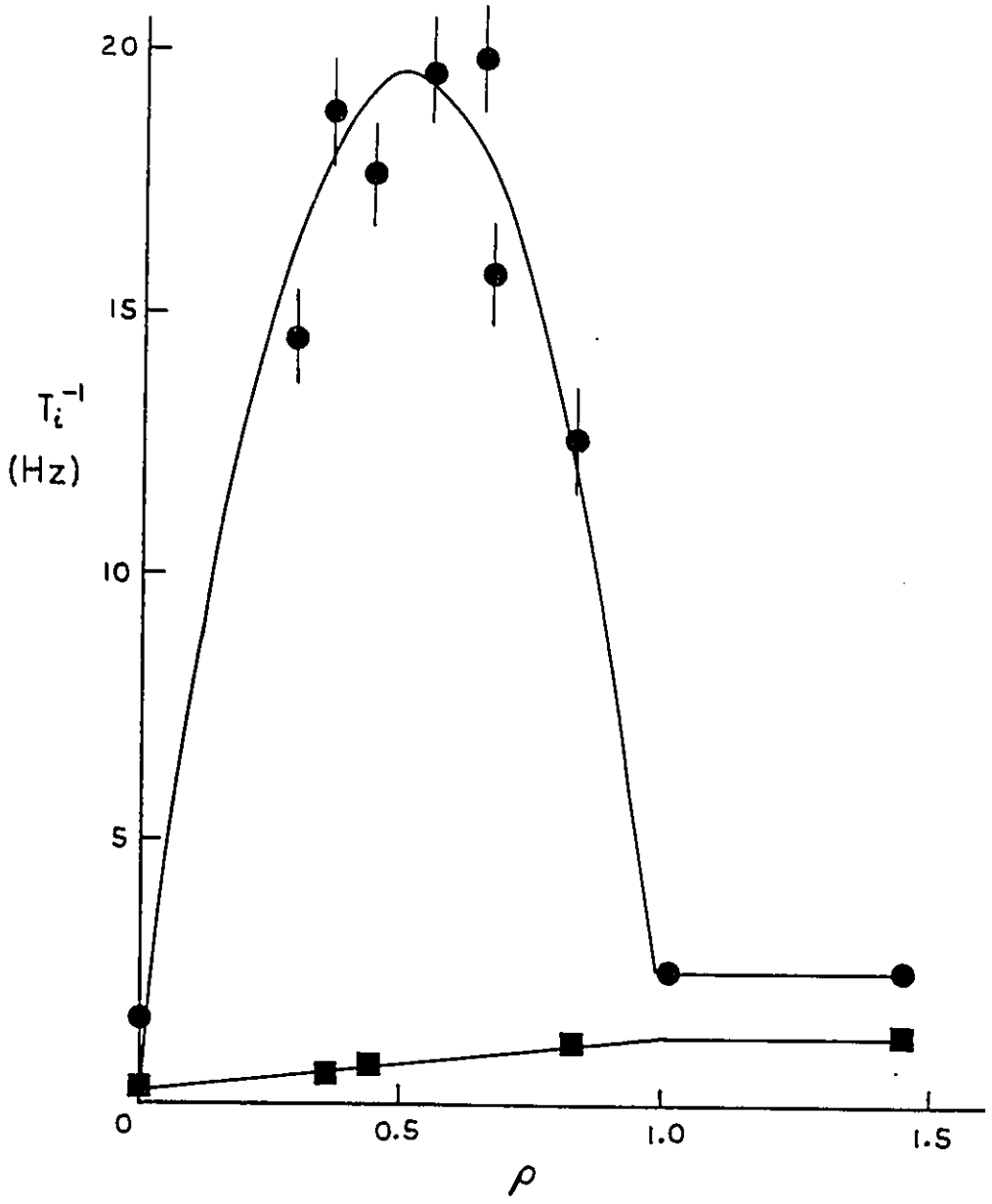

Figure 5.2: ^{7}Li transverse (i = 2; ●) and longitudinal (i = 1; ■) relaxation rates as a function of the ratio ρ = $[B15C5]_T$ / $[LiClO_4]_T$ in nitromethane. T = 300.0 ± 0.5 K and $[LiClO_4]_T$ = 10.6 mM. The data points are experimental and the T_2^{-1} curve has been calculated using an average value of k_2 (k_2 = 2.00 × 10^5 $M^{-1}s^{-1}$) determined from calculated values of (k_A + k_B) for each data point (equation 25) assuming associative exchange only.

In the experimental conditions corresponding to the plots in Figure 5.1, T = 300.0 K and $[LiClO_4]_T$ = 10.6 mM, only one ^7Li resonance is observed which is characteristic of the population average of $(Li^+)_S$ and $(Li{:}B15C5)^+$. The lines are broadened however, and the relationship between the ^7Li longitudinal and transverse relaxation rates, shown in Figure 5.2, is characteristic of moderately rapid exchange of lithium between the two sites. The two sites are again characterized by solvated (site A) and complexed (site B) alkali metal cation. The general appearance of this figure can be compared with the analogous sodium case shown in Figure 4.4. The transverse relaxation rate is affected by chemical exchange resulting in a broadening of the line, whereas the longitudinal relaxation rate is not. It is noteworthy that the values for the relaxation rates of $(Li^+)_S$ (ρ = 0) and $(Li^+)_C$ (ρ = 1.0) are both approximately 2 Hz. This is in contrast with the ^{23}Na study: when B15C5 was complexed to Na^+ in NM, a large relative increase in both the transverse and longitudinal relaxation rates (see Figure 4.4 and Table 4.2) was observed due to a decreased relative symmetry around the sodium cation. The low values of the ^7Li relaxation rates, compared to that of ^{23}Na, are a result of the low quadrupole moment of the lithium cation.

As is also the case with sodium, decreasing the concentration of alkali metal cation salt results in spectacular changes in the NMR spectra which are illustrated in Figures 5.3 and 5.4. At 300 K, (Figure 5.3) a coalescence is observed at approximately 2 mM but lowering the temperature to 263 K (Figure 5.4) also lowers the overall rate of exchange and a coalescence is observed at a higher concentration of lithium ($\sim$ 11 mM). In section 4.4, two possible mechanisms were postulated for a two-site chemical exchange: dissociative (equation 26) and associative (equation 31).

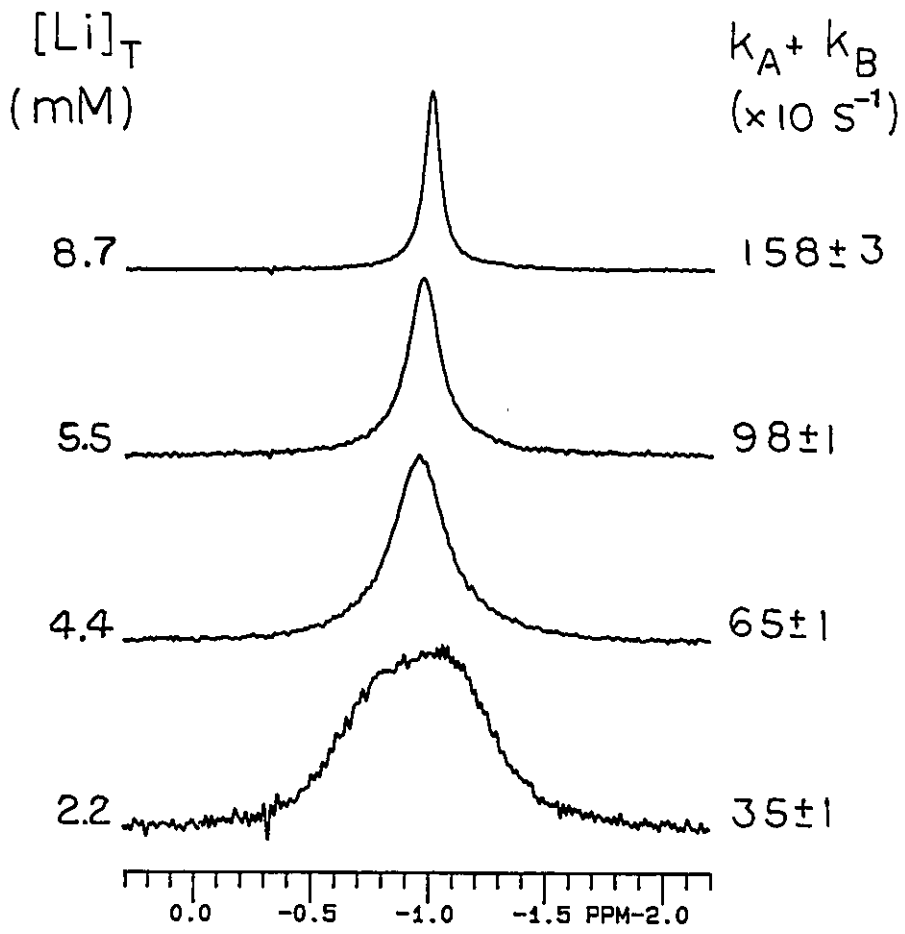

Figure 5.3: ^{7}Li spectra of solutions containing equal populations (ρ = 0.50) of $(Li^{+})_S$ and $(Li{:}B15C5)^{+}$ in nitromethane at 300.0 ± 0.5 K. From top to bottom the $[LiClO_4]_T$ and $(k_A + k_B)$, determined from lineshape analyses, vary as shown.

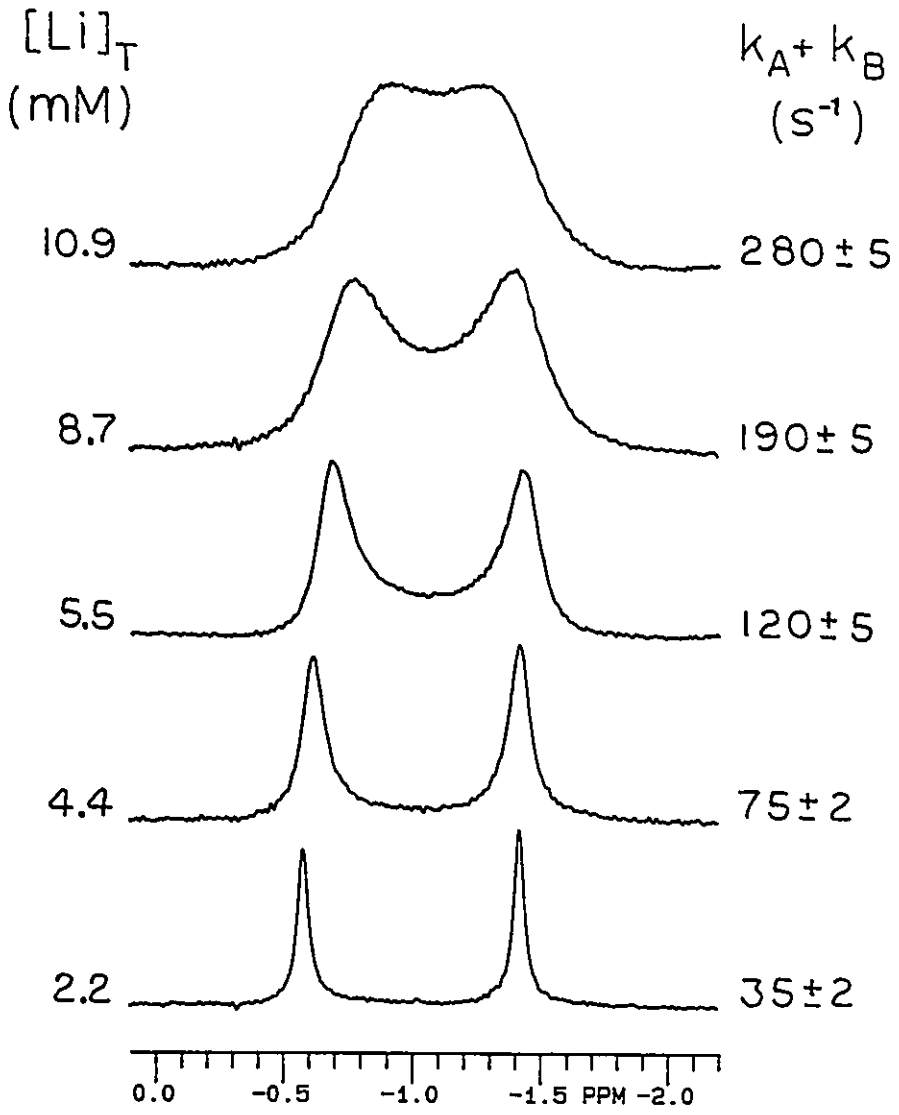

Figure 5.4: ^{7}Li spectra of solutions containing equal populations (ρ = 0.50) of $(Li^{+})_S$ and $(Li{:}B15C5)^{+}$ in nitromethane at 263.0 ± 0.5 K. From top to bottom the $[LiClO_4]_T$ and $(k_A + k_B)$, determined from lineshape analyses, vary as shown.

The ^{7}Li NMR kinetic analysis parallels that of ^{23}Na NMR. From Figures 5.3 and 5.4 it is evident there is a relatively large contribution of the associative exchange mechanism in the overall chemical exchange since there is a proportional variation of $(k_A + k_B)$ with $[LiClO_4]_T$ at both temperatures. Further analysis using the mechanistic test equation (equation 35) and plotting $(k_A + k_B)$ as a function of $[Li^+]_T$, shown in Figures 5.5 and 5.6, reveals that the associative pathway for chemical exchange is preferred with both 15C5 and B15C5. The plots shown in Figures 5.5 and 5.6 clearly indicate that within experimental error there is no measurable contribution of the dissociative exchange mechanism since the lines all extrapolate very close to the origin. The values of the corresponding associative rate constants, k_2, shown in Table 5.1, come directly from the slope measurements . The activation parameters for the associative exchange of lithium in $(Li^+)_S$ and $(Li{:}15C5)^+$ or $(Li{:}B15C5)^+$, also shown in Table 5.1, have been determined with variable temperature studies. The corresponding Eyring plots are shown in Figure 5.7. For comparison, Table 5.1 also includes results obtained by ^{23}Na NMR for the sodium cation with the same crown ethers and solvent at similar temperatures. The associative nature of the lithium exchange is reflected in the entropies of activation which are still largely negative. The free energies of activation for each system are overall very comparable, again suggesting that the origin of the associative exchange has a common basis. A discussion of the nature of the associative mechanism, as it pertains to sodium, was given in chapter 4 where the energy barrier for chemical exchange by this mechanism was postulated to be conformational in nature (see Scheme 1). If this is the case and since it was observed that the solution conformations of both $(Li{:}B15C5)^+$ and $(Na{:}B15C5)^+$ in NM are very similar (see section 3.2.2), *a priori* one would expect the activation parameters for the associative exchange to be very close for both B15C5 complexes of lithium and sodium.

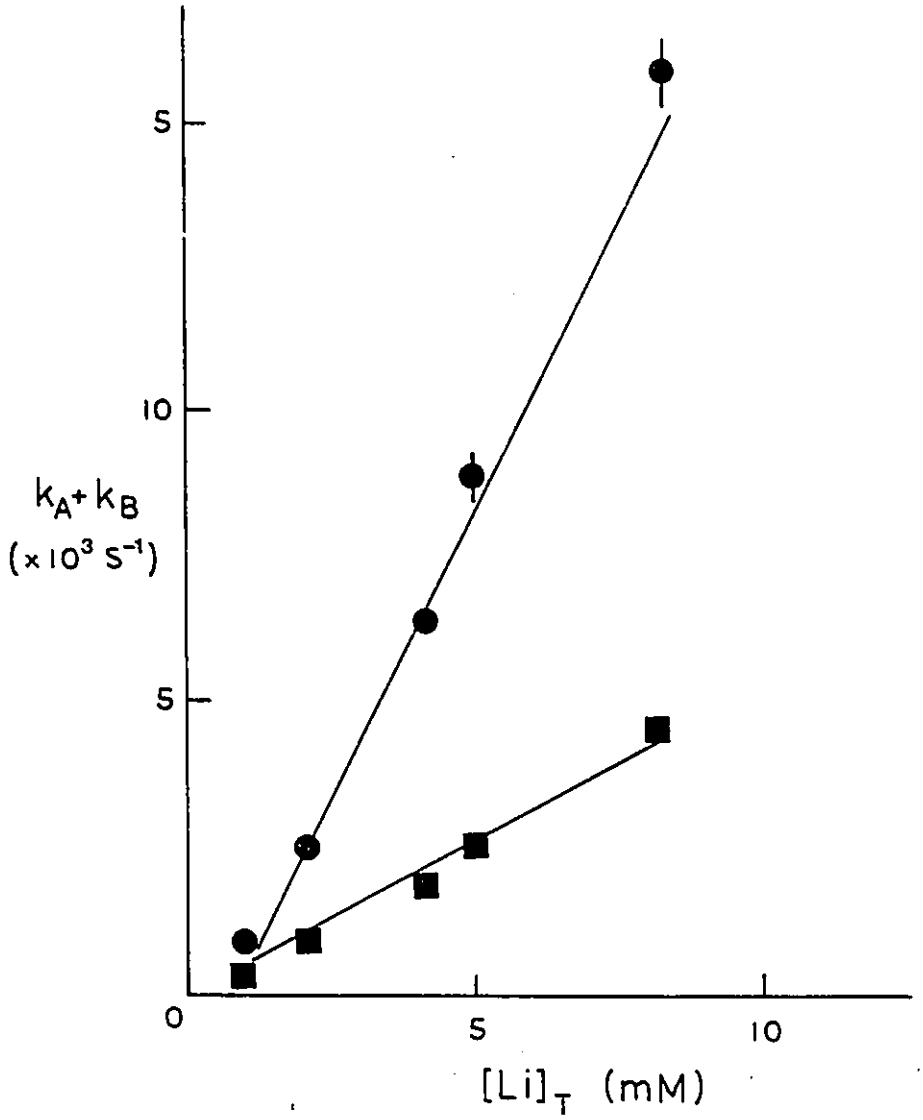

Figure 5.5: $(k_A + k_B)$ as a function of $[LiClO_4]_T$ in NM. $\rho = [15C5]_T / [LiClO_4]_T = 0.53$ in all cases. The data points are experimental and the lines are results of linear regressions: (●) at 300.0 K; $(k_A + k_B) = (-1.2 \pm 0.3) \times 10^3 + (1.9 \pm 0.1) \times 10^6\ [Li]_T$ and (■) at 263.0 K; $(k_A + k_B) = (-4 \pm 1) \times 10^2 + (6.2 \pm 0.4) \times 10^5\ [Li]_T$.

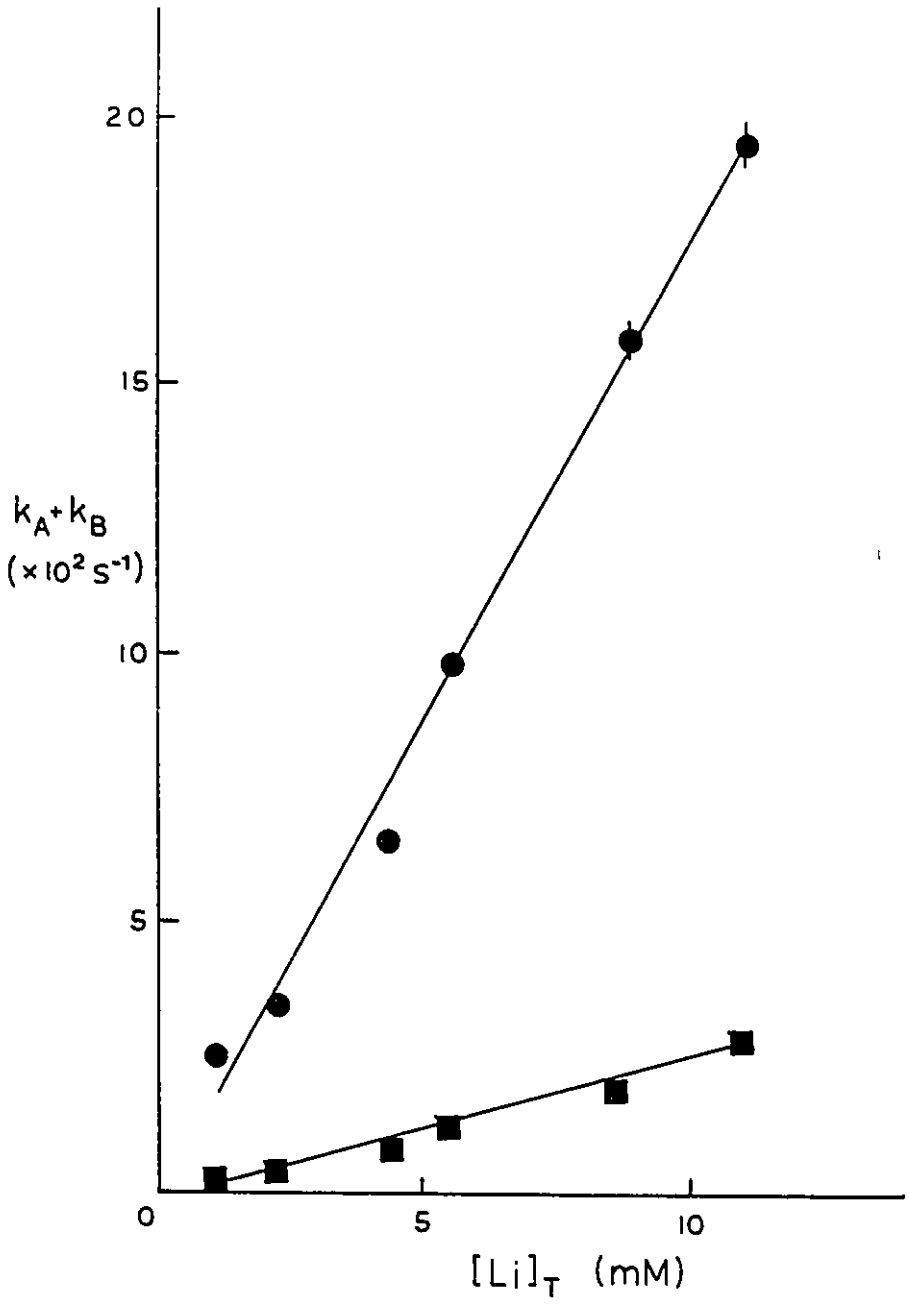

Figure 5.6: ($k_A + k_B$) as a function of $[LiClO_4]_T$ in NM. $\rho = [B15C5]_T / [LiClO_4]_T$ = 0.51 in all cases. The data points are experimental and the lines are results of linear regressions: (●) at 300.0 K; $(k_A + k_B) = (9 \pm 6) \times 10^2 + (1.88 \pm 0.08) \times 10^5\ [Li]_T$ and (■) at 263.0 K; $(k_A + k_B) = (2 \pm 1) \times 10^2 + (2.6 \pm 0.2) \times 10^4\ [Li]_T$.

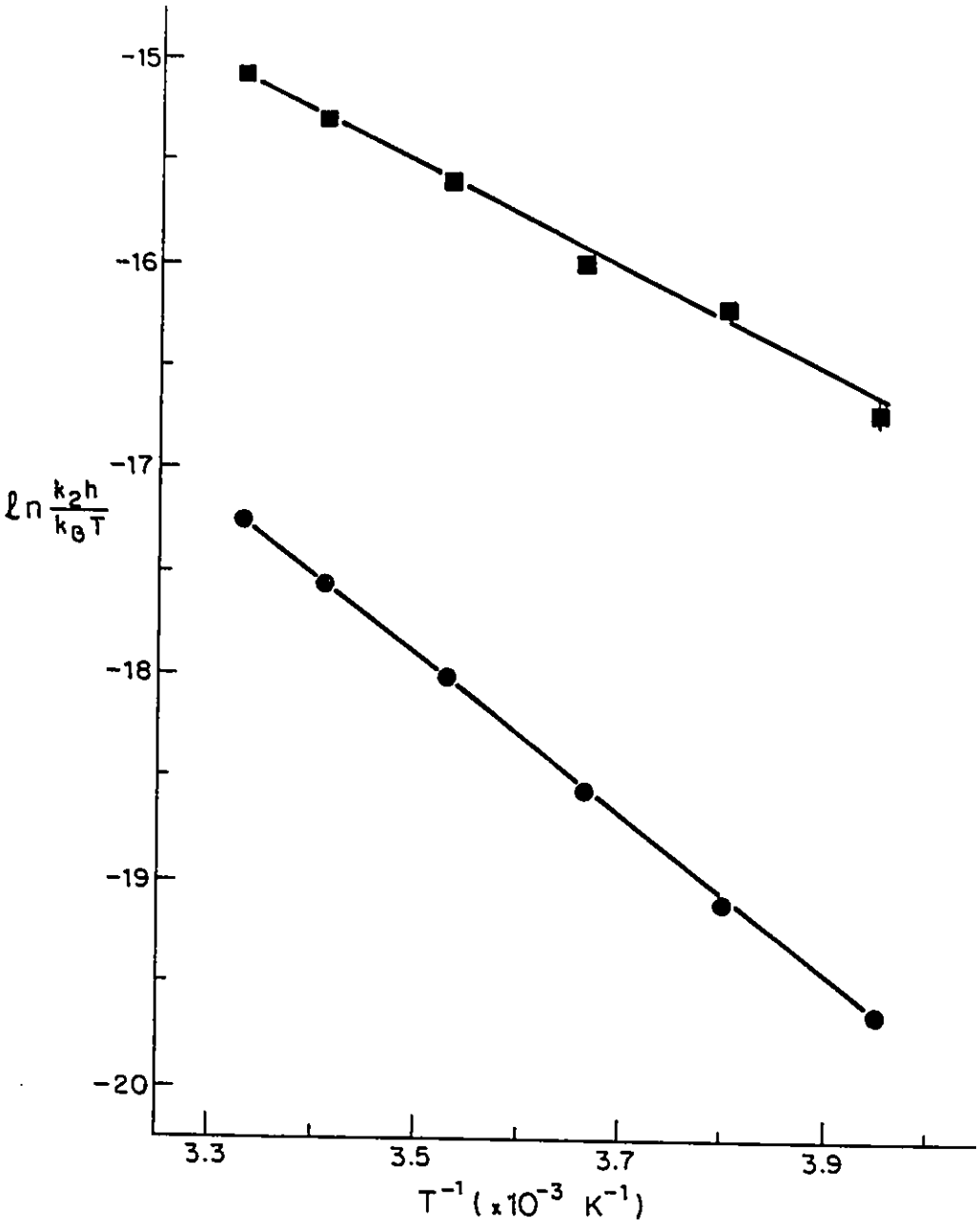

Figure 5.7: $\ln(k_2h / k_BT)$ as a function of T^{-1}. For 15C5 (■), the $[LiClO_4]_T = 5.0$ mM and $\rho = 0.53$; for B15C5 (●), the $[LiClO_4]_T = 10.6$ mM and $\rho = 0.53$.

Table 5.1: Rate Constants, k_2, and Activation Parameters for the Associative Exchange of $(M:C)^+$ in Nitromethane.

$(M:C)^+$	k_2 $\times 10^5\ M^{-1}s^{-1}$	ΔG^*_{as} $kJ.mol^{-1}$	ΔH^*_{as} $kJ.mol^{-1}$	ΔS^*_{as} $J.mol^{-1}.K^{-1}$
$(Li:15C5)^{+a}$	19 ± 1	37.4 ± 0.1	21 ± 1	-54 ± 3
$(Li:B15C5)^{+a}$	1.88 ± 0.08	43.2 ± 0.1	32 ± 1	-36 ± 1
$(Na:15C5)^{+b}$	1.45 ± 0.05	44.1 ± 0.1	21 ± 1	-76 ± 2
$(Na:B15C5)^{+b}$	1.09 ± 0.04	44.8 ± 0.1	28 ± 3	-57 ± 3
$(Na:B15C5)^{+c}$	1.97 ± 0.05	43.1 ± 0.1	–	–

(a) Counteranion is ClO_4^- and T = 300.0 ± 0.5 K. (b) counteranion is BPh_4^- and T = 301.5 ± 0.5 K. (c) counteranion is ClO_4^- and T = 300.0 ± 0.5 K; assuming associative exchange only (see Table 4.5).

The k_2 values and free energies of activation of ($LiClO_4$:B15C5) and ($NaClO_4$:B15C5), shown in Table 5.1, are identical within experimental error. This strongly supports the proposed scenario for associative exchange, illustrated in Scheme 1, since a mechanism which would be influenced by other factors such as cation solvation / desolvation would result in activation parameters significantly different for different cations. Moreover, the enthalpy of activation is independent of the cation involved: ΔH^*_{as} of ($LiClO_4$:B15C5) is the same as that of ($NaBPh_4$:B15C5) as well as ΔH^*_{as} of ($LiClO_4$:15C5) is the same as that of ($NaBPh_4$:15C5) within experimental error. That the free energy of activation is slightly lower with ($LiClO_4$:15C5) compared to ($NaBPh_4$:15C5) and ($LiClO_4$:B15C5) compared to ($NaBPh_4$:B15C5) may be due to a small counteranion effect. The coordinating power of the counteranion has been observed to affect the resulting free

energy of activation for the associative exchange of $(Na:DB24C8)^+$ in NM where a counteranion with a high coordinating power, such as thiocyanate, resulted in a lower free energy of activation [130]. The higher free enthalpies of activation for cation exchange with B15C5 compared to 15C5 is plausibly a reflection of the higher rigidity of B15C5.

5.3 Kinetics by 2D ^{7}Li NMR Exchange Spectroscopy

The investigation of exchange processes by 2-dimensional NMR spectroscopy was first demonstrated by Jeener, Ernst and coworkers in 1979 [57]. The pulse sequence for this technique, referred to as exchange spectroscopy (EXSY), is shown in Figure 5.8.

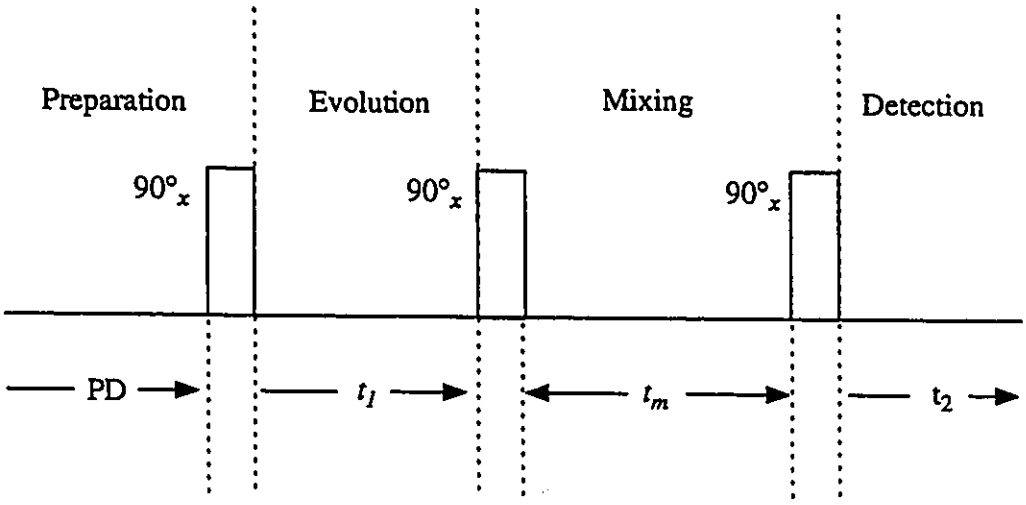

Figure 5.8: Basic scheme for 2-dimensional exchange spectroscopy.

This 2D technique is characterized by four periods of time: the preparation, evolution and detection periods, as in a normal 2D experiment (see for example heteronuclear correlation in Figure 3.14), as well as a mixing period which is of central importance for obtaining rate information. After the preparation period and the first 90° pulse, which converts *z*-magnetization to *y*-magnetization, the various components of the created transverse spin magnetization are frequency labeled by letting them precess at their characteristic resonance frequencies during the evolution period of length t_1. The exchange process takes place during the mixing period of fixed length t_m after a second 90° pulse which restores the *y* component of the magnetization along the *z*-axis. A final third 90° pulse rotates the longitudinal magnetization into the *xy*-plane for detection during t_2. As is usual in any 2D experiment the pulse sequence shown in Figure 5.8 is repeated for a number of equally spaced values of the evolution time t_1. Free precession of the spins during t_1 forms the first time domain while the signal acquisition time, t_2, constitutes the second time domain. Fourier transformation in both dimensions results in a 2D spectrum containing the normal 1D spectrum along the diagonal and cross-peaks off the diagonal due to the occurrence of magnetization transfer during the mixing time. An increase in t_m results in increased information transfer which is reflected by the increased volumes of the spectral cross-peaks. The relationship between the volumes of the cross peaks and t_m can give access to the rate constant of a process, as will be shown later, and therefore to obtain quantitative information about exchange rates it is usual to perform several 2D experiments each of them with different mixing times.

The use of two-dimensional EXSY for qualitative and quantitative kinetic investigations has been limited compared to the conventional one-dimensional lineshape analysis approach. This method works best when the sites undergoing chemical exchange are not coupled to each other since spin-spin coupling may also result in the appearance of cross-peaks masking the chemical exchange. Another drawback of this

method is that the acquisition of data necessary for quantitative interpretation can be very time consuming, as it usually the case with any 2D technique. Two-dimensional EXSY has been recently applied in various situations with various NMR nuclei such as ^{1}H [184], ^{13}C [185], ^{19}F [186], ^{119}Sn [187] and ^{23}Na [188] (for a more complete description of the various applications of 2D EXSY see reference 189). We believe this to be the first application of 2-dimensional ^{7}Li NMR EXSY.

In order to apply this NMR method, chemical exchange must be slow on the NMR timescale so that each nuclear site involved in the chemical exchange must have resonances which are well separated. As can be seen in Figure 5.4, there is the possibility for fulfilling this condition in the present studies. In order to demonstrate ^{7}Li 2D EXSY, we have selected a system in which the specific experimental conditions allow the application of this technique. The corresponding 1D spectrum of the system in question is shown in Figure 5.9.

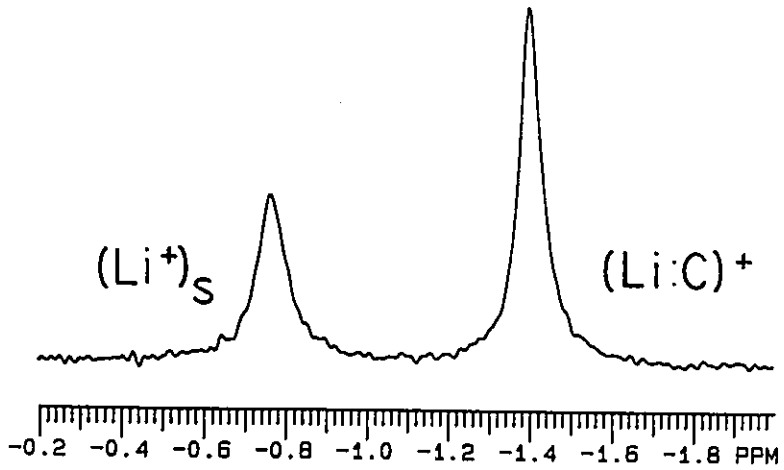

Figure 5.9: ^{7}Li spectrum of a solution containing $(Li^{+})_S$ (P_A = 0.40) and $(Li{:}B15C5)^{+}$ (P_B = 0.60) in nitromethane at 250.0 ± 0.5 K. $[LiClO_4]_T$ = 2.6 mM.

As we have previously seen, the lineshape of the NMR spectrum, and therefore the observed ($k_A + k_B$), is mainly affected by two experimental variables: the temperature and the total concentration of metal salt. For the system $(Li:B15C5)^+$ in NM, two separate resonances are observed at 250.0 K and a $[LiClO_4]_T$ equal to 2.6 mM for a solution containing both solvated (in this case $P_A = 0.40$) and complexed (in this case $P_B = 0.60$) lithium cations. Several 2D EXSY experiments were done with this solution where the mixing time, t_m, was varied between 0.005 and 0.10 s. The stacked plots for three of these experiments (t_m = 0.007, 0.02 and 0.05 s) and the corresponding contour plots are shown in Figures 5.10 and 5.11 respectively where it can be seen that as the t_m increases so does the volume of the cross-peaks.

A quantitative interpretation of the results obtained is straightforward and is based on the following equations for a non-coupled two-site exchange [57]:

$$a_{AA}(t_m) = P_A e^{-\sigma t_m} [\cosh(Dt_m) - (\delta/D) \sinh(Dt_m)] \quad (53)$$

$$a_{BB}(t_m) = P_B e^{-\sigma t_m} [\cosh(Dt_m) + (\delta/D) \sinh(Dt_m)] \quad (54)$$

$$a_{AB}(t_m) = a_{BA}(t_m) = -P_A P_B (R_c/D) e^{-\sigma t_m} \sinh(Dt_m) \quad (55)$$

where

$$\sigma = 1/2 (R_{AA} + R_{BB}) \quad (56)$$

$$\delta = 1/2 (R_{AA} + R_{BB}) \quad (57)$$

$$D = (\delta^2 + P_A P_B R_c^2)^{1/2} \quad (58)$$

$$R_{AA} = R_{1A} + P_B k \quad (59)$$

$$R_{BB} = R_{1B} + P_A k \quad (60)$$

$$R_c = -k \quad (61)$$

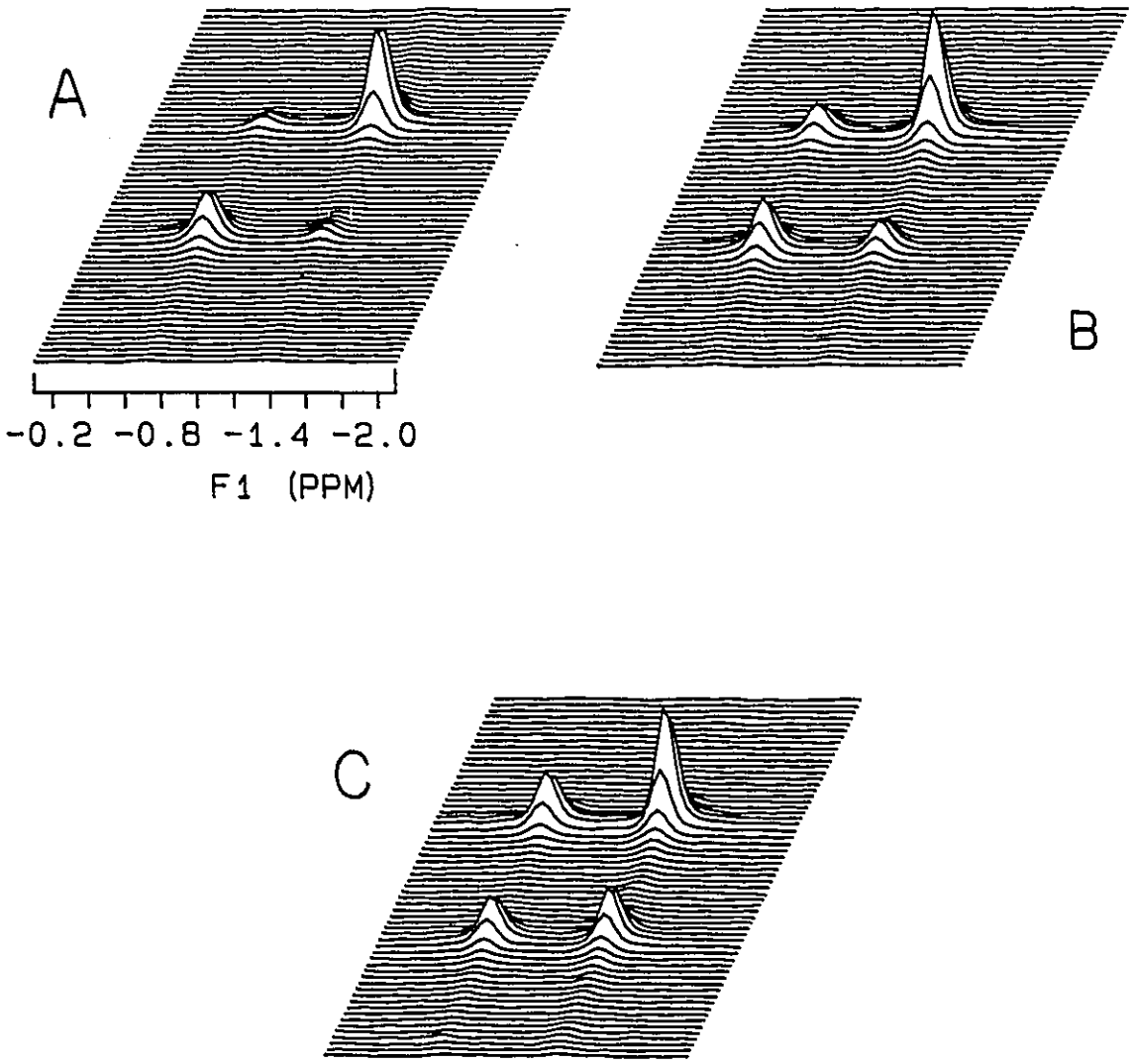

Figure 5.10: Stacked 2D EXSY plots of a solution containing $(Li^+)_S$ (P_A = 0.40) and $(Li:B15C5)^+$ (P_B = 0.60) in nitromethane at 250.0 ± 0.5 K and $[LiClO_4]_T$ = 2.6 mM. t_m = (A) 0.007 s, (B) 0.02 s and (C) 0.05 s.

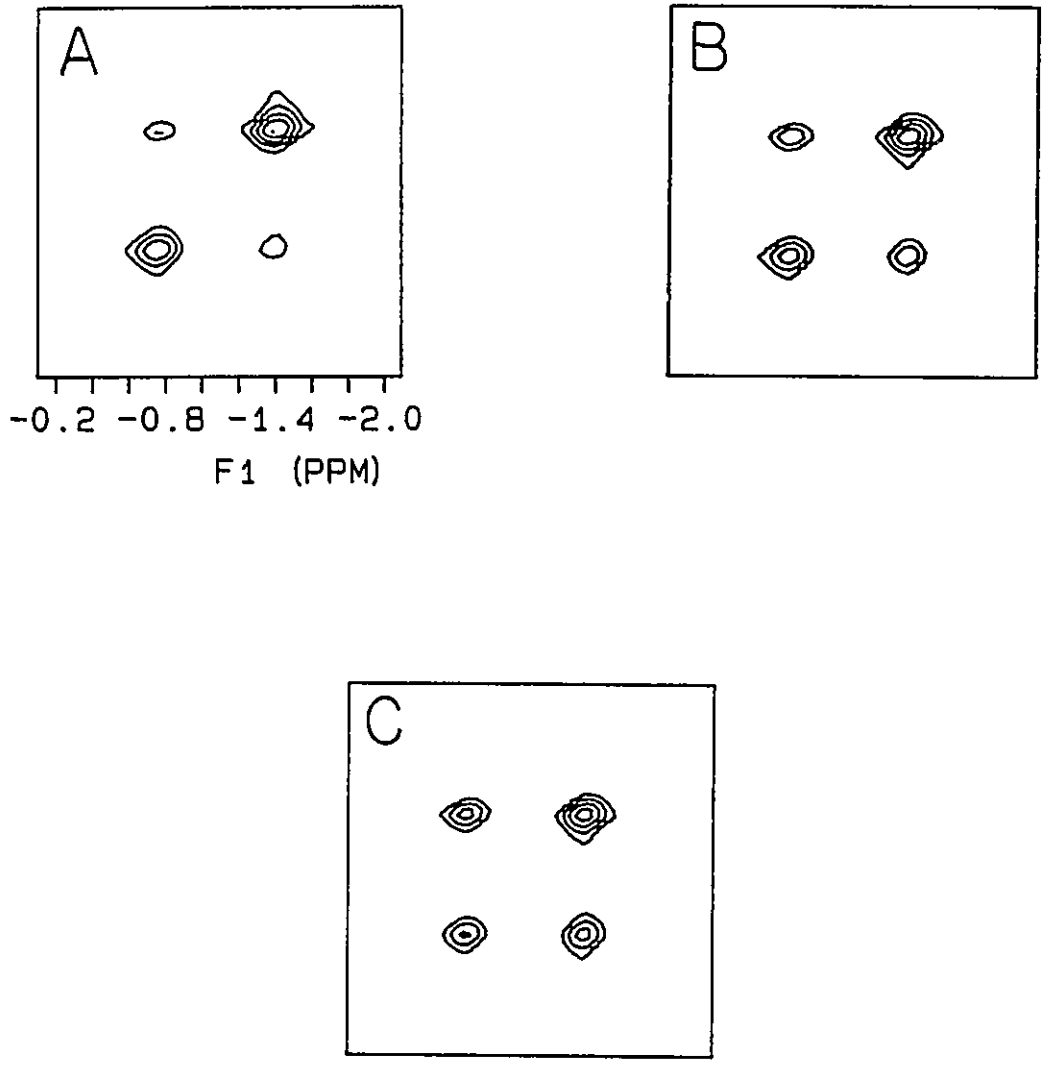

Figure 5.11: Contour 2D EXSY plots of a solution containing $(Li^+)_S$ ($P_A = 0.40$) and $(Li{:}B15C5)^+$ ($P_B = 0.60$) in nitromethane at 250.0 ± 0.5 K and $[LiClO_4]_T = 2.6$ mM. t_m = (A) 0.007 s, (B) 0.02 s and (C) 0.05 s.

The values for a_{AA}, a_{BB} and $a_{AB} = a_{BA}$ correspond respectively to the normalized volume integrations (i.e. the sum of all volume integrations of any one spectrum is taken to be equal to 1.0) of the peaks at sites A, B and the cross peaks. The populations of the two sites are represented by P_A (equal to 0.40 in this case) and P_B (equal to 0.60 in this case) with longitudinal relaxation rates R_{1A} (T_{1A}^{-1}) and R_{1B} (T_{1B}^{-1}) respectively. The longitudinal relaxation rates of lithium in both sites have been determined independently in the desired experimental conditions by the inversion-recovery method; $R_{1A} = 0.94 \pm 0.03$ s^{-1} and $R_{1B} = 3.02 \pm 0.12$ s^{-1}. In this analysis the value for the rate constant **k**, is equivalent to $(k_A + k_B)$ in the conventional 1D analysis. The above equations clearly show the relationship between the experimentally determined peak volumes and the desired rate constant, **k**, for the chemical exchange. The relationship between a_{AB} and t_m is shown in Figure 5.12, where a nonlinear increase in cross-peak volumes is observed as the mixing time increases. The experimental data agree well with the result of the nonlinear regression represented by the drawn curve (there is a slight discrepancy when t_m is large). Error estimates for the cross-peak volumes, shown in Figure 5.12, comes from the knowledge that the volumes of two cross-peaks in each individual experiment should be the same. Perhaps the errors reported have been underestimated in which case the data points at the larger mixing times would fall on the theoretical curve.

A comparison of the rate results obtained by conventional lineshape analysis and 2D EXSY is shown in Table 5.2. By the conventional 1D approach, the preferred exchange mechanism for Li^+ with B15C5 in NM was determined to be exclusively associative and therefore the rate constant for this process can be simply calculated: $k_2 = (k_A + k_B) / [LiClO_4]_T$. Since the results obtained by both methods are identical within experimental errors, the reliability of the application of 2D ^7Li EXSY for kinetic investigations of lithium cations complexed with the crown ether B15C5 is confirmed.

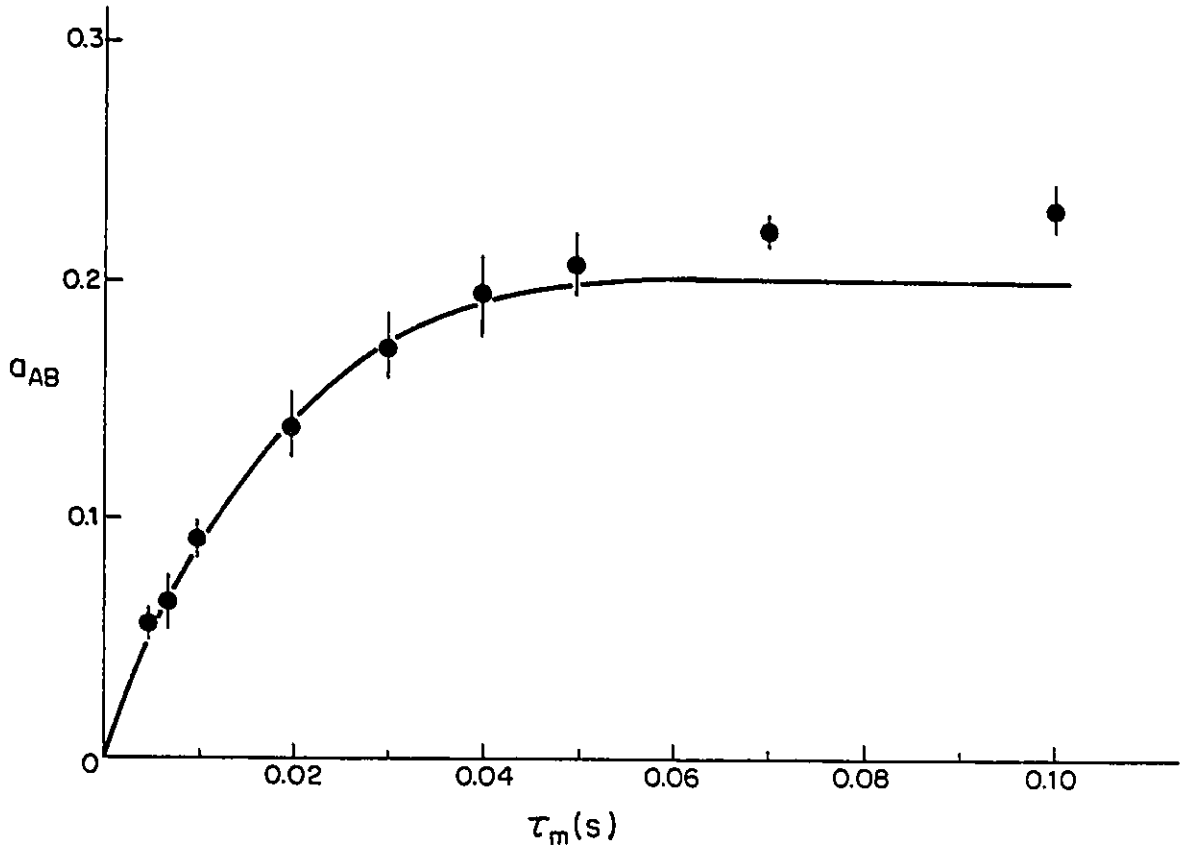

Figure 5.12: The normalized cross-peak volume, a_{AB} determined from 2D ^{7}Li spectra, as a function of the mixing time, t_m. The data points are experimental and the drawn curve is a result of a nonlinear regression based on equations 53-61.

Table 5.2: A Comparison of the Rate Constants Obtained with One- and Two-Dimensional ^{7}Li NMR.

Method	k or $(k_A + k_B)^a$ s^{-1}	$k_2{}^b$ $\times 10^4\ M^{-1}s^{-1}$
1D-lineshape	47 ± 2	1.84 ± 0.08
2D-EXSY	49 ± 14	1.9 ± 0.6

(a) $T = 250.0 \pm 0.5$ K; $\rho = [B15C5]_T / [LiClO_4]_T = 0.6$; $[LiClO_4]_T = 2.6$ mM. (b) associative exchange: $k_2 = (k_A + k_B) / [LiClO_4]_T$.

5.4 Competition between Na^+ and Li^+ for Benzo-15-crown-5

So far we have demonstrated that the associations of lithium and sodium cations individually with 15C5 and B15C5 in NM exhibit many similar structural and kinetic characteristics. The NMR studies have provided some insight into the solution structures of the complexes. Linear variations in the respective ^{23}Na and ^{7}Li chemical shifts as the concentration of the ligand increased (see Figures 4.1a and 5.1) have indicated a formation of highly stable $(Na:15C5)^+$, $(Na:B15C5)^+$, $(Li:15C5)^+$ and $(Li:B15C5)^+$ complexes in nitromethane where $\log K_F > 4$. Whereas ^{1}H NMR studies indicate that the specific solution conformational status of B15C5 in both $(Na:B15C5)^+$ and $(Li:B15C5)^+$ in NM is similar, ^{23}Na and ^{7}Li NMR studies indicate that there is a difference in the positions of both cations within the cavity of B15C5. The ^{23}Na and ^{7}Li chemical shift data in NM indicates a stronger tendency for the formation of sandwich complexes with Na^+. This observation is expected since Na^+ is larger than Li^+ and in all probability, the solution sodium cation sits above the ring plane of the ligand as is

observed in solid $(Na:B15C5)^+$ [77]. The smaller lithium cation on the other hand, probably sits directly within the cavity of this crown ether.

Previous alkali metal NMR investigations by Popov and coworkers have provided insight into the selectivities of the formations of alkali metal-crown ether complexes based upon cation and ligand cavity sizes [88,102]. One such ^7Li NMR study of the interactions of lithium cations with 12C4, 15C5 and 18C6 has indicated a formation of lithium complexes, in various solvents, which are generally more stable with 15C5 [102]. On the other hand, a similar ^{23}Na NMR study has indicated sodium complexes more stable with 18C6 compared to 15C5 and B15C5 [88]. Although an actual value of K_F for both $(Li:B15C5)^+$ (K_{Li}) and $(Na:B15C5)^+$ (K_{Na}) in NM could not be determined by alkali metal NMR, based on our observations and the preceding statements one could *a priori* predict a preference of lithium over sodium in the complexation of B15C5. In order to obtain specific qualitative and quantitative information about the competition of these two cations for B15C5, solutions containing Li^+, Na^+ and B15C5 were studied concurrently by ^7Li and ^{23}Na NMR.

Upon the addition of B15C5 to a solution containing both lithium and sodium cations, a competition between the following two equilibria, each characterized by K_{Li} and K_{Na} respectively, is set up:

$$Li^+ + B15C5 \rightleftharpoons (Li:B15C5)^+ \quad (62)$$

$$Na^+ + B15C5 \rightleftharpoons (Na:B15C5)^+ \quad (63)$$

where in the low donicity solvent NM with the non-coordinating ClO_4^- counteranion, competition involving the solvent and/or counteranion in cation coordination can be neglected. As in the individual cases, the lithium equilibrium shown in equation 62 can be followed by ^7Li NMR and the sodium equilibrium shown in equation 63, by ^{23}Na

NMR. A system such as this can be represented by the following overall equilibrium:

$$Li^+ + (Na{:}B15C5)^+ \underset{k_b}{\overset{k_f}{\rightleftharpoons}} Na^+ + (Li{:}B15C5)^+ \qquad (64)$$

where k_f and k_b are the rate constants for the forward and reverse reactions respectively. The overall equilibrium constant, $K_{eq} = k_f / k_b$, is equivalent to the ratio K_{Li} / K_{Na}.

In order to investigate the equilibrium shown in equation 64, B15C5 was added in varying amounts to nitromethane solutions containing equal concentrations of $NaClO_4$ and $LiClO_4$. A plot of the ^7Li chemical shift as a function of $\rho_T = [B15C5]_T / ([Na^+]_T + [Li^+]_T)$ is shown in Figure 5.13. In the absence of sodium, the ^7Li chemical shift shown in Figure 5.13 would decrease linearly until $\rho_T = 0.5$ at which point a plateau would be observed. This would indicate the quantitative formation of $(Li{:}B15C5)^+$ where $\log K_{Li} > 4$. The added presence of sodium in the system decreases the efficiency of the formation of $(Li{:}B15C5)^+$ and results in a nonlinear relationship of the observed ^7Li chemical shift. A ^7Li chemical shift of -0.62 ppm at $\rho_T = 0$ confirms that lithium is in its solvated state (in NM) and when there is excess ligand a plateau is reached at -1.15 ppm indicating that all the lithium present is complexed to B15C5. In this situation, the chemical exchange is "moderately fast" (see section 4.3) on the ^7Li NMR timescale and the chemical shift observed is representative of a weighted population average of lithium in its two sites.

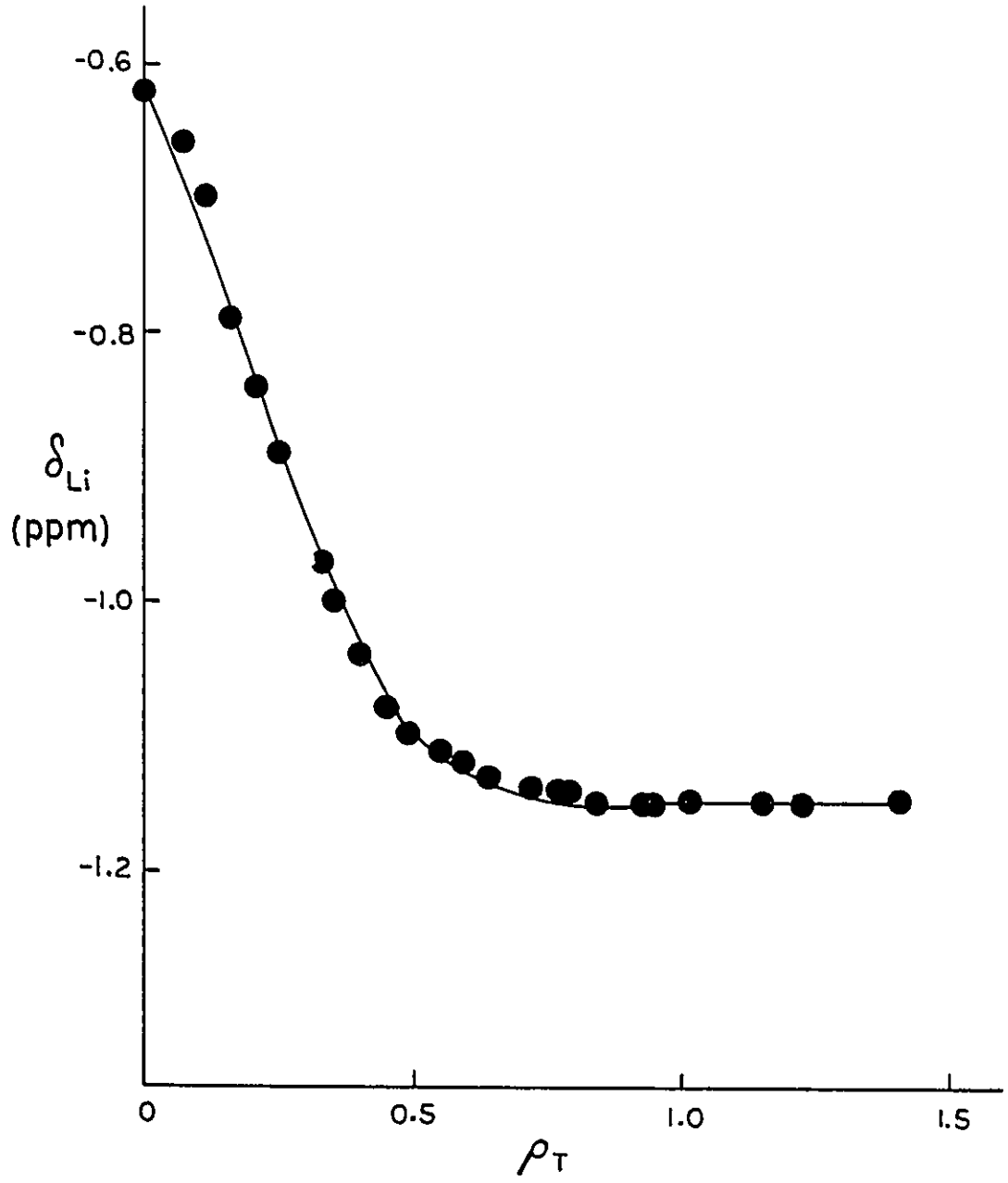

Figure 5.13: ^{7}Li chemical shift as a function of $\rho_T = [B15C5]_T / ([Na]_T + [Li]_T)$ in nitromethane. The total concentration of metal cation, $[M^+]_T = [Na^+]_T + [Li^+]_T = 10.1$ mM, ($[Na^+]_T = [Li^+]_T$) and T = 300.0 ± 0.5 K. The data points are experimental and the curve is theoretical based on a determined value for log $K_{eq} = 2.0$ (equation 64).

The relative populations of the solvated (site A) and complexed (site B) lithium sites can be determined from the chemical shift (see equation 19). Since the data observed in Figure 5.13 are also representative of the equilibrium shown in equation 64, a value for K_{eq} is determined from a nonlinear regression (see Appendix 5): log K_{eq} = 2.0 ± 0.3. This indicates that B15C5 binds preferentially to lithium cations in the presence of sodium.

On the other hand, the status of sodium in the system can be monitored by ^{23}Na NMR. Figure 5.14 shows the ^{23}Na chemical shift again as a function of ρ_T. At $\rho_T = 0$, a ^{23}Na chemical shift of -14.0 ppm is indicative of solvated sodium (in NM) and in the presence of excess ligand all the sodium is complexed to B15C5 resulting in the observed plateau at -3.7 ppm. In the absence of lithium and at this low $[Na^+]_T$ (5 mM), the chemical exchange is expected to be slow on the ^{23}Na NMR chemical shift timescale (see Figure 4.6) and non-Lorentzian spectra would be observed in the region $0 < \rho_T < 0.5$. The presence of lithium greatly hinders the formation of $(Na{:}B15C5)^+$ since the chemical shift does not significantly change until ρ_T is approximately 0.4. When both sodium sites are present however, chemical exchange is still slow on the ^{23}Na chemical shift timescale and the spectra observed are non-Lorentzian. Although the data in Figure 5.14 is still representative of the equilibrium in equation 64, a separate determination of K_{eq} is not possible since chemical exchange is slow and we do not observe one population averaged signal. The curve drawn in this figure was calculated using the value for log K_{eq} = 2.0 determined with the ^{7}Li NMR data and a broken line simply denotes that the ^{23}Na chemical shift was not actually measured. A knowledge of the relative populations of the two sodium sites is still possible since P_A or P_B can be determined from a complete lineshape analysis. This is accomplished by introducing P_B as a variable in the nonlinear regressions of the lineshape analysis (see Appendix 1).

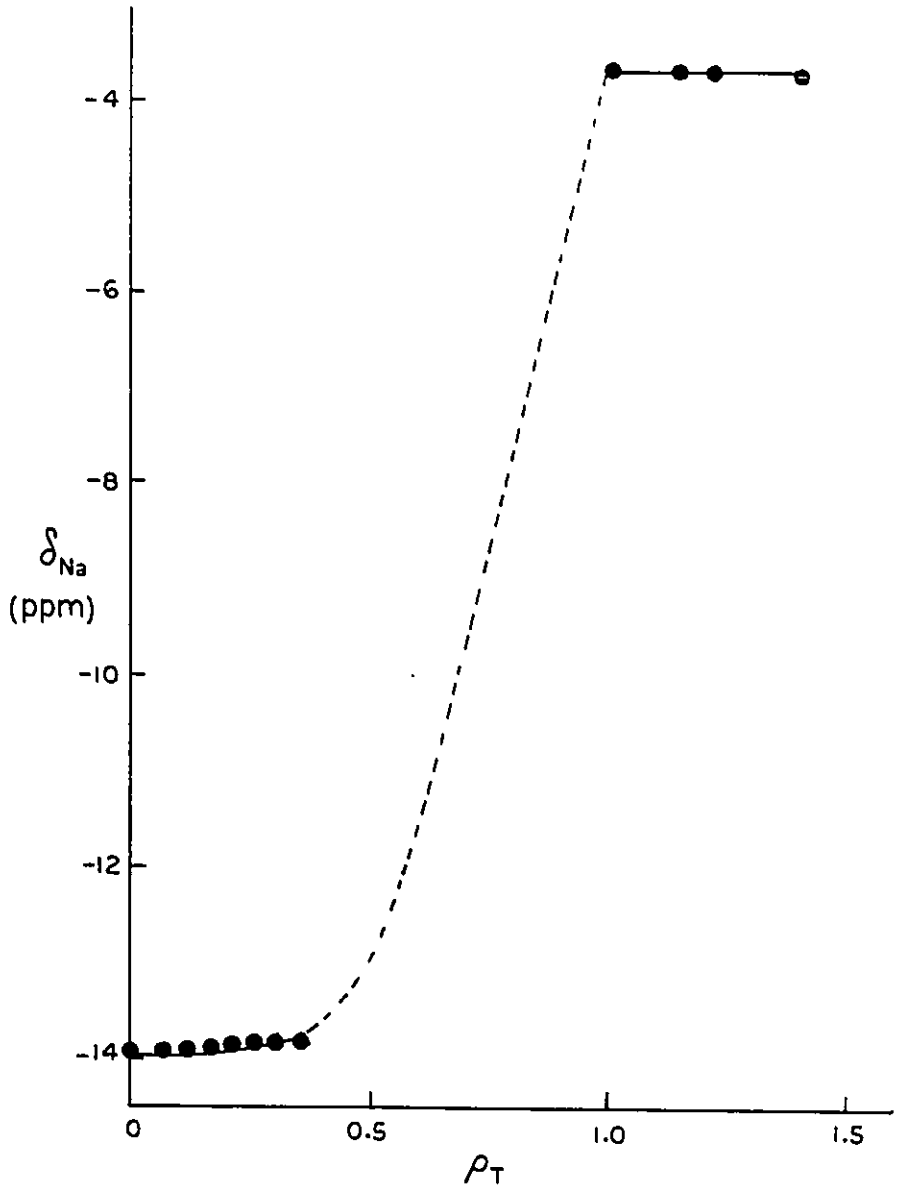

Figure 5.14: ^{23}Na chemical shift as a function of $\rho_T = [B15C5]_T / ([Na^+]_T + [Li^+]_T)$ in nitromethane. The concentration of the total metal, $[M^+]_T = [Na^+] + [Li^+]_T = 10.1$ mM, ($[Na^+] = [Li^+]$) and T = 300.0 ± 0.5 K. The data points are experimental and the curve is theoretical based on a determined value for log $K_{eq} = 2.0$. The middle portion of the curve is drawn as a broken line since in these conditions the spectra observed were non-Lorentzian due to slow chemical exchange.

Since

$$K_{eq} = ([Li{:}B15C5^+] / [Li^+]) \times ([Na^+] / [Na{:}B15C5^+]) \quad (65)$$

and therefore:

$$K_{eq} = (P_B / P_A)_{Li} \times (P_A / P_B)_{Na} \quad (66)$$

this provides another method for determining a value for K_{eq}. The relative populations of lithium in sites A and B can be determined from the ^7Li chemical shift data and those of sodium from the ^{23}Na lineshape analyses. Data for each sample is acquired by the NMR of two different nuclei, and as a result several values of K_{eq} can be calculated. An average value of K_{eq}, where $\log K_{eq} = 1.7 \pm 0.2$, was determined by this approach. This value agrees, within experimental errors, to that previously determined where $\log K_{eq} = 2.0 \pm 0.3$ (the average of the two is 1.9 ± 0.2). Again we can conclude that in nitromethane B15C5 displays selectivity of lithium over sodium.

We have also demonstrated that the well characterized kinetic activities of lithium and sodium individually with B15C5 in NM are the same. That is, in both cases the associative mechanism (equation 31) is preferred for chemical exchange of the cations in the two sites. When one cation is put into the presence of the other, two questions may be asked about the kinetic influence of the added cation on the one studied: does the overall exchange mechanism change and/or are the actual rates of exchange affected? One could visualize a possible synergistic effect where the presence of one cation could actually lower the energy barrier for the chemical exchange of another cation.

In the cation mixture study described above, the chemical exchange of the

lithium cations in its two sites can be studied since the population averaged ^{7}Li NMR lines are broadened due to the moderate rate of chemical exchange. It is reasonable to assume that the associative mechanism for lithium chemical exchange, which is preferred over dissociative exchange, is still in effect for lithium when sodium is present. That is:

$$Li^{*+} + (Li{:}B15C5)^{+} \underset{}{\overset{k_{2Li}}{\rightleftharpoons}} Li^{+} + (Li^{*}{:}B15C5)^{+} \qquad (67)$$

where k_{2Li} is the associative rate constant for this specific exchange in the presence of sodium. One may also envisage a second path for lithium exchange involving the sodium cation, which could have an impact on the behaviour of lithium:

$$Li^{+} + (Na{:}B15C5)^{+} \underset{k_b}{\overset{k_f}{\rightleftharpoons}} Na^{+} + (Li{:}B15C5)^{+} \qquad (68)$$

These two associative mechanisms account for the exchange of lithium in its two sites, and the following relationship for the observed $(k_A + k_B)$ can be obtained (see Appendix 6):

$$(k_A + k_B)_{Li} = k_{2Li}[Li^{+}]_T + k_b[Na^{+}]_T \{(K_{eq} - 1)(\Delta/\Delta_o)_{Na} + 1\} \qquad (69)$$

where $(k_A + k_B)_{Li}$ refers to that parameter measured for the lithium exchange by ^{7}Li NMR lineshape analysis and $(\Delta/\Delta_o)_{Na}$ is a parameter based on the ^{23}Na NMR chemical shifts reflecting the relative populations of the sodium species in solution (see Appendix

6). Since a value for K_{eq} is known (log K_{eq} = 1.9 ± 0.2) a plot of $(k_A + k_B)_{Li}$ as a function of $(\Delta/\Delta_o)_{Na}$ should be linear where a value of k_{2Li} and k_b could be determined from the intercept and the slope respectively. This plot, constructed from our observations and shown in Figure 5.15, is indeed linear and a resulting value for k_{2Li} is shown in Table 5.3.

The same approach can be used in the kinetic observation of sodium in the presence of lithium where the chemical exchange is slow on the ^{23}Na NMR chemical shift timescale. The usual individual sodium associative mechanism is considered:

$$Na^{*+} + (Na{:}B15C5)^+ \overset{k_{2Na}}{\rightleftharpoons} Na^+ + (Na^*{:}B15C5)^+ \qquad (70)$$

where k_{2Na} is the associative rate constant for this specific exchange in the presence of lithium. The second path involving the lithium cations shown in equation 68, is also considered for the associative exchange of sodium. In this case the following relationship for the $(k_A + k_B)_{Na}$ is obtained (see Appendix 6):

$$(k_A + k_B)_{Na} = k_{2Na}[Na^+]_T + k_f[Li^+]_T \{1 + ((1-K_{eq})/K_{eq}))(\Delta/\Delta_o)_{Li}\} \qquad (71)$$

where $(k_A + k_B)_{Na}$ refers to that parameter measured for the sodium exchange by ^{23}Na NMR lineshape analysis and $(\Delta/\Delta_o)_{Li}$ is a parameter based on the ^7Li NMR chemical shifts reflecting the relative populations of the lithium species in solution (see Appendix 6). A plot of $(k_A + k_B)_{Na}$ as a function of $(\Delta/\Delta_o)_{Li}$ should be linear where a value for k_f and k_{2Na} could be determined from the slope and intercept respectively. This plot is shown in Figure 5.16.

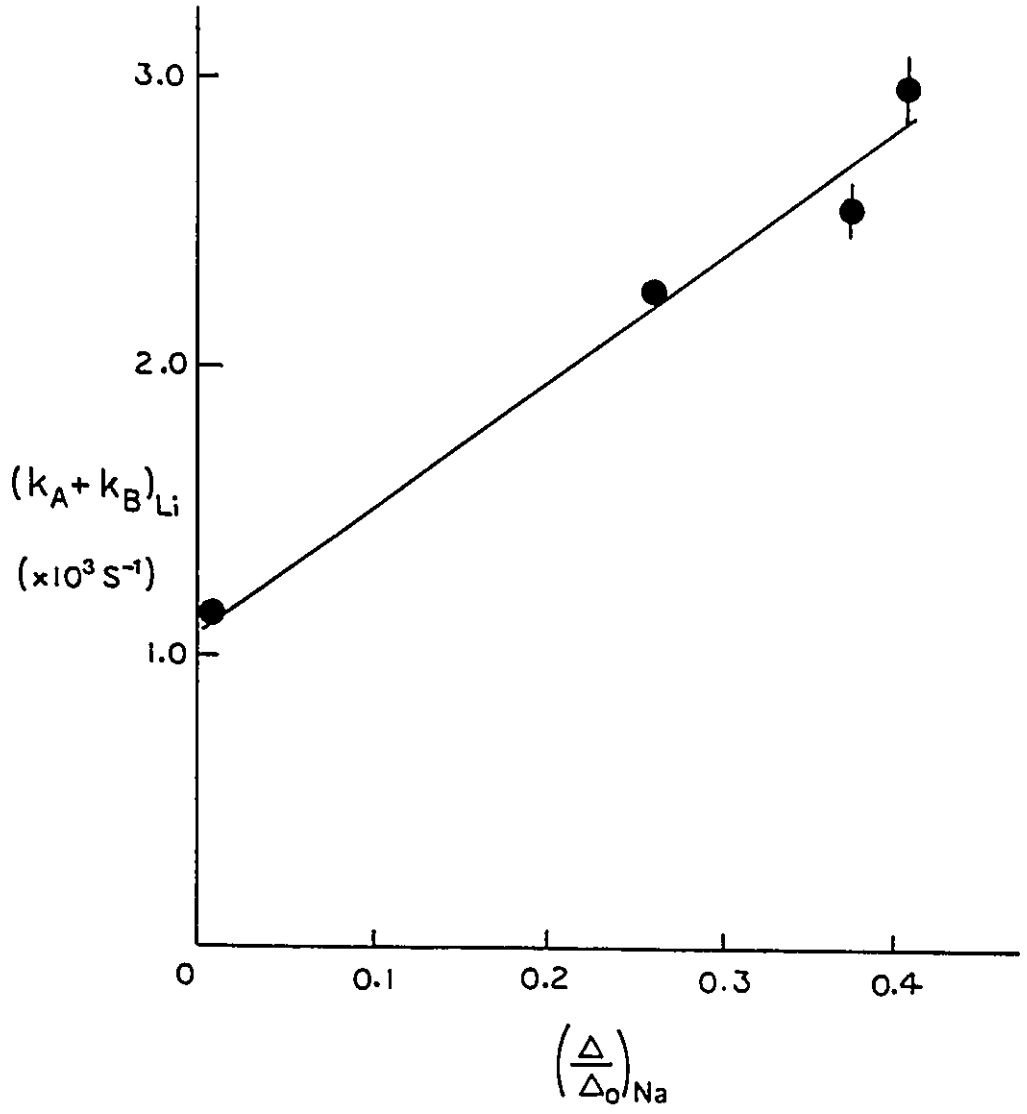

Figure 5.15: $(k_A + k_B)_{Li}$ as a function of $(\Delta/\Delta_o)_{Na}$. $[Na^+]_T = [Li^+]_T = 5.0$ mM in nitromethane at 300.0 ± 0.5 K.

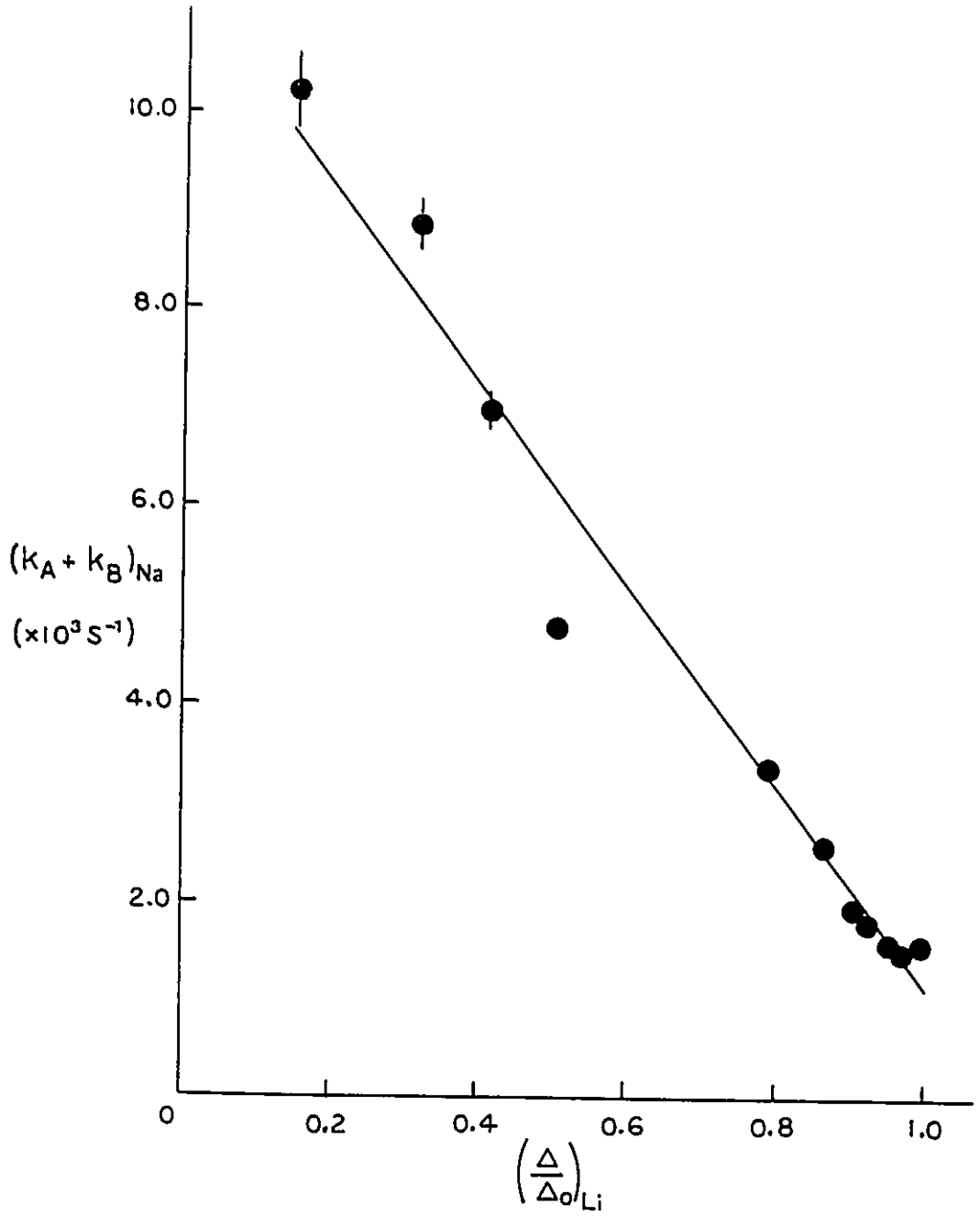

Figure 5.16: $(k_A + k_B)_{Na}$ as a function of $(\Delta/\Delta_o)_{Li}$. $[Na^+]_T = [Li^+]_T = 5.0$ mM in nitromethane at 300.0 ± 0.5 K.

Table 5.3: Rate Parameters for the Associative Exchange of $(Li:B15C5)^+$ and $(Na:B15C5)^+$ in NM; Individually (ind) or in Cation Mixtures (mix).[a]

Cation[b]	k_2 $\times 10^5\ M^{-1}s^{-1}$	$\Delta G^{\ddagger}$ $kJ.mol^{-1}$
Li^+ (ind)	1.88 ± 0.08	43.2 ± 0.1
Li^+ (mix)	2.0 ± 0.3	43.0 ± 0.4
Na^+ (ind)	2.03 ± 0.06[c]	43.0 ± 0.1
Na^+ (mix)	2.0 ± 0.4	43.0 ± 0.5

(a) at 300.0 ± 0.5 K. (b) Counteranion is ClO_4^- in each case. (c) average value taken from data in Table 4.5.

A summary of the rate constants and free energies of activation for the associative exchange of the sodium and lithium cations with B15C5 determined in the cation mixtures as well as for the individual cations, is shown in Table 5.3. The rate constants for the associative exchange, k_2, determined in the cation mixtures agree very well with the values determined in the studies involving individually both cations. There is thus no synergistic effect of one cation on the other. Again the preference of lithium over sodium can be concluded when comparing the rate constants for the forward, k_f, and reverse, k_b, reactions in equation 68: $k_f = (2.1 \pm 0.1) \times 10^6\ s^{-1}$ (determined from a nonlinear regression of the data in Figure 5.16) and $k_b = (1.1 \pm 0.1) \times 10^4\ s^{-1}$ (from Figure 5.15). One can again determine a value for $K_{eq} = k_f / k_b$, where $\log K_{eq} = 2.3 \pm 0.1$. This separate determination of K_{eq} is in excellent agreement with previous determinations (average $\log K_{eq} = 1.9 \pm 0.2$).

SUMMARY AND CONCLUSIONS

In the third chapter of this thesis, the structural aspects of crown ethers and alkali metal cation-crown ether complexes were studied in solution. The ^{1}H NMR spectra of B15C5, DB18C6, DB24C8 and DB30C10 as well as their respective alkali metal complexes, exhibited spectral patterns reflecting both a rapid conversion between two separate conformers and the ^{1}H-^{1}H spin coupling of the 4-spin systems in the crown ethers. From spin simulations, the coupling of the protons in the separate O-CH_2-CH_2-O fragments could be fully characterized by three coupling constants: J_{gem}, J_{cis} and J_{trans}. Subsequently, it was possible, based on a modified Karplus correlation, to obtain values for the dihedral angle, ϕ, between the two oxygen atoms in the ether fragments. An average value of ϕ equal to approximately 60° was obtained for all the systems studied and no trends were detected differentiating between crown ethers which were complexed and those which were not. A dihedral angle of 60° corresponds to a *gauche* orientation of the oxygen atoms which is also generally observed in the solid counterparts.

The proton spectra were partially assigned with heteronuclear chemical shift correlation (HETCOR) experiments which also served to assign the ^{13}C resonances. Long-range HETCOR experiments provided data for the unambiguous assignment of resonances close in value to each other.

In chapters 4 and 5, insight into sodium and lithium complexes of 15C5 and B15C5 in solution was obtained by ^{23}Na and ^{7}Li NMR. The extent of complex formation was significantly reduced in solvents which could compete with the ligand for cation coordination. This was the case for the formation of $(Na{:}B15C5)^{+}$ in dimethylformamide (DN = 26.6) and pyridine (DN = 33.1), whereas in nitromethane (DN = 2.7) and acetonitrile (DN = 14.1), a quantitative formation of lithium and sodium complexes was observed. A study in nitromethane solutions containing mixtures of both

sodium and lithium cations indicated that B15C5 displays a selectivity for the complexation of lithium.

The main focus of the work presented in this thesis, lies in the kinetic and mechanistic behaviors of alkali metal cation - crown ether complexes. The ^{23}Na and ^{7}Li dynamic NMR results which were obtained for $(Na:15C5)^+$, $(Na:B15C5)^+$, $(Li:15C5)^+$ and $(Li:B15C5)^+$, with the counteranions BPh_4^-, ClO_4^- and PF_6^-, could be accounted for by two possible mechanistic contributions to the chemical exchange of the cation. The *dissociative* exchange could only be observed in acetonitrile which has a higher donor value than nitromethane. Studies in binary solvent mixtures have indicated a direct implication of the solvent at the molecular level which governs this mechanism. The *associative* exchange however, was observed to be independent of the nature of the solvent as well as the cation or the crown ether; indeed the activation parameters for many systems implicating the associative mechanism were very consistent, indicating a common origin in all cases. Conformational rearrangements were postulated to be the governing factor for cation exchange by this mechanism.

Although it was generally known before the studies presented in this thesis, that the solvent played an important role in the kinetic interactions of alkali metal cations with macrocyclic ligands, the results obtained in this work provide information about the specific molecular role of the solvent. Until now, solvent effects had been treated and rationalized on a "global" level but the kinetic studies in binary solvent mixtures, presented in this work, have for the first time provided insight into the direct solvent participation in the coordination sphere of the cation. The DMF-NM solvent mixtures provided an excellent medium for this since very small amounts of DMF, which were in the order of the sodium concentrations, gave rise to large increases in the overall rate of exchange and corresponding $(k_A + k_B)$ for the chemical exchange of sodium in the solvated and complexed to B15C5 sites. This was related to an increase in the

dissociative contribution of the overall exchange. The ^{23}Na NMR chemical shifts and longitudinal relaxation rates provided a direct line to the complexed sodium cation coordination sphere which could be characterized by the participation of one DMF molecule. As a result the lability of $(Na:B15C5)^+$ was increased.

In the study of lithium exchange, 2D - ^{7}Li exchange spectroscopy (EXSY) was for the first time applied. The rate constants obtained by this method for the exchange of lithium in the two sites $(Li)^+_S$ and $(Li:B15C5)^+$ in nitromethane were comparable to those obtained by conventional 1D approaches. Although there was no advantage for using ^{7}Li EXSY in our case we have demonstrated that it can be successfully applied. This method may prove very useful in future studies of slow processes involving transport of lithium cations across membranes.

PUBLICATIONS AND CONFERENCES

PUBLICATIONS:

– ***Mechanism of Dissociation of Sodium Monobenzo-15-crown-5 in the Solvent Nitromethane***. K.M. Brière and C. Detellier, *J. Phys. Chem.* (1987), **91**, 6097-6099.

– ***Mechanisms of Dissociation of Sodium 15-Crown-5 and Sodium Monobenzo-15-crown-5 in the Solvents Nitromethane and Acetonitrile***. K.M. Brière and C. Detellier, *New J. Chem.* (1989), **13**, 145-150.

– ***^{23}Na Nuclear Magnetic Resonance Study of the Complexation of Sodium Tetraphenylborate by [5,5]-Dibenzo-30-Crown-10 in Nitromethane, Acetonitrile, Acetone and Pyridine***. K.M. Brière, H.P. Graves, T.S. Rana, L.J. Maurice and C. Detellier, *J. Phys. Org. Chem.* (1990), 435-442.

– ***Alkali Metal NMR Studies of Synthetic and Natural Ionophore Complexes***. Christian Detellier, Helen P. Graves and Kathleen M. Brière, Chapter 4 in "Isotopic Applications in NMR Studies", Volume in "Isotopes in the Physical and Biomedical Sciences", E. Buncel and J.R. Jones editors, Elsevier, in press.

CONFERENCE COMMUNICATIONS:

– ***The Competition Between Li^+ and Na^+ in the Complexation of Benzo-15-crown-5 in the Solvent Nitromethane: A Thermodynamic and Kinetic ^{23}Na NMR Study***. K.M. Brière and C. Detellier, poster presented at the XXI International Conference on Solution Chemistry, Ottawa, Canada, August 5-10, 1990.

– ***Le Rôle du Solvant sur la Cinétique et les Mécanismes de Dissociation du Complexe Benzo-15-couronne 5-sodium: Étude par rmn du ^{23}Na***. K.M. Brière and C. Detellier, communication presented at the 58th congress of L'Association Canadienne Française pour l'Avancement des Sciences, Quebec City, May 17, 1990.

– ***A Kinetic, Mechanistic and Structural Study of the Dissociation of Lithium - 15-Crown-5 and Lithium - Monobenzo-15-Crown-5 in Nitromethane Using ^{7}Li, ^{13}C and ^{1}H NMR***. K.M. Brière, H.D. Dettman and C. Detellier, poster presented at the 72nd Canadian Chemical Conference at the University of Victoria, Victoria, June 4-8, 1989.

– ***Mechanisms of Dissociation of Sodium - Monobenzo-15-Crown-5 in the Solvents Nitromethane and Acetonitrile***. K. M. Brière and C. Detellier, poster presented at the Inorganic Discussion Weekend at York University, North York, October 14-15, 1988.

– ***Role of the Solvent on the Mechanisms of Dissociation of Crown Ether Alkali Metal Complexes***. C. Detellier, K.M. Brière and H.P. Graves, communication presented at the XIX International Conference on Solution Chemistry, University of Lund, Sweden, August 15-19, 1988.

– ***Mechanisms of Dissociation of Crown-Ether Metal Cation Complexes. Role of the Solvent***. C. Detellier, K.M. Brière and H.P. Graves, communication presented at the 4th North American Chemical Congress, June 4-9, 1988.

– ***Benzo-15-couronne-5-sodium: Mise en Évidence d'un Méchanisme D'échange Cationique Bimoléculaire dans le Nitrométhane***. K.M. Brière and C. Detellier, communication presented at the 55th congress of L'Association Canadienne Française pour l'Avancement des Sciences, Ottawa, May 20, 1987.

APPENDIX 1: SAS Program for Full Lineshape Analysis.

This program was used in order to determined the sum of the two pseudo-first order rate constants, ($k_A + k_B$), in the two-site (A and B) exchange of sodium and lithium.

```
1.  DATA TWO;
2.      CMS FILEDEF TWO DISK INPAR DATA A;
3.      INFILE TWO;
4.      INPUT VA VB RA RB PA PB;
5.  PROC PRINT;
6.  DATA ONE;
7.      CMS FILEDEF ONE DISK XXX NMR A;
8.      INFILE ONE;
9.      INPUT X Y;
10. IF _N_=1 THEN SET TWO;
11.     PI=3.14159;
12. PROC NLIN METHOD=DUD;
13.     PARMS CO=1E4 KAB=1E3;
14.     BOUNDS 1<CO<1E6, 0<KAB<5E5;
15.     TAU=1/KAB;
16.     DV=(VA-VB);
17.     DELV=0.5*(VA+VB)-X;
18.     P=TAU*(RA*RB-4*PI**2*DELV**2+PI**2*DV**2)
        +PA*RA+PB*RB;
19.     Q=TAU*(2*PI*DELV-PI*DV*(PA-PB));
20.     R=2*PI*DELV*(1+TAU*(TA+TB))+(PI*DV*TAU*(RB-RA))
        +PI*DV*(PA-PB);
21.     YCAL=CO*(P*(1+TAU*(PB*RA+PA*RB))+Q*R)/(P**2+R**2);
22.     MODEL Y=CO*(P*(1+TAU*(PB*RA+PA*RB))+Q*R)/(P**2+R**2);
23.     OUTPUT OUT=PUT PARMS=CO PARMS=KAB;
24.     ID YCAL;
25. PROC PLOT DATA=PUT;
26.     PLOT Y*X='0' YCAL*X='+'/OVERLAY;
```

NOTES:

– in lines 1-4, the main frame file INPAR DATA A is set for SAS recognition; this file contains the initial parameters corresponding to the particular analysis: VA and VB, RA and RB, and PA and PB are the frequencies in Hz, transverse relaxation rates and populations of sites A and B respectively.

– in lines 6-9, the main frame file XXX NMR A is set for SAS recognition; this file contains the frequency in Hz (X) and arbitrary intensities (Y) of the NMR spectrum.

– in lines 12-14 the nonlinear regression (PROC NLIN) is initialized; there are two variable parameters: CO is an arbitrary intensity factor, and KAB is the desired $k_A + k_B$. Each of these are given reasonable initial values and boundaries. PB can be added as a variable parameter and therefore lines 4, 13, 14 and 23 must be altered and the following line is inserted between lines 14 and 15:

14b. PA=1-PB;

– lines 15-22 contain the equations describing the lineshape (see reference 46).

– lines 23-26 are concerned with the output and plot of the experimental data points as well as the ones calculated from the nonlinear regression.

– to obtain a graphics plot (see Figure 2.5), line 25 can be replaced by:

25a. % INCLUDE QMS;

25b. GPLOT;

APPENDIX 2: Formation Constant (K_{F1}) of the 1:1 Complex.

The following equations were used in determining the K_{F1} for the formation of $(Na:B15C5)^+$ in DMF and PY from ^{23}Na chemical shift (δ_{obs}) or longitudinal relaxation rate (T_1^{-1}) as a function of $[B15C5]_T$ / $[Na^+]_T$ (ρ) data (Figures 4.1 and 4.2). This analysis is appropriate for determining K_{F1} of any M^+-C complex in the absence of other competing reactions.

$$(M^+)_S + (C)_S \underset{}{\overset{K_{F1}}{\rightleftharpoons}} (M:C)^+_S$$

A B

$$[M]_T = [M] + [M:C]; \quad [C]_T = [C] + [M:C]; \quad \rho = [C]_T / [M]_T$$

$$K_{F1} = [M:C] / ([M][C]) = ([M]_T - [M]) / ([M]([C]_T - [M]_T + [M]))$$

$$X = K_{F1}; \quad Y = K_{F1}[C]_T - K_{F1}[M]_T + 1; \quad Z = -[M]_T$$

$$[M] = (-Y + (Y^2 - 4XZ)^{1/2}) / (2X);$$ derived from a quadratic equation for [M]

$$\delta_{obs} = ([M]/[M]_T)\,\delta_A + ([M:C]/[M]_T)\,\delta_B; \quad \delta_{obs} = ((\delta_A - \delta_B)\,([M] / [M]_T)) + \delta_B$$

– δ_{obs}, δ_A and δ_B can be replaced by $T_{1,obs}^{-1}$, $T_{1,A}^{-1}$ and $T_{1,B}^{-1}$ respectively.

APPENDIX 3: Master Table of Published Kinetic Results of Alkali Metal-Macrocyclic Complexes Obtained by Alkali Metal NMR[21].

	Ligand	Alkali Nucleus	Counter-anion	Solvent	Mech.[a]	Rate constant[b]
1.	15C5	^{7}Li	ClO_4^-	NM	II	$(1.9 \pm 0.1) \times 10^6$
2.	B15C5	^{7}Li	ClO_4^-	NM	II	$(1.88 \pm 0.08) \times 10^5$
3.	OM16C4	^{7}Li	ClO_4^-	NM	II	67
4.	C211	^{7}Li	I^-	H_2O	I	$(4.9 \pm 2.0) \times 10^3$
5.	C211	^{7}Li	ClO_4^-	PY	I	$(0.12 \pm 0.24) \times 10^3$
6.	C211	^{7}Li	ClO_4^-	DMSO	I	$(2.32 \pm 0.54) \times 10^1$
7.	C211	^{7}Li	ClO_4^-	DMF	I	$(1.30 \pm 0.33) \times 10^4$
8.	C211	^{7}Li	ClO_4^-	FOR	I	$(7.4 \pm 2.9) \times 10^3$
9.	C221	^{7}Li	ClO_4^-	PY	I	$(1.23 \pm 0.20) \times 10^6$
10.	C221	^{7}Li	ClO_4^-	AN	II	680 ± 42
11.	C221	^{7}Li	ClO_4^-	PC	II	892 ± 50
12.	C222	^{7}Li	ClO_4^-	AN	I	420 ± 14
13.	C222	^{7}Li	ClO_4^-	PC	I	507 ± 31
14.	C222	^{7}Li	ClO_4^-	AC	I	794 ± 42
15.	15C5	^{23}Na	BPh_4^-	NM	II	$(1.45 \pm 0.05) \times 10^5$
16.	B15C5	^{23}Na	BPh_4^-	NM	II	$(1.09 \pm 0.04) \times 10^5$
17.	B15C5	^{23}Na	BPh_4^-	NM	I	$(1.1 \pm 0.1) \times 10^2$
18.	B15C5	^{23}Na	BPh_4^-	AN	I	$(3.5 \pm 0.1) \times 10^3$
19.	B15C5	^{23}Na	BPh_4^-	AN	II	$(0.9 \pm 0.3) \times 10^5$
20.	18C6	^{23}Na	Br^-	MA	I	4.3×10^5
21.	18C6	^{23}Na	BPh_4^-	THF	I	53 ± 6
22.	18C6	^{23}Na	SCN^-	THF	II	$(9.16 \pm 0.12) \times 10^4$
23.	18C6	^{23}Na	SCN^-	MeOH	I	$(3.65 \pm 0.07) \times 10^4$
24.	18C6	^{23}Na	BPh_4^-	PC	II	$(1.30 \pm 0.07) \times 10^5$
25.	18C6	^{23}Na	BPh_4^-	THF/MeOH (0.6/0.4)	I	$(3.56 \pm 0.09) \times 10^3$
26.	18C6	^{23}Na	BPh_4^-	THF/PC (0.8/0.2)	I	$(9.15 \pm 0.13) \times 10^2$
27.	18C6	^{23}Na	BPh_4^-	THF/PC (0.4/0.6)	II	$(5.00 \pm 0.23) \times 10^4$
28.	18C6	^{23}Na	SCN^-	AC	I	4.34×10^5
29.	18C6	^{23}Na	SCN^-	MeOH	I	7.2×10^4
30.	18C6	^{23}Na	SCN^-	PY	I	1.03×10^4
31.	18C6	^{23}Na	BPh_4^-	AN	I	$(3.8 \pm 0.5) \times 10^3$
32.	18C6	^{23}Na	BPh_4^-	AN	II	$(2.6 \pm 0.4) \times 10^5$
33.	18C6	^{23}Na	BPh_4^-	PC	I	$(1.6 \pm 0.2) \times 10^3$
34.	18C6	^{23}Na	BPh_4^-	PC	II	$(6.9 \pm 0.3) \times 10^5$
35.	18C6	^{23}Na	BPh_4^-	AC	I	$(1.48 \pm 0.02) \times 10^4$
36.	18C6	^{23}Na	BPh_4^-	PY	I	$(5.3 \pm 0.2) \times 10^2$
37.	18C6	^{23}Na	BPh_4^-	PY	II	$(2.0 \pm 0.3) \times 10^4$
38.	DB18C6	^{23}Na	BF_4^-	AN	I	4×10^3
39.	DB18C6	^{23}Na	BPh_4^-	AN	I	4×10^3
40.	DB18C6	^{23}Na	BPh_4^-	NM	I	2×10^2
41.	DB18C6	^{23}Na	BPh_4^-	NM	II	3×10^4
42.	DB18C6	^{23}Na	PF_6^-	NM	I	2×10^2
43.	DB18C6	^{23}Na	PF_6^-	NM	II	4×10^4
44.	DB18C6	^{23}Na	SCN^-	DMF	I	1×10^5
45.	DB18C6	^{23}Na	SCN^-	DME	I	1.5×10^4

	Temp. K	ΔG° kJ.mol^{-1}	ΔH° kJ.mol^{-1}	ΔS° J.mol^{-1}.K^{-1}	Reference
1.	300	37.4 ± 0.2	21 ± 1	-54 ± 3	142
2.	300	43.2 ± 0.2	32.2 ± 0.4	-36 ± 1	142
3.	373	79	-	-	161
4.	298	86.3 ± 0.8	86 ± 5	2 ± 12	146
5.	298	95 ± 5	80 ± 14	-52 ± 39	146
6.	298	82.4 ± 0.4	65 ± 2	-58 ± 6	146
7.	298	83.7 ± 0.4	65 ± 2	-65 ± 6	146
8.	298	87.0 ± 0.8	57 ± 3	-95 ± 8	146
9.	298	74.9 ± 0.4	54 ± 2	-62 ± 4	146
10.	298	56.90 ± 0.04	28.7 ± 0.6	-101 ± 2	147
11.	298	56.8 ± 0.4	26.2 ± 0.7	-109 ± 2	147
12.	298	58.28 ± 0.04	11.6 ± 0.5	-157 ± 2	147
13.	298	57.53 ± 0.08	15.0 ± 0.4	-143 ± 2	147
14.	298	56.32 ± 0.08	20.2 ± 0.8	-121 ± 3	147
15.	301.5	44.1 ± 0.1	21 ± 1	-76 ± 2	137
16.	301.5	44.8 ± 0.1	28 ± 3	-57 ± 3	136
17.	301.5	62.1 ± 0.3	-	-	136
18.	258	45.4 ± 0.4	-	-	137
19.	258	38.4 ± 0.8	-	-	137
20.	298	41	25	-54	158
21.	298	63.1 ± 0.4	47 ± 1	-52 ± 5	132
22.	298	44.66 ± 0.04	12 ± 2	-113 ± 4	132
23.	298	46.96 ± 0.08	38 ± 1	-30 ± 4	148
24.	298	43.82 ± 0.17	17 ± 2	-91 ± 7	148
25.	298	52.7 ± 0.1	39 ± 1	-47 ± 4	148
26.	298	56.08 ± 0.08	40.4 ± 0.4	-53 ± 2	148
27.	298	16.9 ± 0.1	36 ± 2	-35 ± 6	148
28.	298.2	40.8	36.7	-14.0	155
29.	298.2	45.3	53.6	27.8	155
30.	298.2	50.1	50.5	1.4	155
31.	301.5	53.2 ± 0.4	32 ± 2	-65 ± 8	143
32.	301.5	42.6 ± 0.4	-	-	143
33.	301.5	55.4 ± 0.3	54 ± 6	-5 ± 20	143
34.	301.5	40.2 ± 0.1	35 ± 1	-16 ± 3	143
35.	301.5	49.8 ± 0.1	44 ± 1	-21 ± 2	143
36.	301.5	58.1 ± 0.1	49 ± 4	-30 ± 10	143
37.	301.5	49.0 ± 0.4	-	-	143
38.	300	53	40 ± 2	-44 ± 8	145
39.	300	53	40 ± 2	-44 ± 8	145
40.	300	60	37 ± 3	-78 ± 8	145
41.	300	48	-	-	145
42.	300	60	-	-	145
43.	300	47	-	-	145
44.	298	45	51	21	140
45.	298	50	53	12	141

	Ligand	Alkali Nucleus	Counter-anion	Solvent	Mech.[a]	Rate constant[b]
46.	DB18C6	^{23}Na	SCN^-	MeOH	I	1.4×10^4
47.	DC18C6 (cis-anti-cis)	^{23}Na	SCN^-	THF	II	$(4.0 \pm 0.2) \times 10^5$
48.	DC18C6 (cis-syn-cis)	^{23}Na	SCN^-	THF	II	$(2.2 \pm 0.2) \times 10^6$
49.	DC18C6 (cis-anti-cis)	^{23}Na	SCN^-	MeOH	I	5.2×10^4
50.	DC18C6 (cis-trans)	^{23}Na	SCN^-	MeOH	I	$> 9.6 \times 10^2$
51.	DA18C6	^{23}Na	SCN^-	THF	I	$(2.34 \pm 0.09) \times 10^3$
52.	DA18C6	^{23}Na	SCN^-	THF	I	$(1.74 \pm 0.05) \times 10^3$
53.	DA18C6	^{23}Na	SCN^-	THF	II	$(9.8 \pm 0.4) \times 10^4$
54.	DAMDB18C6	^{23}Na	SCN^-	DMF	I	1.9×10^5
55.	DNDB18C6	^{23}Na	SCN^-	DMF	I	2.0×10^5
56.	DB24C8	^{23}Na	BPh_4^-	NM($>10^{-3}$M)	II	$(2.8 \pm 0.2) \times 10^5$
57.	DB24C8	^{23}Na	BPh_4^-	NM($<10^{-3}$M)	I	19
58.	DB24C8	^{23}Na	PF_6^-	NM($>10^{-3}$M)	II	$(3.5 \pm 0.2) \times 10^5$
59.	DB24C8	^{23}Na	PF_6^-	NM($<10^{-3}$M)	I	67
60.	DB24C8	^{23}Na	I^-	NM	II	$(4.5 \pm 1.0) \times 10^5$
61.	DB24C8	^{23}Na	SCN^-	NM	II	$(1.3 \pm 2) \times 10^6$
62.	C211	^{23}Na	ClO_4^-	H_2O	I	47.6 ± 0.5
63.	C211	^{23}Na	ClO_4^-	DMF	I	12.1 ± 0.2
64.	C211	^{23}Na	ClO_4^-	DMSO	I	34.0 ± 0.7
65.	C221	^{23}Na	Br^-	MeOH/H_2O (25/75)	I	36.4
66.	C222	^{23}Na	Br^-	EDA	I	165 ± 5
67.	C222	^{23}Na	Br^-	PY	I	1.14 ± 0.09
68.	C222	^{23}Na	Br^-	THF	I	8.03 ± 0.27
69.	C222	^{23}Na	Br^-	H_2O	I	147.4 ± 2.6
70.	$C21C_5$	^{23}Na	ClO_4^-	AN	I	84.8 ± 1.6
71.	$C21C_5$	^{23}Na	ClO_4^-	PC	I	19.4 ± 0.5
72.	$C21C_5$	^{23}Na	ClO_4^-	AC	I	878 ± 6
73.	$C21C_5$	^{23}Na	ClO_4^-	MeOH	I	1800 ± 50
74.	$C21C_5$	^{23}Na	ClO_4^-	DMF	I	$(2.88 \pm 0.03) \times 10^4$
75.	$C21C_5$	^{23}Na	ClO_4^-	PY	I	93.5 ± 0.5
76.	Enniatin B	^{23}Na	SCN^-	MeOH	I	$> 3.1 \times 10^2$
77.	Valinomycin	^{23}Na	SCN^-	MeOH	I	$> 1.2 \times 10^3$
78.	Nonactin	^{23}Na	SCN^-	MeOH	I	$> 1.0 \times 10^3$
79.	Monensin	^{23}Na	Mon^-	MeOH	I	63
80.	Monensin	^{23}Na	Mon^-	MeOH	I	83 ± 4
81.	18C6	^{39}K	AsF_6^-	AC	II	$(4.1 \pm 0.9) \times 10^5$
82.	18C6	^{39}K	AsF_6^-	AC/1,4DO (80/20)	II	$(5.7 \pm 1.1) \times 10^5$
83.	18C6	^{39}K	AsF_6^-	1,3DO	II	$(1.65 \pm 0.04) \times 10^4$
84.	18C6	^{39}K	I^-	MeOH	II	$(6.8 \pm 2.7) \times 10^5$
85.	18C6	^{39}K	I^-	MeOH	I	$(6.8 \pm 2.7) \times 10^4$
86.	DB18C6	^{39}K	I^-	MeOH	I	610
87.	DB18C6	^{87}Rb	SCN^-	MeOH	I	$> 10^4$
88.	18C6	^{133}Cs	BPh_4^-	PY	I	$(9.5 \pm 0.2) \times 10^3$
89.	DC18C6 (cis-syn-cis)	^{133}Cs	BPh_4^-	PC	I	$(1.1 \pm 0.1) \times 10^4$
90.	DA18C6	^{133}Cs	SCN^-	NM	II	$(2.31 \pm 0.23) \times 10^7$

	Temp. K	ΔG° kJ.mol^{-1}	ΔH° kJ.mol^{-1}	ΔS° J.mol^{-1}.K^{-1}	Reference
46.	298	50	47	-10	141
47.	298	41.06 ± 0.04	8.8 ± 0.8	-109 ± 3	149
48.	298	36.88 ± 0.04	8 ± 2	-98 ± 5	149
49.	298	46.0	32	46	141
50.	294	< 55			17
51.	298	53.74 ± 0.13	5.4 ± 0.8	-162 ± 2	149
52.	273	49.72 ± 0.08	5.9 ± 0.8	-161 ± 2	149
53.	233	33.70 ± 0.04	37 ± 2	10 ± 4	149
54.	298	43	-	-	141
55.	298	43	-	-	141
56.	295	41 ± 3	31 ± 3	-32 ± 10	144
57.	295	≅ 65	-	-	144
58.	300	40 ± 2	30 ± 2	-37 ± 10	145
59.	300	≅ 63	-	-	145
60.	294	40.7	-	-	130
61.	294	38.5	-	-	130
62.	298.2	63.4 ± 0.1	67.2 ± 0.3	12.6 ± 0.7	157
63.	298.2	66.8 ± 0.1	83.5 ± 0.5	55.8 ± 1.2	157
64.	298.2	64.2 ± 0.1	69.5 ± 0.4	17.4 ± 1.2	157
65.	298	64.1	66.0 ± 1.2	6.5 ±3.8	163
66.	298	60.50 ± 0.08	51.5 ± 0.8	-32 ± 3	160
67.	298	72.65 ± 0.02	56.9 ± 0.8	-53 ± 3	160
68.	298	67.96 ± 0.08	57.7 ± 0.8	-34 ± 3	160
69.	298	60.60 ± 0.04	67.4 ± 0.8	22 ± 3	160
70.	298.2	62.0 ± 0.1	57.9 ± 0.7	-13.8 ± 2.1	156
71.	298.2	65.7 ± 0.1	70.3 ± 0.5	15.3 ± 1.4	156
72.	298.2	56.2 ± 0.1	54.4 ± 0.4	-6.1 ± 1.2	156
73.	298.2	54.4 ± 0.1	44.9 ± 0.1	-31.9 ± 0.4	156
74.	298.2	46.6 ± 0.1	40.0 ± 0.1	-25.3 ± 0.5	156
75.	298.2	61.8 ± 0.1	62.8 ± 0.2	3.3 ± 0.5	156
76.	294	< 58	-	-	17
77.	294	< 55	-	-	17
78.	294	< 55	-	-	17
79.	298	63	43.0	-66.2	165
80.	298	62.0 ± 0.2	46.8 ± 0.7	-51.1 ± 2.5	162
81.	298	41.0 ± 0.4	36 ± 2	-17 ± 8	150
82.	298	41.1 ± 0.4	55 ± 2	50 ± 8	150
83.	298	49.02 ± 0.04	68 ± 1	63 ± 4	150
84.	298	40.0 ± 0.8	36 ± 3	-13 ± 12	150
85.	298	45.6 ± 0.8		-33 ± 3	150
86.	239	45	-	-	150
87.	223	< 37	-	-	150
88.	298	50.3 ± 0.1	33 ± 2	-60 ± 2	128
89.	298	49.9 ± 0.2	33 ± 2	-59 ± 8	129
90.	283	27.3 ± 0.1	21.3 ± 0.4	-19 ± 3	153

91.	DB21C7	^{133}Cs	SCN^-	AC	II	$(9.4 \pm 3) \times 10^3$
92.	DB21C7	^{133}Cs	SCN^-	MeOH	II	$(2.7 \pm 0.4) \times 10^4$
93.	DB24C8	^{133}Cs	SCN^-	AC	II	$(7.4 \pm 1.0) \times 10^4$
94.	DB24C8	^{133}Cs	SCN^-	MeOH	II	$(5.6 \pm 2.0) \times 10^4$
95.	DB30C10	^{133}Cs	SCN^-	NM	I	$(1.7 \pm 0.1) \times 10^5$
96.	DB30C10	^{133}Cs	SCN^-	AN	II	$(4.2 \pm 0.3) \times 10^7$
97.	DB30C10	^{133}Cs	SCN^-	PC	II	$(5.4 \pm 0.2) \times 10^6$
98.	DB30C10	^{133}Cs	SCN^-	MeOH	II	$(7.6 \pm 0.2) \times 10^6$
99.	C221	^{133}Cs	SCN^-	NM	I	$(3.90 \pm 0.06) \times 10^2$
100.	C221	^{133}Cs	SCN^-	AN	I	$(2.17 \pm 0.05) \times 10^3$
101.	C221	^{133}Cs	SCN^-	MeOH	I	$(3.29 \pm 0.11) \times 10^3$
102.	C221	^{133}Cs	SCN^-	DMF	I	$(4.49 \pm 0.17) \times 10^4$
103.	C222	^{133}Cs	BPh_4^-	DMF	I	$(9.0 \pm 0.9) \times 10^6$
104.	C22B	^{133}Cs	BPh_4^-	PC	I	344 ± 35

91.	220	36 ± 1	34 ± 2	-11 ± 10	152
92.	220	34.7 ± 0.4	25 ± 1	-44 ± 6	152
93.	220	32.6 ± 0.4	28 ± 1	-21 ± 6	152
94.	220	34 ± 1	12 ± 2	-97 ± 10	152
95.	253	36.3 ± 0.1	13.8 ± 0.4	-90 ± 2	151
96.	253	27.8 ± 0.2	34 ± 1	26 ± 6	151
97.	253	29.0 ± 0.1	46 ± 2	69 ± 6	151
98.	253	28.4 ± 0.1	38 ± 1	36 ± 3	151
99.	298	58.2 ± 0.1	-	-	153
100.	298	53.82 ± 0.04	31 ± 1	-75 ± 4	153
101.	298	52.4 ± 0.1	25 ± 1	-93 ± 3	153
102.	298	46.50 ± 0.04	21.7 ± 0.4	-83 ± 1	153
103.	298	33.3 ± 0.3	54 ± 1	69 ± 4	154
104.	298	41.4 ± 0.3	60 ± 3	63 ± 8	129

(a) Mechanism I: dissociative exchange (equation 26); Mechanism II; associative exchange (equation 31). (b) In mechanism I units for k: s^{-1}; in mechanism II units for k: $M^{-1}s^{-1}$.

APPENDIX 4: Equilibrium Constant (K_{CS}) for the Formation of a Sodium Complex Implicating one Molecule of DMF.

The following model has been developed to account for the ^{23}Na chemical shift ($\delta_{C,obs}$) and longitudinal relaxation rate ($T_{1,C,obs}^{-1}$) as a function of $[DMF]_T$ data in DMF-NM solvent mixtures (Figure 4.25).

$$(Na{:}B15C5)^+ + DMF \underset{}{\overset{K_{CS}}{\rightleftharpoons}} (Na{:}B15C5{:}DMF)^+$$

A B

$$K_{CS} = [Na{:}C{:}DMF] / ([Na{:}C][DMF])$$

$$[Na]_T = [Na{:}C] + [Na{:}C{:}DMF]$$

METHOD 1: Assume that $[DMF] = [DMF]_T$

$$\delta_{C,obs} = ([Na{:}C]\delta_A + [Na{:}C{:}DMF]\delta_B) / [Na]_T$$

$$\delta_{C,obs} = (\delta_A + K_{CS}[DMF]\delta_B) / (1 + K_{CS}[DMF])$$

METHOD 2: Full Model

$$K_{CS} = [Na:C:DMF] / (([Na]_T - [Na:C:DMF]) ([DMF]_T - [Na:C:DMF]))$$

$$[Na:C:DMF] = Z[Na]_T;\ Z = (\delta_{C,obs} - \delta_A) / (\delta_B - \delta_A)$$

$$\delta_{C,obs} = \{((\delta_B - \delta_A) / [Na]_T) (K_{CS}[Na]_T - ZK_{CS}[Na]_T) ([DMF]_T - Z[Na]_T)\} + \delta_A$$

– nonlinear regressions using both models gave results which were identical within experimental errors, therefore the assumption that $[DMF]_F = [DMF]_T$ is valid under our experimental conditions.

APPENDIX 5: Equilibrium Constant (K_{eq}) for Li^+-Na^+ Competition.

The following equations describe the competition between Li^+ and Na^+ for complexation with B15C5 in NM. The determination of K_{eq} comes from nonlinear regressions of ^7Li chemical shift as a function of ρ_T data (Figure 5.13).

$$\underset{\text{A}}{Li^+ + (Na{:}B15C5)^+} \overset{K_{eq}}{\rightleftharpoons} \underset{\text{B}}{Na^+ + (Li{:}B15C5)^+}$$

$$[Na]_T = [Na{:}C] + [Na]; \quad [Li]_T = [Li{:}C] + [Li]; \quad [M]_T = [Na]_T + [Li]_T;$$
$$[C]_T = [Li{:}C] + [Na{:}C]; \quad \rho_T = [C]_T / [M]_T$$

$$K_{eq} = ([Na][Li{:}C]) / ([Li][Na{:}C]) = ([Na]_T-[C]_T + [Li{:}C])\,[Li{:}C] / (([Li]_T - [Li{:}C])\,([C]_T - [Li{:}C]))$$

$$X = K_{eq} - 1; \quad Y = -[Na]_T + [C]_T - K_{eq}[Li]_T - K_{eq}[C]_T; \quad Z = K_{eq}[Li]_T[C]_T$$

$$[Li{:}C] = (-Y - (Y^2 - 4XZ)^{1/2}) / (2X);\ \text{derived from a quadratic equation for [Li:C]}$$

$$\delta_{Li} = (([Li]_T - [Li{:}C])\,\delta_A + [Li{:}C]\,\delta_B) / [Li]_T$$

APPENDIX 6: Kinetic Analysis for Li^+-Na^+ Competition.

The following equations are based on a model describing the observed $k_A + k_B$ in the presence of the 2 competing Li^+ and Na^+ cations. In addition to the individual associative pathways for chemical exchange (see equation 68), another associative pathway is postulated:

$$Li^+ + (Na{:}C)^+ \underset{k_b}{\overset{k_f}{\rightleftharpoons}} Na^+ + (Li{:}C)^+$$

$$K_{eq} = k_f / k_b = ([Na][Li{:}C]) / ([Li][Na{:}C])$$

$$[Na]_T = [Na] + [Na{:}C]; \quad [Li]_T = [Li] + [Li{:}C]$$

1) for lithium exchange:

$$(k_A + k_B)_{Li} = k_{2Li}[Li]_T + k_b[Na] + k_f[Na{:}C]$$

$$\delta_{obs,Na} = (([Na]_T - [Na{:}C]) / [Na]_T)\, \delta_A + ([Na{:}C] / [Na]_T)\, \delta_B$$

$$(\delta_{obs,Na} - \delta_A) / (\delta_B - \delta_A) = [Na{:}C] / [Na]_T = (\Delta / \Delta_o)_{Na}$$

$$(k_A + k_B) = k_{2Li}[Li]_T + k_b[Na]_T((K_{eq} - 1)(\Delta / \Delta_o)_{Na} + 1)$$

2) for sodium exchange:

$$(k_A + k_B)_{Na} = k_{2Na}[Na]_T + k_b[Li:C] + k_f[Li]$$

$$(\delta_{obs,Li} - \delta_A) / (\delta_B - \delta_A) = [Li:C] / [Li]_T = (\Delta / \Delta_o)_{Li}$$

$$(k_A + k_B)_{Na} = k_{2Na}[Na]_T + k_f[Li]_T \{1 + ((1-K_{eq}) / K_{eq}) (\Delta / \Delta_o)_{Li}\}$$

CLAIMS TO ORIGINAL RESEARCH

– The conformations of the ether fragments of B15C5, DB18C6, DB24C8 and DB30C10 in nitromethane-d_3, and acetonitrile-d_3 were determined by ^1H NMk at 300 MHz. Coupling constants reflecting the ^1H-^1H coupling were determined from spin simulations and values for the dihedral angles of the oxygens in the ether fragments were determined.

– The assignment of the ^{13}C resonances of several crown ether-sodium and lithium complexes was done by ^1H-^{13}C heteronuclear chemical shift correlation (HETCOR) and the partial assignment of the ^1H resonances was done with long-range HETCOR experiments.

– The ^{23}Na and ^7Li NMR kinetic results were accounted for by two main exchange mechanisms: associative and dissociative exchange. The rate constants for this chemical exchange were determined by calculating the exchange contribution to the transverse relaxation rate in cases of "moderately fast" chemical exchange (Lorentzian lineshape). In cases where slow exchange was exhibited, full lineshape analyses were performed.

– The chemical exchange of sodium in its solvated and complexed to 15C5 and B15C5 states was determined to proceed via an associative pathway in nitromethane. The kinetic behavior of lithium with the same crown ethers in the same solvent paralleled that of sodium. This mechanism was shown to be highly independent of the nature of the solvent, cation or crown ether. It was postulated that the associative exchange is governed by conformational rearrangements. Based on the solution structural results for

B15C5 and $(Na:B15C5)^+$ in comparison with the known crystal structures [77,79], a scheme was proposed for the associative mechanism in the case of Na-B15C5.

– The chemical exchange of sodium in its solvated and complexed to B15C5 states was determined to proceed via a dissociative pathway in acetonitrile. This change in predominant exchange mechanism was attributed to a change in the donor properties of the solvent. With studies in binary solvent mixtures, a model was proposed for the direct participation of the solvent on a molecular level, for this mechanism. This was the first such qualitative and quantitative description of the solvent effect.

– A competition study between the lithium and sodium cations with B15C5 in nitromethane by ^7Li and ^{23}Na NMR, showed that B15C5 exhibits a selectivity for lithium complexation. In the associative exchange of the individual cations, it was determined that there is no synergistic effect.

– The first application of 2D-^7Li exchange spectroscopy was illustrated in the study of lithium chemical exchange with B15C5 in nitromethane. Quantitative results obtained with this method agreed with the conventional 1D approach.

REFERENCES

[1] C.J. Pedersen, *J. Am. Chem. Soc.* (1967), **89**, 7017.

[2] B. Dietrich, J.M. Lehn and J.P Sauvage, *Tetrahedron Lett.* (1969) 2885.

[3] E.P. Kyba, M.G. Siegel, L.R. Sousa, G. Sogah and D.J. Cram, *J. Am. Chem. Soc.* (1973), **95**, 2691.

[4] C.J. Pedersen, *Angew. Chem. Int. Ed. Eng.* (1988), **27**, 1021.

[5] J.M. Lehn, *Angew. Chem. Int. Ed. Eng.* (1988), **27**, 89.

[6] D.J. Cram, *Angew. Chem. Int. Ed. Eng.* (1988), **27**, 1009.

[7] C.J. Pedersen, *J. Am. Chem. Soc.* (1970), **92**, 386.

[8] C.J. Pedersen and H.K. Frensdorff, *Angew. Chem. Int. Ed. Eng.* (1972), **11**, 16.

[9] H.K. Frensdorff, *J. Am. Chem. Soc.* (1971), **93**, 600.

[10] A.V. Bajaj and N.S. Poonia, *Coord. Chem. Rev.* (1988), **87**, 55.

[11] R.M. Izatt, J.S. Bradshaw, S.A. Nelson, J.D. Lamb and J.J. Chritensen, *Chem. Rev.* (1985), **85**, 271.

[12] F. Vögtle, ed. *"Topics in Current Chemistry"*, Vols. 98, 101 and 121, Springer Verlab, New York, 1981, 1982, 1984.

[13] S. Patai, ed. *"The Chemistry of Ethers, Crown Ethers, Hydroxyl Groups, and their Sulfur Analogs"*, Springer Verlab, New York, 1982.

[14] G.A. Melson, ed. *"Coordination Chemistry of Macrocyclic Compounds"*, Plenum Press, New York, 1979.

[15] S. Patai and Z. Rappoport, eds. *"Crown Ethers and Analogs"*, John Wiley and Sons, Great Britain, 1989.

[16] R.M. Izatt and J.J. Christensen, *"Synthetic Multidentate Macrocyclic Compounds"*, Academic Press, New York, 1978.

[17] D.H. Haynes, B.C. Pressman and A. Kowalsky, *Biochem.* (1971), **10**, 852.

[18] B.G. Cox, J. Garcia-Rosas and H. Schneider, *J. Am. Chem. Soc.* (1981), **103**, 1054.

[19] J.C. Lockhart, *J. Chem. Soc., Faraday Trans. 1* (1986) **82**, 1161.

[20] J.C. Lockhart, *"Advances in Inorganic and Bioinorganic Mechanisms"*, vol. 1, A.G. Sykes, ed., Academic Press, New York, 1982

[21] C. Detellier, H.P. Graves and K.M. Brière, *" Alkali Metal NMR Studies of Synthetic and Natural Ionophore Complexes"*, Chapter 4 in *"Isotopes in the Physical and Biomedical Sciences"*, E. Buncel and J.R. Jones eds., Elsevier, in press.

[22] C. Brevard and P. Granger, *"Handbook of High Resolution Multinulear NMR"*, John Wiley and Sons, New York, 1981.

[23] R.K. Harris, *"Nuclear Magnetic Resonance Spectroscopy: 2nd Edition"*, Longman Group UK Limited, England, 1986.

[24] P. Laszlo, *Angew. Chem. Int. Ed. Eng.* (1978), **17**, 254.

[25] J. Mason, ed., *"Multinuclear NMR"*, Plenum Press, New York, 1987.

[26] G.A. Webb, *"NMR of Newly Accessible Nuclei"*, Chapter 4 in Vol.1, P. Laszlo ed., Academic Press, New York, 1983.

[27] A. Delville, C. Detellier, A. Gerstmans and P. Laszlo, *J. Magn. Reson.* (1981), **42**, 14.

[28] C. Detellier, *"NMR of Newly Accessible Nuclei"*, Chapter 5 in Vol. 2, P. Laszlo ed., Academic Press, New York, 1983.

[29] C. Deverell, *Mol. Physics* (1969), **16**, 491.

[30] A.I. Popov, *Pure Appl. Chem.* (1979), **51**, 101.

[31] R.H. Erlich and A.I. Popov, *J. Am. Chem. Soc.* (1971), **93**, 5620.

[32] (a) V. Gutmann and E. Wychera, *Inorg, Nucl. Chem. Lett.* (1966), **2**, 257. (b) V. Gutmann, *"The Donor-Acceptor Aproach to Molecular Interactions"*, Plenum

Press, New York, 1978.

[33] H. Kistenmacher, H. Popkie and E. Clementi, *J. Chem Phys.* (1974), **61**, 799.

[34] J.S. Shih and A.I. Popv, *Inorg. Nucl. Chem. Lett.* (1977), **11**, 105.

[35] W.J. DeWitte, L. Lui, E. Mei, J.L. Dye and A.I. Popov. *J. Sol. Chem.* (1977), **6**, 337.

[36] Y.M. Cahen, P.R. Hardy, E.T. Roach and A.I. Popov, *J. Phys. Chem.* (1975), **79**, 80.

[37] G.E. Maciel, J.K. Hancock, L.F. Lafferty, P.A. Mueller and W.K. Musker, *Inorg Chem.* (1966), **5**, 554.

[38] J.K.M. Sanders and B.K. Hunter, *"Modern NMR Spectroscopy: A Guide for Chemists"*, Oxford University Press, New York, 1987.

[39] T.C. Farrar and E.D. Becker, *"Pulse and Fourier Transform NMR"*, Academic Press, New York, 1971.

[40] A. Abragam, *"The Principles of Nuclear Magnetism"*, Oxford University Press, New York, 1985.

[41] F. Bloch, *Phys. Rev.* (1946), **70**, 460.

[42] F. Bloch, W.W. Hansen and M. Packard, *Phys. Rev.* (1946), **70**, 474.

[43] P.S. Hubbard, *J. Chem. Phys.* (1970), **53**, 985.

[44] T.E. Bull, *J. Magn. Reson.* (1972), **8**, 344.

[45] A. Gierer and K. Wirtz, *Z. Naturforsch.* (1953), **8A**, 532.

[46] J. Sandström, *"Dynamic NMR Spectroscopy*, Academic Press, New York, 1982.

[47] P. Laszlo, *Progr. NMR Spectr.* (1979), **13**, 257.

[48] S.F. Lincoln, *Progr. Reaction Kinetics* (1977), **9**, 1.

[49] M.T. Rogers and J.C. Woodbrey, *J. Phys. Chem.* (1962), **66**, 540.

[50] J.A. Riddick, W.B. Bunger and T.K. Sakana, *"Organic Solvents: 4th Edition"*, John Wiley and Sons, New York, 1986.

[51] J. Homer, *J. Magn. Reson.* (1984), **57**, 171.

[52] R.C. Weast, ed. *"Handbook of Chemistry and Physics*: 63rd *Edition"*, CRC Press Inc., Boca Raton, 1982-1983.

[53] H.Y. Carr and E.M. Purcell, *Phys. Rev.* (1954), **94**, 630.

[54] D.L. Fontaine, D.K. Ross and B. Ternai, *J. Magn. Reson.* (1975), **18**, 276.

[55] (a) R.K. Gupta, G.H. Weiss, J.A. Ferretti and E.D. Becker, *J. Magn. Reson.* (1979), **35**, 301. (b) G.H. Weiss, J.A. Ferretti, J.E. Kieffer, L. Jacobson, *J. Magn. Reson.* (1983), **53**, 7.

[56] G.A. Morris, *Magn. Reson. Chem.* (1986), **24**, 371.

[57] J. Jeener, B.H. Meier, P. Bachmann and R.R. Ernst, *J. Chem. Phys.* (1979), **71**, 4546.

[58] S.N. Deming and S.S. Morgan, *Anal. Chem.* (1973), **45**, 278A.

[59] SAS Institute Inc., *"SAS® User's Guide: Statistics, Version 5 Edition"*, Carry NC, USA: SAS Inst. Inc., 1985.

[60] R.R Johnson, *"Elementary Statistics: 3rd Edition"*, Duxbury Press, North Scituate, USA, 1980.

[61] reference 46 page 109.

[62] S. Castellano and A.A. Bothner-By, *J. Chem. Phys.* (1964), **41**, 3863.

[63] R.C. Ferguson and D.W. Marquardt, *J. Chem. Phys.* (1964), **41**, 2087.

[64] reference 15 page 272.

[65] M.A. Bush and M.R. Truter, *J. Chem. Soc., Perkin II* (1972), 345.

[66] C. Detellier and M. Robillard, *Can. J. Chem.* (1987), **65**, 1684.

[67] M. Shamsipur, G. Rounaghi and A.I. Popov, *J. Sol. Chem.* (1980), **9**, 701.

[68] M. Bisnaire, C. Detellier and D. Nadon, *Can. J. Chem.* (1982), **60**, 3071.

[69] H.D.H. Stöver, A. Delville and C. Detellier, *J. Am. Chem. Soc.* (1985), **107**, 4167.

[70] D.L. Hughes, *J. Chem. Soc. Dalton Trans.* (1975), 2374.

[71] M. Mercer, M.R. Truter, *J. Chem. Soc. Dalton Trans.* (1973), 2469.

[72] E. Mei, J.L. Dye and A.I. Popov, *J. Am. Chem. Soc.* (1976), **98**, 1619.

[73] M. Dobler and R.P. Phizackerley, *Acta Cryst.* (1974), **B30**, 2748.

[74] S. Khazaeli, A.I. Popov and J.L. Dye, *J. Phys. Chem.* (1982), **86**, 5018.

[75] S. Khazaeli, J.L. Dye and A.I. Popov, *J. Phys. Chem.* (1983), **87**, 1830.

[76] M.A. Bush and M.R. Truter, *J. Chem. Soc., Perkin II* (1972), 341.

[77] J.D. Owen, *J. Chem. Soc., Dalton Trans.* (1980), 1066.

[78] P. Seiler, M. Dobler and J.D. Dunitz, *Acta Cryst.* (1974), **B30**, 2744.

[79] I.R. Hanson, *Acta Cryst.* (1978), **B34**, 1026.

[80] P.R. Mallinson, M.R. Truter, *J. Chem. Soc., Perkin Trans. II* (1972), 1818.

[81] J.D. Dunitz, M. Dobler, P. Seiler and R.P. Phizackerley, *Acta Cryst.* (1974), **B30**, 2733.

[82] J.D. Dunitz and P. Seiler, *Acta Cryst.* (1974), **B30**, 2739.

[83] M. Dobler, J.D. Dunitz and P. Seiler, *Acta Cryst.* (1974), **B30**, 2741.

[84] M. Dobler and R.P. Phizackerley, *Acta Cryst.* (1974), **B30**, 2746.

[85] D. Bright and M.R. Truter, *J. Chem. Soc. (B),* (1970), 1544.

[86] J. Hašek, D. Hlavatá and K. Huml, *Acta Cryst.* (1980), **B36**, 1782.

[87] (a) J.D. Owen and M.R. Truter, *J. Chem. Soc. Dalton Trans.* (1979), 1831. (b) J.D. Owen, M.R. Truter, J.N. Wingfield, *Acta Cryst.* (1984), **C40**, 1515.

[88] J.D. Lin and A.I. Popov, *J. Am. Chem. Soc.* (1981), **103**, 3773.

[89] (a) J.W.H.M. Uiterwijk, S. Harkema, B.W. van de Waal, F. Göbel and H.T.M. Nibbeling, *J. Chem. Soc. Perkin Trans. II* (1983), 1843. (b) J.W.H.M. Uiterwijk, S. Harkema and D. Feil, *J. Chem. Soc. Perkin Trans. II* (1987), 721.

[90] G. Wipff, P. Weiner and Peter Kollman, *J. Am. Chem. Soc.* (1982), **104**, 3249.

[91] D.L. Live and S.I. Chan, *J. Am. Chem. Soc.* (1976), **98**, 3769.

[92] J.C. Lockhart, A.C. Robson, M.E. Thompson, P.D. Tyson and I.H.M. Wallace, *J. Chem. Soc. Dalton Trans.* (1978), 611.

[93] E. Kleinpeter, M. Gäbler, W. Schroth, J. Mattinen and K. Pihlaja, *Magn. Reson. Chem.* (1988), **26**, 387.

[94] E. Kleinpeter, M. Gäbler and W. Schroth, *Magn. Reson. Chem.* (1988), **26**, 380.

[95] F.A.L. Anet, J. Krane, J. Dale, K. Daasvatn and P.O. Kristiansen, *Acta Chem. Scand.* (1973), **27**, 3395.

[96] J. Krane, E. Amble, J. Dale and K. Daasvatn, *Acta Chem. Scand.* (1980), **B34**, 255.

[97] J. Krane, J. Dale and K. Daasvatn, *Acta Chem. Scand.* (1980), **B34**, 59.

[98] K.M. Aalmo and J. Krane, *Acta Chem. Scand.* (1982), **A36**, 219.

[99] J. Dale, *Tetrahedron* (1974), **30**, 1683.

[100] J. Dale, *Is. J. Chem.* (1980), **20**, 3.

[101] H.D.H. Stöver, L.J. Maurice, A. Delville and C. Detellier, *Polyhedron* (1985), **4**, 1091.

[102] A.J. Smetana and A.I. Popov, *J. Sol. Chem.* (1980), **9**, 183.

[103] K.M. Brière, H.P. Graves, T.S. Rana. L.J. Maurice and C. Detellier, *J. Phys. Org. Chem.* (1990), **3**, in press.

[104] H.S. Gold and M.R. Rice, *Talanta* (1982), **29**, 637.

[105] P.A. Mosier-Boss and A.I. Popov, *J. Am. Chem. Soc.* (1985), **107**, 6168.

[106] E. Amble and E. Amble, *Polyhedron* (1983), **2**, 1063.

[107] K. Torizuka and T. Sato, *Org. Magn. Reson.* (1979), **12**, 190.

[108] M. Shamsipur and A.I. Popov, *J. Am. Chem. Soc.* (1979), **101**, 4051.

[109] E. Schmidt, J.M. Tremillon, J.P. Kintzinger and A.I. Popov, *J. Am. Chem. Soc.* (1983), **105**, 7563.

[110] M.R. Johnson, C.A. Colburn, S.J. Canion, B. Son, J.A. Mosbo and L.R. Sousa,

Magn. Reson. Chem. (1988), **26**, 197.

[111] B. Eliasson, K.N. Larsson and J. Kowalewski, *J. Phys. Chem.* (1985), **89**, 258.

[112] L. Echegoyen, A. Kaifer, H. Durst, R.A. Schultz, D.M. Dishong, D.M. Goli and G.W. Gokel, *J. Am. Chem. Soc.* (1984), **106**, 5100.

[113] M.C. Fedarko, *J. Magn. Reson.* (1973), **12**, 30.

[114] M. Geringer and H. Sterk, *J. Magn. Reson.* (1989), **85**, 470.

[115] G.W. Buchanan, R.A. Kirby and K. Bourque, *Can. J. Chem.* (1989), **67**, 449

[116] G.W. Buchanan and K. Bourque, *Tet. Lett.* (1984), **25**, 3963.

[117] R.M. Silverstein, G.C. Bassler and T.C. Morril, *"Spectrometric Identification of Organic Compounds: 4th Edition"*, John Wiley and Sons, New York, 1981, p. 209.

[118] N. Shepard and J.J. Turner, *Proc. R. Soc. London, Ser. A* (1959), **252**, 506.

[119] M. Karplus, *J. Chem. Phys.* (1959), **30**, 11.

[120] M. Karplus, *J. Am. Chem. Soc.* (1963), **85**, 2870.

[121] J.B. Lambert, *Accounts Chem. Res.* (1971), **4**, 87.

[122] H.R. Buys, *Rec. Trav. Chim.* (1969), **88**, 1003.

[123] J.B. Stothers, *"Carbon-13 NMR Spectroscopy"*, Academic Press, New York, 1972.

[124] R. Freeman and G.A. Morris, *J. Chem. Soc., Chem. Commun.* (1978), 684.

[125] G.E. Martin and A.S. Zektzer, *Magn. Reson. Chem.* (1988), **26**, 631.

[126] M. Hofer, *"Transport across Biological Membranes"*, Pitmann, London, 1981.

[127] H.J. Buschmann, *J. Sol. Chem.* (1987), **16**, 181.

[128] E. Mei, J.L. Dye and A.I. Popov, *J. Am. Chem. Soc.* (1977), **99**, 5308

[129] E. Mei, A.I. Popov and J.L. Dye, *J. Phys. Chem.* (1977) **81**, 1677.

[130] H.D.H. Stöver and C. Detellier, *J. Phys. Chem.* (1989), **93**, 3174.

[131] H.P. Graves Smith and C. Detellier, to be submitted for publication.

[132] B.O. Strasser, K. Hallenga and A.I. Popov, *J. Am. Chem. Soc.* (1985), **107**, 789.

[133] C. Deverell and R.E. Richards, *Mol. Phys.* (1966), **10**, 551.

[134] (a) C. Detellier and P. Laszlo, *Bull. Soc. Chim. Belg.* (1975), **84**, 1081. (b) M.S. Greenberg, R.L. Bodner and A.I. Popov, *J. Pys. Chem.* (1973), **77**, 2449.

[135] A.I. Popov, *"Stereodynamics of Molecular Systems"*, R.H. Sharma, eds., Pergamon Press, New York, 1982.

[136] K.M. Brière and C. Detellier, *J. Phys. Chem.* (1987), **91**, 6097

[137] K.M. Brière and C. Detellier, *New J. Chem.* (1989), **13**, 145.

[138] D.E. Woessner, *J. Chem. Phys.* (1961), **35**, 41.

[139] V. Gold and L. Zdunek, *J. Chem. Soc., Faraday Trans.* (1982), **78**, 1835.

[140] E. Shchori, J. Jagur-Grodinski, Z. Luz and M. Shporer, *J. Am. Chem. Soc.* (1971), **93**, 7133.

[141] E. Shchori, J. Jagur-Grodinski and M. Shporer, *J. Am. Chem. Soc.* (1973), **95**, 3842.

[142] K.M. Brière, H.D. Dettman and C. Detellier, to be submitted for publication.

[143] H.P. Graves and C. Detellier, *J. Am. Chem. Soc.* (1988), **110**, 6019.

[144] A. Delville, H.D.H. Stöver and C. Detellier, *J. Am. Chem. Soc.* (1985), **107**, 4172.

[145] A. Delville, H.D.H. Stöver and C. Detellier, *J. Am. Chem. Soc.* (1987), **109**, 7293.

[146] Y.M. Cahen, J.L. Dye and A.I. Popov, *J. Phys. Chem.* (1975), **79**, 1292.

[147] M. Shamsipur and A.I. Popov, *J. Phys. Chem.* (1986), **90**, 5997.

[148] B.O. Strasser and A.I. Popov, *J. Am. Chem. Soc.* (1985), **107**, 7921.

[149] P. Szczygiel, M. Shamsipur, K. Hallenga and A.I. Popov, *J. Phys. Chem.* (1987), **91**, 1252.

[150] E. Schmidt and A.I. Popov, *J. Am. Chem. Soc.* (1983), **105**, 1873.

[151] M. Shamsipur and A.I. Popov, *J. Phys. Chem.* (1988), **92**, 147.

[152] B.O. Strasser, M. Shamsipur and A.I. Popov, *J. Phys. Chem.* (1985), **89**, 4822.

[153] M. Shamsipur and A.I. Popov, *J. Phys. Chem.* (1987), **91**, 447.

[154] E. Mei, A.I. Popov and J.L. Dye, *J. Am. Chem. Soc.* (1977), **99**, 6532.

[155] S. F. Lincoln, A. White and A.M. Hounslow, *J. Chem. Soc., Faraday Trans. I* (1987), **83**, 2459.

[156] S.F. Lincoln, I.M. Brereton and T.M. Spotswood, *J. Am. Chem. Soc.* (1986), **108**, 8134.

[157] S.F. Lincoln, I.M. Brereton and T.M. Spotswood, *J. Chem. Soc., Faraday Trans. I* (1985), **81**, 1623.

[158] R.C. Philips, S. Khazaeli and J.L. Dye, *J. Phys. Chem.* (1985), **89**, 600.

[159] J.M. Ceraso and J.L. Dye, *J. Am. Chem. Soc.* (1973), **95**, 4432.

[160] J.M. Ceraso, P.B. Smith, J.S. Landers and J.L. Dye, *J. Phys. Chem.* (1977), **81**, 760.

[161] K.M. Aalmo and J. Krane, *Acta Chem. Scand.* (1982), **A32**, 219.

[162] E. Amat. B.G. Cox and H. Schneider, *J. Magn. Reson.* (1987), **71**, 259.

[163] E. Amat. B.G. Cox, J. Rzeszotarska and H. Schneider, *J. Am. Chem. Soc.* (1988), **110**, 3368.

[164] M. Shporer and Z. Luz, *J. Am. Chem. Soc.* (1975), **97**, 665.

[165] H. Degani, *Biophys. Chem.* (1977), 6, 354.

[166] J.M. Lehn, J.P. Sauvage and B. Dietrich, *J. Am. Chem. Soc.* (1970), **92**, 2916.

[167] M.S. Greenberg and A.I. Popov, *Spectrochim. Acta* (1975), **31A**, 697.

[168] R.H. Erlich, M.S. Greenberg and A.I. Popov, *Spectrochim. Acta* (1973), **29A**, 543.

[169] A.L. Van Geet, *J. Am. Chem. Soc.* (1972), **94**, 5583.

[170] K.H. Michaelian and M. Moskovits, *Nature*, (1978), **273**, 135.

[171] A.V. Hill, *J. Physiol* (1910), **40**, 4.

[172] A. Delville, C. Detellier, A. Gerstmans and P. Laszlo, *Helv. Chim. Acta* (1981), **64**, 547.

[173] C. Detellier and P. Laszlo, *Proc. Indian Acad. Sci. (Chem. Sci.)* (1985), **94**, 291.

[174] D. Lafleur, fourth year honours thesis, Chemistry Department, University of Ottawa, 1986.

[175] A. Hourdakis and A.I. Popov, *J. Sol. Chem.* (1977), **6**, 299.

[176] J.J.R. Frausto da Silva and R.J.P. Williams, *Nature (London)* (1976), **263**, 237.

[177] J.W. Pettegrew, J.F.M. Post, K. Panchalingam, G. Withers and D.E. Woessner, *J. Magn. Reson.* (1987), **71**, 504.

[178] M.C. Espanol and D. Mota de Freitas, *Inorg. Chem.* (1987), **26**, 4356.

[179] D.P. Cobranchi, G.R. Philips, D.E. Johnson, R.M. Barton, D.J. Rose, E.M. Eyring, L.J. Rodriguez and S. Petrucci, *J. Phys. Chem.* (1989), **93**, 1396.

[180] M.L. Kaplan. E.A. Rietman, R.J. Cava, L.K. Holt and E.A. Chandross, *Solid State Ionics* (1987), **25**, 37.

[181] J.B. Lambert and F.G. Riddell, eds., *"The Multinuclear Approach to NMR Spectroscopy"* D. Reidel Publishers, Boston, 1982.

[182] Y.M. Cahen, J.L. Dye and A.I. Popov, *Inorg. Nucl. Chem. Letters* (1974), **10**, 899.

[183] Y.M. Cahen, J.L. Dye and A.I. Popov, *J. Phys. Chem.* (1975), **79**, 1289.

[184] F.L. Dickert, W. Gmeiner, W. Gumbrecht and H. Meissner, *Angew. Chem. Int. Ed. Eng.* (1987), **26**, 228.

[185] Y. Huang, S. Macura and R.R. Ernst, *J. Am. Chem. Soc.* (1981), **103**, 5327.

[186] P. Baine, *Magn. Reson. Chem.* (1986), **24**, 304.

[187] R. Ramachandran, C.T.G. Knight, R.F. Kirkpatrick and E. Oldfield, *J. Magn. Reson.* (1985), **65**, 136.

[188] D.C. Shungu and R.W. Briggs, *J. Magn. Reson.* (1988), 77, 491.

[189] C. Detellier, *"Reaction Kinetics and Exchange"*, Chapter 9 in *" Modern NMR Techniques and Their Application to Chemistry"*, A.I. Popov and K. Hallenga, eds., Marcel Dekker Inc., New York, 1990.

Date: July 18, 1990

Permissions Department:

Academic Press
465 South Lincoln Drive
Troy, Missouri
63379 USA

I am preparing a PhD. thesis entitled:

The Complexation of Alkali Metal Cations by Crown Ethers: A Multinuclear NMR Study

I would greatly appreciate your permission to use material from one of your publications, as specified below:

Title:	Advances in Inorganic and Bioinorganic Mechanisms
Editor / Author:	A.G. Sykes / J.C. Lockhart
Year of Publication:	1982
Material Requested:	Figure 3 on page 232 in the chapter entitled: "Rates and Mechanisms of Reaction for Elements in Groups I-III"

Credit will be given at the source.

Signed: Kathleen Brière

Name and address: Kathleen M. Brière
Department of Chemistry
University of Ottawa
Ottawa, Ont., K1N 6N6, Canada

July 31, 1990

PERMISSION GRANTED, provided that 1) complete credit is given to the source, including the Academic Press copyright line; 2) the material to be used has appeared in our publication without credit or acknowledgement to another source and 3) if commercial publication should result, you must contact Academic Press again.

Martha Strassberger
Contracts, Rights and Permissions
ACADEMIC PRESS, INC.
Orlando, Florida 32887